“The riddle of the sands” – Luminescence dating of coastal sediments from the southern Baltic Sea and southern North Sea coast

Inaugural-Dissertation
zur Erlangung des akademischen Grades Dr. rer. nat.
am Fachbereich Geowissenschaften der Freien Universität Berlin

vorgelegt von
Tony Reimann
aus Berlin-Mitte

Eingereicht am: 21. März 2011

Tag der Disputation: 9. Juni 2011

“The riddle of the sands“ is a spy novel by Erskine Childers published 1903 in London UK.

Gutachter:

Prof. Dr. Manfred Frechen (Erster Gutachter)

Prof. Dr. Margot Böse (Zweiter Gutachter)

Table of contents

4 Paper II: Luminescence dating of coastal sediments from the Baltic Sea coastal barrier Darss-Zingst, NE Germany

5 Paper III: OSL dating of mixed coastal sediments (Sylt, German Bight, North Sea)

6 Paper IV: The Potential of using K-rich feldspars for optical dating of young coastal sediments – a test case from Darss-Zingst peninsula (southern Baltic Sea coast)

7 Paper V: Single-grain dating of young feldspar sediments using post-IR infrared stimulated luminescence

Table of figures[2]

[2] The figures of the research papers (chapter 3-7) are not listed.

Abstract

A better understanding of coastal sedimentary processes and the relating controlling environmental parameters (e.g. climate, sea-level, sediment supply, and vegetation cover) is crucial for developing concepts of enhanced coastal protection. Past changes of the environmental parameters are recorded in coastal sedimentary archives. Thus, Holocene barrier-spits are an important natural laboratory to investigate the cause-effect relationship between developments of coastal sedimentary systems (e.g. beach plains, foredune plains) and the controlling environmental parameters and furthermore to study the regional and local significance of e.g. supraregional sea-level or climate fluctuations. This task requires, in addition to investigations of the coastal sedimentary setting, a reliable estimation of depositional ages from different sedimentary settings.

The main objective of the thesis is to establish significantly improved chronologies of three barrier-spits located at the southern Baltic Sea (Świna-barrier, Darss-Zingst) and the southern North Sea coast (northern spit of Sylt) by means of luminescence dating. The second main objective is to improve the applicability of luminescence dating methods for the reconstruction of Holocene coastal evolution in general.

The luminescence dating of the very detailed foredune succession at the Świna-barrier reveals that progradation of the foredune plain and thus development of the Holocene barrier-spit started subsequently after the main phase of the Littorina transgression when the fast sea-level rise decelerated (after ~5500-5000 BC). The minor sea-level fluctuations after 5000 BC are not recorded in the investigated sediment sequences of the southern Baltic Sea. However, the data reveals that the late Subatlantic transgression (~800 AD) caused a significant decrease of the progradation dynamics at the Świna-barrier and an alteration of the sediment dynamics in Darss-Zingst. Furthermore, the data indicate that the formation of foredunes and swash-bars (i.e. foredune or beach plain progradation) likely correlates to warmer, milder and calmer phases within the mid- to late-Holocene, whereas time gaps within the chronology of the Świna-barrier foredune progradation (i.e. periods of an erosive or stagnant foredune plain) correlate to phases of enhanced aeolian activity (at ~2200 BC, ~900 BC, ~100 AD, ~600 AD, ~1000 AD, and ~1550 AD) and in four out of six cases to general climatic shifts (at ~2200 BC, ~900 BC, ~600 AD, and ~1550 AD) to colder and stormier conditions within the Holocene.

It is well proven for the investigated Holocene coastal sediments that optically stimulated luminescence (OSL) of quartz applying the single-aliquot regenerative-dose (SAR) protocol is a reliable dating method. Single-grain quartz OSL makes it possible to date incomplete bleached sediments as well as sediment mixtures. Moreover, it is shown for the investigated sediments that the measurement of approved small aliquots of quartz can be used as reliable proxy for single-grain measurements.

Nevertheless, in a few regional and sedimentary settings quartz is not suitable as luminescence dosimeter. The thesis shows that feldspar can be used as an alternative dosimeter if the post-IR IRSL (pIRIR) signal and a modified pIRIR measurement protocol are used for dating. However, residual doses and thermal transfer are more significant for the pIRIR signal than for quartz OSL and the conventional IRSL feldspar signal. Furthermore, luminescence signal zeroing of the pIRIR is slow and thus the probability of incomplete bleached feldspar is significantly higher than for quartz OSL.

However, distinct populations of well-bleached feldspar grains within incomplete bleached sediment samples are detected by single-grain pIRIR measurements.

Zusammenfassung

Ein besseres Verständnis von küstennahen Sedimentationsprozessen und den bedingenden natürlichen Steuerungsfaktoren (z.B. Klima, Meeresspiegel, Sedimentverfügbarkeit und Vegetationsbedeckung) ist Grundvoraussetzung für die Entwicklung von verbesserten Küstenschutzkonzepten, da die Veränderlichkeit der natürlichen Steuerungsfaktoren in der Vergangenheit in Küstensedimentarchiven dokumentiert ist. Holozäne Nehrungssysteme sind somit ein wichtiges natürliches Labor, um die Wechselbeziehung zwischen der Entwicklung von küstennahen Sedimentsystemen (z.B. Strandwallsysteme) und den natürlichen Steuerungsfaktoren zu untersuchen. Darüber hinaus kann die regionale und lokale Wirksamkeit von überregionalen Meeresspiegel- und Klimaschwankungen erforscht werden. Dazu ist neben der Untersuchung der Küstensedimentsysteme eine verlässliche Altersbestimmung verschiedener küstennaher Sedimente unbedingt erforderlich.

Das Hauptziel dieser Arbeit ist es mittels der Lumineszenz-Datierungsmethode, einen nachhaltig verbesserten geochronologischen Rahmen für drei Nehrungssysteme der südlichen Ostseeküste (Świna-Pforte, Darss-Zingst) und der südlichen Nordseeküste (nördliche Nehrung Sylt) aufzustellen. Ein zweites Hauptaugenmerk liegt auf der Verbesserung der Anwendbarkeit der Lumineszenz-Methode zur Rekonstruktion holozäner Küstenentwicklungen.

Die Lumineszenz-Datierung der sehr detaillierten Abfolge von überdünten Strandwällen der Świna-Pforte zeigt, dass die Progradation des Strandwallsystems und somit auch die Entwicklung des Nehrungssystems unmittelbar nach der Hauptphase der Littorina-Transgression, als sich der zunächst schnelle Meeresspiegelanstieg verlangsamte (nach ca. 5500-5000 v. Chr.), startete. Die kleineren Meeresspiegelschwankungen nach 5000 v. Chr. sind dagegen in den untersuchten Sedimentsequenzen der südlichen Ostseeküste nicht dokumentiert. Nur die jungsubatlantische Transgression um ca. 800 n. Chr. verursachte eine nachweisbare Verringerung der Progradationsdynamik an der Świna-Pforte und eine Umstellung der Sedimentdynamik auf Darss-Zingst. Des Weiteren lassen die Daten schließen, das die Bildung von überdünten Strandwällen und somit die Progradation eines Strandwallsystems, sehr wahrscheinlich mit wärmeren, milderen und ruhigen klimatischen Phasen innerhalb des mittleren bis späten Holozäns korreliert. Die Zeitlücken in der Chronologie der Strandwallprogradation der Świna-Pforte, das heißt ein stagnierendes oder erosives Strandwallsystem, hingegen, korrelieren mit Phasen erhöhter äolischer Aktivität (um ca. 2200 v. Chr., 900 v. Chr., 100 n. Chr., 600 n. Chr., 1000 n. Chr. und ca. 1550 n. Chr.), die in vier von sechs Fällen (2200 v. Chr., 900 v. Chr., 600 n. Chr. und ca. 1550 n. Chr.) mit generellen klimatischen Verschlechterungen innerhalb des Holozäns in Verbindungen stehen.

Es ist erwiesen, dass die Optisch Stimulierte Lumineszenz (OSL) von Quarz unter Anwendung des „single-aliquot regenerative-dose“ (SAR) Messprotokolls eine verlässliche Methode ist, um die zu untersuchenden holozänen Küstensedimente zu datieren. Die Analyse von Quarz-Einzelkörnern ermöglicht darüber hinaus die Datierung von schlecht gebleichten Sedimenten oder Sedimentgemischen. Des Weiteren konnte gezeigt werden, dass die Messung von überprüften kleinen Quarz-Aliquots als ein zuverlässlicher Proxy für die Messung von Quarz-Einzelkörnern genommen werden kann.

In einigen Regionen oder sedimentären Umgebungen ist die Verwendung von Quarz als Lumineszenz-Dosimeter eingeschränkt oder unmöglich. Die vorgelegte Arbeit zeigt, dass Feldspat als alternatives Lumineszenz-Dosimeter verwendet werden kann, wenn das post-IR IRSL (pIRIR) Signal und ein modifiziertes pIRIR Messprotokol zur Anwendung kommt. Jedoch haben „residual doses“ und „thermal transfer“ eine größere Signifikanz für das pIRIR Feldspatsignal als für das Quarz- (OSL) und das konventionelle (IRSL) Feldspatsignal. Darüber hinaus, ist die Signalnullsetzung des pIRIR Feldspatsignales langsamer und somit ist die Wahrscheinlichkeit von schlechter Bleichung signifikant erhöht im Vergleich zur Quarz OSL. Dennoch konnten Alterspopulationen von gut gebleichten Feldspatkörnern in schlecht gebleichten Sedimenten mittels der pIRIR Einzelkorndatierung identifiziert werden.

Acknowledgements

This PhD thesis is part of the „Leibniz-Pakt für Lumineszenz“(2008-2010) and was funded by the „Leibniz-Pakt für Innovation und Forschung“.

First of all I’d like to thank my “Doktorvater” Prof. Dr. Manfred Frechen (LIAG, Hannover) for initiating the Leibniz project, which gave four PhDs and one Postdoc the great opportunity to work on excellent projects. Furthermore, I’d like to thank Manfred for helping me in all necessary aspects for conducting this PhD, for having always an open door, for critical reading every line of this thesis, and in particular for always being not a typical (German) boss.

I’d also like to thank Dr. Sumiko Tsukamoto (LIAG, Hannover) for teaching me luminescence, for always showing me the new methodological gimmicks, and for co-supervising my PhD with patience and effort. In particular, you helped me so much to write up some good scientific papers and to deal with sometimes very detailed reviews.

Moreover, I’d like to thank Prof. Dr. Margot Böse (Free University of Berlin) for convincing me in 2007 to apply for a PhD in the Leibniz project, for reviewing my thesis and last but not least for hosting me at the FU Berlin during the last months of the PhD. Furthermore, I am very grateful for the help and discussions with Christopher Lüthgens and Dirk Wenske.

During my PhD I had the great opportunity to visit (and to stay there for a few months) the laboratory in Risø (Denmark) and to collaborate with Dr. Kristina Thomsen (Risø-DTU), Prof. Andrew Murray (NLL, Århus University), and Dr. Mayank Jain (Risø-DTU). It was both, fun and a brilliant scientific experience to work with you. In particular, I’d like to express my special thank to Kristina for teaching me all aspects of single-grain dating and for carefully reviewing (and of course improving) three of my papers. Moreover, my thank goes to Dr. Jan-Peter Buylaert (who saved me from more than 1 m snow in Dec. 2010), Dr. Torben Lapp, Vicki Hansen, Reza Sobathi and all the others of the Risø/NLL team.

Moreover, I had the opportunity to join very fruitful collaborations with Dr. Sebastian Lindhorst (University of Hamburg), Michael Naumann (IOW, Greifswald University), Dr. Krystyna Osadczuk (University of Szczecin), and Prof. Dr. Jan Harff (IOW, University of Szczecin). A special thank goes to Sebastian and Michael who introduced me in coastal Sedimentology, Geomorphology, the Stratigraphy of the southern North Sea and Baltic Sea coast. In particular, I enjoyed a few very exciting weeks and many fun moments in the field with you.

I am grateful to the whole team of the section 3 (Geochronology and Isotophydrology) at the LIAG in Hannover where the main part of my PhD was carried out. In particular, the help and support of Dr. Astrid Techmer, Jolanthe Losse, Petra Posimowski, Gudrun Drewes, Sabine Mogwitz, Dr. Paul Königer, Dr. Axel Suckow, Frank Oppermann, and Karsten Vollmer is very much appreciated. A special thank goes to my fellow luminescence PhD students (Esther, Lara, Christine, Agi, Tobias, Alex and Linto) for sharing their knowledge, for discussions and of course for changing samples.

Finally, I’d like to thank my friends and my family, although I was far away from Berlin and things were not always easy during the last three years, I knew that I always could count on your help and support. In particular, I am very grateful to Anita for holding my back when it was most needed.

Moreover, without the financial support of my grandmother Christel, my mother Renate, and my father Michael my university degree and the PhD would be unthinkable. Above all, I met a beautiful woman named Annika in 2009. This indeed means more to me than the PhD.

March 2011,

Tony Reimann

1 Introduction

Against the background of an ongoing environmental change (global warming, global sea-level rise, see e.g. IPCC, 2007) it is an essential task for geosciences to systematically investigate the cause-effect relationship between changing environmental parameters and coastal processes and dynamics (Harff and Lüth, 2007). A better understanding of past coastal processes and dynamics provides a crucial input for forecast models of coastal change. Thus, it is essential for planning coastal protection, infrastructure and settlements along our coasts.

Holocene coasts are an important natural laboratory to examine the development of sediment systems resulting from the interaction between natural controlling parameters e.g. relative sea-level fluctuations, sediment supply, accommodation space of the area, climate parameters, vegetation cover (Forbes et al., 1995; Hoffmann et al., 2005), and in addition anthropogenic factors such as deforestation, land use or coastal protection (e.g. Grunewald, 2006; Labuz, 2009). These complex interactions are reflected in a variety of Holocene coastal sedimentary archives (e.g. sandy barrier-spits). A thorough analysis and interpretation of these archives requires detailed sedimentological and geomorphological investigations. Furthermore, a reliable and robust geochronological frame is essential.

During the last decades great effort has been made in studying Holocene coastal sediment successions and sedimentary features along the southern Baltic Sea and southern North Sea coast by sedimentological as well as geomorphological methods (e.g. Keilhack, 1912, 1914; Schütze, 1939; Gripp and Simon, 1940; Borówka et al., 1986; Borówka, 1990; Müller, 1996; Janke and Lampe, 1998; Schumacher, 2000; Oszadczuk, 2002; Hoffmann et al., 2005, 2009; Hoffmann and Lampe, 2007; Lindhorst, 2008, 2010). However, until 2008 the chronologies of sediment archives along the southern Baltic Sea and the German part of the southern North Sea coast were only poorly established owing to a limited number of radiocarbon ages (i.e. mainly ages of peat formation or ages from marine shells) and occasional archaeological findings.

During the last two decades, various studies of coastal regions around the world showed that luminescence dating, in particular if quartz can be used as luminescence dosimeter, is best suited to establish reliable and high-resolution chronologies of Holocene coastal sediment successions (e.g. see reviews by Jacobs, 2008; Madsen and Murray, 2009). However, some applications of the luminescence dating method (e.g. dating of young feldspars, dating of sediment mixtures) are still in an early experimental stage. These applications still merit a systematic examination regarding their potential and reliability.

1.1 Overall aims and objectives

The main objective of this work is to establish a more detailed and robust chronology for some Holocene coastal sediment archives along the southern Baltic Sea and southern North Sea coast. Furthermore, it is aimed to interpret the Holocene coastal sedimentary archives, i.e. the cause-effect relationship of coastal processes and controlling parameters. Thirdly, it is aimed to test the potential of new analytical set-ups (measurement equipment, statistical models) in order to reliably date incomplete bleached or mixed Holocene coastal sediments. A fourth main objective is to

systematically test the potential of feldspar minerals as an alternative luminescence dosimeter in Holocene coastal settings.

1.2 Outline of thesis

The thesis is subdivided into eight chapters. Chapter 1 is the introduction of the thesis. In chapter 2 the current state of research is outlined. The first part of chapter 2 is focussed on Holocene coastal sediment systems and sedimentary processes. The three coastal areas under study are briefly introduced in the second part. The third part of chapter 2 introduces luminescence dating methods. All three parts of chapter 2 underline the most relevant problems of the current state of research, which are addressed in the following chapters.

Chapter 3 presents the well established application of optically stimulated luminescence (OSL) dating method to foredune and coastal dune sediments from the Świna barrier (southern Baltic Sea, NW Poland). The Świna barrier provides one of the most detailed successions of established foredunes along the southern Baltic Sea coast and is regarded as a key area to study the cause-effect relationship between the Holocene evolution of a foredune plain and the controlling parameters. In particular, the correlation of periods of a stagnant or erosive foredune plain with phases of enhanced aeolian activity, general climatic deterioration and regressive vegetation cover is discussed in chapter 3. The following chapter 4 deals with OSL dating of two generations of beach ridge systems situated at the Darss-Zingst peninsula (southern Baltic Sea, NE Germany). The high-resolution chronology of a currently prograding beach ridge plain (Zingst Windwatt) is correlated with similar coastal areas along the Danish and Dutch North Sea coast. Moreover, the established chronology is correlated with the climate development of the last millenium. Chapter 3 and 4 are based on manuscripts, which are accepted for publication (chapter 3) and published (chapter 4) in the international peer-reviewed journal Geomorpholgy.

Chapter 5 presents the application of OSL to date contaminated swash-bar (shallow marine) sediments from the North Frisian island Sylt (German Bight, North Sea). In order to identify the burial age of swash-bars within a sediment mixture OSL is applied to single-grains of quartz. Reliable burial ages for these swash-bar sediments are crucial to understand the sea-level and climate control on the evolution of the northern spit of Sylt. Different measurement set-ups and statistical methods are tested and discussed. Chapter 5 is based on a study which is submitted to the international peer-reviewed journal Quaternary Geochronology.

In chapter 6 the application of K-rich sand-size feldspars to dating of young coastal sediments is systematically tested. The samples are taken from a coastal sediment core from the western part of Zingst peninsula (NE Germany). It is one of the first studies that used a post-IR IRSL (pIRIR) signal (Thomsen et al., 2008) from feldspar for dating. The study shows for the first time that a modified pIRIR measurement protocol can be used to date Holocene sediments. Furthermore, the study shows that the conventional IRSL signal from feldspar gives unreliable results. In chapter 7 the results of the modified pIRIR protocol applied to feldspar single-grains are discussed. This pioneer study systematically investigates feldspar single-grain dose distributions of well-bleached and incompletely bleached sediment samples. Chapter 7 shows for the first time that feldspar single-grain measurements can be used to identify a population of well-bleached feldspar grains in an incompletely bleached sediment sample and thus that this technique can be used to obtain reliable burial ages for young incompletely bleached feldspar samples. Chapter 6 is based on a study that is

published in the international peer-reviewed journal Quaternary Geochronology; chapter 7 based on a manuscript, which is currently under review.

In chapter 8 an overall conclusion of the previous chapters and of the thesis is given. It underlines the most important outcome of this work and gives an outlook to future research.

2 Current state of research

2.1 Holocene coastal evolution

2.1.1 Coastal sediments and sedimentary features

Holocene coastal plains along the southern Baltic Sea and southern North Sea coast are made up of shallow marine depositions (e.g. swash-bars, tidal sediments), aeolian depositions (e.g. aeolian cover sands, dune sediments) or sedimentary features, which are a result of a combination of shallow marine and aeolian depositional processes e.g. beach ridges or foredune ridges. Both, beach ridges and foredune ridges are cited as sensitive indicators of ancient shoreline positions (e.g. Bristow et al., 2000; Otvos et al., 2000) and have thus significance for studies of Holocene coastal evolution.

The term beach ridge is used in the literature for relict, parallel to semi-parallel, either wave-built or wind-built ridges, which usually form beach plains (Otvos, 2000). Foredunes are defined as shore-parallel dunes formed by aeolian sediments within vegetation at the upper limit of wave action on prograding beach platforms (Hesp, 1988, 2002; Bristow et al., 2000). However, both terms are often used synonymous in the literature and Otvos (2000) concluded that the term beach ridge should include all relict beach plain ridges, whether made up by wave/swash-built (berm ridge) or by aeolian sediments (foredune ridge). Thus, if a significant aeolian component is present most beach plain ridges are characterised as foredunes. Based on ground-penetrating radar (GPR) measurement, which is a non-invasive geophysical method, accompanied with sedimentological investigations, Bristow et al. (2000) proposed a model of beach plain development and foredune evolution at sandy coasts under moderate climate conditions. The model reveals the interdependence of shallow marine (e.g. wave and swash-built) and aeolian processes.

According to the model of Bristow et al. (2000) a basic requirement of a prograding beach or foredune plain is a positive sediment budged i.e. a sufficient sediment supply to the beach (Fig. 2.1a, d). A second requirement of a prograding beach or foredune plain is a progressive vegetation cover (e.g. Hesp, 1988, 2002) to trap the wind-blown sediment and to stabilise foredunes as well as the beach platform (Fig. 2.1b, c). Lindhorst et al. (2010) recently suggested a slightly modified model based on investigations of a hooked spit on the North Frisian island Sylt (North Sea). They found by means of GPR measurements that the accumulation of aeolian sand is associated with the proximal terminations of erosional scarps in the backshore. They concluded that the formation of erosional scarps (e.g. by storms) serves as a trap i.e. it initialise the formation of foredune ridges. However, the model of Bristow et al. (2000) (Fig. 2.1) as well as the study of Lindhorst et al. (2010) reveal that the successive accretion of foredune ridges (i.e. a prograding foredune plain) results from an interplay of shallow marine and aeolian processes.

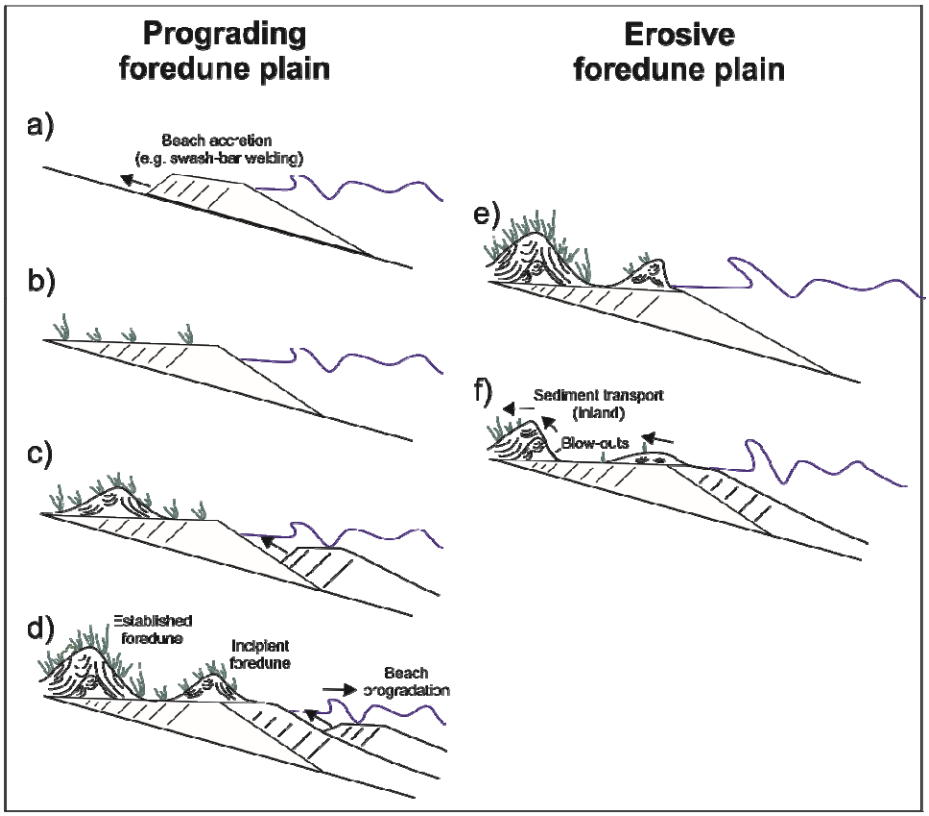

Figure 2.1: Model of beach and foredune plain accretion modified after Bristow et al. (2000). **a)** Where the sediment budged is positive beach accretion results from e.g. swash-bar welding. **b)** Once a stable backshore platform has formed by ongoing beach progradation, dune initiation is accompanied by vegetation growths **c)**. The initial dunes (incipient foredunes according to Hesp, 1988) are stabilised by fast-growing plants, this vegetation cover plays an important role in trapping of aeolian sand (e.g. Hesp, 1988, 2002; Lindhorst et al., 2010) and forming an established foredune **d)**. A continued accretion of beach sediment bodies (beach progradation) may lead to the initiation of a new incipient foredune ridge (Bristow et al., 2000). In contrast, a rising seal-sea level may cause erosion of the foredunes **e)** and thus negative sediment budged of the foredune plain. If the vegetation cover is regressive dune blow-outs occur and sediment is transported from the foredune plain and backshore platform to the coastal hinterland **f)**. As a result transgressive and/or parabolic dunes may form.

Foredune plains turn into an erosive or instable mode for three main reasons. Firstly, a significant reduction in sand supply (e.g. sediment cut-off) effectively halts foreslope accretion (Bristow et al., 2000) and thus reduces sand supply for foredune formation. Secondly, a significant relative sea-level rise effectively causes erosion of the beach and foredune plain (Fig. 2.1e). Thirdly, a regressive vegetation cover effectively reduces the quantity of sand being trapped at the beach, which causes an interruption of foredune accretion and a sediment transport further inland (Fig. 2.1f). This can happen e.g. as a result of an increased frequency and magnitude of wave and storm erosion, of changes in the vegetation period or due to a change in land-use (e.g. Grunewald, 2006). If so, foredune blow-outs occur and accordingly sand is transported inland, forming transgressive and parabolic dunes (Bird, 1990; Hesp, 2002). Transgressive or parabolic dunes are in contrast to established foredunes genuine aeolian features. Thus, transgressive or parabolic dunes are formed in phases of enhanced aeolian activity i.e. these dunes are no indicators for ancient shorelines (unlike foredunes). Bird (1990) characterised these aeolian features as secondary dunes. Secondary dunes differ from the primary foredunes by dune orientation, the shape of the axis and the height.

However, it is often concluded in the literature (e.g. Hesp, 1988, 2002; Forbes et al., 1995; Bristow et al., 2000; Hoffmann et al., 2005; Lindhorst et al., 2010) that the Holocene evolution of beach and foredune plains is in combination with the local geology and morphology controlled by the

development of the sea-level and the climate. Fluctuation of the relative sea-level as well as past changes of Holocene climate may be manifested in these coastal sediment archives. If so, these sedimentary archives provide geological chronologies to study the regional and local significance of global sea-level and climate changes.

2.1.2 Evolution of a Holocene barrier-spit

The evolution of the recent southern Baltic Sea and North Sea coastline started with the Littorina transgression and Flandrian transgression, respectively (e.g. Streif, 2004; Lampe, 2005). The transgressions (8.0-7.0 ka) caused the flooding of a paraglacial landscape, which was primarily shaped during the last glaciations. After the main phase of transgression the former fast seal-level rise became slower. Sandy Holocene spits attached to higher elevated islands and started to develop. Thus, the coastlines consist of Pleistocene headlands (cliffs) and Holocene sandy lowlands (mainly beach plains and/or foredune plains) and are classified as paraglacial coasts according to Forbes (1995). The evolution of these Holocene spits and barrier-spits is - as mentioned above - controlled by the combination of a variety of natural parameters (e.g. sea-level, sediment supply, climate, vegetation) and anthropogenic parameters (e.g. land use, coastal protection). As this thesis is mainly focussed on the Holocene coastal development at the southern Baltic Sea coast a conceptual model (according to Hoffmann et al., 2005) of Holocene barrier evolution is introduced, which considers conditions at a low-energy, sand-dominated, and tideless paraglacial coast. Note that the environmental conditions at the southern North Sea are different from the Baltic Sea coast e.g. it is a high-energy and tidal coast.

According to Hoffmann et al. (2005) the barrier evolution along the southern Baltic Sea is primarily influenced by the transgressive history and the pre-transgressive morphology. The evolutionary stages of the barrier evolution proposed by Hoffmann et al. (2005) are shown in Figure 2.2. During the main phase of transgression (8.0-7.0 ka) the paraglacial landscape (Fig. 2.2a) was flooded. The sediment supply was insufficient to compensate the expansive accommodation space growth and thus the landscape was submerged (Fig. 2.2b). Furthermore, initial proto-beach ridges attached to the Pleistocene headlands and migrated with the transgressing sea (Lampe et al., 2007). At about 7.5 ka the sea-level rise decelerated (Lampe et al., 2007). Thus, the accommodation space growth decreased, coastal barriers started to develop, and the erosion of Pleistocene headlands led to the formation of cliffs and barrier-spits (Fig. 2.2c). Furthermore, large wind flats were accumulated behind the beach ridge or foredune plains. When the successive accretion of beach ridges or foredune ridges closed the coastal inlets the barriers are either stabilised or eroded resulting in alongshore sediment transport. In areas with positive sediment budged progradation of the coastline occurred (Fig. 2.2d). The coastal plains of established beach ridges or foredune ridges potentially provided the sediment to form coastal dunes (e.g. parabolic dunes) on top.

The ongoing evolution of Holocene coastal barriers has altered the previous strongly varying coastline to a straight coastline. A regional description for this special composition of coastal landforms and sedimentary dynamics is called Bodden equilibrium coast (“Bodden-Ausgleichsküste” in German) where “Bodden” is the local synonym for lagoon. The final stage of this potential equilibrium can be observed at the SE Baltic Sea, along the Polish coast. In the final stage former bays or lagoons are isolated from the open sea and transformed into coastal lakes by coastal barriers.

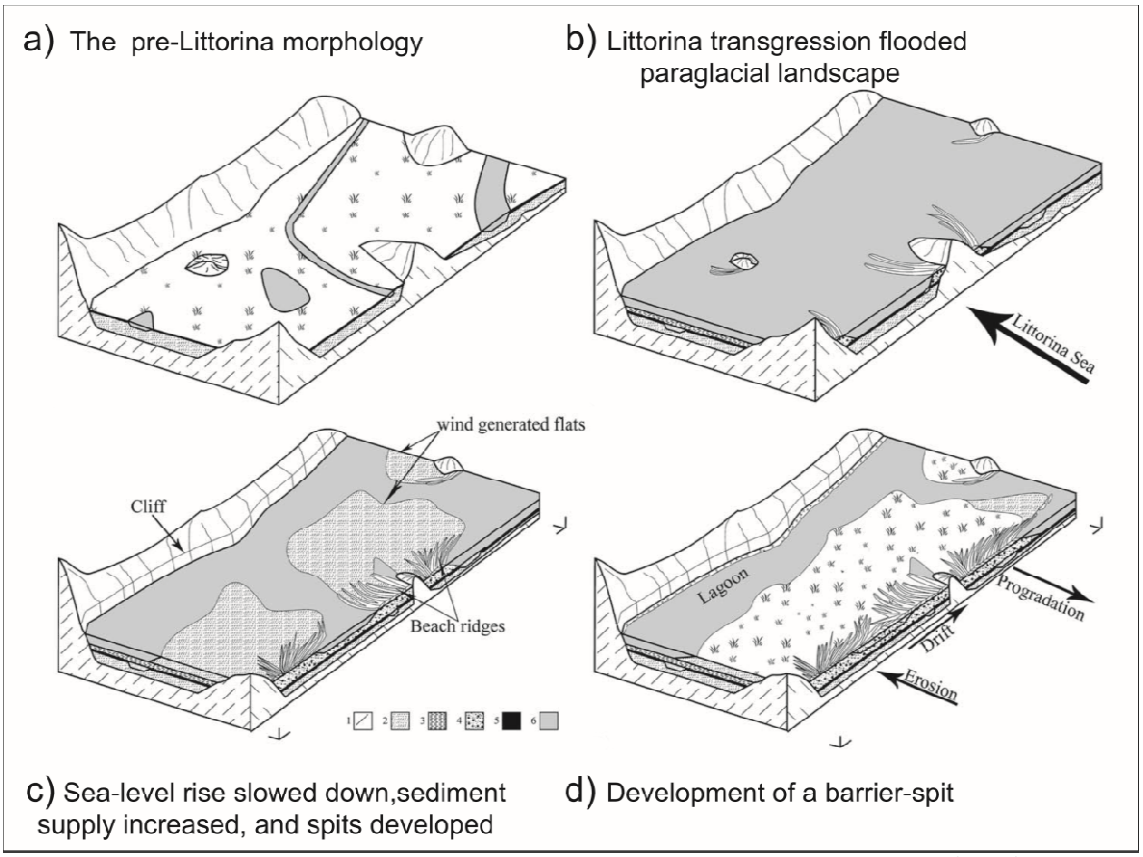

Figure 2.2: Evolution of Holocene barriers at the SW Baltic coast after Hoffmann et al. (2005). (1) Till, (2) fine sand, (3) mud, (4) fine to medium sand, (5) peat and (6) water. **a)** The pre-Littorina morphology is characterised by elevations made up of Pleistocene glacial deposits bordering by depressions which are partly filled with fluvial and lacustrine sediments. **b)** During the main phase of the Littorina transgression the water level rose rapidly and flooded the depressions. Initial proto-beach ridges began to build up attached to the Pleistocene headlands. **c)** Sediment supply increased as the erosion intensified. Cliffs were formed and the coastline was cut back. Wind flats developed behind the foredune ridges. Coastal lakes were disconnected from the open sea. **d)** The successive accretion of foredune ridges closed the connection to the open sea; lagoons came into being. The barrier can either be eroded and the sediment transported further longshore or stabilised. Progradation occurs where sediment accumulates (Hoffmann et al., 2005).

However, Lampe (2005) as well as Hoffmann et al. (2009) note that the time interval from ~6.5 ka to present is poorly documented by radiocarbon data from peat because the siliciclastic sediments of the barrier spits contain very little organic material suitable for radiocarbon dating. The post-Littorina sea-level fluctuations and resulting coastal processes have been reconstructed mainly by occasional archaeological findings and sedimentological evidence. Thus, the chronologies of these important sediment successions are only poorly established. In order to establish are significant improved geochronological frame for the Holocene coastal barriers it is a matter of urgency to date the siliciclatic coastal sediments directly. Moreover, the evolutional model of Hoffmann et al. (2005) needs to be specified by a numerical chronology.

2.2 Study areas

Three Holocene barrier-spit systems were selected for case studies. These areas are located along the southern Baltic Sea and southern North Sea coast (Fig. 2.3). The different study areas are briefly introduced in the following section (2.2.1-2.2.3).

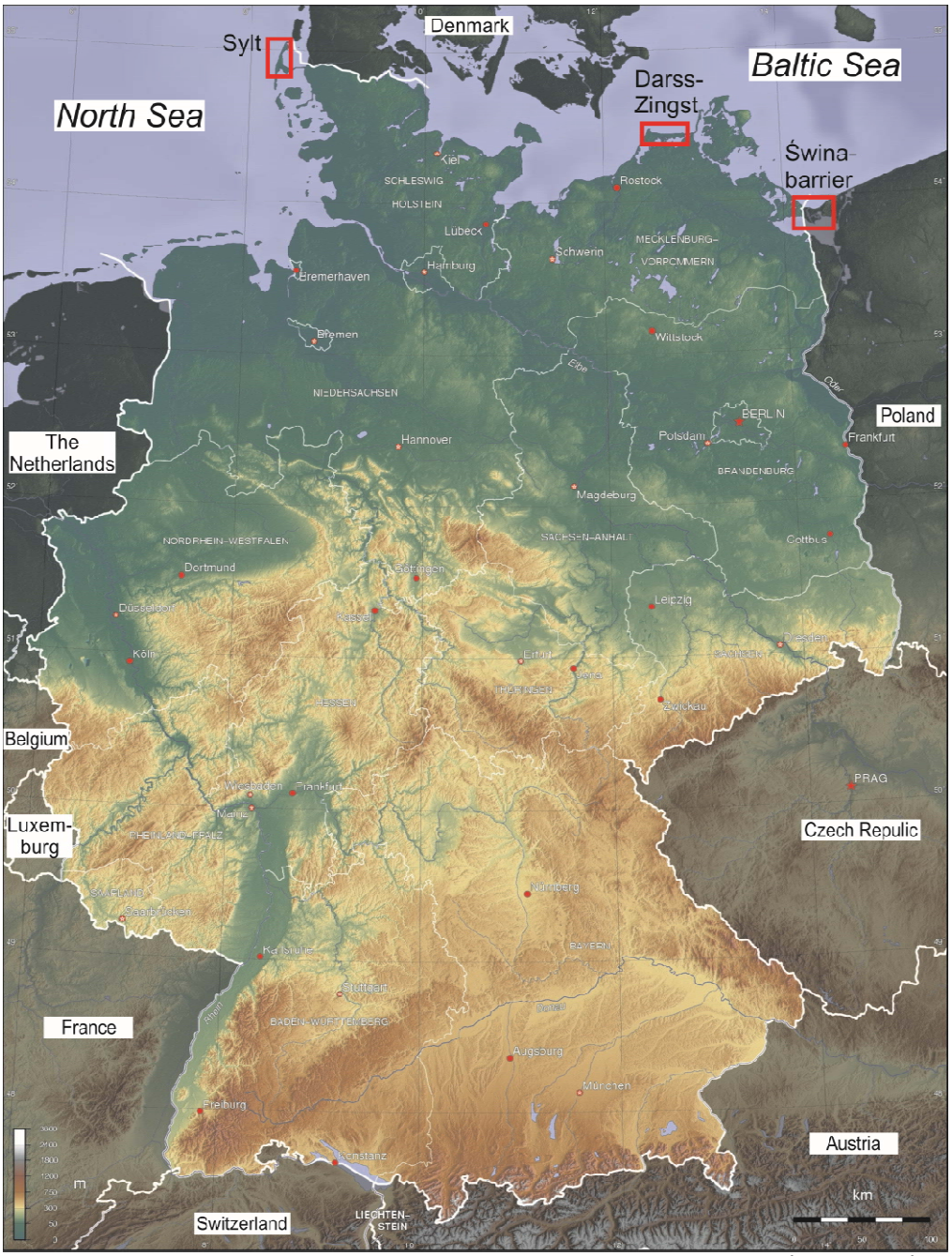

Figure 2.3: Topographic map of Germany. Map is modified after: **www.mygeo.info/landkarten/deutschland/Deutschland_Topograhie_2007.jpg**. The study areas are indicated by red rectangles.

2.2.1 Świna barrier

The Świna barrier is located at the border of Poland and Germany (Fig. 2.3). A detailed description of the study area (including maps and figures) is given in chapter 3. The barrier consists of two sandy spit systems (i.e. foredune plains) situated between two Pleistocene headlands on Uznam and Wolin (Usedom und Wollin in German). The barrier separates the Szczecin Lagoon from the Pomeranian Bight (Baltic Sea). Both spits provide one of the most detailed successions of foredunes. The stratigraphy and the formation of the more than one hundred foredunes of the Świna barrier were already investigated by Keilhack (1912, 1914). He subdivided the foredune successions of Uznam and Wolin into three generations (brown, yellow, and white) varying in size, in the orientation of the

ridges but mainly in the degree of soil profile (podzol) development. Keilhack established a classic coastal foredune stratigraphy for the southern Baltic Sea. Therefore, the Świna barrier can be regarded as a key area to investigate the Holocene evolution of foredune plains at the southern Baltic Sea coast. Until 2008, the Holocene history of these important sediment successions has been studied based on geomorpholocial, pedological and sedimentological investigations (Keilhack, 1912, 1914; Borówka et al., 1986; Borówka, 1990; Osadczuk, 2002). The chronology of the Świna barrier was based on a few isolated radiocarbon estimates from the 1960s (Prusinkiewicz and Noryśkiewicz, 1966), which actually date the time of peat formation in the inter dune troughs. Thus, it is timely and crucial to establish an improved and more detailed chronology for the foredune successions at the Świna barrier.

2.2.2 Darss-Zingst

The Darss-Zingst peninsula is the north-eastern part of the Darss-Zingst-Fischland peninsula chain, which is located at the south-western Baltic Sea coast of NE Germany. The peninsula chain is the westernmost part of the Bodden equilibrium coast (see section 2.1.2). A detailed description of the study area is given in chapter 4. Darss-Zingst is a relatively flat Holocene barrier-spit, which is attached to the Pleistocene headland Altdarss in the west. The barrier-spit consists of different beach plains (e.g. succession of foredunes or windflats) which are separated from each other by coastal inlets. Some of these coastal inlets are artificially closed (e.g. Prerowstrom). The present sediment transport is mainly alongshore from the west (Darss) to the east (Zingst). However, according to the sediment budged calculations of Naumann and Lampe (submitted) it is unlikely that the Altdarss cliff (in the west) is the exclusive sediment source for the Holocene barrier-spit Darss-Zingst. Naumann and Lampe (submitted) found potential sediment sources in the northward sea area and proposed a simultaneous closing of the barrier-spit during the Holocene rather than an exclusive west-east directed beach progradation. However, the chronology of the beach plains is too patchy to verify their working hypothesis.

2.2.3 Northern spit Sylt

The island Sylt is situated at the border of Germany and Denmark (Fig. 3) and belongs to the North Frisian islands in the German Bight (southern North Sea). A more detailed description of the study area is given in chapter 5. Sylt is built on a Pleistocene core of Saalian and Elsterian moraines, as well as reworked earlier Cenozoic sediments (Gripp and Becker, 1940). Two Holocene barrier-spit systems are attached towards the north and the south. The area under study is located on the northern barrier-spit. The Holocene evolution was first described by Gripp and Simon (1940). Lindhorst et al. (2008, 2010) presented in process-orientated studies a high-resolution three-dimensional sedimentary model of the northern spit. This model is based on GPR measurements and sediment cores. They show that the sedimentary architecture reflects both phases of erosion and accumulation (e.g. by swash-bar welding). However, the timing of these phases is not well established (Lindhorst et al., 2008, 2010). In order to correlate the evolution of the northern spit with sea-level fluctuations and/or climate shifts (as controlling factors) a detailed chronology of these sediment successions is essential.

2.3 Luminescence dating of Holocene coastal sediments

A better understanding of coastal sedimentary processes and the relating controlling factors (e.g. climate, sediment supply, and sea level) is fundamental to developing concepts of improved coastal protection. This task requires, in addition to investigations of the sedimentary setting, a reliable estimation of depositional ages of different sedimentary units. During the last decade luminescence dating became a powerful tool to date Holocene coastal sediments.

Nevertheless, until 2008 the majority of geochronological studies, which investigated Holocene coastal sediment successions along the southern Baltic Sea coast and the German North Sea coast, were based mainly on radiocarbon data (e.g. Lampe, 2005; Hoffmann et al., 2005; Lindhorst et al., 2008). However, chronologies, which are only based on radiocarbon are problematical; firstly, due to a general lack of suitable organic material (wood, peat, shells) for radiocarbon dating. Secondly, if organic material is present in coastal settings, it is always questionable whether this material is in situ or not. Thirdly, radiocarbon dating of sediments younger than 450 years is problematic (Nielsen et al., 2006; Madsen et al., 2007; Madsen and Murray, 2009) owing to calibration problems of short-term atmospheric ^{14}C-variations caused by fluctuations of the solar activity and the climate during the recent centuries (Stuiver, 1978; Hua, 2009). Finally, marine organic material (e.g. shells) requires a correction for the marine-reservoir effect. However, this task is not straightforward (see e.g. Lindhorst, 2007).

Luminescence dating has the potential to provide dates with an accuracy of 5-10% (Murray and Olley, 2002) from the depositional event itself. Luminescence estimates the time elapsed since mineral grains (e.g. sedimentary quartz and feldspar) were last exposed to daylight and it can reliably date sediments ranging from ~10 to 150 000 years. The principles of luminescence dating were reviewed by Aitken (1985, 1998) and more recently by Preusser et al. (2008). The method uses an optical (optically stimulated luminescence, OSL) or thermally (thermoluminescence, TL) sensitive luminescence signal in the minerals. During exposure to sunlight, e.g. during sediment transport, the luminescence signal in the mineral grains is erased until it is completely zeroed. After burial, the mineral grains are sealed from sunlight; the luminescence signal starts to accumulate again, being induced by naturally occurring radioactivity. For dating, the amount of absorbed energy, known as the equivalent dose (D_e in Gy), since the last zeroing is determined within a laboratory luminescence measurement. The burial time is calculated by dividing the equivalent dose by the dose rate. The dose rate is the radiation exposure acting on a sample over a certain time (Preusser et al., 2008). This relation is expressed by following equation:

$$\text{Luminescence age} = \frac{\text{Equivalent dose } D_e}{\text{Dose rate}} \left[\frac{Gy}{Gy/a} \right] \qquad \text{(Eq. 2.1)}$$

During the past 20 years, it is mainly OSL dating that is applied to establish chronologies for a variety of sedimentary settings (e.g. see reviews by Wallinga, 2002; Bateman, 2008; Fuchs and Owen, 2008; Roberts, 2008; Madsen and Murray, 2009).

During recent years, the majority of studies have used quartz as a natural dosimeter and quartz has generally been found to yield precise and accurate ages in particular for young samples (Madsen and Murray, 2009). Thus, OSL on sedimentary quartz minerals is a powerful method to determine reliable depositional ages. The application of quartz to dating Holocene coastal sediments is introduced in section 2.3.1. However, there are regional and sedimentary settings where the use of quartz as luminescence dosimeter is limited or in some cases impossible due to a low OSL sensitivity of the quartz minerals (see review by Preusser et al., 2009). In such cases K-rich feldspar minerals can be used as alternative luminescence dosimeters. Commonly, K-rich feldspars are stimulated in the near infrared and thus this method is known as infrared stimulated luminescence (IRSL). The application to dating of Holocene sediments is introduced in section 2.3.2. Incomplete zeroing (bleaching) of the luminescence signal prior to burial or post-depositional mixing have in some samples been shown to result in false estimated luminescence ages, this false estimation is of significance in particular for young samples (<5ka). To overcome the problem of incomplete bleaching and post-depositional mixing, the luminescence technique has been applied to single-grains in an attempt to identify the grain population most likely to have been well-bleached at burial or not affected from mixing processes. The single-grain technique is introduced in section 2.3.3.

2.3.1 OSL dating of quartz

OSL dating of quartz is commonly used for geochronological studies in coastal or marine environment (see review by Jacobs, 2008) and for the dating of young sediments (see review by Madsen and Murray, 2009). The OSL of quartz was firstly introduced by Huntley et al. (1985) and further developed in the following years. A major breakthrough in OSL dating was the development of reliable single-aliquot techniques in the 1990s (e.g. Duller, 1991, 1994; Mejdahl and Bøtter-Jensen, 1994; Murray and Roberts, 1998; Murray and Wintle, 2000). The main advantage of a single-aliquot approach is that all measurements are carried out on an aliquot of the same grains, which circumvents the problem of individual properties of grains from different aliquots. A review of different single-aliquot techniques as well as the alternative multi-aliquot techniques is given by Vandenberghe (2004) and Preusser et al. (2008).

Most studies during the last decade apply the single-aliquot regenerative-dose (SAR) measurement protocol (according to Murray and Wintle, 2000, 2003) for quantifying the D_e. The basic premise of the SAR is that the OSL signal is zeroed during each measurement. Following the measurement of the luminescence induced in nature (natural signal), it is possible to monitor the OSL response of the same grains (in an aliquot) to a known laboratory irradiation (regenerative doses). Using varying amounts of laboratory irradiation allows the construction of a dose response curve by the measurements of regenerative doses (Preusser et al., 2009). In the SAR procedure, the response to a constant test dose (T_N) is measured after each natural and regenerative dose measurement (Fig. 2.4a). A typical quartz OSL signal is shown in Fig. 2.4b. The T_N response changes with any change in OSL sensitivity, and thus by dividing the natural or regenerated OSL signal by the T_N response a sensitive-corrected response and so a sensitive-corrected dose response curve can be derived (Fig. 2.4c). A detailed review of this approach and the included quality tests is provided by Wintle and Murray (2006).

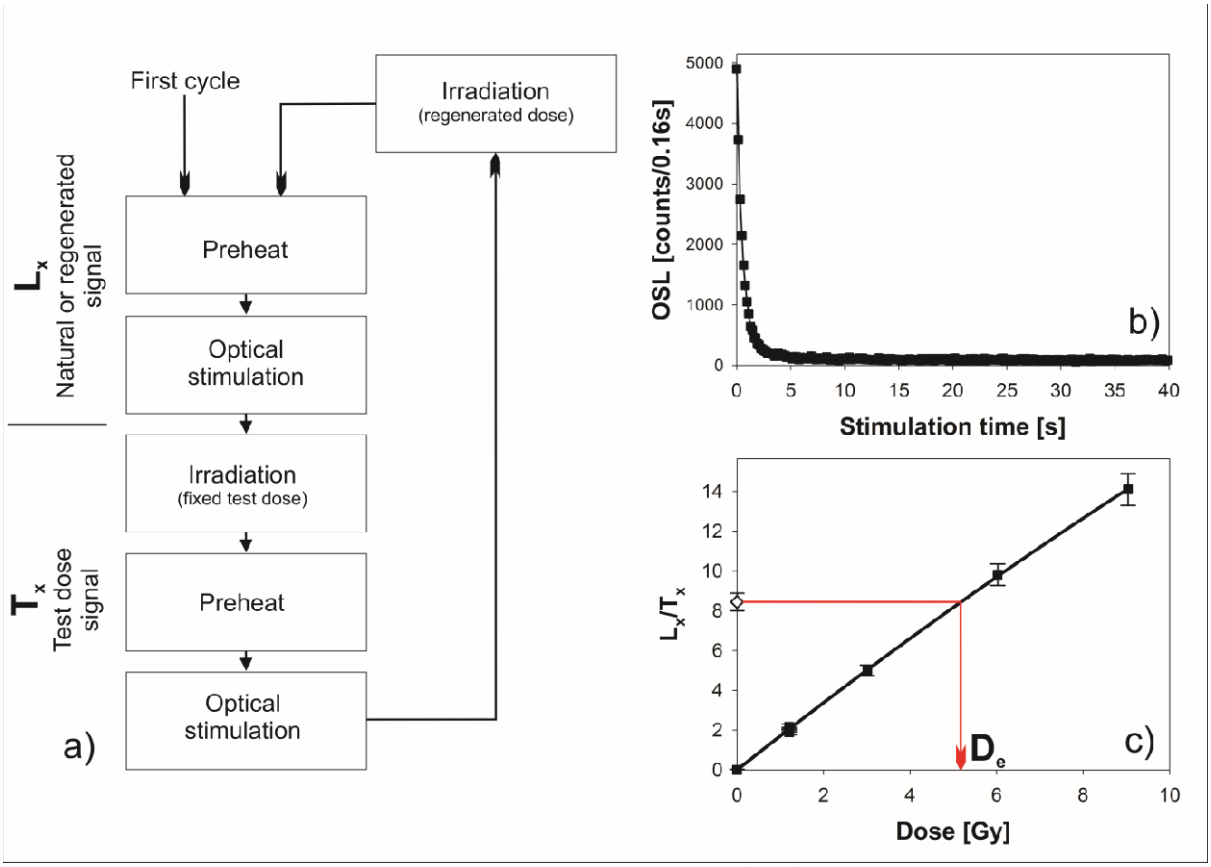

Figure 2.4: Quartz OSL applying the single-aliquot regenerative-dose (SAR) protocol. A generalised SAR protocol (according to Murray and Wintle, 2000) is shown in **a)**. In **b)** a typical OSL signal curve is shown. In **c)** a SAR dose response curve is shown. The natural L_x/T_x is indicated as open diamond; the regenerative L_x/T_x is indicated as black square. The D_e of the aliquot is obtained by interpolation of the natural sensitivity corrected (L_x/T_x) natural signal on the SAR dose response curve. The data shown are for quartz extracted from a coastal sample from Zingst (Baltic Sea, W-Zi3).

Madsen and Murray (2009) summarized in their review paper the main problems associated to dating of very young (<1 ka) coastal and aeolian sediments, e.g. signal-to-noise ratio, thermal transfer, resetting of the OSL signal. Nevertheless, it is well proved for Holocene coastal aeolian, beach or shallow marine sediments along the world that OSL measurements of quartz based on the SAR protocol provides reliable ages estimates (e.g. Bailey et al., 2001; Murray-Wallace et al., 2002; Wilson et al., 2004; Murray and Mohanti, 2006; Lopez and Rink, 2007; Sommerville et al., 2007; Roberts and Plater, 2007; Madsen et al., 2009; Kunz et al., 2010a). In recent years, in particular, plenty of studies along the North Sea coast of the Netherlands and Denmark had proven the suitability of quartz OSL applying SAR to dating of Holocene coastal sediments (e.g. Ballarini et al., 2003; Madsen et al., 2005, 2007, 2010; Clemmensen and Murray, 2006; Nielsen et al., 2006). However, until 2008 similar investigations along the German North Sea coast and the southern Baltic Sea coast were generally lacking. Only the paper of Mauz and Bungenstock (2007) studied tidal sediments from East Friesland to reconstruct sea-level trends by applying OSL dating method. Thus, it is timely and a matter of urgency to establish quartz OSL based chronologies for coastal sediments along the German coasts.

2.3.2 Luminescence dating of K-rich feldspar

Although, quartz OSL is generally a very robust technique (see previous section) in several regional and sedimentary settings the use of quartz as a dosimeter is limited or not possible due to a very poor OSL sensitivity of the quartz minerals (e.g. Preusser et al. 2006; Lukas et al., 2007; Steffen et al., 2009; Hülle et al., 2010; Kunz et al., 2010b). Low OSL sensitivity of quartz can be found in numerous parts of the world, mostly where the quartz grains have only recently been released from the source rock. These problems encountered in application of quartz are reviewed by Preusser et al. (2009). It is well known that K-rich feldspar minerals provide very bright and reproducible luminescence signals (higher intrinsic luminescence) even if the quartz provides nearly undetectable OSL signals (e.g. Preusser et al., 2005; Lukas et al., 2007; Kunz et al., 2010b). In addition, Davids et al. (2010) showed that the significant higher intrinsic luminescence sensitivity of K-rich feldspars results in an improved signal-to-noise ratio compared to quartz, even if the quartz gives well detectable OSL signals. An improved signal-to-noise ratio is an advantage particularly with regard to young samples. However, in the past ten years the use of feldspar as a natural dosimeter has be held back for two main reasons: (i) the presence of anomalous fading (athermal signal decrease) in the IRSL signals (e.g. Wintle, 1973; Aitken, 1985, 1998; Huntley and Lamothe, 2001; Wallinga et al., 2007; Davids et al., 2010), which results in systematic age underestimation, and (ii) a slower zeroing of the luminescence signal by exposure to sunlight (e.g. Godfrey-Smith, 1988; Thomsen et al., 2008), which make problems of incompletely bleaching more severe in feldspar than in quartz.

The infrared stimulated luminescence (IRSL) was invented by Hütt et al. (1988). A review of the methodological principles of IRSL and the different luminescence spectra from K-rich feldspars is given by Krbetschek et al. (1997). The IRSL SAR protocol applied to sand-size K-rich feldspars was mainly introduced by Wallinga et al. (2000) and Blair et al. (2005). In contrast to the OSL SAR protocol in Fig. 2.4 the aliquots are stimulated by infrared LED or infrared laser. However, ages derived from SAR IRSL dating of K-feldspars need to be corrected for anomalous fading (e.g. Huntley and Lamothe, 2001; Lamothe et al., 2003). The limitations of the common fading correction procedures are e.g. shown by Wallinga et al. (2007). Therefore, in recent years, enormous effort has been made in finding luminescence signals from feldspar which are less affected by anomalous fading (e.g. Trautmann et al., 1999; Erfurt and Krbetschek, 2003; Tsukamoto et al., 2006; Thomsen et al., 2008). Thomsen et al. (2008) proposed the use of a post-IR IRSL (pIRIR) signal measured at an elevated temperature, which is less affected by anomalous fading than the conventional IRSL signal. The proposed pIRIR single-aliquot regenerated-dose measurement protocol (pIRIR protocol), a typical pIRIR signal and a resulting dose response curve are shown in Fig. 2.5a, b and c, respectively.

Buylaert et al. (2009) and Thiel et al. (2010) successfully applied the proposed pIRIR protocol to dating of older (>100 ka) sediments. However, signal zeroing might be a problem for the pIRIR protocol. Furthermore, Buylaert et al. (2009) reported a measureable residual dose/thermal transfer, which does not affect for their old samples but be important for young Holocene samples. Indeed, they analysed in their paper three Holocene samples as well and obtained an average overestimation of ~20% (Buylaert et al., 2009). In order to apply the proposed pIRIR protocol to Holocene coastal samples thorough experimental tests on young K-rich feldspars are required. A systematic testing may allow an optimisation of the pIRIR protocol with regard to dating of Holocene coastal samples.

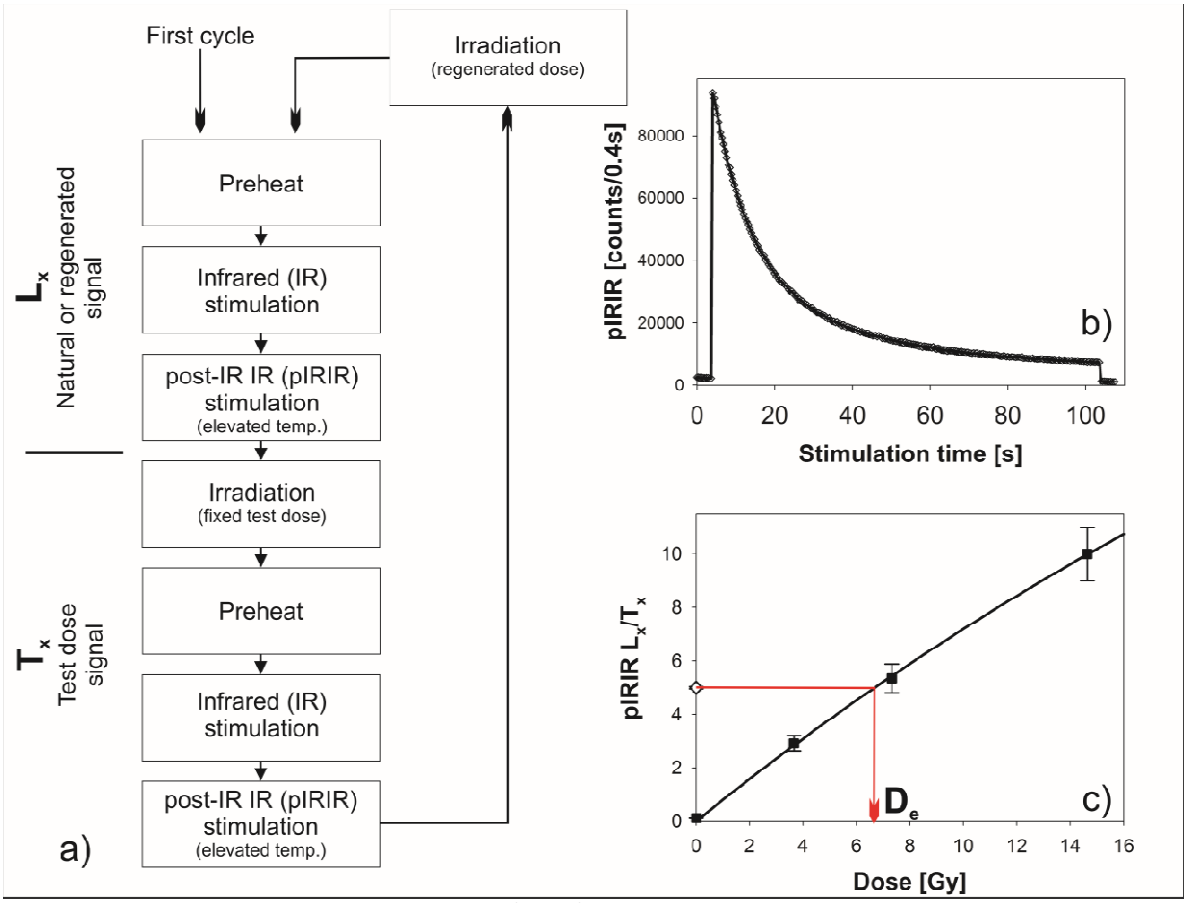

Figure 2.5: Feldspar IRSL applying post-IR IRSL (pIRIR) SAR protocol. A generalised pIRIR protocol (according to Thomsen et al., 2008) is shown in a). The first IRSL stimulation is carried out at 50 °C; the post-IR IRSL (pIRIR) is carried out at an elevated temperature (150-290 °C). In b) a typical pIRIR signal curve is shown. In c) a pIRIR SAR dose response curve is shown. The natural L_x/T_x is indicated as open diamond; the regenerative L_x/T_x is indicated as black square. The D_e of the aliquot is obtained by interpolation of the natural sensitivity corrected (L_x/T_x) natural signal on the pIRIR SAR dose response curve. The data shown are for K-rich feldspar extracted from a coastal sample from Zingst (Baltic Sea, W-Zi3).

2.3.3 Single-grain analyses of complex D_e distributions

One advantage of the single aliquot technique is that it easily allows multiple replicates of D_e measurements from the same sediment sample. The resulting D_e distributions always show a certain variation among the individual D_e estimates. In general, the observed variation in a D_e distribution is attributed to intrinsic factors (e.g. counting statistics, instrument reproducibility, thermal transfer and other luminescence characteristics) and extrinsic factors (e.g. small scale variations of the radiation field, partial bleaching of the luminescence signal prior to deposition, post-depositional mixing of the sediment). Thus, it is first and foremost important to assign appropriate intrinsic uncertainties to the individual D_e estimates in order to study extrinsic sources of D_e variation (Thomsen et al., 2007). During the last decade plenty of luminescence studies investigated incomplete bleaching of the luminescence signal prior to deposition in various sedimentary environments (e.g. fluvial, glacifluvial, coastal, proglacial, alluvial, periglacial) as the main extrinsic source of D_e variation (e.g. Olley et al., 1999, 2004; Fuchs and Lang, 2001; Wallinga, 2002; Arnold et al., 2007).

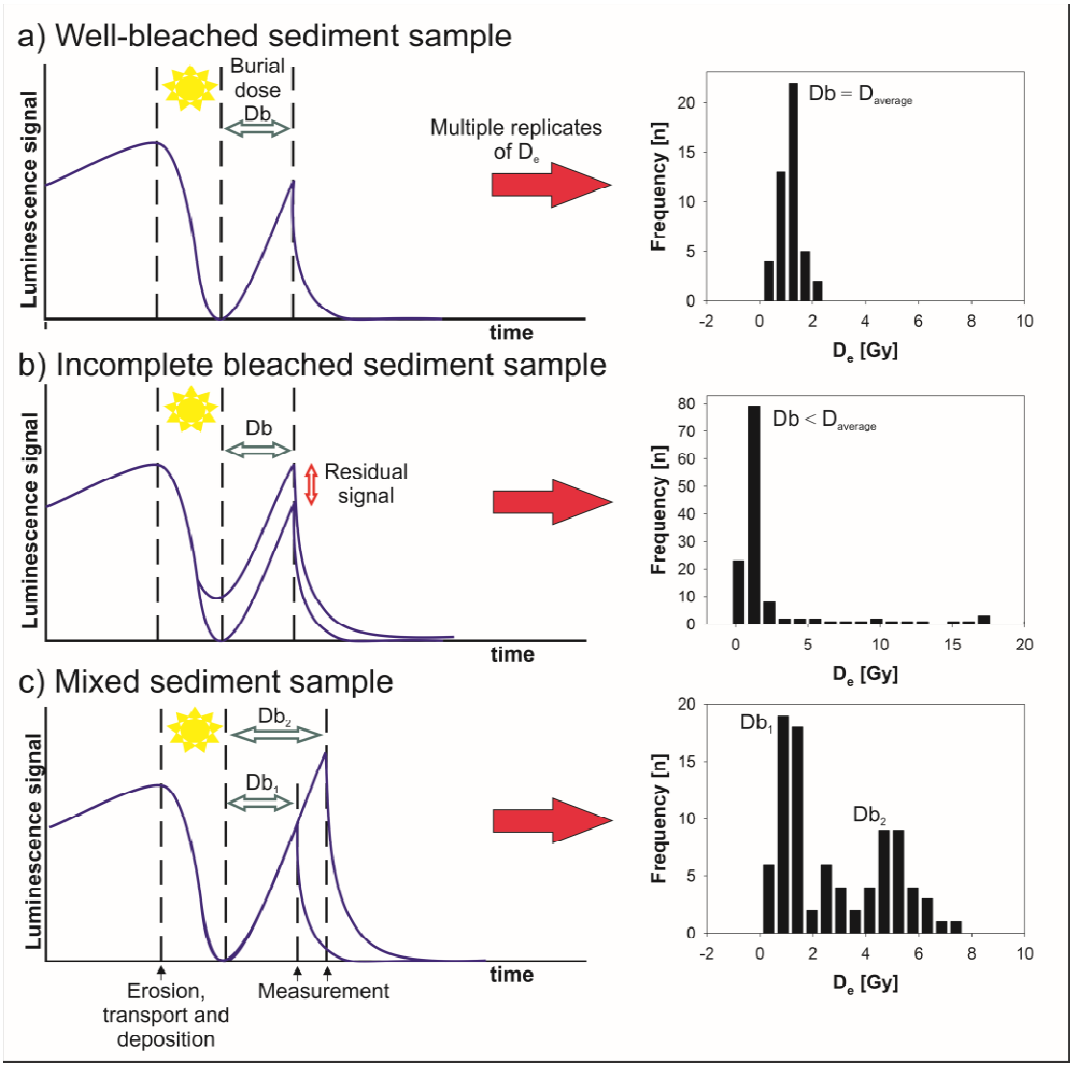

Figure 2.6: Luminescence signal zeroing, sediment mixing and resulting D_e distributions. During erosion, transport and deposition the minerals are exposed to sunlight and the previously accumulated luminescence signal is zeroed (bleached). In **a)** a well-bleached sample is shown, a sufficient sunlight exposure removed all the luminescence (left). The resulting gaussian distribution of multiple replicate D_e measurements is shown on the right and thus the burial dose (Db) is equivalent to the average D_e ($D_{average}$). In **b)** the sunlight exposure during erosion, transport and deposition was not sufficient for some grains, for these incomplete bleached grains a residual signal remains (left). The resulting positive skewed D_e distribution is shown on the right. Note that the majority of the grains are well-bleached. However, the Db of the well-bleached grain population is smaller than the average $D_{average}$ of the distribution. In **c)** well-bleached minerals, which were buried for different time intervals, were mixed after the deposition (e.g. bioturbition). The resulting multi-modal D_e distribution (with Db_1 and Db_2) is shown on the right.

If the signal resetting (zeroing) of some sedimentary grains is incomplete a residual luminescence signal remains, which results in an overestimation of the equivalent dose for these grains, although this overestimation is generally only of significance for young samples (<5ka). The difference of a typical well-bleached sample and a typical incomplete bleached sample is shown in Fig. 2.6a and Fig. 2.6b, respectively. Furthermore, post-depositional processes (e.g. due to bioturbation) are discussed as significant source for D_e variations (e.g. Bateman et al., 2003, 2007). However, incomplete bleaching as well as sediment mixing cause complex (non-gaussian) D_e distribution (see Fig. 2.6b, c) and dating such samples is not a straightforward task since it requires detailed analyses of non-gaussian D_e distributions as the mean or weighted mean of such D_e distributions is unlikely to be an appropriate estimate of the true burial dose (e.g. Rodnight et al., 2006).

Given that, single sedimentary grains (quartz or feldspar) are the smallest unit of sediment transport and sediment reworking, it is prudent to observe the D_e variations on a single-grain scale of analysis. If furthermore, the intrinsic sources of D_e variation are quantified by laboratory experiments (see Thomsen et al., 2005, 2007; Duller, 2008) and the expected variation in a well-bleached and/or unmixed D_e distribution is defined, e.g. by investigating aeolian samples from the same regional setting (e.g. Rodnight et al., 2006), well-bleached grain populations and incomplete-bleached grain populations can be identified by applying statistical models to single-grain D_e distributions (e.g. Galbraith et al., 1999; Thomsen et al., 2007).

The OSL dating of single-grains was invented by Murray and Roberts (1997) and has since the late 1990s undergone several evolutionary steps, which were recently reviewed by Duller (2008). However, to this day, single-grain dating technique is primarily applied to quartz minerals.

For quartz it is known that in various regional settings (e.g. north European plain, Scandinavia) only 1-5% of the grains emit a detectable OSL signal and as a consequence the signal in a multi-grain aliquot is dominated by only a few bright grains (e.g. Duller, 2000; Lüthgens et al., accepted). In such cases, the measurement of multi-grain aliquots containing less than 100 grains (small aliquots) are a sufficient proxy for true single-grain measurements as the average luminescence signal in a small aliquot is dominated by one or two bright grains (e.g. Thomsen et al., 2002; Rodnight et al., 2006; Lüthgens et al., accepted). The analysis of small aliquots is often advantageous as it is less time-consuming and statistically less challenging than single-grain analysis. However, the appropriateness of small aliquot as proxy for single-grain measurement is in recent years subject of controversies (e.g. Olley et al., 2004; Rodnight et al., 2006; Arnold and Roberts, 2009). Thus, it is crucial to systematically apply both measurement set-ups to coastal samples of the north European plain (here: southern North Sea or southern Baltic Sea coast) that suffer from incomplete bleaching or sediment mixing.

In contrast to quartz, feldspar has a great advantage because it seems to have inherently strong IRSL signals regardless of the regional and sedimentary setting. However, only a very few single-grain feldspar studies (reasons see previous section) have been published so far, but Duller (2003) as well as Li et al. (2010) showed that in contrast to quartz ~40% of the individual feldspar grains emit a significant IRSL signal and stated that the large proportion of feldspar grains giving a significant signal is of great benefit when measuring feldspar single-grains. However, no single-grain study of feldspar pIRIR is published so far. Thus, neither the intrinsic sources of variation in a pIRIR single-grain D_e distribution nor the natural signal zeroing of the promising feldspar pIRIR signal are examined to this day.

Chapter 3, Paper I:

Tony Reimann[a], Sumiko Tsukamoto[a], Jan Harff[b,c], Krystyna Osadczuk[c], Manfred Frechen[a] 2011.

[a] Leibniz Institute for Applied Geophysics (LIAG): Geochronology and Isotope Hydrology, Stilleweg 2, 30655 Hannover, Germany
[b] Leibniz Institute for Baltic Sea Research, Department for Marine Geology, Warnemünde, Germany
[c] Institute of Marine and Coastal Sciences, University of Szczecin, Szczecin, Poland

Reconstruction of Holocene coastal foredune progradation using luminescence dating – an example from the Świna barrier (southern Baltic Sea, NW Poland).

Geomorphology 132, 1-16.

(www.sciencedirect.com/science/article/pii/S0169555X11001863)

Abstract

Two sandy spits on the Świna barrier (Wolin and Uznam) provide a very detailed succession of Holocene coastal foredunes and dunes and are regarded as key sites along the southern Baltic Sea coast. Optically Stimulated Luminescence (OSL) dating is proven to be a powerful tool for the reconstruction of Holocene coastal spit evolution and foredune accretion; quartz extracted from the coastal sediments in the study area provides excellent properties for OSL dating. The OSL age from the innermost dune indicates that spit development of the Świna barrier started immediately after rapid sea level rise of the Littorina transgression decelerated at ~6.6 ka. A significant change in the foredune progradation rate occurred during the late Subatlantic transgression at ~1.2 ka (800 AD), when migration rates decreased from 2.6 ± 0.7 m a^{-1} to 1.3 ± 0.4 m a^{-1}. Progradation accelerated again during the "Little Ice Age" between 1550 and 1850 AD.

The systematic dating of 28 samples reveals six hiatuses during foredune succession, at ~2100 BC, ~900 BC, 200 BC-200 AD, ~600 AD, ~1000 AD, and ~1600 AD. The timing of these hiatuses correlates with the phases of transgressive dune development in the surrounding area (Troszyn and Świna) and with phases of increased aeolian activity in other parts of North- and West-Europe. We conclude that four of these phases of foredune erosion/instability and aeolian sediment mobilisation were caused by general climate shifts to cooler and stormier conditions at ~2200 BC, ~900 BC, ~600 AD, and at ~1600 AD, the latter corresponding to the "Little Ice Age". The period of increased aeolian activity around 1000 AD is likely related to a phase of intensive forest clearance in Central Europe. In contrast, the systematic foredune accretion and foredune plain growth correlates to periods of positive sediment budget, milder and calmer climate, and an intact vegetation cover.

3.1 Introduction

The evolution of paraglacial coasts is controlled by sediment supply, morphology and climate (Forbes et al., 1995). The development of the southern Baltic Sea coastlines and coastal landforms (e.g. spits, coastal barriers) results from the complex interaction between natural factors e.g. relative sea-level fluctuations, local geology, the amount of sediment and accommodation space of the area, the energy and direction of waves and winds, and vegetation cover (Hoffmann et al., 2005). Furthermore, anthropogenic factors, such as deforestation, land use and coastal protection have to be considered for a better understanding of the Holocene coastal evolution. A detailed investigation of coastal development and the sediment dynamics along the southern Baltic Sea provides an insight into both natural and anthropogenic processes and their interaction. Due to ongoing environmental change (such as sea-level rise, global warming, and excessive land use), it is an important task for the geoscience community to understand the very complex cause-effect relationships between coastal processes and their relative importance (Harff and Lüth, 2007).

The Świna barrier is a key area for a better understanding of spit and coastal barrier evolution along the southern Baltic Sea because it provides one of the most detailed successions of coastal foredunes and dunes in the region (Keilhack, 1912, 1914). Based on the degree of podzolisation Keilhack (1912) sub-divided these dunes into three generations (brown, yellow and white; Fig. 3.1) and established a "classic" dune classification for the southern Baltic Sea coast. Furthermore, the Świna barrier is also a key area for providing an insight into Holocene aeolian activity for the so-called "European sand belt" (Zeeberg, 1998) and the relationship between the evolution of coastal foredune plains and coastal parabolic or transgressive dunes. This barrier is composed of two spits (the Wolin and Uznam spits; Fig. 3.1) which developed in opposite directions during the Holocene, although it is not certain, whether development of the two spits was simultaneous.

The Holocene history of barrier evolution and aeolian activity in this area has been studied based on geomorphologic and geological investigations of the aeolian and coastal sediment succession (e.g. Keilhack, 1912, 1914; Borówka et al., 1986; Borówka, 1990; Osadczuk, 2002). However, the chronologies of these landforms were based on a few isolated radiocarbon estimates, mainly of peat from the inter dune troughs (Prusinkiewicz and Noryśkiewicz, 1966). Hoffmann et al. (2005, 2009) provided radiocarbon ages from the basal peat from Pudagla lowland (Uznam, Fig. 3.1b), and this basal peat represents the onset of the coastal evolution. To obtain a better insight into the interaction between sediment dynamics and sea level change, the wind regime or the vegetation cover, a reliable, accurate and systematic geochronology of the shallow water and aeolian sand succession is necessary. Clarke and Rendell (2009) suggested in their review paper the importance of luminescence dating for studying the timing of Holocene sand movement. Optically stimulated luminescence (OSL) was first proposed by Huntley et al. (1985) which made it possible to date the time elapsed since the last exposure to sunlight of mineral grains (quartz or feldspar), and therefore OSL dating can be used to determine the depositional age of sand- or silt-size sediments. Aitken (1998) gives a general overview of OSL dating methods including the theoretical background. During the last decade, the OSL dating of quartz using the single-aliquot regenerative-dose protocol (SAR) (Murray and Wintle, 2000) was successfully applied in a plenty of studies to Holocene shallow water sediments (e.g. Murray-Wallace et al., 2002; Madsen et al., 2005, 2007, 2009; Nielsen et al., 2006; Roberts and Plater, 2007; Alappat et al., 2010) and dunes (e.g. Murray and Clemmensen, 2001; Ballarini et al., 2003; Aagaard et al., 2007; Kunz et al., 2010) from numerous coasts along the world.

The first OSL dates from the southern Baltic Sea were obtained by Kaiser et al. (2006) and Hilgers (2007) for Late Pleistocene aeolian sands and paleosols. Reimann et al. (2010; 2011) dated Holocene coastal sediments at the southern Baltic Sea from the Darss-Zingst peninsula (NE Germany).

The aim of this study is to illustrate the potential of OSL based chronologies for coastal and aeolian sediments, and to establish a detailed and reliable chronology based on OSL dating for the coastal sediment succession from the Świna barrier. The chronology and the existing models of barrier spit evolution along the southern Baltic Sea (e.g. Hoffmann et al. 2005), the local relative sea level curve (Hoffmann et al., 2009), the stratigraphy of Holocene coastal dunes and foredunes in particular the classification of Keilhack (1912, 1914) are then used to debate mid- to long-term controlling factors (e.g. sea level, climate, land use) for foredune accretion. Furthermore, the relationship between the phases of foredune development and aeolian sand movement during the Holocene will be discussed.

3.2 Study Area

3.2.1 Holocene coastal evolution and sea level history

The Baltic Sea is an almost tideless, semi-enclosed sea with brackish water masses. It occupies an intracontinental basin, linked to the Atlantic Ocean through the Danish Straits (Øresund, Storebælt and Lillebælt, Fig. 3.1a). During the Last Glacial Maximum (LGM), the Fenno-Scandinavian ice sheet covered the Baltic Sea basin. After the area became ice-free (Late Pleistocene), proglacial lakes and marine phases alternated. The later phases were triggered by complex interactions of eustatic sea level fluctuations, isostatic adjustments and ice sheet-decay between 14.0 and 8.0 ka (see reviews by Björk 1995 and Lampe 2005). The development of the recent southern Baltic Sea coastline started with the Littorina transgression at around ~8.0 ka (Janke and Lampe, 1998; Lampe, 2005; Hoffmann et al., 2005, 2009). This coastline consists of Late Pleistocene headlands (cliffs) and Holocene sandy lowlands (barriers and dune coasts) and was classified by Hofmann and Lampe (2007) as paraglacial coast according to the definition of Forbes et al. (1995).

Hoffmann et al. (2005) provide a conceptual model of barrier evolution, which considers low-energy, sand-dominated, and tideless conditions in the paraglacial coast. They observe that barrier evolution along the southern Baltic coast is primarily influenced by the transgressive history of the Baltic Sea and the pre-transgressive relief. According to their model, the Littorina transgression (8.0–6.0 ka) caused the flooding of paraglacial landscapes, characterised by Pleistocene headlands (glacial deposits) bordering depressions partly filled by freshwater or fluvial sands. The rise of the sea level was initially very rapid, with a mean rate of 15 mm a^{-1} between ~8.0 ka cal. BP and ~7.0 ka cal. BP (Hoffmann and Lampe, 2007). During this main phase of transgression, the sediment supply was insufficient to compensate the expanding accommodation space due to a rapid rise in water level, and the landscape was submerged. After ~7.0 ka cal. BP, the rate of sea level rise is assumed to have decreased to approximately 1 mm a^{-1}. Sediment supply increased, the amount of accommodation space decreased, and therefore, the coastal barriers started to develop. The erosion of the Pleistocene headlands led to the formation of cliffs and barrier spits. Large wind-flats were formed behind the beach ridge plains, disconnecting the coastal lakes from the open sea. When the beach ridges had closed the coastal inlets the barriers either stabilised or eroded, resulting in sediment transport along the shoreline. If the sediment budget was positive, progradation of the coastline occured and coastal dunes began to develop on the top of the beach ridges (Hoffmann et al., 2005).

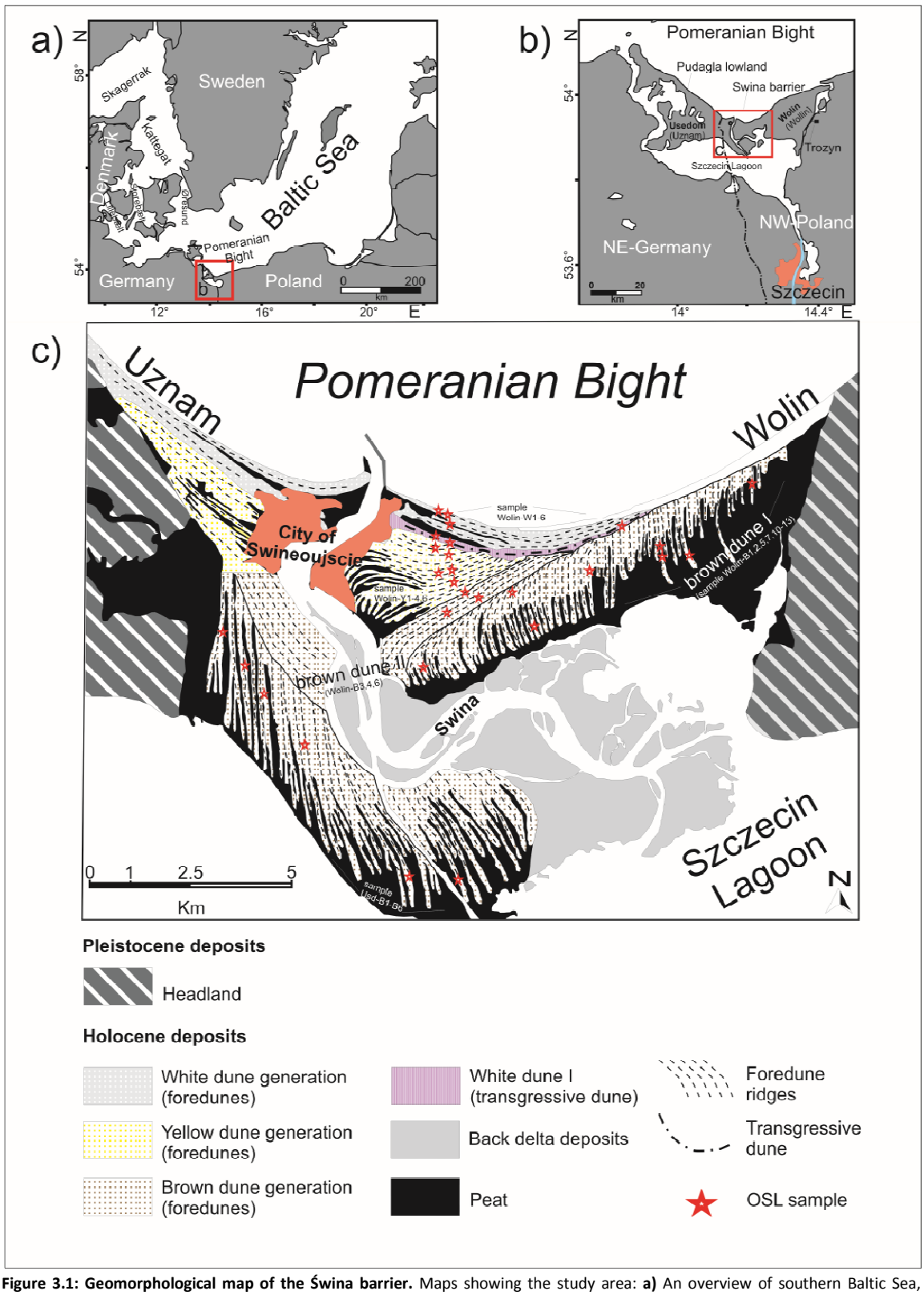

Figure 3.1: Geomorphological map of the Świna barrier. Maps showing the study area: **a)** An overview of southern Baltic Sea, **b)** the Pomeranian Bight and **c)** a geomorphological map of the study area based on Keilhack (1912, 1914), Borówka et al. (1986) and Osadczuk (2002).

According to this model, the formations of the barriers are mostly controlled by the relative sea level. Apart from eustatic sea level rise since the Late Glacial, tectonic and isostatic crustal movements have influenced relative sea level change (Lampe, 2005, Harff and Meyer, 2007) due to the location

of the southern Baltic sea in the transition area between Fennoscandian Uplift and the Central European Subsidence Zone (Harff et al., 2005). Relative sea level change during the Holocene has been investigated using a number of peat and archaeological findings, and the chronology based upon radiocarbon dating, mainly of basal peat layers (e.g. Borówka et al., 2005; Lampe, 2005; Uścinowicz, 2006; Hoffmann et al., 2009). The relative sea level curve reported by Hoffmann et al. (2009) for the western Pomeranian Bight differs from the relative sea level curve of Wismar Bay, indicating a reduction in the rate of sea level rise at ~6.0 ka cal. BP (Lampe, 2005). According to Hoffmann et al. (2009) the differences in the curves reflect different glacio-isostatic crustal movements. After ~6.5 and 6.0 ka cal. BP, only minor fluctuations in sea level (around ± 0.5 m) are assumed (Lampe, 2005; Hoffmann et al., 2009). However, Hoffmann et al. (2009) note that the time interval from ~6.5 ka cal. BP to present day is poorly documented by radiocarbon data from peat. The post-Littorina sea level fluctuation has been reconstructed mainly from archaeological findings and sedimentological evidence, because the siliciclastic sediments of the barrier-spit and beach ridge plains contain very little organic material suitable for radiocarbon dating (Lampe, 2005). The widespread appearance of a peat horizon, dated by radiocarbon to ~1.2-1.0 ka cal. BP, indicates a rising sea level (late Subatlantic transgression) with a rate of approximately 1 mm a^{-1} (Hoffmann and Lampe, 2007; Lampe et al., 2007). A regression of the relative sea level is assumed by Lampe (2005) and correlated to the “Little Ice Age” (LIA) between 0.45 ka and 0.15 ka cal. BP.

3.2.2 Geomorphology and dune generations of Świna barrier

The Świna barrier consists of two sandy spits situated between two Pleistocene headlands on Uznam and Wolin (Usedom and Wollin in German) separating the Szczecin Lagoon from the Pomeranian Bay (Baltic Sea) (Fig. 3.1c). Aeolian sediments cover the marine and fluvial basement of the barrier. The evolution of the Świna barrier spits and the formation of more than one hundred coastal foredunes and dunes have been investigated by Keilhack (1912, 1914). In these studies, the dunes were sub-divided into three generations varying in size, in orientation of the ridges and mainly in the degree of soil profile (podzol) development (Fig. 3.2). The oldest, brown dunes have a thick developed brown illuvial horizon (EA). Peat-filled, inter-dune troughs separate these long and narrow ridges of 2 to 8 m height, which generally have a meridional orientation (north-south striking). In Wolin, the brown dunes can be subdivided into two sub-generations, brown dunes I and II. Brown dunes II also have a brown illuvial horizon, but the foredune ridges are oriented in W-E direction (Fig. 3.1c). Borówka et al. (1986) and Osadczuk (2002) characterised the brown dunes as succession of parallel beach ridges, which were transformed into coastal foredunes. These dune ridges are classified as established foredunes, according to Hesp (2002). The foredunes of brown dune I formed during the development of the Wolin and the Uznam spit and imply meridional beach progradation because the orientations of these ridges are almost perpendicular to the recent coastline. The morphology indicates that the Uznam spit grows to southeast and Wolin spit grows to southwest. The orientation of the second brown dune generation (brown dune II) indicates a south-north growth (alongshore progradation) of the Wolin spit. The second brown dune does not exist in the Uznam spit. Five peat samples from the inter-dune troughs have been dated by radiocarbon to Subboreal and Early Subatlantic ages (between 5.46 ± 0.47 ka cal. BP and 1.30 ± 0.24 ka cal. BP; Prusinkiewicz and Noryśkiewicz, 1966). These were calibrated from radiocarbon to calendar years using the programme CALIB 5.0 (Stuiver and Reimer, 1993; Reimer et al., 2004) to allow for better comparison with the OSL ages.

The yellow dune generation consists of 3 to 10 m high foredune ridges, which have a weakly developed podzol soil profile with a yellow illuvial horizon (Fig. 3.2). Since the ridges are oriented

almost parallel to the coastline (west-east striking), the yellow dune generation is regarded as an alongshore prograding coastline. Borówka et al. (1986) and Osadczuk (2002) believed the yellow dunes formed between 2.0 and 0.5 ka, although they did not have any independent geochronological evidence to substantiate this. The youngest dune generation, the white dunes (Keilhack 1912, 1914), are also orientated parallel to the coastline but do not contain an illuvial soil horizon, given their recent development (Fig. 3.2). Osadczuk (2002) distinguishes between the transgressive white dune I which has an irregular morphological axis (parabolic shape) and is up to 22 m in height, and a series of straight foredune ridges situated further north called white dunes II (see Fig. 3.1). Using historical maps, Keilhack (1912, 1914) reported that pronounced white dunes I developed between 1500 and 1650 AD.

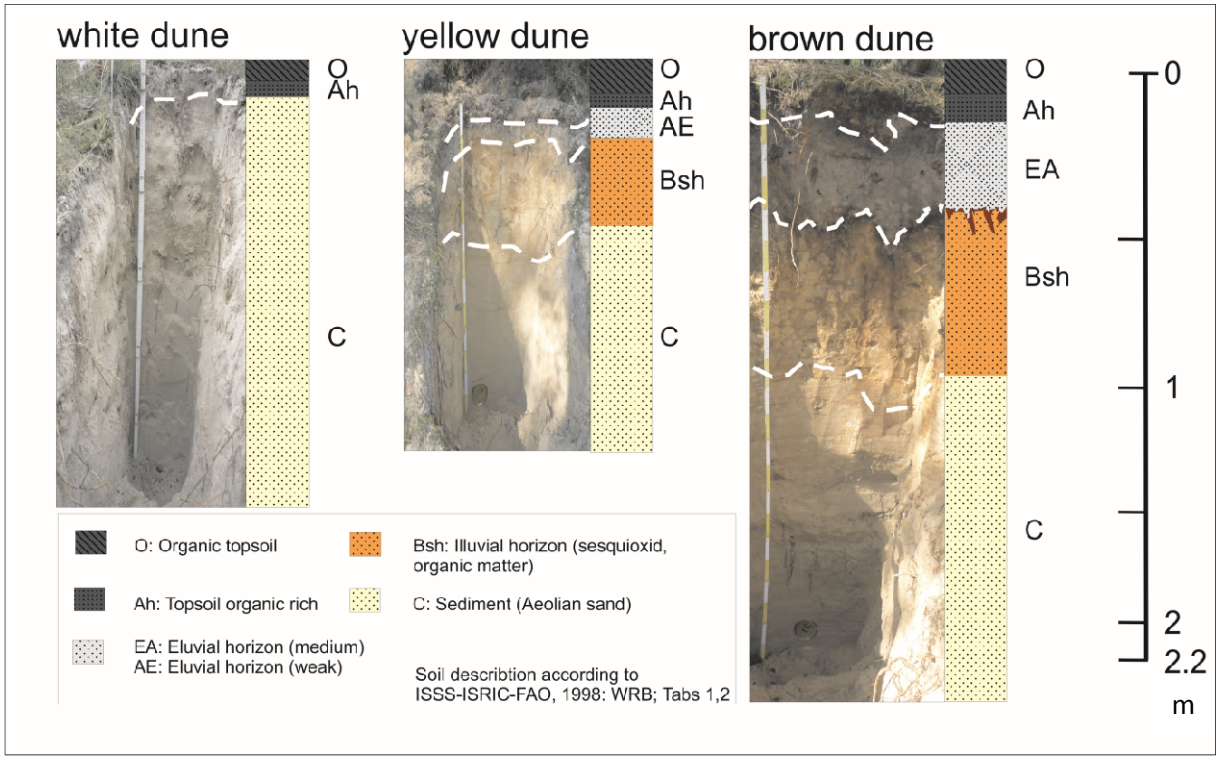

Figure 3.2: Soil profiles of the dune generations. Typical soil profiles of the brown, yellow and white dunes are shown.

The two spits consist mainly of continuous successions of established foredune ridges which one could characterise as foredune plains. According to Hesp (2002), the evolution of established foredunes depends on various factors e.g. the sediment supply, the degree of vegetation cover, the plant species, the rate of aeolian sand accretion, the frequency and magnitude of wave and wind forces,, as well as and the extent of human impact. Mainly the beach width, sediment supply, vegetation characteristics and wind velocity act as controlling factors of foredune height, volume and morphology. Large foredunes usually develop on dissipative beaches whereas smaller ones occur on narrower beaches. Thus, the accretion of the first (oldest) brown narrow and low foredune ridges with heights of about 2 m, relates to a narrow beach-surfzone type. The formations of the yellow foredunes, with heights up to 10 m, are related to a more expanded beach-surfzone type.

When the vegetation cover is locally breached due to trampling (e.g. Grunewald, 2006), intensive land use or more frequent wave and storm erosions triggered by a climate deterioration, the successive accretion of foredunes can be interrupted. The development of dune blow-outs occurs

and accordingly sand is transported inland, producing transgressive and parabolic dunes (Bird, 1990; Hesp, 2002). The white dune I type is one example of a transgressive dune. Borówka et al. (1986) studied a parabolic dune field at Troszyn, which is approximately 15 km further inland (Fig. 3.1c). They distinguished three aeolian series (Troszyn II, III and IV) in the upper part and dated the onset of the dunes indirectly using radiocarbon dating to 3.35 ± 0.09, 2.19 ± 0.12, and 0.89 ± 0.09 ka cal. BP, respectively. These radiocarbon ages were also calibrated according to Stuiver and Reimer (1993) and Reimer et al. (2004).

3.2.3 Sampling

All the samples were taken from the undisturbed original sediment (C-horizon, Fig. 3.2) to avoid post-depositional mixing of the sediment (due to roots or animals) and inhomogeneities of the natural radioactivity (due to soil formation processes). Six samples were taken from the brown dunes of Uznam spit (Usd-B1-6) following a northwest to southeast transect (Fig. 3.1c). The OSL samples were taken as evenly as possible along the northeast to southwest transect and the south to north transect of Wolin spit as well as the northwest to southeast transect of Uznam spit (Fig. 3.1). Furthermore, a few dune ridges were sampled twice to check the reproducibility of ages obtained from the same ridge.

Eight samples were taken (Wolin-B1-2, -B5, -B7 and -B10-13) from the brown dune generation of Wolin spit following a northeast to southwest transect. Two samples were taken from the brown dune II generation. These dune ridges (Wolin-B3-4) have an orientation almost coastline-parallel and a well developed podzol profile. Sample Wolin-B6 was taken from the border between the yellow and brown dunes. Five samples (Wolin-Y1-4 and –Y6) were taken from the yellow dune generation of Wolin spit following a south-north transect. Furthermore, three samples were taken from the white dune I (Wolin-W1-2 and –W6) and another three from the second generation of white dunes (Wolin-W3-5) (Fig. 3.1c).

3.3 Methods

3.3.1 Experimental details

The preparation of the coarse grain (sand-sized) quartz samples was carried out under subdued red light. The samples were dry-sieved to recover grains of either 100-150 µm, 150-200 µm or 200-250 µm in diameter (see Table 3.1). The sand was treated with hydrochloric acid (HCl) to dissolve carbonate, sodium oxalate ($Na_2C_2O_4$) to disperse the aggregates and hydrogen peroxide (H_2O_2) to remove the organic matter. The quartz minerals were isolated using heavy liquid density separation with sodium polytungstate. The sample material was then treated with 40% hydrofluoric acid (HF) for ~60 min to etch the outer surface of the grains and to remove the remaining feldspar minerals. After HF-etching, the quartz grains were resieved again with a 100, 150 and 200 µm mesh to remove smaller particles.

For luminescence measurement, two automated luminescence readers (Risø TL/OSL DA-15 and 20; Bøtter-Jensen et al., 2003) were used. Both were fitted with a blue LED array (470 Δ 20 nm) and 7.5 mm Hoya U-340 detection filters. The sand-size quartz grains were mounted on stainless steel discs with a diameter of 6 mm (medium aliquots) using silicon oil. The single-aliquot regenerative-dose

(SAR) protocol (Murray and Wintle, 2000, 2003) was applied for performance tests and the measurement of the equivalent doses (D_e).

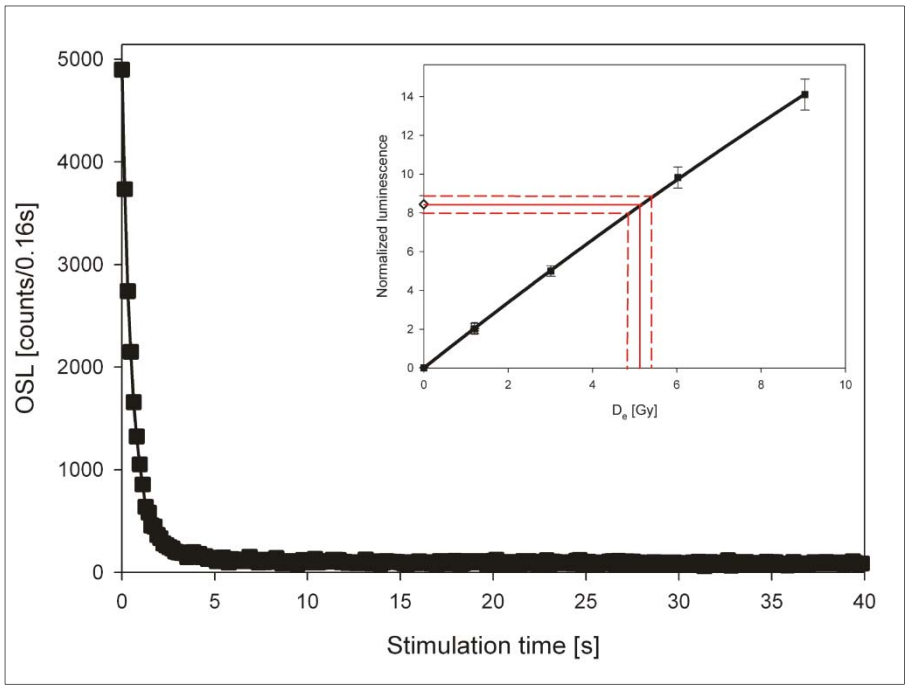

Figure 3.3: A quartz OSL decay curve and dose response curve. A typical quartz decay curve of sample Wolin-B1 is shown. The inset shows a SAR (Murray and Wintle, 2000) dose response curve from the same aliquot.

The SAR protocol was applied without the hot clean out at the end of each cycle (according to Murray and Wintle, 2003) because the performance test measurements reveal no advantage (e.g. a reduced recuperation) by this step. Beside the recycling ratio and the recuperation test, which are normally incorporated within a SAR protocol (Wintle and Murray 2006), the OSL/IR depletion ratio (Duller, 2003) was applied to detect feldspar contamination. Aliquots with a recycling ratio or OSL IR depletion ratio >10% from unity were rejected, as suggested by Wintle and Murray (2006) and Rodnight (2008). A typical quartz signal curve and SAR dose response curve of sample Wolin-B 1 is shown in Figure 3.3.

3.3.2 Dose rate determination

The radionuclide concentrations of the sediment surrounding the OSL sample were measured using high-resolution gamma spectrometry. The samples were measured in Marinelli-beakers filled with 700 g of sediment. The Marinelli-beakers have measurement-adapted geometry with a hole in the bottom to enclose the HPGe (High-Purity Germanium) N-type coaxial detector during measurement. The gamma rays from the radionuclides ^{214}Pb and ^{214}Bi were used to obtain the uranium (^{238}U) content and the gamma rays of ^{208}Tl, ^{212}Pb and ^{228}Ac, were measured to calculate the thorium (^{232}Th) content. For the potassium activity, the release of gamma rays from the decay of ^{40}K to ^{40}Ar was observed. The samples were measured for periods between two and five days. The conversion factors of Adamiec and Aitken (1998) and the β-attenuation dependency on grain size, according to Mejdahl (1979) were used to calculate the β- and γ-dose rates. The α-irradiated part of the grains was removed by HF treatment and the water content was estimated to correct the β- and γ-dose rates for the water content attenuation (Aitken, 1985). The water content was estimated to be 6 ± 3 %, which is in agreement with values reported by Hilgers et al. (2001), Ballarini et al. (2003) or Madsen et al. (2007) for European coastal dunes; a more detailed justification for a water content of 6 ± 3 % is given in Reimann et al. (2010). The cosmic dose rate was calculated according to Prescott

and Hutton (1994) and Prescott and Stephan (1982). The results of the dose rate determination are listed in Table 3.1.

Table 3.1: Results of the dose rate determination.

Dune generation	Sample ID	Geographic latitude	Geographic longitude	Depth [m]	Grain size [µm]	Water content[a] [%]	Cosmic dose rate [Gy/ka]	Sediment dose rate [Gy/ka]	Total dose rate [Gy/ka]
brown I	Wolin-B1	53°54.71	14°23.20	1.70	150-250	6 ± 3	0.16 ± 0.02	0.92 ± 0.05	1.08 ± 0.15
brown I	Wolin-B2	53°54.85	14°23.22	1.60	150-250	6 ± 3	0.16 ± 0.02	0.85 ± 0.05	1.01 ± 0.15
brown I	Wolin-B3	53°53.99	14°18.82	1.70	150-200	6 ± 3	0.16 ± 0.02	0.60 ± 0.05	0.76 ± 0.15
brown I	Wolin-B4	53°53.64	14°19.00	1.60	150-200	6 ± 3	0.16 ± 0.02	0.57 ± 0.05	0.73 ± 0.15
brown I	Wolin-B5	53°53.93	14°19.92	1.70	150-200	6 ± 3	0.16 ± 0.02	0.75 ± 0.05	0.91 ± 0.15
yellow	Wolin-B6	53°53.80	14°19.06	1.80	150-200	6 ± 3	0.15 ± 0.02	0.68 ± 0.05	0.83 ± 0.15
brown I	Wolin-B7	53°55.74	14°25.28	1.80	150-250	6 ± 3	0.15 ± 0.02	0.74 ± 0.05	0.89 ± 0.15
brown I	Wolin-310	53°54.56	14°23.24	1.80	150-200	6 ± 3	0.15 ± 0.02	0.70 ± 0.05	0.85 ± 0.15
brown I	Wolin-311	53°53.68	14°20.26	1.70	150-200	6 ± 3	0.16 ± 0.02	0.61 ± 0.05	0.77 ± 0.15
brown I	Wolin-312	53°52.64	14°18.49	1.90	200-250	6 ± 3	0.15 ± 0.02	0.85 ± 0.05	1.00 ± 0.15
brown I	Wolin-313	53°53.88	14°21.35	2.00	200-250	6 ± 3	0.15 ± 0.02	0.72 ± 0.05	0.87 ± 0.15
brown	Usd B1	53°50.44	14°19.00	1.80	150 200	6 ± 3	0.15 ± 0.02	0.97 ± 0.05	1.12 ± 0.15
brown	Usd-B2	53°50.55	14°17.00	1.80	150-200	6 ± 3	0.15 ± 0.02	0.66 ± 0.05	0.81 ± 0.15
brown	Usd-B3	53°52.48	14°15.06	1.50	150-200	6 ± 3	0.16 ± 0.02	0.71 ± 0.05	0.87 ± 0.15
brown	Usd-B4	53°52.76	14°13.30	2.10	150-200	6 ± 3	0.15 ± 0.02	0.66 ± 0.05	0.81 ± 0.15
brown	Usd-B5	53°52.58	14°14.31	1.90	150-200	6 ± 3	0.15 ± 0.02	0.61 ± 0.05	0.76 ± 0.15
brown	Usd-B6	53°52.65	14°13.20	2.00	150-200	6 ± 3	0.15 ± 0.02	0.66 ± 0.05	0.81 ± 0.15
yellow	Wolin-Y1	53°54.30	14°17.79	1.70	150-200	6 ± 3	0.16 ± 0.02	0.91 ± 0.05	1.07 ± 0.15
yellow	Wolin-Y2	53°54.24	14°16.06	1.80	150-200	6 ± 3	0.15 ± 0.02	0.96 ± 0.05	1.11 ± 0.15
yellow	Wolin-Y3	53°54.47	14°17.93	1.80	100-150	6 ± 3	0.15 ± 0.02	0.93 ± 0.05	1.09 ± 0.15
yellow	Wolin-Y4	53°54.43	14°16.12	1.70	100-150	6 ± 3	0.16 ± 0.02	0.81 ± 0.05	0.97 ± 0.15
yellow	Wolin-Y6	53°54.09	14°17.91	1.10	150-200	6 ± 3	0.17 ± 0.02	0.85 ± 0.05	1.02 ± 0.15
white	Wolin-W1	53°54.55	14°17.96	1.40	100-150	6 ± 3	0.16 ± 0.02	0.94 ± 0.05	1.10 ± 0.15
white	Wolin-W2	53°54.55	14°18.11	1.50	100-150	6 ± 3	0.16 ± 0.02	0.93 ± 0.05	1.09 ± 0.15
white	Wolin-W3	53°54.55	14°17.11	1.30	100-150	6 ± 3	0.17 ± 0.02	0.98 ± 0.05	1.15 ± 0.15
white	Wolin-W4	53°55.05	14°17.98	1.20	100-150	6 ± 3	0.17 ± 0.02	0.86 ± 0.05	1.03 ± 0.15
white	Wolin-W5	53°55.04	14°17.99	1.40	100-150	6 ± 3	0.17 ± 0.02	0.85 ± 0.05	1.02 ± 0.15
white	Wolin-W6	53°54.73	14°22.99	1.30	150-200	6 ± 3	0.17 ± 0.02	0.60 ± 0.05	0.77 ± 0.15

Foot note:
[a] Water content is expressed as mass of dry sediment.

3.3.3 Performance of quartz-SAR

For the thorough testing of the applied SAR protocol and for the selection of the most appropriate thermal treatment, dose recovery, thermal transfer and preheat plateau tests were applied at six different preheat temperatures (160 – 260 °C) with a fixed low temperature cutheat at 160 °C, which is recommended in dating of young samples (e.g. Bailey et al., 2001; or review by Madsen and Murray, 2009). The preheat temperature for equivalent dose (D_e) measurements should be selected from the plateau region of the preheat plateau test and should have a dose recovery ratio (ratio of the measured to given dose) close to unity. More details of the theoretical background of the dose recovery and preheat plateau test are given by Wintle and Murray (2006). A thermal transfer test was conducted using bleached aliquots to observe the contribution of thermal transferred OSL signal with the intention of minimising this.

A preheat plateau is obtained for preheat temperatures between 160 and 260°C for a brown dune and a white dune sample (Wolin B1 and Wolin-W 1, Fig. 3.4a). Thermal transfer increases with preheat temperatures above 220 °C for both samples (Fig. 3.4b). Dose recovery ratios for all samples are close to unity and are independent of the preheat temperature for the brown dune sample (Fig 3.4c). For the white dune sample, a decreasing trend within the range of acceptability (0.9 to 1.1) was observed. According to these results, we selected a preheat temperature of 180 °C for D_e measurements. Additionally, the SAR protocol was tested using a dose recovery test for the selected preheat temperature of 180 °C for each sample. The obtained ratios were all within the acceptable range (Table 3.2) and assure the appropriateness of the applied protocol for the measurement of equivalent doses.

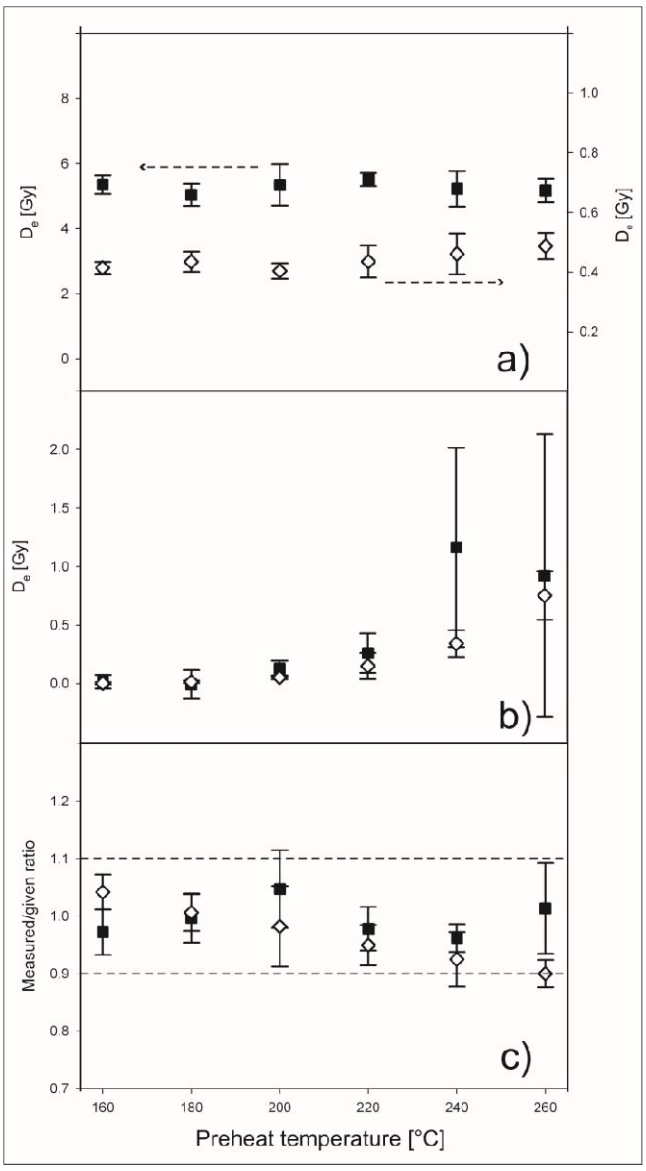

Figure 3.4: Performance tests of samples Wolin-B1 and Wolin-W1. a) Preheat plateau test, **b)** thermal transfer test and **c)** dose-recovery test. Sample Wolin-B1 (brown dunes) is shown by the filled squares and Wolin-W1 (white dunes) by the open diamonds.

3.3.4 Equivalent doses and ages

One of the fundamental assumptions of OSL dating is the complete resetting of the signal prior to the deposition (Aitken, 1998). If the exposure of a grain to light is insufficient, a residual OSL signal will remain and the time since burial will be overestimated. Usually aeolian or coastal sediments do not suffer from incomplete bleaching (Aitken, 1998; Duller, 2008). The D_e distributions from many subsamples (aliquots) of a sample can be used to assess if the signal has been reset sufficiently prior to the deposition; normally distributed D_e values indicate the sediment was well bleached, whereas incomplete bleaching is indicated by asymmetric (positively skewed) distributions of D_e values (e.g. Olley et al., 1999, Arnold et al., 2007). Dose distributions from 6 samples are shown in Figure 3.5. The overdispersion value (σ_{OD}) according to Galbraith et al. (1999) represents the relative standard deviation of the D_e distribution allowing for measurement uncertainties (Olley et al., 2004) and is listed in Table 3.2. Undisturbed samples, which have been bleached uniformly, should give σ_{OD}-values of 20 % or less (Olley et al., 2004; Duller, 2008). In this study, only two very young samples with low De values (Wolin-W4 and –W6, Tab. 2) are above (~23 %) the suggested threshold, which according to Arnold et al. (2009), is due to the increasing influence of “natural” sources of D_e scatter in very

young samples. Most of the samples have σ_{OD}-values below 15 %. A Kolmogorov-Smirnov-Test was also conducted, and was also used by Hülle et al. (2010) and Kunz et al. (2010), to check if the sample D_e distributions can be considered Gaussian. All samples give a P-value below the significance level, and are therefore considered to have a Gaussian distribution.

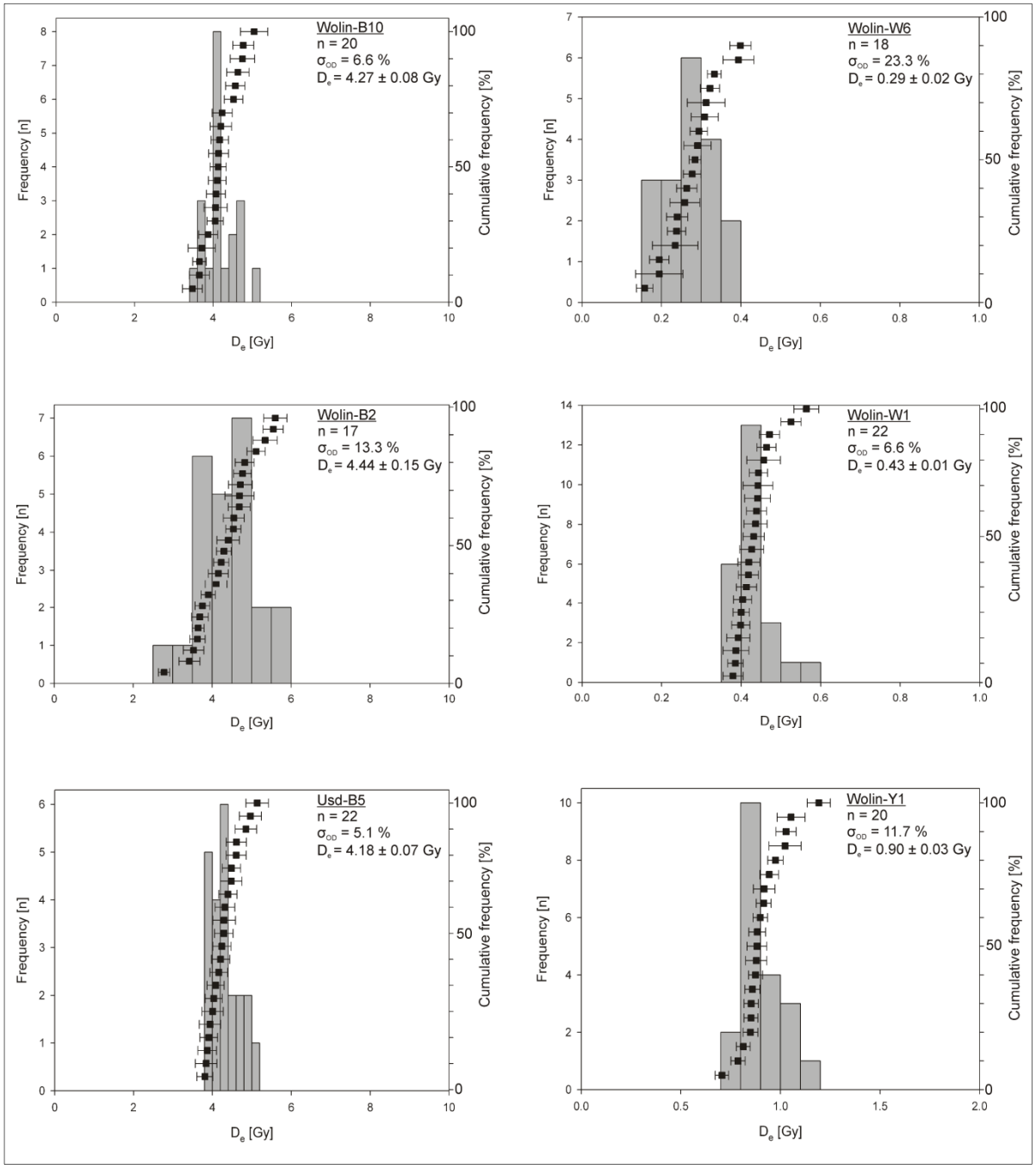

Figure 3.5: D_e distributions of examples from the brown, yellow and white dune generations. The sample ID, the number of accepted aliquots (n), the overdispersion value (σ_{OD}) and the equivalent dose (D_e) is shown for the six selected D_e distributions.

The central age model (CAM) according to Galbraith et al. (1999) was used for D_e calculation of each sample as recommended by Bailey and Arnold (2006) and Arnold et al. (2007) for well-bleached sediments. The OSL age was then calculated by dividing the D_e by the total dose rate.

Table 3.2: Results of the OSL dating.

Dune generation	Sample ID	Dose recovery ratio	Aliquots [n]	σ_{OD} value[a] [%]	CAM D_e[b] [Gy]	Age[c] [ka]	Age range [a]
brown I	Wolin-B1	1.01 ± 0.04	18	10.1	5.12 ± 0.14	4.74 ± 0.25	2980-2480 BC
brown I	Wolin-B2	0.97 ± 0.05	17	13.3	4.44 ± 0.15	4.40 ± 0.26	2650-2130 BC
brown II	Wolin-B3	1.00 ± 0.06	18	5.7	1.24 ± 0.02	1.65 ± 0.11	250-470 AD
brown II	Wolin-B4	1.02 ± 0.04	18	5.3	1.25 ± 0.02	1.72 ± 0.12	170-410 AD
brown I	Wolin-B5	0.99 ± 0.06	21	11.3	2.35 ± 0.06	2.60 ± 0.15	750-440 BC
yellow	Wolin-B6	1.00 ± 0.10	20	10.6	0.95 ± 0.03	1.14 ± 0.07	800-940 AD
brown I	Wolin-B7	0.99 ± 0.05	19	17.0	4.80 ± 0.19	5.39 ± 0.37	3750-3010 BC
brown I	Wolin-B10	1.00 ± 0.06	20	6.6	4.27 ± 0.08	4.98 ± 0.30	3270-2670 BC
brown I	Wolin-B11	1.01 ± 0.03	16	8.5	2.79 ± 0.07	3.65 ± 0.25	1890-1390 BC
brown I	Wolin-B12	1.02 ± 0.06	15	12.3	2.47 ± 0.09	2.45 ± 0.15	590-290 BC
brown I	Wolin-B13	1.03 ± 0.06	14	13.3	3.72 ± 0.15	4.28 ± 0.30	2570-1970 BC
brown	Usd-B1	0.99 ± 0.03	18	7.9	3.53 ± 0.08	3.15 ± 0.15	1290-990 BC
brown	Usd-B2	0.97 ± 0.03	16	9.1	3.76 ± 0.10	4.62 ± 0.29	2900-2320 BC
brown	Usd-B3	0.99 ± 0.05	18	12.7	3.76 ± 0.12	4.33 ± 0.27	2590-2050 BC
brown	Usd-B4	0.99 ± 0.03	21	7.1	5.31 ± 0.10	6.62 ± 0.42	5030-4190 BC
brown	Usd-B5	0.99 ± 0.04	22	5.1	4.18 ± 0.07	5.48 ± 0.37	3840-3100 BC
brown	Usd-B6	1.01 ± 0.05	18	5.6	5.14 ± 0.10	6.35 ± 0.40	4740-3940 BC
yellow	Wolin-Y1	1.01 ± 0.01	20	11.7	0.90 ± 0.03	0.85 ± 0.04	1120-1200 AD
yellow	Wolin-Y2	1.04 ± 0.03	20	20.0	1.00 ± 0.05	0.90 ± 0.04	1070-1150 AD
yellow	Wolin-Y3	0.99 ± 0.02	19	6.4	0.62 ± 0.01	0.59 ± 0.03	1390-1450 AD
yellow	Wolin-Y4	0.97 ± 0.05	21	6.7	0.68 ± 0.01	0.69 ± 0.04	1280-1360 AD
yellow	Wolin-Y6	0.98 ± 0.03	19	8.4	1.18 ± 0.03	1.18 ± 0.07	760-900 AD
white	Wolin-W1	1.01 ± 0.03	22	6.6	0.43 ± 0.01	0.39 ± 0.02	1600-1640 AD
white	Wolin-W2	1.00 ± 0.01	18	7.4	0.49 ± 0.01	0.45 ± 0.02	1540-1580 AD
white	Wolin-W3	0.96 ± 0.06	19	19.0	0.15 ± 0.01	0.13 ± 0.01	1870-1890 AD
white	Wolin-W4	1.00 ± 0.03	19	23.0	0.06 ± 0.01	0.06 ± 0.01	1940-1960 AD
white	Wolin-W5	0.98 ± 0.01	18	15.7	0.08 ± 0.01	0.08 ± 0.01	1920-1940 AD
white	Wolin-W6	1.00 ± 0.03	18	23.3	0.29 ± 0.02	0.38 ± 0.03	1600-1660 AD

Foot notes:
[a] Overdispersion (σ_{OD} value) was calculated according to Galbraith et al. (1999).
[b] The Central Age Model (CAM) according to Galbraith et al. (1999) was applied for D_e calculation.
[c] Age was calculated by dividing the D_e by the total dose rate and is indicated in years ago (before 2008).

3.4 Results

28 samples for OSL dating were analysed, and the dose rates, equivalent doses and ages are listed in Tables 3.1 and 3.2. The OSL ages are also shown in Figure 3.6. The dose rates range from 0.73 ± 0.05 Gy ka^{-1} to 1.15 ± 0.05 Gy ka^{-1}, which are typical for coastal dunes (e.g. Berger et al., 2003; Kunz et al., 2010). The D_e values are between 0.06 ± 0.01 and 5.13 ± 0.10 Gy. With the exception of two samples from the youngest dune (Wolin-W4-5), which have higher D_e uncertainties due to their very low signal to noise ratio, the relative age errors are within 10 %. This is regarded as a normal range for OSL age uncertainties (Murray and Olley, 2002).

The OSL ages of the brown dunes range from 1.65 ± 0.11 ka to 6.62 ± 0.42 ka. The oldest brown dune sample from Uznam spit yielded an OSL age of 6.62 ± 0.42 ka and from Wolin, 5.39 ± 0.37 ka. With the exception of sample Usd-B5, the brown dune samples are in stratigraphic order within the 1-sigma error range and decrease in age from the Pleistocene headlands of Uznam and Wolin to the Świna (Fig. 3.6). Sample Usd-B5 gives an OSL age of 5.48 ± 0.37 ka, which is expected to be older than Usd-B6 (6.35 ± 0.40 ka) from the southeast neighbour, however these two ages can be interpreted as the same within the 2-sigma uncertainty. The yellow dunes have OSL ages between 0.59 ± 0.03 ka and 1.18 ± 0.07 ka. The OSL age of white dune I range from 0.38 ± 0.02 ka to 0.45 ± 0.02 ka. The foredune ridges of the second white dune generation give OSL ages ranging from 0.06 ± 0.01 ka to

0.13 ± 0.01 ka. All yellow and white dune samples are in stratigraphic order and decrease in age from south to north indicating a northward prograding coastline.

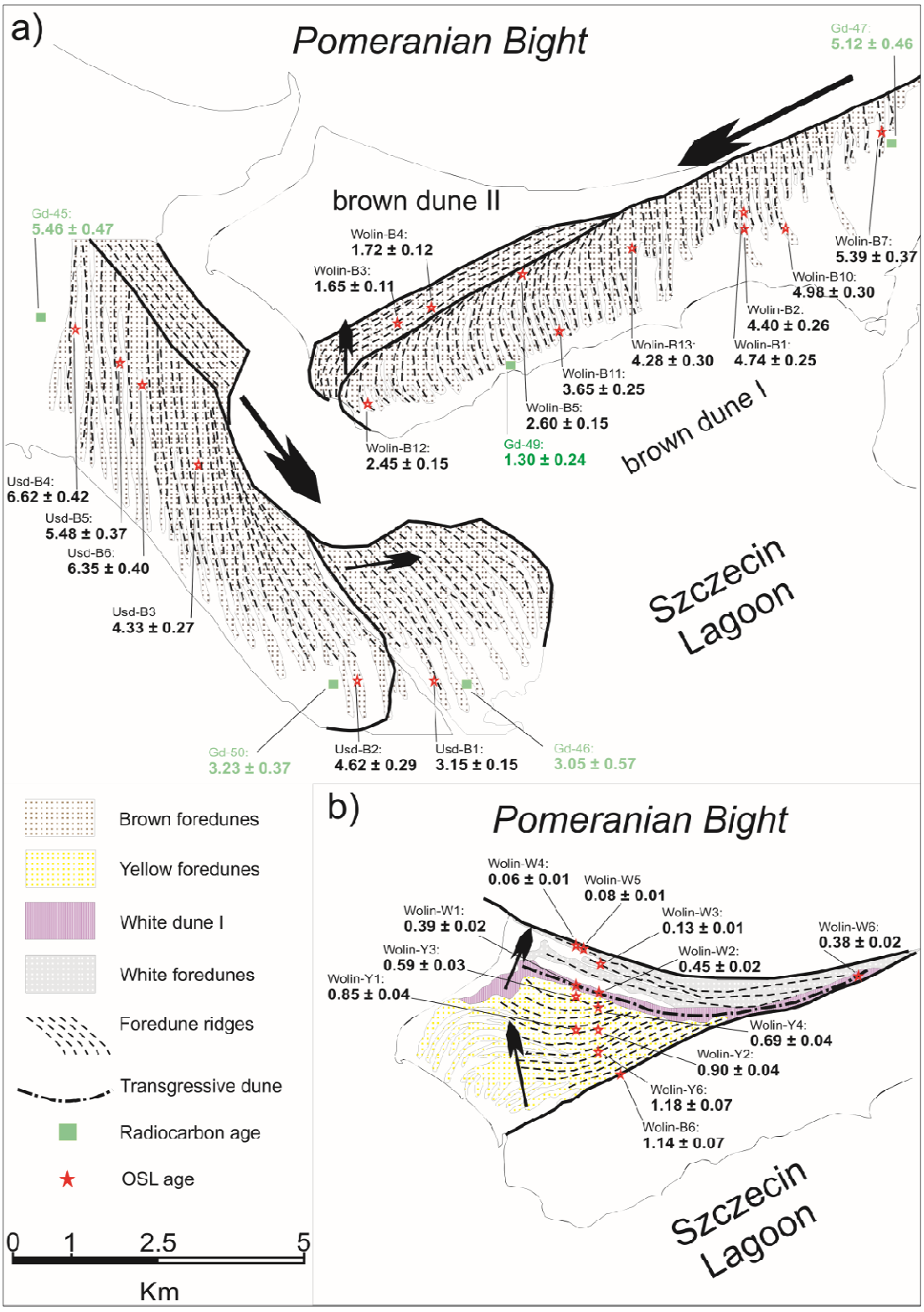

Figure 3.6: Maps showing a) the OSL ages of the brown dunes at Uznam and Wolin spit and b) the ages of the yellow and white dunes at Wolin spit. OSL ages are indicated in ka before 2008, and radiocarbon ages are indicated in calibrated ka BP.

3.5 Discussion

All OSL ages are presented in thousands of years (ka) before the sampling in 2008. The radiocarbon ages are presented in calibrated thousands of years before present (cal. ka BP), where BP is years before 1950 AD. Furthermore, these ages are given in calendar years before Christ (BC) and anno Domini (AD), for a better comparison.

3.5.1 Chronology and chronostratigraphy

The OSL based chronostratigraphy is in agreement with the relative stratigraphy of this cover sand succession, which was first established by Keilhack (1912, 1914) based upon phases of soil development. Furthermore, the OSL chronology presented in this study is based upon more samples than the radiocarbon based chronostratigraphies of Prusinkiewicz and Noryśkiewicz (1966), Borówka et al. (1986) and Osadczuk (2002) and provides direct depositional ages for the foredunes and dune succession.

The OSL chronology is supported by three lines of independent evidence. The oldest OSL age from the cover sand succession is 6.62 ± 0.42 ka (Usd-B4; Fig. 3.5), which is younger than the radiocarbon age of ~7.5 cal. ka BP (Hoffmann et al., 2009) from the underlying basal peat layers from Uznam Island. Secondly, the OSL ages of the foredune ridges are similar in age or older than the peat from the corresponding inter-dune troughs (e.g. Usd-B4 and Gd-45 or Wolin-B 7 and Gd-47, see Fig. 3.6), which is in agreement with the stratigraphic interpretation of Keilhack (1912) and Borówka et al. (1986). Finally, the three OSL ages from the white dune I (0.39 ± 0.02 ka, 0.45 ± 0.2 ka, and 0.38 ± 0.3 ka) from Wolin-W 1, 2 and Wolin-W 6, respectively (Table 3.2 and Fig. 3.6), agree well with the historical map interpretations of Keilhack (1912) who concluded that the formation of this dune complex occurred between 1500 and 1650 AD. Hence, the OSL chronology is considered to be reliable.

The aggradation of the first brown dune generation as straight and meridional foredune ridges took place during the Atlantic and Subboreal period at Wolin and Uznam spit. The accretion of these foredunes started around 6.6 ka shortly after the sea level rise decelerated in the Pomeranian Bight (Hoffmann et al., 2009) and ceased at ~3.0 ka at Uznam and ~2.5 ka at Wolin spit. The onset of barrier evolution is therefore older than previously suggested by Prusinkiewicz and Noryśkiewicz (1966) and Borówka et al. (1986, 2005) who concluded that the onset of barrier evolution occurred in the Subboreal period, based on radiocarbon ages (Gd-45: 5.46 ± 0.47 ka cal. BP and Gd-47: 5.12 ± 0.46 ka cal. BP). However, these indirect radiocarbon ages (from peat) have to be younger than the corresponding foredunes because the sampled peat is the overlying strata. Between samples Usd-B2 and Usd-B1 (Uznam) and Wolin-B13 and Wolin-B11 (Wolin), a small time gap (hiatus) in foredune succession of the two spits is recorded (Fig. 3.6) at about 4.1 ka (2100 BC) indicating a reduction of progradation rate for this period. Brown dunes II were accumulated between 1.8 and 1.5 ka (170-470 AD) in the Early Subatlantic period, with a ~500 a hiatus (290 BC -170 AD) after the formation of the Brown dunes I. The change of foredune ridge orientation from north-south (brown dunes I) to west-east (brown dunes II) is likely to be related to relatively slow sea-level rise or stable sea-level conditions in combination with a high sediment supply due to a long-shore transport. This pattern agrees e.g. with previous findings of Hoffmann and Lampe (2007) for the northern part of Uznam (Nord-Usedom).

The exact morphological transition between brown and yellow dunes is not distinguishable. However, aggradation of the yellow dunes (with west-east orientation and almost straight ridges) started at ~1.2 ka (800 AD). A hiatus between the formation of the brown dunes II and yellow dunes between 1.5 and 1.2 ka (470-760 AD) is confirmed by the OSL ages (Fig. 3.6). This hiatus correlates with a general climatic shift to cooler and stormier condition after the Roman Warm Period (RWP), which probably also caused a change of the vegetation cover and thus a change in stability of established foredunes (see review by Hesp, 2002). Formation of the yellow dunes was completed ~0.6 ka (~1400 AD) during the Medieval Warm Period (MWP). The chronostratigraphic position of the yellow dunes is in agreement with the assumptions made by Borówka et al. (1986), Borówka (1990) and Osadczuk (2002).

The pronounced white dune I developed in post-mediaeval times between 0.47 and 0.36 ka (1530-1650 AD) (Osadczuk, 2002), with aggradation corresponding to the "Little Ice Age" (LIA). Lampe (2005) suggested a regressive sea level for the LIA period, which covers the period between 1350 and 1900 AD (Hass, 1996) and is characterised by a relatively low sea level and a colder, stormier climate. The northward following series of straight foredune ridges (white dune II according to Osadczuk, 2002) developed within the last 150 years.

3.5.2 Migration rates of the foredune plains

If the foredune succession of both spits is subdivided into generations, which are separated from each other by an erosional hiatus and/or a morphological change, average migration rates can be calculated for each generation (Fig. 3.7). Until ~4.5 ka, migration rates of 3.9 ± 1.1 m a^{-1} and 4.2 ± 1.9 m a^{-1} were calculated for the north-south oriented brown foredunes (brown dunes I) of Uznam and Wolin, respectively. After ~4.5 ka, the migration rate in Wolin decreases to 2.7 ± 0.6 m a^{-1}. It is likely that the migration rate in Uznam also decreased after ~4.5 ka, although only one OSL date is available (Usd-B1; 3.15 ka) and the calculation of migration rate was not possible. This early shift of migration dynamics is possibly related to the initial stage of the Świna barrier closure and a general change in sediment supply to both spits. On the other hand, the decrease of the lateral migration rate is not surprising as it can be presumed that the thickness of the sediment and thus the accumulated sediment volume increases to the centre of the barrier. If so, the sediment supply was relatively constant although the lateral migration decreased.

The average migration rate of the west-east striking foredunes on Wolin (brown dunes II to white dunes II) is lower (~1.8 m a^{-1}) than those of the north-south striking foredunes. The significant shift of migration rates occurred after ~1.2 ka (~800 AD) when migration dynamics decreased from 2.6 ± 0.7 m a^{-1} before 800 AD to 1.3 ± 0.4 m a^{-1} and 1.1 ± 0.1 m a^{-1} afterwards (Fig. 3.7). This change in mean migration rates is likely to be related to the late Subatlantic transgression, which induced a general alteration of sediment dynamics at the southern Baltic coast at 800 AD (Lampe et al., 2007). These recent findings, based on radiocarbon data from coastal mires, are confirmed by OSL ages presented in this study. During the most recent succession (after ~1550 AD) progradation of the plain accelerated (2.0 ± 0.2 m a^{-1}), during the regressive sea level conditions of the LIA (Lampe, 2005) and transgressive sea level conditions within the last 150 years. This migration rate of about 2.0 m a^{-1} is comparable with those reported by Nielsen et al. (2006) for a beach ridge plain in Jerup (Northern Jutland, Denmark). Keilhack (1912) counted ~150 brown dune ridges from the Wolin spit and deduced a mean formation rate of 35 years per ridge. In this study, the formation of brown dunes

(both generations) within a time frame of ~3.7 ka (from 5.4 to 1.7 ka) was dated, and an aggradation rate of ~25 years per ridge for the 150 brown established foredunes was obtained).

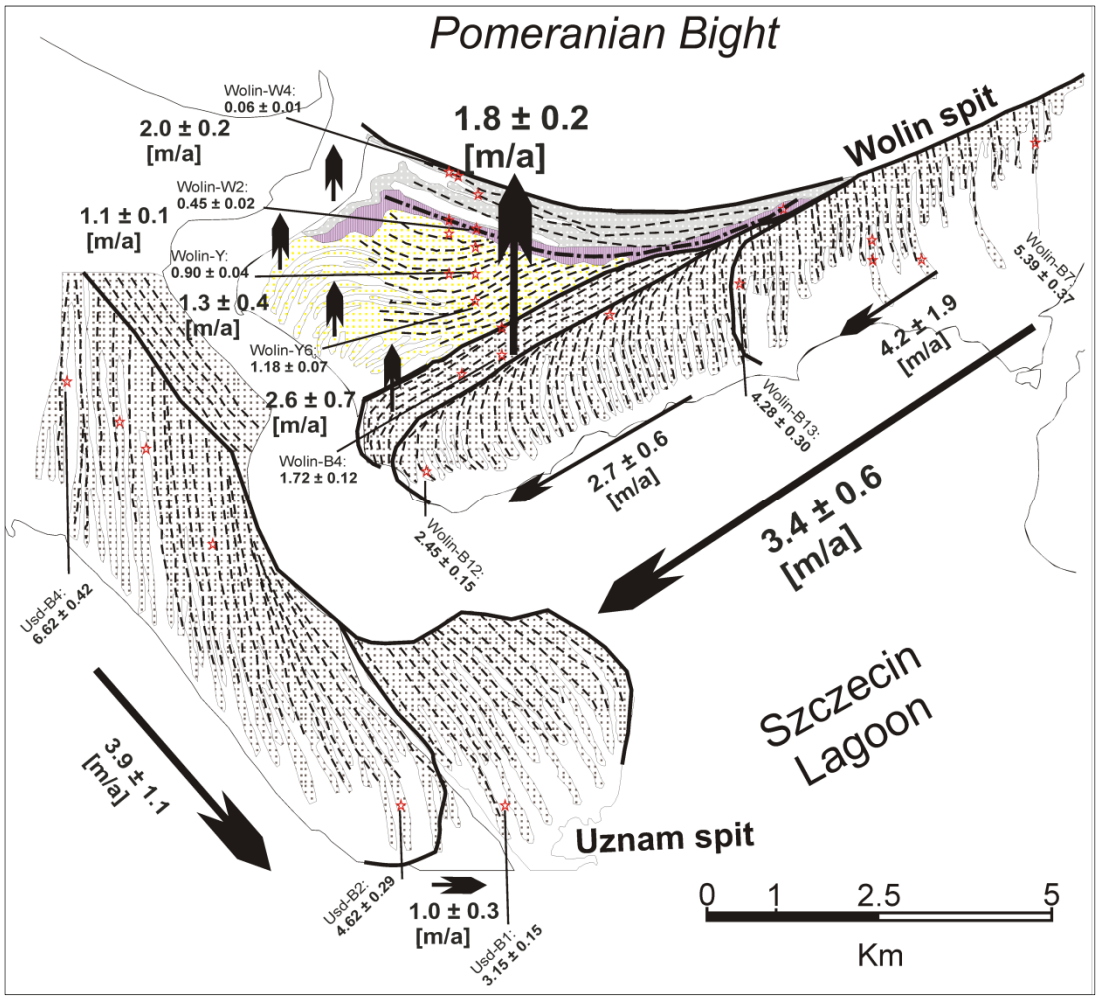

Figure 3.7: Migration rates of spit development. The migration rates of the spits for the brown, yellow and white foredune succession at Uznam and Wolin spit are given in metres per year (m/a). The OSL ages which border between each group of dunes are also indicated (see text). See Figure 6 for signs and symbols.

The detailed chronology of both coastal foredune plains (Wolin and Uznam) provides an important insight into the development of coastal landforms affected by sea-level fluctuation, which is an important contribution to the current controversies regarding the ongoing environmental change (e.g. global warming, sea-level rise). This study reveals that minor sea-level fluctuations do not always result in a drowned coastal landscape but foredune plains can grow even under conditions of a moderate sea-level rise (e.g. immediately after the main phase of the Littorina transgression at ~7.0-6.5 ka) if the sediment supply is sufficient to keep balance with the accommodation space growth and the vegetation cover is able to fix the sediment. Thus, beside the sediment supply the vegetation cover is an important control on the evolution of coastal plains.

3.5.3 Foredune plain evolution and aeolian sand movement

The growth of the two spits has occurred primarily as a result of the systematic accretion of established foredunes (beach progradation). The evolution of a foredune plain is summarised in the review paper of Hesp (2002), where it was shown that a foredune plain develops during phases of moderate sea level regression and transgression, as long as there is a significant sediment supply and progressive plant cover. Under such conditions, the sediment is fixed and beach progradation continues. However, in phases of foredune instability or erosion, additional sediment is transported over the foredune ridge and the formation of parabolic or transgressive dunefields is possible (Bird, 1990; Hesp, 2002). To prove this interaction in a supra-regional context, the OSL ages are compared with chronologies of aeolian sand movement and parabolic dune development along the North and West European coasts, shown in Figure 3.8. These chronologies provide information on the phases of enhanced aeolian activity along the European Atlantic and North Sea coasts.

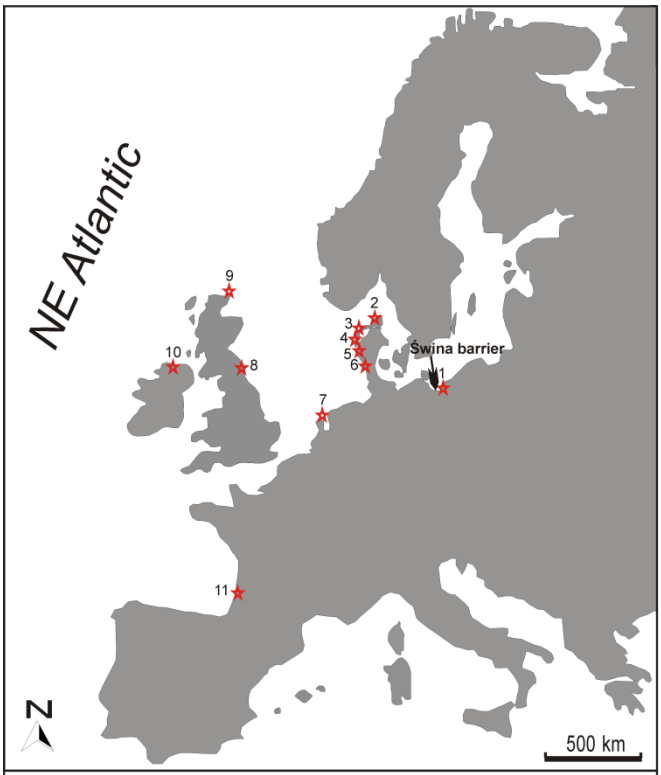

Figure 3.8: Map of dune studies along North- and West European coasts.

Foredune instability occurs when vegetation cover is sparse, due to sediment oversupply during periods of regressive sea level and/or climate deterioration. Foredune erosion occurs due to increased storminess (Klijn, 1990) and/or sea level transgression. Aagaard et al. (2007) investigated the interaction between a negative or stagnant sediment budget at the beach and a trangressive dunefield development Skallingen peninsula (Jutland). This negative correlation of beach progradation with phases of aeolian activity is also observed in our data (Fig. 3.9). The presence of time gaps within the foredune succession may indicate that the evolution of both foredune plains (Wolin and Uznam) is correlated to warmer, milder and calmer phases within the mid- to late-

Holocene, whereas the hiatuses (e.g. at ~2100 BC, ~900 BC, 400-600 AD, and ~1600 AD) within the foredune successions may correlated with colder and stormier periods (Bond et al., 1997). These climatic conditions caused foredune instability or erosion, sediment remobilisation and the formation of parabolic dune fields. Additionally the phases of foredune instability, aeolian reactivation and sand movement are caused by increased land-use and settlement activity and the consequent deforestation. Periods of intensive forest clearance are known during the timing of the Late Roman Empire at ~300 AD and during medieval times at ~1100 AD (Hilgers, 2007) in the region. Alternatively, the hiatus within the foredune succession may result from a too low spatial density of the samples. Stone and Thomas (2008) and Telfer et al. (2010) recently pointed out that the palaeoclimatic interpretation e.g. the presents of hiatuses within linear (desert) dune chronologies is dependent upon the sampling resolution. However, some of the hiatuses are found between nearby ridges (e.g.Usd-B1 and B2; Wolin-B3 and B6, Wolin-B5 and B11; see Fig. 3.6 and Fig. 3.9) whereas otherages of the ridges, which are far away from each other (e.g. Usd-B2 and B3; Wolin-B5 and B12), are overlapping with uncertainties. We presume it is more likely that the observed hiatuses within the foredune succession correlate with phases of an interrupted accretion of established foredunes.

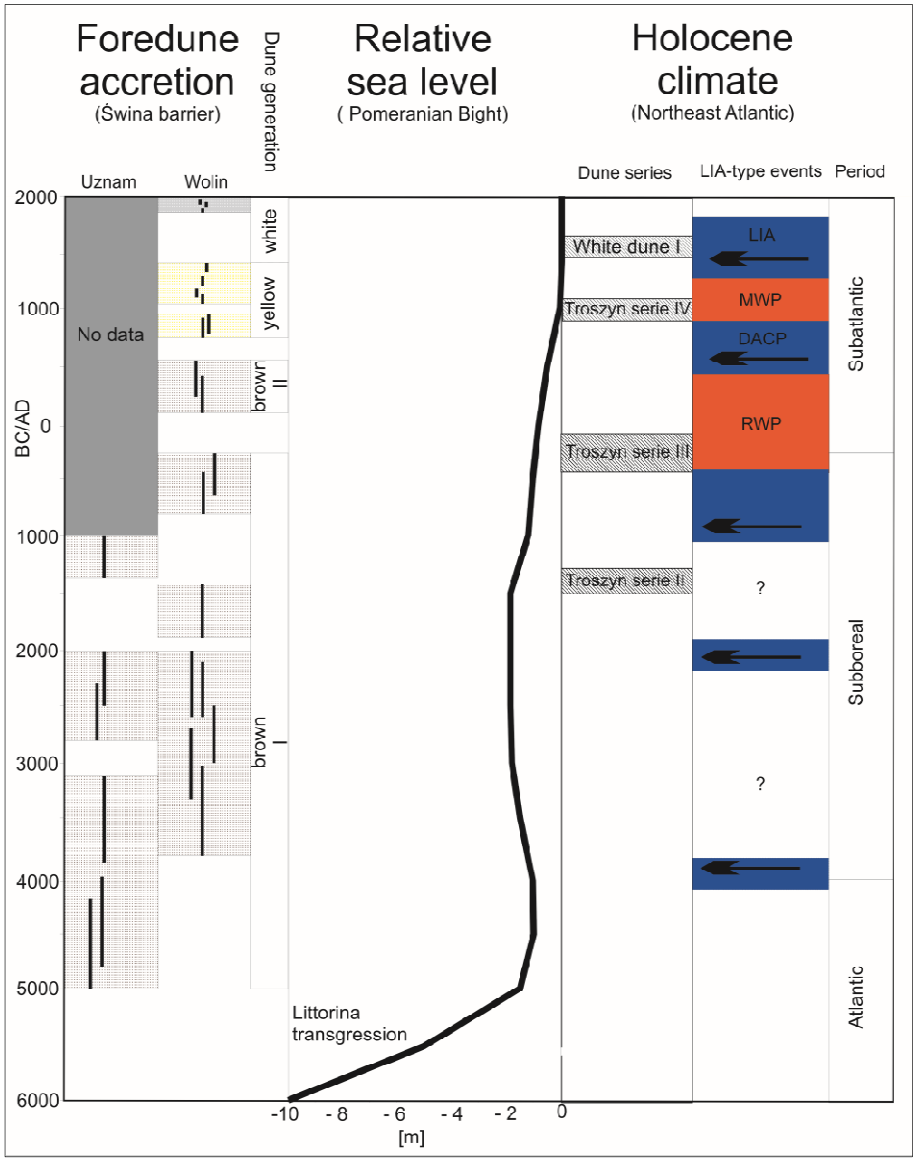

Figure 3.9: Correlation between foredune accretion, aeolian sand movement and the Holocene climate. The correlation between the hiatuses within the foredune succession and phases of increased aeolian activity and general climate trends during the Holocene are shown. The black vertical bars are the OSL ages and errors of the Uznam and Wolin foredunes. The sea level curve for the Pomeranian Bight is based on Hoffmann et al. (2009). The Troszyn dune series reported by Borówka et al. (1986) and the white dune I of the Świna barrier represent phases of sand movement in NW Poland. LIA-type event, according to Bond et al. (1997) and McDermott et al, 2001, are shown, with colder periods shown in blue and warmer periods shown in red. LIA refers to "Little Ice Age, DACP the "Dark Age Cold Period", MWP the "Medieval Warm Period" and RWP, the "Roman Warm Period".

Bond et al. (1997) and McDermott et al. (2001) reported several cooling events (at ~6100 BC, ~3900 BC, ~2200 BC, 800 BC, and 600 AD) in the North Atlantic during the Holocene. These events were reconstructed from the records of $\delta^{18}O$ variability in the Greenland ice cores and speleothems from SW Ireland, respectively. These cooling events correlate with general climatic shifts to cooler and stormier conditions, which are comparable to the condition during the LIA (1350-1900 AD). Therefore, the characterisation as LIA-type events is common for the cooling events at ~6100 BC, ~3900 BC, ~2200 BC, 800 BC, and 600 AD. Clemmensen et al. (2009) reported phases of increased aeolian activity at about 2200 BC, 800 BC, 100 AD, 1050-1200 AD, and 1550-1650 AD which were initiated during colder and stormier climate conditions in Jutland (North Denmark). Their findings are based on a combination of the radiocarbon and OSL dating of several dunefields (Skagen Odde, Hanstholm, Hvidbjerg, Lodbjerg, Fig. 3.8). Wilson et al. (2001) also found evidence for coastal dune development in Northumberland (NE England, Fig. 3.8) within cooling (LIA-type) events (at ~2200 BC, ~700 BC, ~600 AD); however, their chronology of aeolian sand movement is less robust because it was based on the indirect radiocarbon ages. In Northern Ireland (Fig. 3.8) two phases of dune activity during cooling (LIA-type) events were reported, around 1100-600 BC and ~1350 AD, based on radiocarbon and OSL evidence (Wilson et al., 2004). Sommerville et al. (2007) dated aeolian sand accumulation at the Orkney islands (N Scotland, Fig. 3.8) to ~2200 BC, ~1000 BC and ~1500 AD using OSL and correlated these phases to Holocene climatic deterioration.

In the results presented, the first hiatus was found at 2100 BC, which appears in both foredune successions and correlates with a general climatic shift at 2200 BC in the North Atlantic (Bond et al., 1997; McDermott et al., 2001) and a phase of aeolian activity, which was found by Clemmensen et al. (2001a, 2009) in Jutland (Denmark) and by Wilson et al. (2001) and Sommerville et al. (2007) in Great Britain. The LIA-type event at 900 BC is also found in our sediment records. A pronounced hiatus within the Wolin foredune succession is apparent between 1390 BC and 750 BC. This hiatus correlates also with a phase of increased aeolian activity (aeolian series Troszyn II) in NW Poland (Borówka et al., 1986) (see Figure 3.9). Furthermore, Clemmensen et al. (2009) reported a phase of increased dune activity in Northern Denmark at ~800 BC. Other authors have reported phases of aeolian sand movement in North- and West-Europe for this period as well (Wilson et al., 2001, 2004; Sommerville et al., 2007).

Between the first and the second generation of brown foredunes a hiatus is apparent between 290 BC and 170 AD, which correlates well with the dune series Troszyn III of Borówka et al. (1986). This period correlates to the Roman Warm Period (RWP) that is known for a moderate and mild climate in Europe. However, this hiatus is probably related to the closing of the barrier and the general shift in the sediment dynamics of the whole barrier system. The beach progradation direction has changed from meridional to coastline-parallel, and a phase of foredune instability and regional aeolian sediment mobilisations is likely to have been accompanied with the increased dune activity further inland (Troszyn III). Furthermore, Hilgers (2007) reported a phase of sand mobilisation, which correlates to a period of forest clearance caused by an increased settlement activity of German tribes in NE Germany for the time of the Late Roman Empire between 250 AD and 400 AD. This could be an alternative explanation for the period of sand movement in Troszyn and the hiatus within the Świna foredune succession.

The hiatus between the brown and the yellow dunes from 470 AD to 760 AD (Fig. 3.9) correlates with a cold and stormy period that is known as the Dark Age Cold Period (DACP). This period is well known as cooling (LIA-type) event in the climatic records of the North Atlantic (Bond et al., 1997;

McDermott et al., 2001) and in marine sediment cores from Skagerrak (Hass, 1996). Wilson et al. (2001) reported a phase of increased aeolian activity in correlation with the DACP in Northumberland (NE England). Historically, this period is well-known for the migration of the German tribes in Europe and the end of the Roman Empire. The aeolian series of Troszyn IV accumulated around 1050 AD (Borówka et al., 1986) a few centuries later. A similar phase of aeolian activity is referred to by Clemmensen et al. (2009) for Jutland (Denmark). It also appears that there was a short halt in the foredune accretion in Wolin at ~950 AD, which was reactivated after ~1070 AD. This hiatus within the foredune succession correlates to a period of deforestation owing to an increased population and an expansion of settlements during medieval times in NE Germany and other parts of Central Europe (Hilgers, 2007).

The cold and stormy LIA (Hass, 1996) correlates to the formation of the transgressive white dune I in the sediment successions, which were dated to between 1540 and 1660 AD (Table 3.2). During this period the foredune accretion was inactive (Fig. 3.9). The LIA is documented in North and West Europe in plenty of coastal dunefields, and resulted in sand mobilisation and development of transgressive dunes (e.g. Clemmensen et al., 2001a, 2009; Wilson et al., 2001, 2004; Clarke et al., 2002; Ballarini et al., 2003; Aagaard et al., 2007; Sommerville et al., 2007; Clarke and Rendell, 2009) due to increased storminess and a colder climate related to periodic shifts of the atmospheric circulation system NAO (North Atlantic Oscillation) (Dawson et al. 2002).

3.6 Conclusion

The OSL dating of quartz, utilising the SAR protocol (Murray and Wintle, 2000, 2003; Wintle and Murray, 2006) appears to be a powerful tool for the reconstruction of foredune progradation dynamics and their relation to the sea level and climate fluctuations. Furthermore, the OSL ages provide an insight into the development of foredune plains associated with transgressive dunes evolution (phases of increased aeolian activity) and the climate and/or human activity as controlling factors.

- The sedimentary quartz of the investigated dunes and foredunes reveal excellent properties for OSL dating. The quartz luminescence signal was sufficiently bleached prior to the deposition, and the obtained luminescence ages are in good agreement with independent historical evidence and radiocarbon ages (Keilhack, 1912; Prusinkiewicz and Noryśkiewicz, 1966; Hoffmann et al., 2009).
- Spit development and foredune accretion of the Świna barrier started at ~6.6 ka at Uznam spit, after the rapid sea level rise of Littorina transgression decelerated. The foredune accretion of Wolin spit started approximately 1000 years later at ~5.4 ka.
- The progradation rate of the Wolin spit decreased significantly after the late Subatlantic transgression (800 AD) and accelerates again during the last 450 years. No significant difference in the migration rates was observed between the Wolin and Uznam spits.
- Under conditions of positive sediment budget, phases of foredune plain growth were interrupted by stagnant or erosional phases, which are related to foredune instability, resulting in discontinuities in the sediment record. These phases of foredune instability correlate with transgressive dune development in Troszyn or Świna (white dune I). Furthermore, the hiatuses within the foredune records correlate with phases of general climatic deterioration during the

Holocene (LIA-type events) at ~2200 BC, ~800 BC, ~600 AD, and 1400-1850 AD (Hass, 1996; Bond et al. 1997; McDermott et al., 2001) and phases of increased aeolian activity in North and West Europe at (~2200 BC, ~900 BC, ~100 AD, ~600 AD, ~1000 AD, ~1600 AD) reported by Wilson et al. (2001, 2004), Sommerville et al. (2007) and Clemmensen et al. (2009). For the hiatus at ~1000 AD is likely to correlate with a period of medieval forest clearance according to Hilgers (2007).

- The results presented in this study support the model of foredune plain development proposed by Bird (1990) and Hesp (2002). Under conditions of moderate sea level fluctuations and positive sediment budget, the systematic accretion of foredunes is accompanied by a moderate climate and a progressive plant cover. Foredune instability and hence an inactive or erosional foredune plain is related to aeolian sand mobilisation within phases of a decreased plant cover caused by colder and stormier conditions and/or anthropogenic land use.

Acknowledgements

This study was supported by the “Leibniz-Pakt für Innovation und Forschung”. The authors thank Prof. R. Borówka and Dr. A. Osadczuk for guidance and help in the field and for providing great knowledge about the area under study. We also thank Petra Posimowski for recalibration of the radiocarbon data. Julie Durcan is thanked for improving the English of the manuscript and providing helpful comments. The comments of Dr. Gösta Hoffmann and an anonymous reviewer have greatly improved the manuscript.

References

- Aagaard, T., Orford, J., Murray, A.S., 2007. Environmental controls on the coastal dune formation; Skallingen Spit, Denmark. Geomorphology 83, 29-47.
- Adamiec, G., Aitken, M., 1998. Dose-rate conversion factors: update. Ancient TL 16, 37-50.
- Aitken, M.J., 1985. Thermoluminescence Dating. Academic Press, London.
- Aitken, M.J., 1998. An Introduction to Optical Dating. Oxford University Press, Oxford.
- Alappat, L., Vink, A., Tsukamoto, S., Frechen, M., 2010. Establishing the Late Pleistocene-Holocene sedimentation boundary in the southern North Sea using OSL dating of shallow continental shelf sediments. Proceedings of the Geologists´ Association 121, 43-54.
- Arnold, L.J., Bailey, R.M., Tucker, G.E., 2007. Statistical treatment of fluvial dose distributions from southern Colorado arroyo deposits. Quaternary Geochronology 2, 162-167.
- Arnold, L.J., Roberts, R.G., Galbraith, R.F., DeLong, S.B., 2009. A revised burial dose estimation procedure for optical dating of young and modern-age sediments. Quaternary Geochronology 4, 306-325.
- Bailey, R.M., Arnold, L.J., 2006. Statistical modelling of single grain quartz D_e distributions and the assessement of procedures for estimating burial dose. Quaternary Science Reviews 25, 2475-2502.
- Bailey, S.D., Wintle, A.S., Duller, G.A.T., Bristow, C.S., 2001. Sand deposition during the last millennium at Aberffraw, Anglesey, North Wales as determined by OSL dating of quartz. Quaternary Science Reviews 20, 701-704.

- Ballarini, M., Wallinga, J., Murray, A.S., van Heteren, S., Oost, A.P., Bos, A.J.J., van Eijk, C.W.E., 2003. Optical dating of young coastal dunes on a decadal time scale. Quaternary Science Reviews 22, 1111-1117.
- Berger, G.W., Murray, A.S., Havholm, K.G., 2003. Photonic dating of Holocene back-barrier coastal dunes, northern North Carolina, USA. Quaternary Science Reviews 22, 1043-1050.
- Bird, E.C.F., 1990. Classification of European dune coast. Catena Supplement 18, 15-24.
- Björck, S., 1995. A review of the history of the Baltic Sea 13.0-8.0 ka BP. Quaternary International 27, 19-40.
- Bond, G., Showers, W., Cheseby, M., Lotti, R., Almasi, P., deMenocal, P., Priore, P., Cullen, H., Hajdas, I., Bonani, M., 1997. A pervasive millennial-scale cycle in North Atlantic Holocene and Glacial climates. Science 278, 1257-1266.
- Borówka, R.K., 1990. Coastal dunes in Poland. Catena Supplement 18, 25-30.
- Borówka, R.K., Gonera, P., Kostrzewski, A., Nowaczyk, B., Zwoliński, Z., 1986. Stratigraphy of eolian deposits in Wolin Island and the surrounding area, North-West Poland. Boreas 15, 301–309.
- Borówka, R.K., Osadczuk, A., Witkowski, A., Wawrzyniak-Wydrowska, B., Duda, T., 2005. Late Glacial and Holocene depositional history in the eastern part of the Szczecin Lagoon (Great Lagoon) basin-NW Poland. Quaternary International 130, 87–96.
- Bøtter-Jensen, L., Andersen, C.E., Duller, G.A.T., Murray A.S., 2003. Developments in radiation, stimulation and observation facilities in luminescence measurement. Radiation Measurements 37, 535-541.
- Clarke, M., Rendell, H., 2009. The impact of North Atlantic storminess on western European coasts: A review. Quaternary International 195, 31-41.
- Clarke M., Rendell, H., Tastet,J.-P., Clave, B., Masse, L., 2002. Late-Holocene sand invasion and North Atlantic storminess along the Aquitaine Coast, southwest France. Holocene 12, 231-238.
- Clemmensen, L.B., Murray, A., 2006. The termination of the last major phase of aeolian sand movement, coastal dunefields, Denmark. Earth Surface Processes and Landforms 31, 795–808.
- Clemmensen, L.B., Pye, K., Murray, A., Heinemeier, J., 2001a. Sedimentology, stratigraphy, and landscape evolution of a Holocene coastal dune system, Lodbjerg, NW Jutland, Denmark. Sedimentology 48, 3-27.
- Clemmensen, L.B., Murray, A., Beck, J.H., Clausen, A., 2001b. Large-scale aeolian sand movement on the west coast of Jutland, Denmark in late Subboreal to early Subatlantic time - a record of climate change or cultural impact? GFF (Geologiska Föreningens i Stockholm Förhandlingar) 123, 193-203.
- Clemmensen, L.B., Murray, A., Heinemeier, J., de Jong, R., 2009. The evolution of Holocene coastal dunefields, Jutland, Denmark: A record of climate change over the past 5000 years. Geomorphology 105, 303-313.
- Dawson, A.G., Hickey, K., Holt, T., Elliott, L., Dawson, S., Foster, I.D.L., Wadhams, P. Jonsdottir, I., Wilkinson, J., McKenna, J., Davis, N.R., Smith, D.E., 2002. Complex North Atlantic Oscillation (NAO) index signal of historic North Atlantic storm-track changes. The Holocene 12, 363–369.
- Duller, G.A.T., 2003. Distinguishing quartz and feldspar in single grain luminescence measurements. Radiation Measurements 37, 161-165.

- Duller, G.A.T., 2008. Single-grain optical dating of Quaternary sediments: why aliquot size matters in luminescence dating. Boreas 37, 589-612.
- Forbes, D.L., Orford, J.D., Carter, R.W.G., Shaw, J., Jennings, S.C., 1995. Morphodynamic evolution, self-organisation, and instability of coarse-clastic barriers on paraglacial coasts. Marine Geology 126, 63-85.
- Galbraith, R.F., Roberts, R.G., Laslett, G.M., Yoshida, H., Olley, J.M., 1999. Optical dating of single and multiple grains of quartz from Jinmium rock shelter, Northern Australia: part 1, experimental details and statistical models. Archaeometry 41, 339-364.
- Grunewald, R., 2006. Assement of damages from recreational activities on coastal dunes of the southern Baltic Sea. Journal of Coastal Research 22, 1145-1157.
- Harff, J., Lampe, R., Lemke, W., Lübke, H., Lüth, F., Meyer, M., Tauber, F., 2005. The Baltic Sea — a model ocean to study interrelations of geosphere, ecosphere, and anthroposphere in the coastal zone. Journal of Coastal Research 21, 441–446.
- Harff, J., Lüth, F., (eds.) 2007. Sincos – Sinking Coast. Geosphere. Ecosphere and Anthroposphere of the Holocene Southern Baltic Sea. Bericht der Römisch-Germanischen Kommission 88, 7-266.
- Harff, J., Meyer, M., 2007. Changing Holocene coastal zones of the Baltic Sea. Bericht der Römisch-Germanischen Kommission 88, 241-266.
- Hass, H.C., 1996. Northern Europe climate variations during late Holocene: evidence from marine Skagerrak. Palaeogeography, Palaeoclimatology, Palaeoecology 123, 121–145.
- Hesp, P., 2002. Foredunes and blowouts: initiation, geomorphology and dynamics. Geomorphology 48, 245-268.
- Hilgers, A., 2007. The chronology of Late Glacial and Holocene dune development in the northern Central European lowland reconstructed by optically stimulated luminescence (OSL) dating. PhD thesis, University of Cologne.
- Hilgers, A., Murray, A.S., Schlaak, N., Radtke, U., 2001. Comparison of quartz OSL protocols using Lateglacial and Holocene dune sands from Brandenburg, Germany. Quaternary Science Reviews 20, 731-726.
- Hoffmann, G., Lampe, R., 2007. Sediment budget calculation to estimate Holocene coastal changes on the southwest Baltic Sea (Germany). Marine Geology 243, 143-156.
- Hoffmann, G., Lampe, R., Barnasch, J., 2005. Postglacial evolution of coastal barriers along the West Pomeranian coast, NE Germany. Quaternary International 133-134, 47-59.
- Hoffmann, G., Schmedeman,N., Schafmeister, M.Th., 2009. Relative sea-level curve for SE Rügen and Usedom Island (SW Baltic Sea Coast, Germany) – using decompacted profiles. Zeitschrift der Deutschen Gesellschaft für Geowissenschaften (ZDGG) 160, 69-78.
- Hülle, D., Hilgers, A., Radtke, U., Stolz, C., Hempelmann, N., Grunert, J., Felauer, T., Lehmkuhl, F., 2010. OSL dating of sediments from the Gobi Desert, Southern Mongolia. Quaternary Geochronology 5, 107-113.
- Huntley, D.J., Godfrey-Smith, D.I., Thewalt, M.L.W., 1985. Optical dating of sediments. Nature 313, 105-107.
- ISSS-ISRIC-FAO, 1998. World reference base for soil resources. FAO, World Soil Resources Report 84, Rome,
- Janke, W., Lampe, R. 1998. Die Entwicklung der Nehrung Fischland-Darß-Zingst und ihres Umlandes seit der Litorina-Transgression und die Rekonstruktion ihrer subrezenten Dynamik mittels historischer Karten. Zeitschrift für Geomorphology N.F., Suppl. Bd. 112, 177-194.

- Kaiser, K., Barthelmes, A., Czakó Pap, S., Hilgers, A., Janke, W., Kühn, P., Theuerkauf, M. 2006. A Lateglacial palaeosol cover in the Altdarss area, southern Baltic Sea coast (northeast Germany): investigations on pedology, geochronology and botany. Netherlands Journal of Geoscience 85, 197–220.
- Keilhack, K., 1912. Die Verlandung der Swinepforte. Jahrbuch der Königliche-Preussischen Geologischen Landesanstalt XXXII, 209-244.
- Keilhack, K., 1914. Erläuterungen zu Geologischen Karten von Preussen und benachtbarten Bundesstaaten. Blatt Swinemünde. Berlin.
- Klijn, J.A.,1990. The younger dunes in the Netherlands; chronology and causation. Catena, Supplement 18, 89-100.
- Kunz, A., Frechen, M., Ramesh, R., Urban, B., 2010. Luminescence dating of late holocene dunes showing remnants of early settlement in Cuddalore and evidence of monsoon activity in south east India. Quaternary International 222, 194-208.
- Lampe, R., 2005 Lateglacial and Holocene water-level variations along the NE German Baltic Sea coast: review and new results. Quarternary International 133-134, 121-136.
- Lampe, R., Meyer, H., Ziekur, R., Janke, W., Endtmann, E., 2007. Holocene evolution of the irregularly sinking southern Baltic Sea coast and the interactions of sea-level rise, accommodation space and sediment supply. In: Harff, J., Lüth, F., (eds.) Sincos – Sinking Coast. Geosphere. Ecosphere and Anthroposphere of the Holocene Southern Baltic Sea. Bericht der Römisch-Germanischen Kommission 88, 14-46.
- Madsen, A.T., Murray A.S., 2009. Optically stimulated luminescence dating of young sediments: a review. Geomorphology 109. 3-16.
- Madsen, A.T., Murray, A.S., Andersen, T.J., Pejrup, M., Breuning-Madsen, H., 2005. Optically stimulated luminescence dating of young estuarine sediments: a comparison with ^{210}Pb and ^{137}Cs dating. Marine Geology 214, 251-268.
- Madsen, A.T., Murray, A.S., Andersen, T.J., 2007. Optical dating of dune ridges on Rømø, a barrier island in the Wadden Sea, Denmark. Journal of Coastal Research 23, 1259–1269.
- Madsen, A.T., Duller, G.A.T., Donnelly, J.P., Roberts, H.M., Wintle, A.G., 2009. A chronology of hurricane landfalls at Little Sippewisset Marsh, Massachusetts, USA, using optical dating. Geomorphology 109, 36-45.
- McDermott, F., Mattey, D.P., Hawkesworth, C., 2001. Centennial-scale Holocene climate variability revealed by a high-resolution speleothem ^{18}O record from SW Ireland. Science 294, 1328–1331.
- Mejdahl, V., 1979. Thermoluminescence dating: beta attenuation in quartz grains. Achaeometry 21, 61-73.
- Murray, A.S., Wintle, A.G., 2000. Luminescence dating of quartz using an improved single-aliquot regenerative-dose protocol. Radiation Measurements 32, 57-73.
- Murray, A.S., Clemmensen, L.B., 2001. Luminescence dating of Holocene aeolian sand movement, Thy, Denmark. Quaternary Science Reviews 20, 751-754.
- Murray, A.S., Olley, J.M., 2002. Precision and accuracy in the optically stimulated luminescence dating of sedimentary quartz: a status review. Geochronometria 21, 1-16.
- Murray, A.S., Wintle, A.G., 2003. The single aliquot regenerative dose protocol: potential for improvements in reliability. Radiation Measurements 37, 377-381.

- Murray-Wallace, C.V., Banerjee, D., Rourman, R.P., Olley, J.M., Brooke, B.P., 2002. Optically stimulated luminescence dating of Holocene relict foredunes, Guichen Bay, South Australia. Quaternary Science Reviews 21, 1077–1086.
- Nielsen, A., Murray, A.S., Pejrup, M., Elberling, B., 2006. Optically stimulated luminescence dating of al Holocene beach ridge plain in Northern Jutland, Denmark. Quarternary Geochronology 1, 305-312.
- Olley, J.M., Caitcheon, G.G., Roberts, R.G., 1999. The origin of dose distributions in fluvial sediments, and the prospect of dating single grains from fluvial deposits using optically stimulated luminescence. Radiation Measurements 30. 207-217.
- Olley, J.M., Pietsch, T., Roberts, R.G., 2004. Optical dating of Holocene sediments from a variety of geomorphic settings using single grains of quartz. Geomorphology 60, 337-358.
- Osadczuk, K., 2002. Evolution of the Świna barrier spit. Greifswalder Geographische Arbeiten 27, 119-125.
- Pedersen, K., Clemmensen, L.B., 2005. Unveiling past aeolian landscapes: a groundpenetrating radar survey of a Holocene coastal dunefield system, Thy, Denmark. Sedimentary Geology 177, 57–86.
- Prescott, J. R., Stephan, L. G. 1982. The contribution of cosmic radiation to the environmental dose for thermoluminescent dating - Latitude, altitude and depth dependences. PACT 6, 17-25.
- Prescott, J.R., Hutton, J.T., 1994. Cosmic ray distributions to dose rates for luminescence and ESR dating: large depths and long-term variations. Radiation Measurements 23, 497–500
- Prusinkiewicz, K., Noryśkiewicz, B., 1966. Zagadnienie wieku bielic na wydmach brunatnych Mierzei Świny w świetle analizy palynologicznej i datowania radioweglem C14. Zeszyty Naukowe Uniwersytetu Mikołaja Kopernika w Toruniu. Geografia 5, 75-88.
- Reimann, T., Naumann, M., Tsukamoto, S., Frechen, M., 2010. Luminescence dating of coastal sediments from the Baltic Sea coastal barrier-spit Darss-Zingst, NE Germany, Geomorphology 122, 264-273.
- Reimann, T., Tsukamoto, S., Naumann, M., Frechen, M., 2011. The potential of using feldspars for optical dating of young coastal sediments – a test case from Darss-Zingst peninsula (southern Baltic Sea coast), Quaternary Geochronology 6, 207-222.
- Reimer, P.J., Baillie, M.G.L., Bard, E., Bayliss, A., Beck, J.W., Bertrand, C.J.H., Blackwell, P.G., Buck, C.E., Burr, G.S., Cutler, K.B., Damon, P.E., Edwards, R.L.,Fairbanks, R.G., Friedrich, M., Guilderson, T.P., Hogg, A.G., Hughen, K.A.,Kromer, B., McCormac, F.G., Manning, S., Bronk Ramsey, C., Reimer, R.W.,Remmele, S.,Southon, J.R., Stuiver, M., Talamo, S., Taylor, F.W., van der Plicht, J., Weyhenmeyer, C.E., 2004. IntCal04 terrestrial radiocarbon age calibration, 0‑26 cal kyr BP. Radiocarbon 46, 1029‑1058.
- Roberts, H.M., Plater, A.J., 2007. Reconstruction of Holocene foreland progradation using optically stimulated luminescence (OSL) dating: an example from Dungeness. The Holocene 17, 495–505.
- Rodnight, H., 2008. How many equivalent dose values are needed to obtain a reproducible distribution? Ancient Tl 26, 1-9.
- Sommerville, A.A., Hansom, J.D., Housley, R.A., Sanderson, D.C.W., 2007. Optically stimulated luminescence (OSL) dating of coastal aeolian sand, Orkney Islands, Scotland. The Holocene 17, 627–637.

- Stone, A.E.C., Thomas, D.S.G., 2008. Linear dune accumulation chronologies from the southwest Kalahari, Namibia: challanges of reconstructing late Quaternary palaeoenvironments from aeolian landforms. Quaternary Science Reviews 27, 1667-1681.
- Stuiver, M., Reimer, P.J., 1993. Extended 14C database and revised CALIB radiocarbon calibration program. Radiocarbon 35, 215–230.
- Szkornik, K., Gehrels, W.R., Murray, A.S., 2008. Aeolian sand movement and relative sea-level rise in Ho Bugt, western Denmark, during the “Little Ice Age”. Holocene 18. 951-965.
- Telfer, M.W., Bailey, R.M., Burrough, S.L., Stone, A.E.S., Thomas, D.S.G., Wiggs, G.S.F., 2010. Understanding linear dune chronologies: Insights from a simple accumulation model. Geomorphology 122, 195-208.
- Uścinowicz, S., 2006. A relative sea-level curve for the Polish Southern Baltic Sea. Quaternary International 145-146, 86-105.
- Wilson, P., Orford, J.D., Knight, J., Braley, S.M., Wintle, A.G., 2001. Late-Holocene (post-4000 yr BP) coastal due development in Northumberland, northeast England, The Holocene 11, 215-229.
- Wilson, P., McGourty, J., Bateman, M.D., 2004. Mid- to late-Holocene coastal dune event stratigraphy for the north coast of Northern Ireland. The Holocene 14, 406-416.
- Wintle, A.G., Murray, A.S., 2006. A review of quartz optically stimulated luminescence characteristics and their relevance in single-aliquot regeneration dating protocols. Radiation Measurements 41, 369–391.
- Zeeberg, J.J., 1998. The European sand belt in Eastern Europe and comparison of Late Glacial dune orientation with GCM simulation results. Boreas 27, 127-139.

Chapter 4, Paper II:

Tony Reimann[a], Michael Naumann[b,c], Sumiko Tsukamoto[a], Manfred Frechen[a]
2010.

[a] Leibniz Institute for Applied Geophysics (LIAG): Geochronology and Isotope Hydrology, Stilleweg 2, 30655 Hannover, Germany
[b] Leibniz Institute for Baltic Sea Research, Department for Marine Geology, Warnemünde, Germany
[c] Institute of Geography and Geology, Greifswald University, Greifswald, Germany

Luminescence dating of coastal sediments from the Baltic Sea coastal barrier-spit Darss-Zingst, NE Germany.

Geomorphology 122, 264-273.

(www.sciencedirect.com/science/article/pii/S0169555X10001054)

Abstract

This study presents the first optically stimulated luminescence (OSL) dating application of young Holocene sediments from the coastal environment along the German Baltic Sea at the barrier-spit Darss–Zingst (NE Germany). Fifteen samples were taken in Zingst–Osterwald and Windwatt from beach ridges to reconstruct the development of the Zingst spit system and separate phases of sediment mobilisation. The single-aliquot regenerative-dose (SAR) protocol was applied to coarse grain quartz for OSL dating. The reliability of OSL data was tested with laboratory experiments including dose recovery, recycling ratio and recuperation as well as the stratigraphy. We conclude that the sediment is suitable for OSL measurements and the derived ages are internally consistent as well as in agreement with the existing stratigraphy and the geological models of sediment aggradation. The beach ridges at Zingst–Osterwald aggregated ~1900 to ~1600 years ago before the alteration of the sediment system related to the late Subatlantic transgression and the closing of the coastal inlets. The sediment of Windwatt area was deposited after the transgression and the ages can be subdivided into four groups ~900, ~500, 260–320, and ~40 years ago. It is assumed that the ages of ~500 years (1500 AD) and between 260 and 320 years ago (1680–1750 AD) represent the phases of sediment mobilisation related to colder and stormier climatic conditions as well as regressive sea level conditions during the Little Ice Age (1350–1900 AD). The subrecent age estimate of ~40 years demonstrates that the sedimentation processes in the Windwatt area are still active and might be related to a storm surge and sediment overwash in the 1960s. This study confirms prior chronological investigations in other coastal regions (e.g. North Sea) that OSL has a great potential to provide a reliable chronological frame in coastal areas.

4.1 Introduction

Luminescence dating has been successfully applied to Holocene deposits in coastal enviroments (e.g. Murray-Wallace et al., 2002; Ballarini et al., 2003; Madsen et al., 2005; Nielsen et al., 2006; Lopez and Rink, 2007; Madsen et al., 2007; Roberts and Plater, 2007). The dating of beach ridge, foredune ridge or coastal dune successions provides reliable and high-resolution chronologies for the Holocene evolution of typical coastal landforms like spits, barrier-spits and beach ridge plains. This study presents the first optical stimulated luminescence (OSL) dating results from coastal sediments of the southern Baltic Sea. The Holocene evolution of the southern Baltic Sea coastline started with the onset of the Littorina transgression between about 8000 and 7800 years before present (Janke and Lampe, 1998; Hoffmann et al., 2005; Lampe, 2005; Lampe et al., 2007). Since that time the sea level of the southern Baltic Sea has been relatively stable with only minor fluctuations (Schumacher and Bayerl, 1999). The pre-Littorina relief was mainly shaped by the Weichselian glaciation. Moraines and outwash planes are modified by glacial tectonic and fluvial processes and build the basement and sediment supply for the coastal evolution (Naumann et al., 2009). During and after the Littotrina transgression the cliffs from the Pleistocene headlands were eroded. Large amounts of sediment subsequently filled up the morphological depressions and provide the material, which connected the islands, formed barrierspits and isolated bays from the coastal hinterland (mainland) by these new coastal barriers. These Holocene coastal landforms are composed of recent and relict beach and foredune ridge and/or coastal dune sequences. A regional description for this special composition of coastal landforms and sedimentary dynamics is called Bodden equilibrium coast ("Bodden-Ausgleichskuste" in German). "Bodden" is the local synonym for bay. The ongoing evolution of young coastal barriers has altered the previous strongly varying coastline to a straight coastline. The final stage of this potential equilibrium is detectable to the east, along the Polish coast, where these former bays are isolated from the open sea by coastal barriers. The evolution of this paraglacial coast is controlled by the sediment supply (local geology, sea level), the morphology (accommodation space) and the impact of the climate system (direction and energy of waves and winds) (Forbes et al., 1995).

Until recently, the chronologies of coastal sediment succession along the southern Baltic Sea were based on radiocarbon data mostly derived from the coastal hinterland and a limited number of archaeological findings (Hoffmann et al., 2005; Lampe, 2005). However, there is a lack of suitable material (shells, and peat) for radiocarbon dating in the investigated beach areas. The basal peat is often eroded or respectively relocated, hence is not in situ. Thus, chronologies which are only based on radiocarbon in the coastal regions of the southern Baltic Sea are complicated. Furthermore, the radiocarbon dating of sediments younger than 450 years is problematic (Nielsen et al., 2006; Madsen et al., 2007; Madsen and Murray, 2009) owing to calibration problems of short-term atmospheric ^{14}C-variations caused by fluctuations of the solar activity and the climate during the recent centuries (Stuiver, 1978; Hua, 2009). OSL datings based on the single-aliquot regenerative-dose (SAR) protocol (Murray and Wintle, 2000, 2003; Wintle and Murray, 2006) have the potential to provide dates with an error of 5–10% (Murray and Olley, 2002) from the depositional event itself. OSL estimates the time elapsed since the last exposure to daylight for quartz grains in sediments. Quartz grains in sediments act as a natural dosimeters, assuming the measured equivalent dose (D_e in Gray) is proportional to the burial time of the sediment. The dose rate is provided by natural radioactivity in the sediment. The total dose rate for coarse grain quartz dating is calculated from the

β- and γ- dose rate (D_β+D_γ in Gy/a) after correcting for the water content attenuation factor and the cosmic dose rate (D_{cosmic} in Gy/a) of the sampling site. The α-irradiated part of the grain is removed by HF-etching. OSL ages are calculated using the equation (Aitken, 1998):

$$Age = \frac{D_e}{w \cdot (D_\beta + D_\gamma) + D_{cosmic}} \left(\frac{Gy}{Gy/a} \right) \qquad \text{(Eq. 4.1)}$$

OSL dating of quartz is widely applicable for sand dominated coastal environments (Jacobs, 2008) like along the Baltic Sea. Therefore, OSL dating provides a chronological tool for setting up a more accurate and more reliable geochronological frame than previously done mainly based on radiocarbon ages. An OSL chronology is based on a dense grid of age estimates. OSL investigations in the hinterland of southern Baltic Sea coast were previously conducted by Kaiser et al. (2006) who dated late Pleistocene palaeosols from the Altdarss.

The aim of this study is to test the suitability of OSL dating in coastal sediments and to establish a more reliable and detailed chronological frame for the Holocene sediment succession of the Baltic coast.

4.2 Study area and sampling

4.2.1 Setting

In general the Bodden coast consists of Late Pleistocene headlands connected by young Holocene lowlands (spits, barrier-spits or barrier islands). The development of this coastline started with the Littorina transgression at around 8000 and 7800 years before present (Janke and Lampe, 1998; Hoffmann et al., 2005; Lampe, 2005; Lampe et al., 2007). According to Schumacher (2002), the Baltic Sea flooded the former mainland and formed an archipelago-like landscape. Between about 8000 and 6000 years before present the sea level rapidly rose with rates up to 2.5 cm/a (Kliewe and Janke, 1991) resulting in a level of around 2 m below the present sea level. The cliffs from the Pleistocene headlands were eroded and the sediment subsequently filled up the morphological depressions. The shallowing of the depressions and the decrease of the sea level rise since 6000 years ago (Schumacher and Bayerl, 1999; Hoffmann et al., 2005; Lemke, 2005; Lampe et al., 2007) led to the development of spits and barrierspits between the islands isolating bays and lagoons from the open sea and forming the typical Bodden equilibrium coast with a system of beach ridges and dunes at the front and peatlands in the coastal hinterland.

The Zingst–Werder–Bock barrier-spit system is the easternmost part of the Fischland–Darss–Zingst peninsula chain located along the south-western Baltic Sea coast in NE Germany (Fig. 4.1). Fischland is situated in the south-west of the Holocene barrier system and connects the mainland with the isolated Pleistocene headlands of Fischland and Altdarss to the northeast (Fig. 4.1).

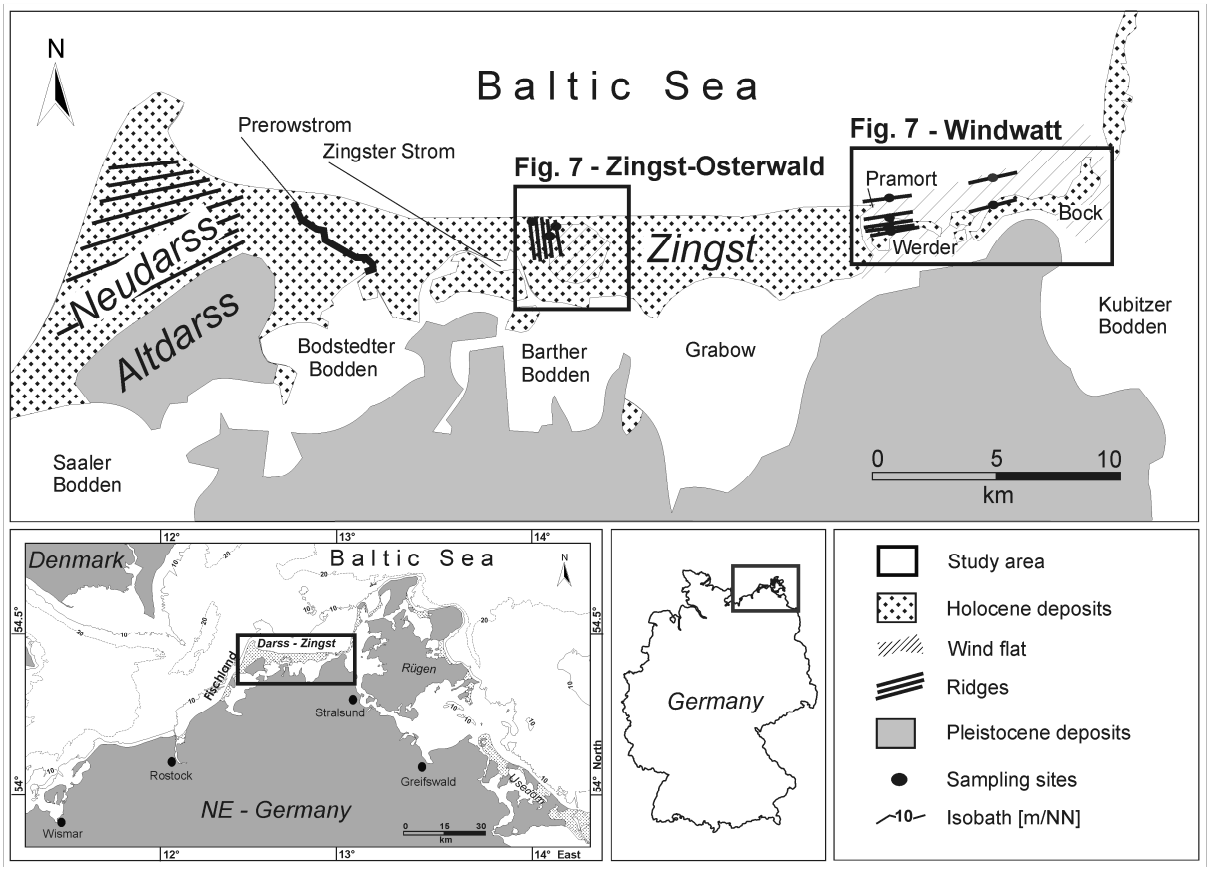

Figure 4.1: Map showing the Darss–Zingst peninsula in the regional context. Investigated locations of Zingst–Osterwald and Windwatt are black bordered.

The Neudarss spit is located to the north of the Altdarss cliff and shows a sequence of beach ridges (Fig. 4.1). The Zingst barrier-spit is located to the east of the Darss. This part of the peninsula is separated by the "Prerowstrom" coastal inlet (Fig. 4.1), which was artificially closed. Zingst is a flat barrier ranging in altitude from slightly below sea level at back sided lagoons to 1–2 m a.s.l. at the direct coastline. The highest elevation is the elevated dune belt in the northeast (8–9 m a.s.l.) next to the Pramort coastal inlet. Eastwards the barrier continues with a wind flat area of about 25 km^2, ranging in altitude from slightly above sea level to 0.5 m below sea level depending on wind strength and wind direction. The southern border of the wind flat area is the island chain of Werder and Bock (Fig. 4.1). These islands have mainly west–east orientations like the Zingst barrier-spit. The Fischland–Darss–Zingst peninsula separates a lagoon system from the open sea including the Saaler Bodden, the Bodstedter Bodden, the Barther Bodden, the Grabow and the Kubitzer Bodden (Fig. 4.1).

Fig. 4.2 shows a generalised overview of the geological structure in a cross section through the Darss–Zingst peninsula system based on 35 sediment cores. The cores were taken with a hydraulic powered extracting tool and half-open testing probes for effective mapping. The marine sedimentation base was reached in all cores. The typical carbonate content of the Upper Pleistocene sediments (Pleistocene base, Fig. 4.2) was taken as the indicator to distinguish terrestrial Pleistocene and marine Holocene sedimentary environments in the core. The marine Holocene sediment succession is subdivided into six litho-facies units. The marine sediment base is marked as a black

dashed line and varies between 1.0 and 13.5 m below mean sea level. The modern surface is often an inherited relief of the marine base. The positions of morphological features like the coastal inlets Pramort, Prerowstrom, Zingster Strom are a result of this inherited relief. The Pleistocene base consists of fine sand, whose origin are glacio-lacustrine or glacio-fluvial deposits, glacio-lacustrine silt and local distribution of till. Basal peat is rare and if present, it is difficult to decide, whether the peat is in situ or not. The marine sediment succession starts with organic–silicate gyttja in the lower parts. A less turbulent waterbody in the lagoons or in higher water depths below the wavebase makes sedimentation of silty material with an organic content up to 20% possible. It is described as slack water facies and covered by fine sand mixed with remnants of marine molluscs. The sedimentation is related to a shallow marine environment and these deposits form around 70–80% of the peninsula. A minor amount of sediment consists of coarse material, typical for more dynamic waterbodies, as beach facies. In some areas a thin top layer of aeolian sands can be identified, but in most cases the aeolian influence cannot be distinguished from fine sands deposited under shallow marine conditions.

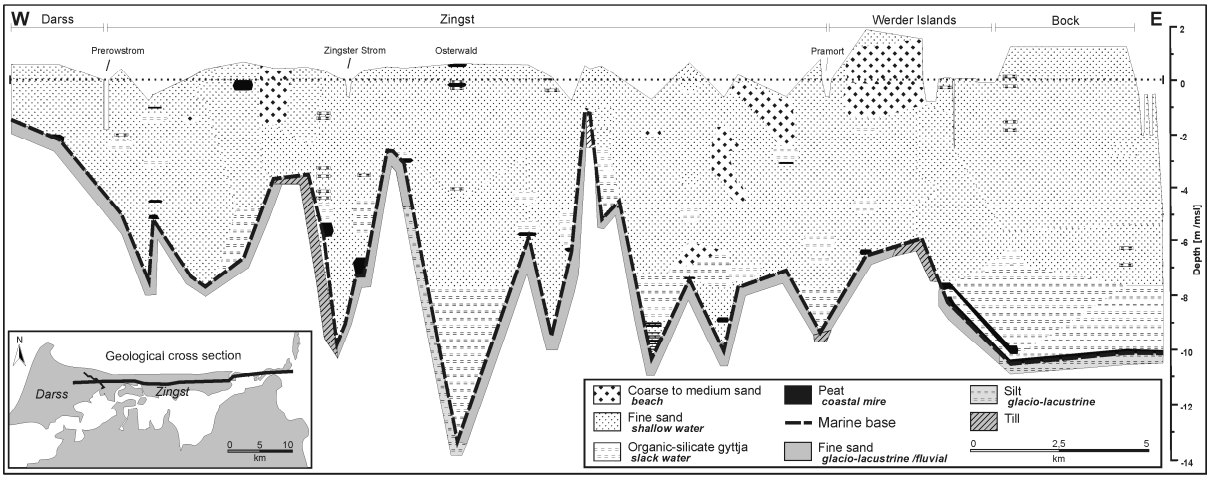

Figure 4.2: Geological cross section through the Darss–Zingst peninsula. Figure is based on 35 sediment cores.

The outstanding dominance of fine clastic sediments is unusual for Holocene barrier systems in this region. The near-distance transport from the cliffs (e.g. Altdarrss, Fig. 4.1), which consist mainly of till provides large amounts of coarse material for the sedimentation system. However, it is unlikely that the Altdarss cliff is the only sediment source for the Darss–Zingst spit. The Pleistocene sediment of the Altdarss (Fig. 4.1) represented an important sediment source in particular for the Neudarss spit. The eroded sediment from the Altdarss cliff formed the northward growing Neudarss spit (Fig. 4.1).

Additionally fine sand was transported from that area (Altdarss, and Neudarss) parallel to the shoreline and accumulating eastward (Zingst, Fig. 4.1). Nevertheless, the formation of the Zingst part of the peninsula is mainly a result of landward overwash of a former island in the sea area to the north (Janke and Lampe, 1998; Lampe, 2002). The process started at around 4000 years (Lampe, 2002) when beach ridges attached perpendicular to the recent coastline to the island and formed a southward growing spit. The remains of this spit are preserved as a succession of beach ridges (German: Reffen) and channels (German: Riegen) in the Zingst–Osterwald area (Janke and Lampe, 1998; Lampe, 2002). Both processes, shoreline-parallel sediment transport and landward overwash,

connected temporary existing islands to a continuous spit (Janke and Lampe, 1998). According to Lampe (2002) and Lampe et al. (2007) the final abrasion of the island and the old spit as well as the elongation of the subrecent spit system started at about 800 AD (1200 years ago) during the late Subatlantic transgression. During this transgression the coastal inlets (e.g. Zingster Strom) were filled up with sediment and closed. The disappearance of the former accommodation space i.e. coastal inlets (e.g. Zingster Strom, Fig. 4.1) induced a general alteration of the sediment dynamics of the Darss–Zingst spit system (Lampe et al., 2007) to a mainly coastline parallel sediment transport. Subsequently a sand flat emerged in the east due to the eastward transport of sediment forming small circular islands around temporary beach ridge remains, shortly after the inlets were closed by an eastward migrating dune belt. Progradation of the coastline has occurred in areas with positive sediment budged (Janke and Lampe, 1998; Hoffmann et al., 2005) for example in the Windwatt area with a shoreline-parallel orientation of the “Reffen” and “Riegen” structures.

4.2.2 Sampling

The sampling was carried out in the Zingst–Osterwald area and the Windwatt area (Fig. 4.1). At the Zingst–Osterwald site six samples (Zi–O1–6) were collected from three outcrops. From each outcrop two samples were taken in a vertical sequence from homogenous light yellowish quartz-rich medium sand layers (C horizon) of marine origin (Fig. 4.1, see also Fig. 4.7) at a depth of 40–80 cm below surface. In the Windwatt area four 1 m-long cores were drilled (WerI-2, I-4, I-5 and I-8, Fig. 4.1) from the barrier island Gros Werder and six samples were taken (Zi–W1–6). Additionally, three samples (Zi–W7–9, see Fig. 4.7) were taken out of two cores from the island Bock (Bock-3 and -4, Fig. 4.1) in a south to north transect (landward to seaward; Fig. 4.1, and also Fig. 4.7). Black PVC liners with a diameter of 80 mm were used for coring to avoid light exposure of the luminescence samples. All the samples were taken from thick homogenous fine sand layers (see Fig. 4.7). The Zingst–Osterwald luminescence samples were collected in black tubes to avoid light exposure. The Windwatt cores were sub-sampled in the luminescence laboratory under subdued red light conditions. Additionally, a sample for dose rate determination was taken from the sediment surrounding of each luminescence sample.

4.3 Method and experimental details

4.3.1 Preparation

The preparation of the coarse grain (sand-sized) OSL samples was carried out under subdued red light. Fifteen samples from two sites were dry-sieved to recover grains of 100–250 μm in diameter. The sand was treated with HCl to dissolve carbonate, with $Na_2C_2O_4$ to dissolve the aggregates and with H_2O_2 to remove the organic matter. Then the quartz minerals were separated by a heavy liquid (sodium polytungstate) and subsequently treated with 40% HF for 45 min to etch the outer surface of the grains to avoid a contribution of the α-irradiated outer part of the quartz mineral and to remove the remaining feldspar minerals. After HF-etching the quartz grains were sieved again with a 100 and 150 μm mesh.

4.3.2 Dose rate determination

The radionuclide concentrations (U-, Th- and ^{40}K-content) of the sediment surrounding were measured using high-resolution gamma spectrometry (Murray et al., 1987). For dose rate measurement different sample sizes (700 g vs. 50 g) and measurement geometries (Marinelli-beakers vs. small containers) were used. The Zingst–Osterwald (Zi–O) samples were measured in Marinelli-beakers filled with 700 g of sediment. The Marinelli-beakers have measurement adapted geometry with a hole in the bottom to enclose the germanium-detector during measurement. The Windwatt samples were measured in small boxes with 50 g of sediment. The samples were measured over periods of three days to five days. The conversion factors of Adamiec and Aitken (1998) and the β-attenuation in dependency of grain size after Aitken (1985) were used to obtain the β- and γ-dose rates (D_β+D_γ).

The "in situ" water content was obtained from exemplary subsamples to calculate the water content attenuation factors (w) to correct the β- and γ-dose rates (Aitken, 1985). The cosmic dose rate (D_{cosmic}) was derived from the altitude and latitude of the sampling sites, the burial depth and the density of the overburden (Prescott and Stephan, 1982; Prescott and Hutton, 1994).

4.3.3 OSL measurements

For the De determination an automated reader (Riso TL/OSL DA-20) with blue light stimulation (at 470 nm) and a 7.5 mm Hoya U-340 detection filter (Botter-Jensen et al., 2000) was used. The fine sand quartz (100–250 µm) was settled on stainless steel discs with a diameter of 6 mm (medium aliquots). A single-aliquot regenerativedose (SAR) protocol (Murray and Wintle, 2000, 2003) was applied for pre-tests and D_e measurements (Table 4.1).

Table 4.1: SAR protocol used for equivalent dose determination (Murray and Wintle, 2000, 2003).

Step	Treatment	Observe
1	Give Dose, Di	
2	Preheat ([1]230°C,[2]200°C)	
3	OSL, 125°C, 40s	Li
4	Give test Dose, Dt	
5	Cutheat ([1]170°C,[2]160°C)	
6	OSL, 125°C,40s	Ti
7	OSL, 280°C,40s	

Foot notes:
[1] Heating conditions for Zingst-Osterwald samples.
[2] Heating conditions for Windwatt samples.

At the end of each run the aliquots were optically stimulated at 280 °C for 40s to bleach the remaining OSL signal as much as possible to minimize the thermal transfer of charges (recuperation; Murray and Wintle, 2003). In each measurement sequence, the 2nd regenerative-dose was given again twice at the end of the SAR cycles. The first recycling ratio (R6/R2) checks, if the sensitivity change is corrected successfully by the test dose OSL. If it is successfuly applied, the value should be close to unity (Wintle and Murray, 2006). For the second recycling ratio, a 100 s infrared (IR) stimulation followed by a 40 s blue stimulation was inserted. The depletion ratio of IR/blue OSL was

used according to Duller (2003) to check if there is feldspar contamination in each disc (aliquot). Additionally the measurement of a zero dose point (recuperation) is conducted to check if there is any thermally transferred charge from light-insensitive traps to the OSL traps (recuperation) (Wintle and Murray, 2006). The prevention of this recuperation has great importance in particular for young samples with a small D_e (Kiyak and Canel, 2006). Aliquots with a recycling ratio (R6/R2, Table 4.1) or IR/blue OSL depletion ratio (R7/R2) >10% from unity were rejected (range of acceptability according to Wintle and Murray, 2006).

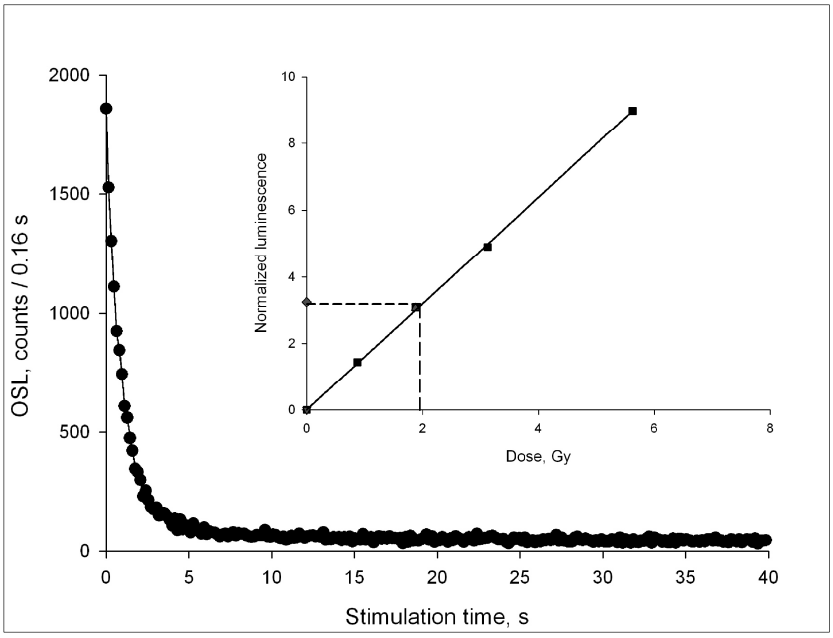

Figure 4.3: Typical OSL decay curve and SAR growth curve (Sample Zi–O1). Regenerated signal points (R_i) are shown as black squares, repeated signals (recycling points) as grey diamonds. The grey diamond is the natural OSL signal which is extrapolated onto the growth curve and gives an equivalent dose (D_e) of about 2 Gy.

To examine the basic conditions (e.g. thermal treatment) of the SAR protocol, the dose recovery and thermal transfer tests with 24 aliquots (4 discs for each temperature step) were applied at 6 different preheat and 5 different cut heat temperatures (only for the dose recovery test). If the protocol works correctly, the dose recovery ratio (ratio of measured to given dose) should be close to unity. More details of the theoretical background of the dose recovery test are given by Wintle and Murray (2006). Within the dose recovery experiments the use of different integration regions for the OSL signal were also tested. According to Ballarini et al. (2007) the relative contribution of slow and medium components of the quartz OSL signal, which are less suitable for OSL dating compared to the fast component, could be minimized by selecting the Early Background Substraction (EBG) instead of the usually used Late Background Subtraction (LBG=36 s to 40 s of the signal). For the EBG the background signals were calculated for the region immediately following the initial signal (1.78 s to 4.8 s of the OSL signal). The OSL of bleached aliquots (thermal transfer test) was used to observe the contribution of thermal treatment to the OSL signal with the intention to minimize this. Typical OSL decay curves of sample Zi–O1 show that the OSL signal is suitable for OSL dating (Fig. 4.3). An example of sensitivity corrected dose response curve is also shown in Fig. 4.3.

4.4 Results

4.4.1 Pretests

Dose recovery tests at different preheat and cutheat temperatures for sample Zi–O1 were carried out. The preheat/cutheat temperatures at 230 °C/170 °C are the most suitable for the Zingst–Osterwald samples. The acceptable range for the measured/given dose ratio is between 0.9 and 1.1 (Wintle and Murray, 2006). Below 240 °C preheat no thermal transfer was observed (Fig. 4.4a). An additional dose recovery test with the selected preheat/cutheat temperatures at 230 °C/170 °C was performed on each sample from Zingst–Osterwald (4 aliquots per sample). The given doses were successfully recovered for all six samples within the acceptable range (Fig. 4.5a).

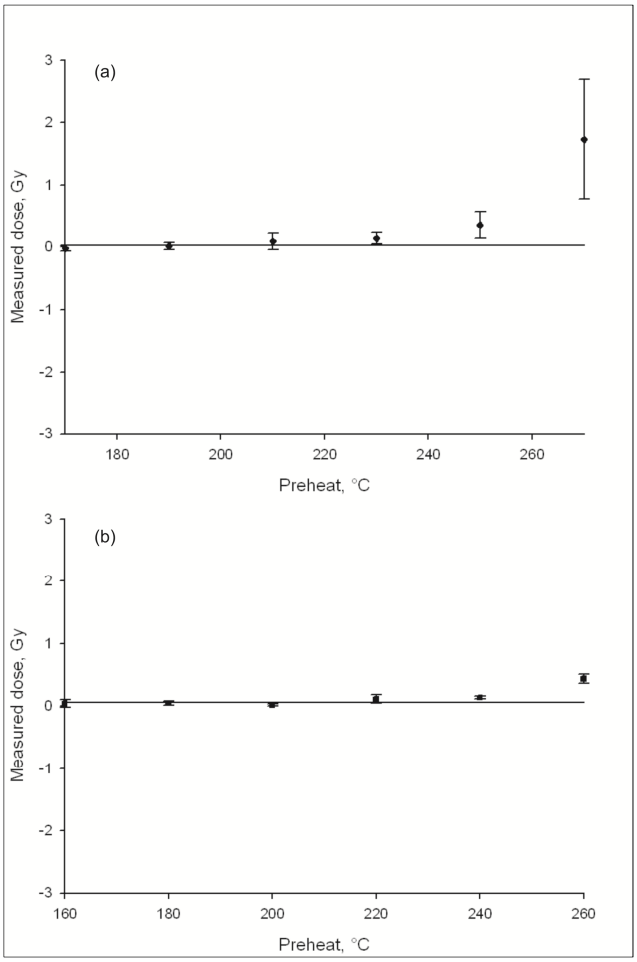

Figure 4.4: Thermal transfer of Zi–O1 (a) and Zi–W4 (b). Equivalent dose is plotted with preheat temperature including six temperature steps between 150 °C and 250 °C (Zi–O1) or rather 160–260 °C (Zi–W4) for aliquots that were bleached prior to the measurement.

The Windwatt samples were measured with a preheat/cutheat at 200 °C/160 °C. The dose recovery test, demonstrated that we were able to recover the given dose for all nine samples within the range of 0.9–1.1 (Fig. 4.5b). To minimize thermal transfer, the preheat temperature was kept below 240 °C (Fig. 4.4b).

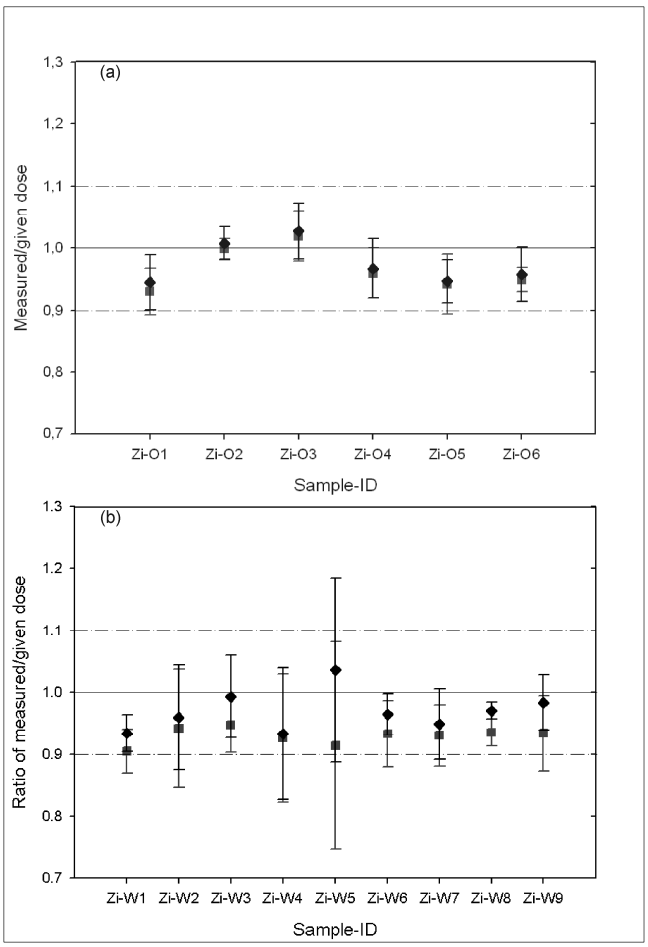

Figure 4.5: Dose recovery test for samples from Zingst–Osterwald Zi–Oi (a) and from Windwatt Zi–Wi (b). Measured/given ratio is plotted for each sample with the preheat/ cutheat temperatures at 230 °C/170 °C for Zi–Oi samples and at 200 °C/160 °C for Zi–Wi samples. Grey squares indicate the measured/given ratio calculated with Late Background Subtraction (36–40 s). The measured/given ratio calculated with Early Background Subtraction (1.76–4.8 s) is shown by black diamonds. The target value is unity (black line). The range of acceptability is between 0.9 and 1.1 (dotted line).

The dose recovery (measured/given) ratio was improved when the early background (EBG) was subtracted from the initial OSL signal instead of the Late Background (LBG) (Fig. 4.5a, b). The medium and/or the slow component from these quartz samples very likely do not recover the given dose.

4.4.2 D_e values and ages

Eighteen aliquots for each sample were measured for D_e determination. OSL signals were evaluated using the EBG approach to avoid a contribution of the medium and/or the slow component. We had to exclude 25 of 270 aliquots from the calculation of D_e due to poor recycling and/or IR/blue OSL depletion ratios (>10% from unity). The standard error, which is calculated from the standard deviation divided by the square root of the number of aliquots, of the D_e values is consistently low (Table 4.2). The D_e values for each sample showed an almost narrow and symmetrical Gaussian distribution with a small standard deviation (Table 4.2). With the applied protocol, we were able to measure a very small D_e of 0.44±0.02 m Gy for Sample Zi–W7 (Table 4.2). That confirms that the local sediment was sufficiently exposed to daylight prior to the deposition and that the measured quartz is very sensitive and suitable for luminescence dating.

Table 4.2: Results of dose rates, moisture content, equivalent doses and OSL ages.

Field-ID		Depth [m]	Sample	Grain size [µm]	Cosmic dose[a] rate [mGy/ka]	Water content[b] [%]	Dose rate[c] [Gy/ka]	De[d] [Gy] (with EBG)	Standard deviation of D_e	n[e] [Aliquots]	OSL age[f] [a]	Age range
Zingst-Osterwald	Zi-1	-0.35	Zi-O1	150-212	195 ± 20	6 ± 4	1.32 ± 0.06	2.03 ± 0.03	0.15	18	1540 ± 90	380-560 AD
		-0.55	Zi-O2	150-200	188 ± 20	6 ± 4	1.31 ± 0.09	2.25 ± 0.07	0.27	16	1710 ± 110	190-410 AD
	Zi-2	-0.45	Zi-O3	150-250	192 ± 20	6 ± 4	1.21 ± 0.08	2.04 ± 0.05	0.20	16	1680 ± 100	230-430 AD
		-0.65	Zi-O4	150-250	185 ± 20	6 ± 4	1.22 ± 0.09	2.17 ± 0.05	0.18	16	1790 ± 110	110-330 AD
	Zi-3	-0.45	Zi-O5	150-212	192 ± 20	6 ± 4	1.06 ± 0.07	1.84 ± 0.04	0.15	18	1730 ± 100	180-380 AD
		-0.70	Zi-O6	150-200	187 ± 20	6 ± 4	1.11 ± 0.07	1.89 ± 0.05	0.21	15	1700 ± 100	210-410 AD
Windwatt	Werl-2	-0.56	Zi-W1	150-212	188 ± 20	6 ± 4	0.97 ± 0.11	0.271 ± 0.009	0.035	16	280 ± 20	1710-1750 AD
	Werl-2	-1.03	Zi-W2	150-250	173 ± 20	6 ± 4	1.07 ± 0.08	0.964 ± 0.034	0.121	13	890 ± 60	1060-1180 AD
	Werl-4	-0.70	Zi-W3	150-200	183 ± 20	15 ± 5	0.86 ± 0.09	0.429 ± 0.017	0.066	16	500 ± 40	1470-1540 AD
	Werl-5	-0.81	Zi-W4	100-150	183 ± 20	15 ± 5	0.91 ± 0.12	0.264 ± 0.023	0.091	16	290 ± 30	1690-1750 AD
	Werl-8-OS	-0.34	Zi-W5	100-150	180 ± 20	15 ± 5	1.13 ± 0.08	0.348 ± 0.014	0.057	17	310 ± 20	1680-1720 AD
	Werl-8-OS	-0.87	Zi-W6	100-150	178 ± 20	15 ± 5	1.11 ± 0.07	0.524 ± 0.009	0.036	16	470 ± 30	1510-1570 AD
	Bock-3	-0.32	Zi-W7	106-150	196 ± 20	15 ± 5	1.05 ± 0.11	0.044 ± 0.002	0.008	18	40 ± 5	1965-1975 AD
	Bock-3	-0.84	Zi-W8	100-150	179 ± 20	15 ± 5	1.27 ± 0.15	0.366 ± 0.016	0.062	15	290 ± 30	1690-1750 AD
	Bock-4-OS	-0.78	Zi-W9	100-150	180 ± 20	15 ± 5	1.12 ± 0.07	0.561 ± 0.008	0.032	17	500 ± 30	1480-1540 AD

Foot notes:

[a] Cosmic dose rate is obtained according to Prescott and Hutton (1994) and Prescott and Stephan (1982).

[b] Water content is expressed as a mass of dry sediment.

[c] Dose rate is calculated after Aitken (1985) using the conversion factors of Adamiec and Aitken (1998) for uranium, thorium and potassium.

[d] D_e is indicate as the mean of accepted aliquots and the standard error of one sigma.

[e] n is the number of accepted aliquots.

[f] OSL ages in years [a] ago are calculated after Aitken (1998).

The detected dose rates were relatively low for all samples and range from 1.32 to 0.86 Gy/ka (Table 4.2) due to a very low uranium and thorium content. The measured uranium content was between 0.26±0.02 and 0.60±0.02 ppm, the thorium content was between 0.67±0.01 and 1.85±0.04 ppm and the potassium content ranged between 0.62 and 1.12%. The measured water content of the subaquatic beach samples samples (Zi–W3–9) was between 10 and 20%. The measured water content of the samples Zi–O1–6, Zi–W1, 2 was between 2 and 9%. We therefore apply a water content of 15±5% for the samples Zi–W3 to Zi–W9 and of 6±4% for the Zingst–Osterwald samples and for Zi–W1 and Zi–W2 for age calculation. The dose rate errors for Zingst–Osterwald and Windwatt are 4–7% and 6–13%, respectively (Table 4.2). The higher error for the Windwatt samples is caused by the smaller sample size for the gamma spectrometry (50 g).

The OSL ages for the Zingst–Osterwald samples, taking the error into consideration, range from 1500 to 1900 years (Table 4.2). The OSL ages of the sediments from Windwatt area are younger than Zingst– Osterwald (Table 4.2). The sediments from the Windwatt ages can be subdivided into at least four age clusters; ∼900, ∼500, 260–320, and ∼40 years. The age errors of the Zingst–Osterwald and Windwatt samples are around 6% and 6–12%, respectively.

4.5 Discussion

4.5.1 Reliability of OSL dates

The performance of SAR protocol in this study (recycling ratio, recuperation and the dose recovery test) showed that the SAR procotol was successfully applied for the samples. The distribution of the recycling ratios of all measured aliquots (266) is well around unity with an average of 1.004±0.004. The small standard deviation of 0.062 (Fig. 4.6a) confirms that the sensitivity correction of the adapted SAR protocol is working perfectly. The average recuperation level is between 2% and 4% of the sensitivity corrected natural signal and therefore generally low and satisfactory. These values are similar to those regarding the effect of preheat temperature to young quartz samples conducted by

Kiyak and Canel (2006). The measured dose recovery ratios for all samples (altogether 59 aliquots) are close to unity (mean value, 0.972±0.008, Fig. 4.6b).

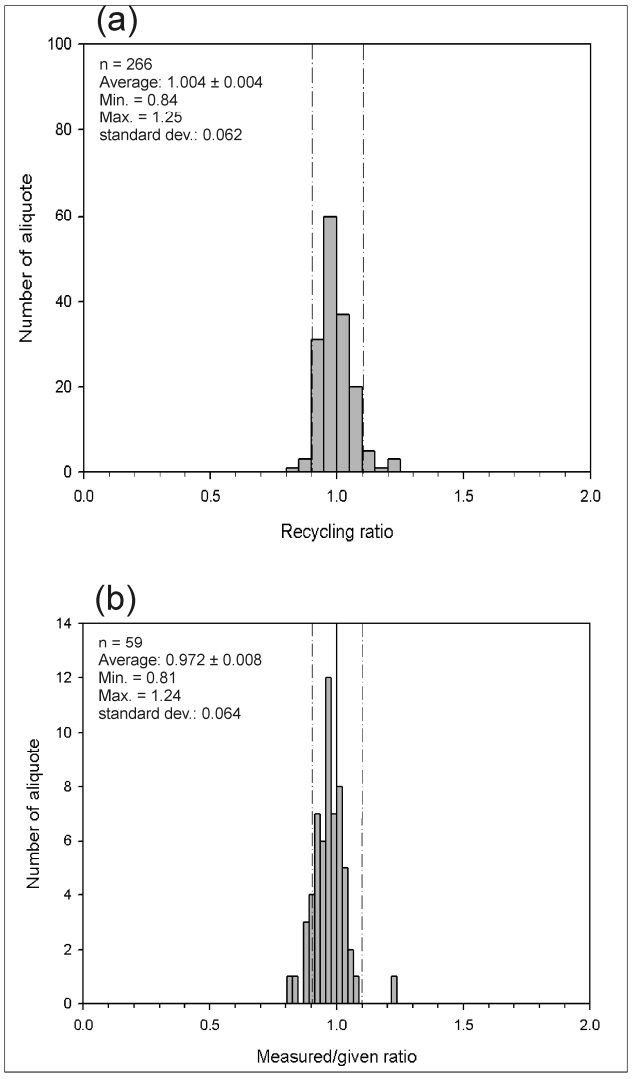

Figure 4.6: Distributions of recycling ratios (a) and dose recoveries (b). (a) Distribution of recycling ratios from all aliquots used for OSL age calculation. **(b)** Distribution of data from all aliquots measured for dose recovery. The dotted lines mark the range of acceptability for (a) and (b) (0.9 to 1.1).

The distributions of D_e values for the investigated samples are rather narrow and symmetrical indicating sufficient bleaching for the investigated sediments (according to Fuchs and Owen, 2008). The standard deviations are mostly between 6 and 12% of the D_e (Table 4.2). For some of the youngest sample (e.g. Zi–W5, Table 4.2) the obtained standard deviations of the D_e are slightly larger due to a bad signal-tonoise ratio. The very low D_e of Zi–W7 (Table 4.2) confirms that the sand was sufficiently bleached and therefore the quartz dosimeter was reset prior to the deposition.

The OSL ages are stratigraphically consistent. All ages derived from the samples are in vertical sequence and increase with depth or rather have the same age when taking the error into account (Zi–O1/Zi–O2, Zi–O3/Zi–O4, Zi–O5/Zi–O6, Zi–W1/Zi–W2, Zi–W5/Zi–W6, and Zi–W7/Zi–W8). However, it was expected that samples from the same ridge would give the same deposition age because each beach ridge was deposited during a very short time span. In fact the Zingst–Osterwald samples (Zi–O3/Zi–O4 and Zi–O5/Zi–O6) from outcrop Zi–1, 2, 3 give the same age within the error for each beach ridge (Fig. 4.7). For the samples Zi–W1/Zi–W2, Zi–W5/Zi–W6 and Zi–W7/Zi–W8 sub-

sampled from the Windwatt cores WerI-2, WerI-8-OS and Bock-3 the lower sample is significantly older than the upper one (Fig. 4.7).

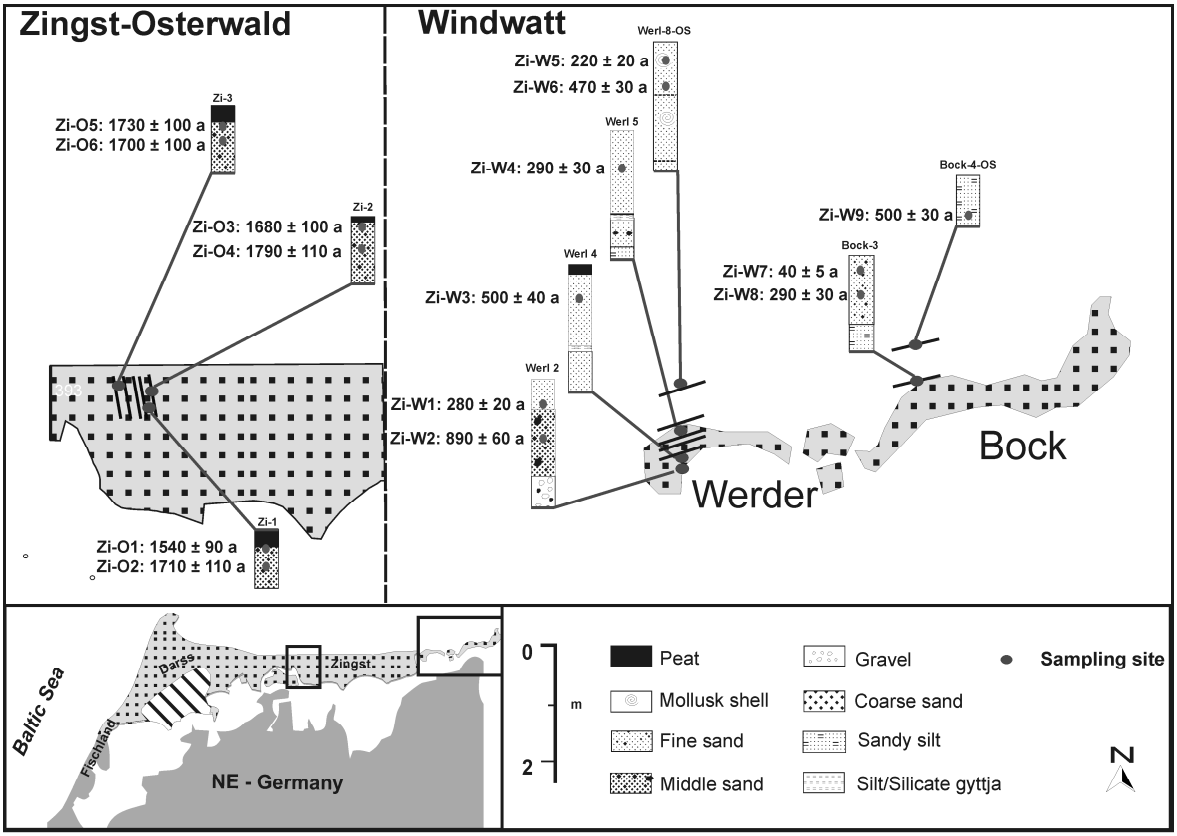

Figure 4.7: Map of Zingst–Osterwald and Windwatt with dating results. Ages are pictured in relation to the lithologic context and the geomorphic setting. For Zingst–Osterwald the lithology of the outcrops are illustrated. The positions of luminescence samples are marked with grey cycles. For the Windwatt area the lithology of the cores is shown; the luminescence samples were taken from the marked positions.

4.5.2 OSL dates in context of setting and the literature review

The beach ridges of the Zingst–Osterwald area yielded OSL ages ranging from 110 to 560 AD (Fig. 4.7, Table 4.2) correlating to the middle Subatlantic period. The orientation of these beach ridges (north/ south) is different from the Windwatt beach ridge sequence (west/east orientation) because the ridges are attached perpendicular to a former island to the north. This succession represents the old spit system before the late Subatlantic transgression (at about 800 AD) and before the final abrasion of the former islands. After this final abrasion the coastal inlets like the “Zingster Strom” (Figs. 4.1 and 4.2) were filled and closed, which subsequently induced a general alteration of the sediment dynamics of the Darss–Zingst spit system with a dominant west–east sediment transport and the appearance of prograding coastline in the easternmost part of the peninsula (Windwatt). Our dates are in agreement with the evolutional model of Janke and Lampe (1998), Lampe (2002), Lampe et al. (2007), which is based on geology, geomorphology and radiocarbon dating. The present data set does not allow the reconstruction of the growth direction of the spit growing at this time because the sampled beach ridges at the Zingst–Osterwald site are too close together to obtain a significant age difference. The investigated ridges at Zingst–Osterwald have at least all the same age within the error and suggest a synchronous formation. However, according to our OSL dates, we

assume that the closing of the former coastal inlets must be younger than the Zingst–Osterwald ridges and hence younger than 560 AD.

The beach ridge succession of the Windwatt area has been deposited since 1060 AD and is an ongoing process (Fig. 4.6, Table 4.2). The Windwatt beach ridge succession is significantly younger than the Zingst–Osterwald beach ridges (Fig. 4.6, Table 4.2) and so younger than the alteration of sediment dynamics. The Windwatt beach ridge succession was deposited after the late Subatlantic transgression, which started at about 800 AD (Lampe et al., 2007). According to Janke and Lampe (1998), Lampe (2002) and Lampe et al. (2007) the Windwatt succession represents the most recent spit system with a dominant west–east sediment transport, which started to develop after the alteration of the sediment system triggered by the closing of the coastal inlets. The obtained OSL ages are in agreement with the geological estimates which are based on interpretation of the sediment structure and a few radiocarbon ages from interstratified peat layers.

The pattern of OSL ages from Windwatt area represents complex sedimentary dynamics. It was expected that the landward ridges are older than the seaward ridges due to a seaward prograding system. Regarding Zi–W2 (lower sample of core WerI-2), Zi–W3 and Zi–W4 (Fig. 4.7) we obtained decreasing ages in a seaward direction. But taking the result of core WerI-8-OS into account (from the most seaward ridge) the lower sample has an age of about 470 years and is significantly older than Zi–W5 from the landward ridge. A similar phenomenon is observed for Zi–W8 and Zi–W9 which are sampled from the same depth in a seaward direction (Fig. 4.7, Table 4.2). The age of the seaward ridge (Zi–W9) is with 500±30 years older than the OSL age from the landward ridge (290±30 years, Zi–W8) (Fig. 4.7, Table 4.2). The sample Zi–W7, which was taken above Zi–W8, has a sub-recent age (40±5 years). The latter age demonstrates that sedimentation processes are still active in this area. It is very likely that the sub-recent sediment is related to a storm surge event which caused sediment overwash. In fact, for every core the uppermost part is significantly younger, indicating that the formation of the ridges is not related to a single depositional event. The complex spatial distribution of age estimates is related to a seaward prograding sediment system but is primarily an effect of phases with different sedimentary dynamics and (re)mobilisation of sediment (e.g. sediment overwash).

Coastal sediment (sand) mobilisation is primarily related to human activity (e.g. deforestation or coast protection), natural climatic factors (e.g. storminess, and storm surge frequency), sediment availability and fluctuation of sea level (Madsen et al., 2007). Our OSL ages between 1470 and 1750 AD (Table 4.2) correlate to the time of the Little Ice Age (LIA) (1350–1900 AD according to Hass, 1996) and it is likely that during that time sediment mobilisation increased. The LIA is characterized by a relatively low sea level and a generally cold and stormy climate. Several phases of increasing storminess related to positive variations of the NAO (North Atlantic Oscillation) (Dawson et al., 2002) were recognised within the period of the LIA. Hass (1996), who investigated marine sediment cores from the Skagerrak, divided the Little Ice Age into three phases 1350–1550 AD, 1550–1750 AD and 1750–1900 AD. The first and the last phase indicate a winter mode of sedimentation with increased (westerly) storm activity, whereas the 2nd period between 1550 and 1750 AD showed less storm activity. However, there are a number of studies in northwest Europe which document increased aeolian sand movement during the LIA due to increased storminess and shifts in the atmospheric circulation system (Szkornik et al., 2008). The ages of Zi–W3, Zi–W6 and Zi–W9 (Fig. 4.7) cluster around 1500 AD and correlate with the first phase of the LIA with increased storm activity according

to Hass (1996). It is likely that the ages of Zi–W1, Zi–W4, Zi–W5 and Zi–W8 (Fig. 4.7) from 1680 to 1750 AD are related to the onset of the third phase of the LIA or rather the ages represent the transition from the second to the third phase (according to Hass, 1996). This is in agreement with OSL dating of coastal dune and beach ridges from the North Sea coast conducted by Ballarini et al. (2003) (Texel island, Netherland) and Madsen et al. (2007) (Rømø, Denmark) who correlated their ages with increased storminess in relation to the third phase of the LIA (around 1720 AD) as well. The lack of age estimates between 1500 and 1680 AD is very likely related to the calmer mode of the middle period of the LIA (according to Hass, 1996).

The general role of the relative sea level position as an important control on the sand movement initiation is still under discussion. Szkornik et al. (2008) summarized two hypotheses regarding sea level position which are common in the literature. Cooper (1958) proposed, that aeolian sand movement is related to relative sea level highs or risings which induced reworking and erosion of sand and led to a transgressive dune system. Whereas Shofield (1975) correlated sand movement to an exposed shore area caused by a falling or low sea level position and therefore an increased availability of sand. For the German Baltic Sea coast, Lampe (2005) described the widespread appearance of a prominent peat oxidation horizon in the coastal peatlands, which is related to the LIA indicating a sea level regression for this period. Since 1850 AD a rising sea level has been observed. The clustering of deposition ages (1470–1750 AD) in the Windwatt area (Fig. 4.7) during the LIA and hence a period of regressive sea level conditions supports the second hypothesis. There is only one age younger than 150 years (Fig. 4.7) which could be related to deposition under transgressive conditions. Thus, the presented OSL dates also support the OSL study of Madsen et al. (2007) who correlate the pronounced beach ridge unit of the North Friesian island Rømø with a relatively low sea level.

4.6 Conclusion

- The local sediment from the beach ridges is suitable for luminescence dating using quartz minerals as natural dosimeter and the chosen SAR protocol for determination of the equivalent dose (D_e).
- The ages derived from these D_e values are consistent within the stratigraphy.
- Our OSL ages are in agreement with the existing evolutional model (Janke and Lampe, 1998; Lampe, 2002; Lampe et al., 2007) of the Darss–Zingst spit development.
- The OSL age estimates from Zingst–Osterwald are significantly older (1900 to 1450 years) than the Windwatt ages (950 years to modern ages). The successions represent the phase before and after the late Atlantic transgression or rather before and after the alteration of the sediment dynamics linked to the closing of the coastal inlets.
- The young ages of the Windwatt beach ridge system with one sub-recent age estimate (Zi–W7) show that the sedimentation process in this part of the spit is still active and reveals the very complex pattern of sedimentation in this beach area. The ages cluster into four groups (~900, ~500, 260–320, and ~40 years). The OSL ages of ~500 years (1500 AD) and 260–360 years (1680–1750 AD) might represent periods of sediment mobilisation caused by phases of a colder and stormy climate and a generally low sea level within the Little Ice Age.

The chronological data of this study confirm that quartz as a dosimeter offers the potential for a precise and accurate geochronology for investigations in the sand dominated coastal environment and of coastal changes. It is possible to reconstruct the movement of shallow marine and aeolian sand in order to prove the existing geological models of this area and correlate them with phases of sedimentation triggered by fluctuations of climate and/or sea level conditions. We therefore conclude that OSL is a convincing geochronological method for studies of coastal evolution. This is part of an ongoing study investigating coastal dynamics along the southern coast of the Baltic Sea.

Acknowledgements

This study was supported by the “Leibniz-Pakt fur Innovation und Forschung”. The authors wish to thank Isabel John and Bjorn Machalett for providing support during sampling. We also thank the reviewers and the editors for providing constructive comments on the paper.

References

- Adamiec, G., Aitken, M., 1998. Dose-rate conversion factors: update. Ancient TL 16, 37–50.
- Aitken, M.J., 1985. Thermoluminescence Dating. Academic Press, London.
- Aitken, M.J., 1998. An Introduction to Optical Dating. Oxford University Press, Oxford.
- Ballarini, M., Wallinga, J., Murray, A.S., van Heteren, S., Oost, A.P., Bos, A.J.J., van Eijk, C.W.E., 2003. Optical dating of young coastal dunes on a decadal time scale. Quaternary Science Reviews 22, 1011–1017.
- Ballarini, M., Wallinga, J., Wintle, A.G., Bos, A.J.J., 2007. A modified SAR protocol for optical dating of individual grains from young quartz samples. Radiation Measurements 42, 360–369.
- Bøtter-Jensen, L., Bulur, E., Duller, G.A.T., Murray, A.S., 2000. Advances in luminescence instrument systems. Radiation Measurements 32, 523–528.
- Cooper, W.S., 1958. Coastal sand dunes of Oregon and Washington. Memoirs of Geological Society of America, vol. 72. Boulder, Co.
- Dawson, A.G., Hickey, K., Holt, T., Elliott, L., Dawson, S., Foster, I.D.L., Wadhams, P., Jonsdottir, I., Wilkinson, J., McKenna, J., Davis, N.R., Smith, D.E., 2002. Complex North Atlantic Oscillation (NAO) index signal of historic North Atlantic storm-track changes. The Holocene 12, 363–369.
- Duller, G.A.T., 2003. Distinguishing quartz and feldspar in single grain luminescence measurements. Radiation Measurements 37, 161–165.
- Forbes, D.L., Orford, J.D., Carter, R.W.G., Shaw, J., Jennings, S.C., 1995. Morphodynamic evolution, self-organisation, and instability of coarse-clastic barriers on paraglacial coasts. Marine Geology 126, 63–85.
- Fuchs, M., Owen, L.A., 2008. Luminescence dating of glacial and associated sediments: review, recommendations and future directions. Boreas 37, 636–659.
- Hass, H.C., 1996. Northern Europe climate variations during late Holocene: evidence from marine Skagerrak. Palaeogeography, Palaeoclimatology, Palaeoecology 123, 121–145.

- Hoffmann, G., Lampe, R., Barnasch, J., 2005. Postglacial evolution of coastal barriers along the West Pomeranian coast, NE Germany. Quaternary International 133–134, 47–59.
- Hua, Q., 2009. Radiocarbon: a chronological tool for the recent past. Quaternary Geochronology 4, 378–390.
- Jacobs, Z., 2008. Luminescence chronologies for coastal and marine sediments. Boreas 37, 508–535.
- Janke, W., Lampe, R., 1998. Die Entwicklung der Nehrung Fischland–Darß–Zingst und ihres Umlandes seit der Litorina-Transgression und die Rekonstruktion ihrer subrezenten Dynamik mittels historischer Karten. Zeitschrift fur Geomorphologie N.F. Supplementband 112, 177–194.
- Kaiser, K., Barthelmes, A., Czakó Pap, S., Hilgers, A., Janke, W., Kuhn, P., Theuerkauf, M., 2006. A Lateglacial palaeosol cover in the Altdarss area, southern Baltic Sea coast (northeast Germany): investigations on pedology, geochronology and botany. Netherlands Journal of Geoscience 85 (3), 197–220.
- Kiyak, K.G., Canel, T., 2006. Equivalent dose in quartz from young samples using the SAR protocol and the effect of preheat temperature. Radiation Measurements 41, 917–922.
- Kliewe, H., Janke, W., 1991. Holozäner Küstenausgleich im südlichen Ostseegebiet bei besonderer Berücksichtigung der Boddenausgleichsküste Vorpommerns. Petermanns Geographische Mitteilungen 135, 1–15.
- Lampe, R., 2002. Holocene evolution and coastal dynamics of the Fischland–Darss–Zingst peninsula. Greifswalder Geographische Arbeiten 27, 155–163.
- Lampe, R., 2005. Lateglacial and Holocene water-level variations along the NE German Baltic Sea coast: reviewand newresults. Quarternary International 133–134, 121–136.
- Lampe, R., Meyer, H., Ziekur, R., Janke, W., Endtmann, E., 2007. Holocene evolution of the irregularly sinking southern Baltic Sea coast and the interactions of sea-level rise, accommodation space and sediment supply. Berichte der Romisch-Germanischen Kommission 88, 15–46.
- Lemke, W., 2005. Die kurze und wechselvolle Entwicklungsgeschichte der Ostsee – Aktuelle meeresgeologische Forschungen zum Verlauf der Litorina-Transgression. Jahrbuch der Bodendenkmalpflege in Mecklenburg-Vorpommern 52, 43–54.
- Lopez, G.I., Rink, W.J., 2007. Characteristics of the burial environment related to quartz SAR-OSL dating at St. Vincent Island, NW Florida, USA. Quaternary Geochronology 2, 65–70.
- Madsen, A.T., Murray, A.S., 2009. Optically stimulated luminescence dating of young sediments: a review. Geomorphology 109, 3–16.
- Madsen, A.T., Murray, A.S., Andersen, T.J., Pejrup, M., Breuning-Madsen, H., 2005. Optically stimulated luminescence dating of young estuarine sediments: a comparison with ^{210}Pb and ^{137}Cs dating. Marine Geology 214, 251–268.
- Madsen, A.T., Murray, A.S., Andersen, T.J., 2007. Optical dating of dune ridges on Romo, a barrier island in the Wadden Sea, Denmark. Journal of Coastal Research 23 (5), 1259–1269.
- Murray, A.S., Wintle, A.G., 2000. Luminescence dating of quartz using an improved single-aliquot regenerative-dose protocol. Radiation Measurements 32, 57–73.
- Murray, A.S., Olley, J.M., 2002. Precision and accuracy in the optically stimulated luminescence dating of sedimentary quartz: a status review. Geochronometria 21, 1–16.

- Murray, A.S., Wintle, A.G., 2003. The single aliquot regenerative dose protocol: potential for improvements in reliability. Radiation Measurements 37, 377–381.
- Murray, A.S., Marten, R., Johnston, A., Martin, P., 1987. Analysis for naturally occuring radionuclides at environmental concentrations by gammaspectrometry. Journal of Radioanalytical and Nuclear Chemistry 115 (2), 263–288.
- Murray-Wallace, C.V., Banerjee, D., Rourman, R.P., Olley, J.M., Brooke, B.P., 2002. Optically stimulated luminescence dating of Holocene relict foredunes, Guichen Bay, South Australia. Quaternary Science Reviews 21, 1077–1086.
- Naumann, M., Lampe, R., Hoffmann, G., 2009. Coastal evolution of a Holocene barrier spit (Bug peninsula/NW Rügen) deducted from geological structure and relative sea-level. E & G (Eiszeitalter und Gegenwart) Quarternary Science Journal 58, 164-173.
- Nielsen, A., Murray, A.S., Pejrup, M., Elberling, B., 2006. Optically stimulated luminescence dating of al Holocene beach ridge plain in Northern Jutland, Denmark. Quaternary Geochronology 1, 305–312.
- Prescott, J.R., Stephan, L.G., 1982. The contribution of cosmic radiation to the environmental dose for thermoluminescent dating — latitude, altitude and depth dependences. PACT 6, 17–25.
- Prescott, J.R., Hutton, J.T., 1994. Cosmic ray distributions to dose rates for luminescence and ESR dating: large depths and long-term variations. Radiation Measurements 23, 497–500.
- Roberts, H.M., Plater, A.J., 2007. Reconstruction of Holocene foreland progradation using optically stimulated luminescence (OSL) dating: an example from Dungeness. The Holocene 17, 495–505.
- Schumacher, W., 2002. Coastal evolution of the Darss Peninsula. Greifswalder Geographische Arbeiten 27, 165–168.
- Schumacher, W., Bayerl, K.A., 1999. The shoreline displacement curve of Rügen Island (southern Baltic Sea). Quaternary International 56, 107–113.
- Shofield, J.C., 1975. Sea-level fluctuations cause periodic postglacial progradation, South Kaipara Barrier, North Island, New Zealand. Journal of Geology and Geophysics 28, 295–316.
- Stuiver, M., 1978. Radiocarbon timescale tested against magnetic and other dating methods. Nature 273, 271–274.
- Szkornik, K., Gehrels, W., Murray, A.S., 2008. Aeolian sand movement and relative sealevel rise in Ho Bugt, western Denmark, during the 'Little Ice Age'. The Holocene 18, 951–965.
- Wintle, A.G., Murray, A.S., 2006. A review of quartz optically stimulated luminescence characteristics and their relevance in single-aliquot regeneration dating protocols. Radiation Measurements 41, 369 391

Chapter 5, Paper III:

Tony Reimann[a], Sebastian Lindhorst[b], Kristina J. Thomsen[c], Andrew S. Murray[d], Manfred Frechen[a].

[a] Leibniz Institute for Applied Geophysics (LIAG), Section S3: Geochronology and Isotope Hydrology, Hannover, Germany
[b] Universität Hamburg, Geologisch-Paläontologisches Institut, Hamburg, Germany
[c] Radiation Research Division, Risø DTU, Roskilde, Denmark
[d] Nordic Laboratory for Luminescence Dating, Department of Earth Sciences, Aarhus University, Risø DTU, Roskilde, Denmark

OSL dating of mixed coastal sediments (Sylt, German Bight, North Sea).

Submitted in revised form to Quaternary Geochronology.

(www.sciencedirect.com/science/journal/18711014)

Abstract

As part of a study on coastal sedimentary processes this paper presents the OSL dating of mixed coastal sediment samples from the southern North Sea island of Sylt (German Bight). During coring of the swash-bar (beach) sediments, five samples were presumably contaminated by younger overwash and aeolian sediments because of the sampling method employed. To obtain reliable burial ages for these swash-bar sediments, single-grain and small aliquot measurements were used together with the Finite Mixture Model (FMM) proposed by Roberts et al. (2000) to identify the grain population containing the largest doses (from the deepest part of the core). Before the FMM was applied to dating, the parameters and performance of the FMM was first investigated by systematically comparing small aliquot (~20 grains) and single-grain measurements of an undisturbed aeolian and swash-bar sample and a laboratory mixture of both sediments. This test case demonstrates the advantage of selecting the time interval immediately following the initial luminescence signals for background subtraction because unsuitable quartz grains were removed from the dose distribution. It is concluded that the measurement of small aliquots can be regarded as a reliable proxy for single-grain dose distribution if the sediment contains only a small proportion of quartz grains emitting a luminescence signal and that the FMM results are relatively insensitive to changes of the over-dispersion parameter between 10 to 40 %.

We show that the burial ages of the contaminated swash-bar samples resulting from the maximum age populations from equivalent dose distributions measured using small aliquots are consistent with the stratigraphy and with ages obtained from uncontaminated samples.

5.1 Introduction

A better understanding of coastal sedimentary processes and the related controlling factors (e.g. climate, sediment supply, and sea level) is fundamental to developing concepts of improved coastal protection. This task requires, in addition to investigations of sedimentary setting, a reliable estimation of the depositional ages of different sedimentary units. Optically simulated luminescence (OSL) using quartz as a natural dosimeter has proved to be a powerful and reliable dating technique to determine depositional ages of young coastal sediments around the world (e.g. Murray-Wallace et al., 2002; Ballarini et al., 2003; Madsen et al., 2005, 2007, 2009; Nielsen et al., 2006; Buynevich et al., 2007; Lopez and Rink, 2007; Jacobs, 2008; Alappat et al., 2011; Reimann et al., 2011b). Nevertheless, there are sources of scatter which can contribute to complex equivalent dose (D_e) distributions; these may lead to inaccurate OSL ages. Recently several studies have addressed the problem of (i) heterogeneous bleaching of sedimentary grains prior to deposition and (ii) post-depositional mixing of the sediment units, as the most common sources of complex and broad D_e distributions (e.g. Roberts et al., 1998; Galbraith et al., 1999; Olley et al., 1999, 2004; Bailey and Arnold, 2006; Pietsch, 2009; Thomsen et al., 2007). Most of these studies made use of small aliquot (containing less than 100 grains) or single-grain measurements and then employed various statistical models to identify the equivalent dose (D_e) of the smallest dose population to obtain appropriate burial ages (e.g. Olley et al., 2004; Rodnight et al., 2006).

Here we present OSL ages of eight beach sediment samples, five of which appear to have been contaminated during sampling by overlying younger over-wash and aeolian sediments. Dating such samples is not a straightforward task since it requires detailed analyses of complex D_e distributions. The mean or weighted mean of D_e distribution made up of more than one component is unlikely to be an appropriate estimate of the true burial dose (Db) (e.g. Rodnight et al., 2006). In this study, we apply the Finite Mixture Model (FMM, Roberts et al., 2000) to identify the population representing the largest D_e i.e. the population derived from the time since burial of the uncontaminated beach sediments. The FMM can be applied to identify discrete D_e populations within a dose distribution containing multiple D_e components. It has been applied to sediment mixtures in a number of single-grain OSL studies (e.g. Roberts et al., 2000, 2001; Jacobs et al., 2006, 2008b; Bateman et al, 2007), and Rodnight et al. (2006) applied the FMM to small aliquot (~30 grains) D_e distributions and obtained burial ages for partial bleached fluvial sediments that were in agreement with independent age control. Arnold and Roberts (2009) more recently suggested that the FMM should only be applied to single-grain D_e distributions to avoid the averaging effect of multi-grain D_e measurements. Their recommendations are based on a stochastic model that simulated multi-grain aliquots and it shows that grain-to-grain averaging effects in multi-grain aliquots should be avoided when using the FMM. Their model assumed one to ten luminescent grains per aliquot and uses a simple weighting factor to define the relative contribution that each luminescent grain will have on the combined multi-grain D_e value of the aliquot. However, this weighting factor and thus the significance of the averaging effects in multi-grain aliquots depends on the contribution of individual grains to the total light sum (i.e. the difference in grain brightness), which can differ between both regional and sedimentary settings (e.g. Duller et al., 2000).

The case study presented here systematically compares the performance of the FMM based on single-grain and small aliquot data sets and makes a contribution to the ongoing debate regarding

the use of small aliquots as a proxy for the more time-consuming analysis of single-grain D_e distributions. The FMM is then used to identify maximum dose populations in mixed sediment samples that had been accidentally contaminated by younger material during sampling.

First and foremost we investigate whether we can date such contaminated samples and secondly we investigate whether single-grain analysis is required in such an analysis or whether small aliquots (each containing ~20 grains) can be used as a reliable proxy. The performance and the parameters of the FMM are systematically investigated to determine if they can be applied successfully to estimate a maximum D_e population from a laboratory sediment mixture. The resulting procedure is then used to date the contaminated beach samples and the ages are discussed within the stratigraphic context. Finally, the importance of the over-dispersion (σ_{OD}) parameter in the FMM and the reliability of small aliquot compared to single-grain analyses are discussed.

5.2 Study area

5.2.1 Geology and Geomorphology

The study area is located on the northern barrier spit of Sylt, an island on the eastern side of the North Sea 11 km from the coast just south of the border between Germany and Denmark (Fig. 5.1a). The island is built on a core of Saalian (380–126 ka, Gibbard et al., 2005) and Elsterian (480–420 ka) moraines, as well as reworked earlier Cenozoic sediments (Gripp and Becker, 1940). Two Holocene barrier spits are attached to the north and south ends (Fig. 5.1b). The southern spit consists of dunes and washover sediments which unconformably overlie clays and silts of a former backbarrier lagoon and are interpreted as resulting from continuous eastward migration of the coastline (Hoffmann, 1974).

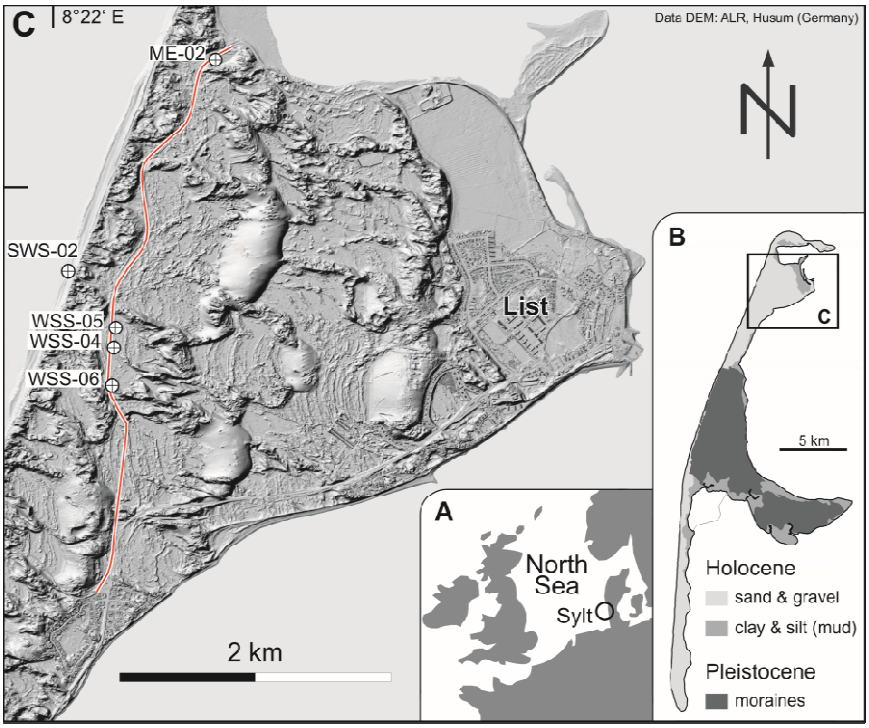

Figure 5.1: Map of the study area. The barrier-spit system on the island Sylt is located in the southern North Sea, near the border of Denmark and Germany **(a).** Sylt consists of a Pleistocene moraine core with two Holocene sandy barrier spits attached towards the north and the south **(b).** The geomorphology of the northern barrier spit is characterized by aeolian dunes, which are partly active migrating **(c).** The sample locations are situated along the western coast of the spit which faces the open sea. Note active swash bars along the recent coast.

The sedimentary evolution of the northern spit was first described by Gripp and Simon (1940) on the basis of analyses of sediment cores. They found that the spit consists of sand and gravel with intercalations of clay and peat. Lindhorst et al. (2008, 2010) presented a process-oriented study based on ground-penetrating radar data (GPR) and sediment cores. They pointed out that the sedimentary architecture of the spit reflects both phases of erosion and construction. During the construction phases, two different processes lead to spit growth: welding of swash-bars is the prevailing process along the western coast, but foreshore beach-drift sedimentation takes place on the hooked spit forming the northern termination of the island.

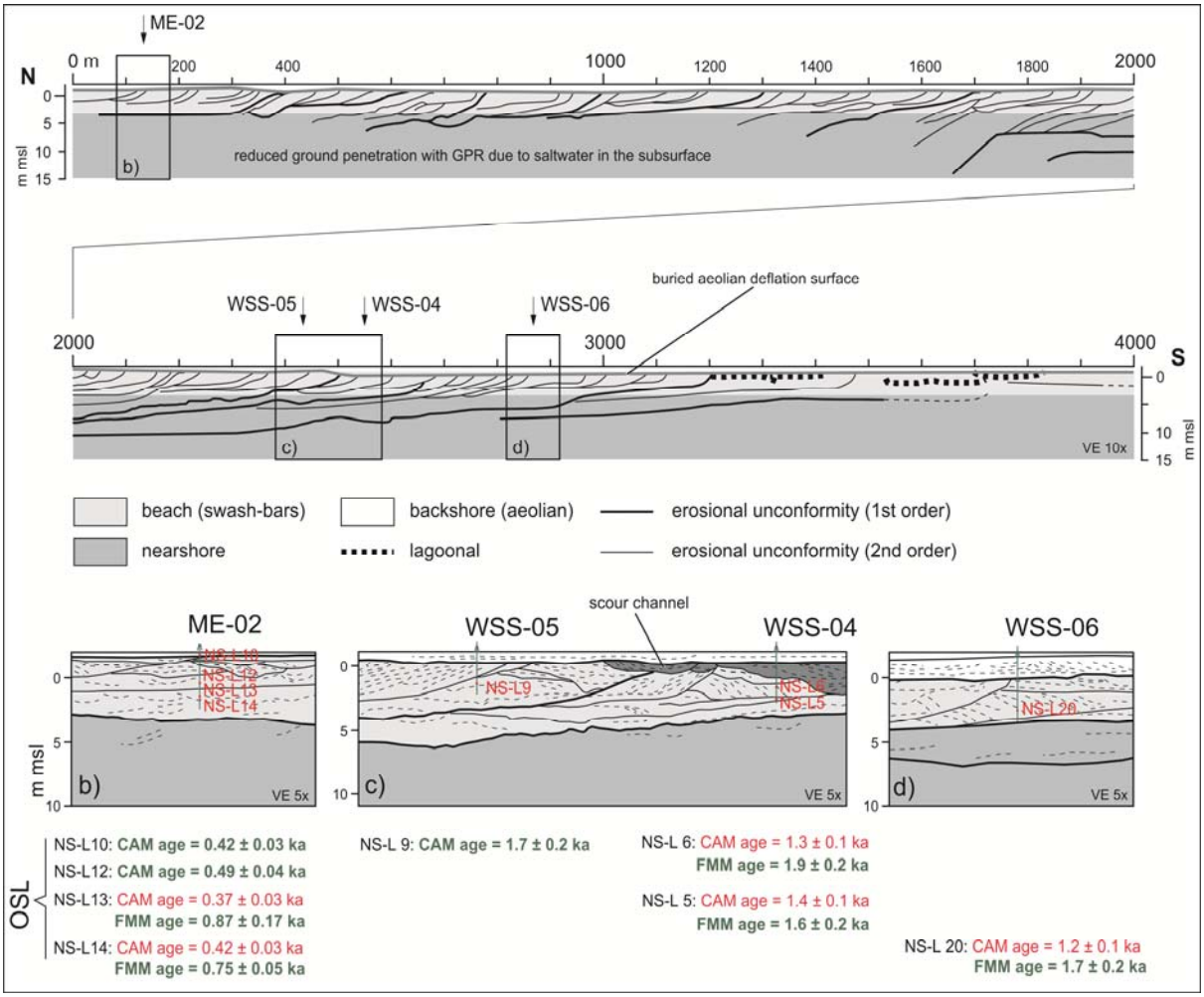

Figure 5.2: Geological section and sample location. The sedimentary architecture of the spit was investigated using ground-penetrating radar (Lindhorst et al., 2008). The sedimentary succession consists of beach deposits bound by northward dipping erosional unconformities **(a).** Two types of unconformities can be recognized. 1st order unconformities reach down to a depth of 15 m below mean sea level (mbsl) that can be traced over more than 1500 m along the spit axis. These unconformities are attributed to rare severe storms that eroded large parts of the spit. 2nd order unconformities reach down to a depth of around 5-6 mbsl that are attributed to annual storms. Beside the recent deflation surface around 1.8 m above sea level, there is a buried aeolian deflation surface at a depth of 1 m below the present land surface. Sediments sampled for OSL are medium to coarse sands deposited as swash bars (**b, c, and d**). Note that the upper part of Core WSS-04 is formed by sediments of a cut-and-fill structure, interpreted as a scour channel, significantly younger than the swash-bar sequence.

The stratigraphic architecture of the northern spit along a 4 km long transect parallel to the recent coast is shown in Fig. 5.2. Two types of erosional unconformities are present. First order unconformities reach down to a depth of around 15 m below present mean sea level (mbsl) and can be traced for more than 1.5 km along the spit axis. These erosional unconformities are interpreted

to result from rare severe storms (Lindhorst et al., 2008). Second order unconformities reach down to a depth of 5 to 6 mbsl and are attributed to annual winter storms. Between the unconformities, sedimentary packages show landward-directed dipping beds. These strata are interpreted as swash-bars welded to the beach under fair-weather conditions; these swash-bar sediment bodies are the main building block of the northern spit. Cut-and-fill structures reaching down to a depth of 3 mbsl are scour channels feeding washover fans towards the east. The whole sedimentary succession is truncated 1 m below the present land surface by an erosional unconformity. This unconformity can be traced over the entire northern spit and is interpreted as a buried deflation surface (Lindhorst et al., 2008). On top of this erosional unconformity, a cover of aeolian transported sands has been deposited. Although the different sedimentary units (swash-bar, washover, and aeolian) are likely to be made up of well-bleached sand, and so have relatively simple D_e distributions reflecting the different ages of these units, a mixture of these sediments must inevitably have a more complex D_e distribution and thus it is appropriate to use the FMM to identify these populations. The present day land surface is formed by the active deflation surface, which is located at 1.8 m above present mean sea level. The position of this modern deflation surface appears to be controlled by the ground-water table. The youngest sedimentary unit on northern Sylt is formed by a dune system that incorporates active migrating dunes (Fig. 5.1 c).

The chronology of this important sediment succession is unkown, and as a result so is the timing of the spit evolution, severe storm events (recorded as large erosional unconformities or washover fans) and aeolian sand mobilisation. OSL dating is probably the only method that can date these events on Sylt, and so give insights into the broader behaviour of the eastern North Sea.

5.2.2 Sampling

To obtain sediment samples for OSL dating, vibracores were drilled to a depth of 5 m below the present surface at selected positions along a transect oriented parallel to the modern coast (Fig. 5.1 c, 5.2 a). For the samples NS-L 9, 10 12 a 63 mm steel probe with 50 mm plastic liner was used. Cutting of liners and sediment sampling was done in the laboratory under subdued light conditions. As the piston needed for this coring method turned out to be very difficult to use in the coarse sediment of the study area, an open percussion coring tube with a diameter of 50 mm was used for the lower samples (NS-L 5, 6, NS-L 13, 14 and NS-L 20). As this coring tube is open along its side, these samples are likely to be contaminated by sediment carryover from above the sampling depth. To avoid exposure of these samples to daylight, drilling was performed at night and sediment sampling was done in the field under the cover of a small tent.

5.3 Experimental details

5.3.1 Sample preparation

The preparation of the sand-sized quartz samples was carried out under subdued red light. The samples were dry-sieved to recover the grain size fraction of either 150-212 µm, 150-250 µm, or 300-355 µm (see Table 5.1). The sediment samples were well-sorted and it was difficult to gather enough material from more than one grain-size fraction. The sand was treated with hydrochloric acid (HCl) and with disodium oxalate ($Na_2C_2O_4$) to break up aggregates, respectively. Hydrogen peroxide (H_2O_2) was used to remove organic matter. Quartz minerals were extracted using a heavy

liquid (sodium polytungstate) separation and subsequently treated with 40% Hydrofluoric acid (HF) for about 60 minutes to etch the surface of the grains and to dissolve any remaining feldspar minerals.

5.3.2 Instrumentation

The measurement of multi-grain aliquots were carried out using automated Risø TL/OSL readers (DA 15 and DA 20) equipped with blue (470 nm) light-emitting diodes (LED) and 7.5 mm Hoya U-340 detection filters (Bøtter-Jensen et al., 2000). In multi-grain measurements the quartz grains were mounted on stainless steel discs using silicon oil. Performance tests were carried out using medium-sized aliquots with a diameter of 6 mm (equivalent to a few hundred or thousand grains depending on the grain size used). For measurement of equivalent doses (D_e) we used small aliquots containing about 20 grains each. This is equivalent to 1 and 2 mm in diameter for the 150-212 µm fraction and 300-355 µm fraction, respectively (see Fig. 5.2 of Duller, 2008). Furthermore, we visually checked representative aliquots of each batch. The multi-grain aliquots were stimulated for 40 s using the blue LEDs.

An automated Risø TL/OSL reader (DA 20) fitted with a single-grain attachment (Duller et al., 1999; Bøtter-Jensen et al., 2000) was used for the OSL measurement of quartz single-grains. The grains (grain size 150-250 or 150-212 µm) were loaded into aluminium single-grain discs with a 10 x 10 grid of 300 µm grain holes and stimulated with a green laser at 532 nm for 0.83 s. To confirm that only one grain was loaded into each hole the single-grain discs were visually inspected using a microscope before measurement.

5.3.3 OSL measurements

A single-aliquot regenerative-dose (SAR) procedure (Murray and Wintle, 2000) was used with four to five regenerative doses, a zero dose measurement and two repeat doses to obtain a recycling ratio and an OSL-IR depletion ratio (Duller, 2003). This allowed the construction of a sensitivity corrected dose response curve for each individual grain or aliquot (see typical decay curves and dose response curves in Fig. 5.3). Our SAR protocol employed a preheat temperature of 180 °C for 10 s and a cutheat of 160 °C (see section 5.4.1). Only multi-grain aliquots with a recycling and IR depletion ratio within 15 % of unity and a test dose response known to better than 15 % were accepted for D_e calculation. For the single-grain data only grains with recycling ratios within two standard deviations of unity and natural test dose responses known to better than 20 % were accepted. Furthermore, we excluded grains with non-monotonically growing dose response curves (e.g. dose response curves not growing with increasing dose). All dose estimates are derived by fitting the regenerated dose points with a linear function.

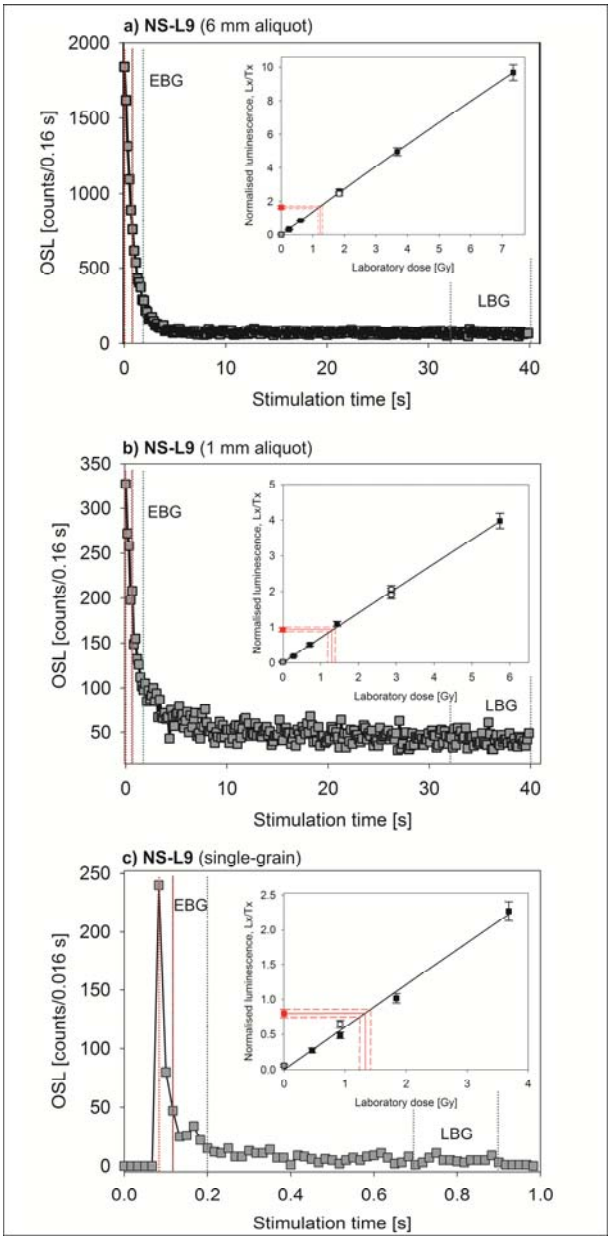

Figure 5.3: Quartz decay curves and dose response curves of sample NS-L 9. (a) Medium (few hundred grains) aliquots, **(b)** small (~20 grains) aliquots and **(c)** single-grains. For multi-grain measurements the time interval from 0.48 s to 1.48 s or from 32 s to 40 s was subtracted from the initial 0.48 s of the OSL signal as early background (EBG) or late background (LBG), respectively. For single-grains the time interval from 0.033 s to 0.119 s or from 0.63 s to 0.83 s was subtracted from the initial 0.033 s of the OSL signal as EBG or LBG, respectively.

In routine analysis the later part of the OSL decay curve (e.g. the last 8 s) is usually subtracted from the initial part (e.g. the first ~0.5 s) to produce a net OSL signal. This approach is called the late background subtraction (LBG) approach. However, Jain et al. (2003) and Singarayer and Bailey (2003, 2004) demonstrated that the quartz OSL stimulation curve can be represented by the linear sum of first order exponential decaying functions. The decay rate of the fast component, used for dating, is about 10 times faster than the next fastest component. Because the intensity of an exponential decay at any point on the curve is proportional to the initial intensity and to the area underlying the decay curve, subtracting a background signal measured close to the beginning of the decay curve (early background, EBG) from the initial signal gives an accurate estimate of an intensity proportional to the area under the fast component, and at the same time minimises the contribution of the slower components, all without the considerable labour of curve fitting. Cunningham and Wallinga (2010) have argued that the contribution from the fast OSL component to this net OSL signal can be maximised by using a time interval for background subtraction ~2.5 times longer than the initial

signal, immediately following the initial integral. Ballarini et al. (2007) concluded based on single-grain analyses that the D_e of dim grains can be overestimated due to the incorporation of a slow OSL component that was apparently not zeroed at the time of burial. The EBG approach has the advantage of reducing the contribution from medium and slow components, resulting in smaller recuperation, thermal transfer and tighter D_e distributions (Cunnigham and Wallinga, 2010); these issues are important for all samples, but particularly to young material such as is investigated here. For multi-grain aliquots we use the signal from 0.48 s to 1.48 s as early background and subtract it from the initial 0.48 s of the OSL signal. For the single-grain measurements, the time interval from 33 ms to 119 ms was subtracted from the initial 33 ms of the OSL signal (Fig. 5.3). For comparison, a LBG between 32 to 40 s and 0.60 to 0.83 was also considered for multi-grain and single-grain analyses, respectively.

The uncertainty on individual D_e values has been assigned using "Analyst 3.24" (Duller, 2007) and consists of contributions from counting statistics and curve fitting errors. An additional uncertainty was added in quadrature to that estimated by "Analyst" to account for other intrinsic sources of uncertainty (e.g. instrumental reproducibility). For small aliquot (~20 grains) and single grain measurements an additional uncertainty of 5 % and 10 %, respectively, was added to account for the dispersion observed in a dose recovery experiment (see section 5.4.2). This additional dispersion found in the gamma-dose recovery experiments quantifies all sources of variability that can be quantified within our experimental set-up; it includes any contribution to the variability caused by instrument reproducibility and other intrinsic sources of variability. In summary, the uncertainties assigned to our individual D_e estimates include counting statistic, curve fitting errors and the additional dispersion observed in a uniform gamma-irradiated sample.

5.3.4 Dose rate determination

The radionuclide concentrations of the surrounding sediment were determined using high-resolution gamma spectrometry. The samples were measured in Marinelli-beakers filled with 700 g of sediment using an HPGe (High-Purity Germanium) N-type coaxial detector. The gamma rays from the radionuclides ^{214}Pb and ^{214}Bi were used to obtain the uranium (^{238}U) content and the gamma rays of ^{208}Tl, ^{212}Pb and ^{228}Ac, were measured to calculate the thorium (^{232}Th) content. In addition, to check if there is a disequilibrium in the uranium decay chain, the activities of the ^{238}U daughter nuclides ^{234}Th and ^{210}Pb (two end members of the uranium decay chain) were compared in three samples (NS-L 5, 6, and NS-L 13). No significant discrepancy of the activities was observed indicating equilibrium for the uranium decay chain. For the potassium activity, the release of gamma rays from decay of ^{40}K to ^{40}Ar was observed. The samples were each measured for several days. The activities of ^{238}U, ^{232}Th and ^{40}K were converted into α- and β-dose rates using the factors of Adamiec and Aitken (1998) and the attenuation of the β-particles in the grains was evaluated according to Mejdahl (1979). An internal α-dose rate of 0.06 ± 0.03 Gy/ka was included. The α-irradiated outer part of the grains was removed by treatment with HF. The β- and γ-dose rates were corrected for the water content attenuation following Aitken (1985). The "in situ" water content is estimated to be 18 ± 4 %. The cosmic dose rate was calculated according to Prescott and Hutton (1994) and Prescott and Stephan (1982). The results of dose rate determination are listed in Table 5.1.

Table 5.1: Results of dose rate determination.

Sample core	sample	depth [m]	Grain size [μm]	Cosmic dose rate [Gy/ka]	β-dose rate [Gy/ka]	γ-dose rate [Gy/ka]	Total dose rate [Gy/ka][a]
ME-02	NS-L 10	0.55-0.65	150-212	0.19 ± 0.02	0.44 ± 0.04	0.22 ± 0.03	0.91 ± 0.06
ME-02	NS-L12	2.40-2.50	150-212	0.14 ± 0.01	0.36 ± 0.04	0.17 ± 0.03	0.73 ± 0.06
ME-02	NS-L13	3.40-3.55	300-355	0.12 ± 0.01	0.60 ± 0.04	0.29 ± 0.03	1.07 ± 0.06
ME-02	NS-L14	3.60-3.80	300-355	0.12 ± 0.01	0.60 ± 0.04	0.28 ± 0.03	1.06 ± 0.06
WSS-04	NS-L5	3.60-3.75	300-355	0.12 ± 0.01	0.30 ± 0.04	0.15 ± 0.03	0.63 ± 0.06
WSS-04	NS-L6	2.60-2.70	300-355	0.14 ± 0.01	0.25 ± 0.04	0.14 ± 0.03	0.58 ± 0.06
WSS-05	NS-L9	2.40-2.50	150-250	0.14 ± 0.01	0.32 ± 0.04	0.16 ± 0.03	0.68 ± 0.06
WSS-06	NS-L20	4.55-4.65	300-355	0.10 ± 0.01	0.31 ± 0.04	0.17 ± 0.03	0.64 ± 0.06
SWS-02	NS-L16	0.10-0.20	300-355	0.21 ± 0.02	0.53 ± 0.12	0.23 ± 0.03	1.03 ± 0.06

Foot notes:
[a] Total dose rate includes cosmic dose rate, β-dose rate, γ-dose rate, and an internal α-dose rate of 0.06 ± 0.03 Gy/ka.

5.4 Results and discussion

5.4.1 Performance of SAR protocol

For the thorough testing of our SAR protocol and for the selection of the most appropriate thermal treatment, we applied preheat plateau, thermal transfer and dose recovery tests at six different preheat temperatures (160-260 °C; see Wintle and Murray, 2006 for a discussion of these tests). Figure 5.4 shows the results for the quartz-SAR measurement based on multi-grain (6 mm diameter aliquots) measurement of sample NS-L 12. The preheat temperature for D_e measurements was selected from the plateau region of the preheat plateau test between 160 and 240 °C (Fig. 5.4 a). A significant thermal transfer was detected for preheat temperatures above 200 °C (Fig. 5.4 b).

The beta-dose recovery ratios (ratio of measured to given dose) are consistent with unity within one sigma for the entire preheat temperature range (Fig. 5.4 c). Based on these results, we selected a preheat temperature of 180 °C and a cutheat temperature of 160 °C for the measurement of the D_e values. To support the validity of this choice, we undertook a beta dose-recovery test using four medium aliquots of each sample. The resulting measured to given dose ratios are all consistent with unity, and the mean ratio is 1.01 ± 0.01 (n = 28), confirming the ability of our protocol to accurately measure a known dose given to these samples before any thermal treatment.

We also undertook gamma-dose recovery experiments (see section 5.4.2) using both small aliquots and single-grains. Using an EBG we obtained ratios of 0.97 ± 0.05 (n = 15) and 1.03 ± 0.03 (n = 29) for small aliquots and single-grains, respectively. For the LBG we obtained ratios of 1.00 ± 0.03 (n = 18) and 1.01 ± 0.02 (n = 51) for small aliquots and single-grains, respectively. Thus, all dose recovery ratios confirm the accuracy of the applied SAR for small aliquots and single-grains independent of the background subtraction (EBG or LBG) used.

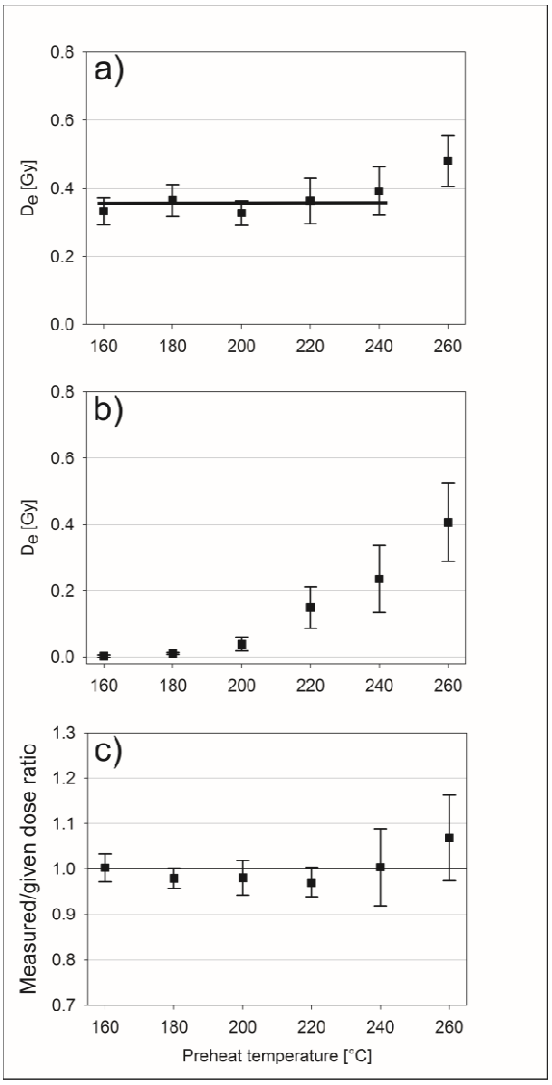

Figure 5.4: Performance of quartz SAR. (a) Preheat plateau test, **(b)** thermal transfer test and **(c)** dose-recovery test results of Sample NS-L 12 are shown. Results are indicated as the mean value of four medium aliquots and the 1-σ standard deviation.

5.4.2 Gamma dose-recovery

In the literature, it has been shown that counting statistics and instrument reproducibility alone are insufficient to account for the observed variability in laboratory gamma-dose recovery experiments (e.g. Thomsen et al., 2005). Thus, in order to quantify intrinsic sources of variability, we first gave a known gamma-dose of 2.0 Gy using a ^{137}Cs point source in a scatter-free geometry at a distance of 2 m to a modern swash-bar analogue (NS-L 16); this was known to have been well bleached prior to deposition (Fig. 5.5). The quartz sample in the irradiation cell was ~1 mm thick, and it was surrounded by ~1.7 mm of glass, ensuring a uniform dose rate throughout the sample volume. This laboratory-irradiated sample was then measured using both small aliquots (~20 grains) and single-grains (data not shown), and the dose recovery ratios were all consistent with unity (see section 5.4.1). Assigning uncertainties to the individual D_e values based on counting statistics and curve fitting errors alone ("Analyst 3.24", Duller, 2007) gives an σ_{OD} value of 5.5 ± 0.5 % (n = 13) and 11.4 ± 1.4 % (n = 51) for small aliquot and single grains, respectively using the LBG approach. Using the EBG approach the calculated σ_{OD} values reduce to 4.6 ± 0.6 % (n = 10) and 9.8 ± 1.5 % (n = 29), respectively.

In what follows we have added (in quadrature) an additional uncertainty of 5 % and 10 % for small aliquots and single grains, respectively to account for the intrinsic sources of uncertainty quantified in the gamma-dose recovery experiment (Note that any instrument variability is included in the dispersion observed when measuring a uniform dose, and should not be separately included). For single-grain measurements, the additional intrinsic uncertainty of ~10 % is in good agreement with those reported earlier by Thomsen et al. (2005) for a heated quartz sample and Thomsen et al. (2007) for heated and unheated samples. In our view, any measurement of the natural dose recorded by a single aliquot (of any size, i.e. including a single-grain) cannot have a smaller dispersion than that derived from such gamma dose-recovery experiment.

5.4.3 Assessing burial doses of sediment mixtures

Because of the sampling techniques employed we expect contamination of the swash-bar sediments by overlying younger sediments for samples NS-L 5, 6, 13, 14, and 20 (see section 5.2.2). To obtain burial doses for these contaminated swash-bar sediments we apply the Finite Mixture Model (FMM, Roberts et al., 2000) to identify the dose populations containing the largest D_es assuming that those grains or aliquots with the smallest D_es are intrusive from the overlying and younger aeolian and overwash deposits. The FMM was introduced for Fission Track Dating by Galbraith and Green (1990). Given that single-grains are the smallest unit of sediment transport, one should investigate single-grain D_e distributions to avoid D_e averaging effects. First we analyse an aeolian sand sample (NS-L 10) and a swash-bar sample (NS-L9), both thought to be uncontaminated, to determine the minimum amount of over-dispersion (σ_{OD}) to be expected in uncontaminated dose populations (see section 5.4.3.1). These two samples and a modern beach analogue were taken with the closed steel probe using closed plastic liners (see section 5.2.2); sediment mixing during sampling is negligible in these cases. We calculated σ_{OD} using the central age model of Galbraith et al. (1999); this parameter is an important input value in the FMM (Jacobs et al., 2006; Rodnight et al., 2006). Secondly, we test the ability of the FMM to extract accurate D_e estimates by preparing a known laboratory mixture of grains from the aeolian (NS-L 10) and swash-bar (NS-L 9) sample (section 5.4.3.2). Finally we examine whether small aliquots can be used as a proxy for single-grains (section 5.4.3.1 and 5.4.3.2).

5.4.3.1 Analyses of uncontaminated dose distributions

The small aliquot D_e of the modern swash-bar sample (Fig. 5.5) is close to symmetric with a dominant D_e population at about 0.015 Gy; the CAM D_e is 0.02 ± 0.01 Gy (equivalent to an age of ~20 ± 10 years) indicating that the light exposure of these grains prior to deposition was sufficient to effectively reset the OSL signal. This observation supports the hypothesis that the older swash-bar sediments were also well-bleached at deposition.

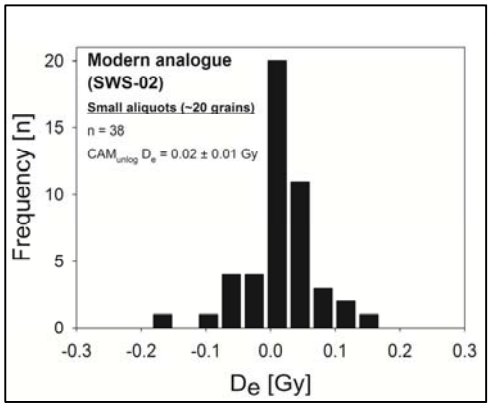

Figure 5.5: D_e distribution of the modern analogue swash-bar sample SWS-02. The D_e value was calculated using a unlog version of the Central Age Model (CAM) according to Galbraith et al. (1999) and Arnold et al. (2009).

A comparison of single-grain and small aliquot D_e distributions for the uncontaminated aeolian (NS-L 10) and swash-bar (NS-L 9) samples is shown in Figure 5.6 and Figure 5.7, respectively. Both Figures 5.6 and 5.7 also compare the use of an early background (EBG) and a late background (LBG) subtraction (see section 5.3.3).

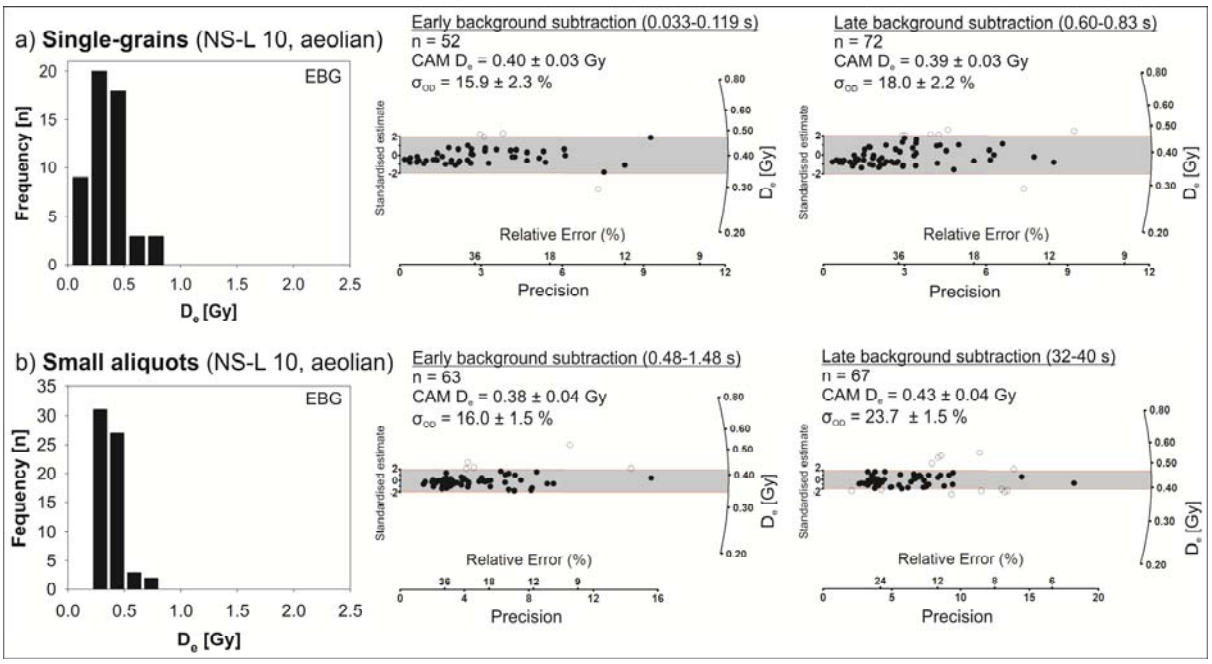

Figure 5.6: D_e distributions of the uncontaminated aeolian sample NS-L10. Histograms (left) and radial plots (centre, right) of D_e distributions derived from single-grain (a) and small aliquot measurement (b) of the aeolian sample NS-L 10. The data in the central radial plots were analysed using the early background (EBG) subtraction; the data in the right radial plots were analysed using the late background (LBG) subtraction.

For the aeolian sample (NS-L 10) we obtained narrow and approximately symmetric D_e distributions for both single-grain (Fig. 5.6 a) and small aliquot (Fig. 5.6 b) measurements, both centred on about 0.4 Gy. The CAM D_es of single-grain and small aliquot analyses are consistent with each other irrespective of the choice of background summation interval. To assess whether the assigned uncertainties on the individual D_e estimates (including the σ_{OD} derived from the gamma-dose recovery experiments) adequately describe the observed variability we calculated the σ_{OD} for each data set using the central age model (CAM) of Galbraith et al. (1999). For both single-grains and small aliquots (Fig. 5.6 a and 5.6 b) we obtain, a σ_{OD} of ~16 % when using the EBG approach. When LBG subtraction is used the σ_{OD} values increase to ~18 % and ~24 %, respectively. These σ_{OD} values indicate that the intrinsic uncertainties assigned to the D_e values (see section 5.3.3, 5.4.2) are too small to account for the observed variability in the D_e distributions from what are very likely to be well-bleached and unmixed samples. There are two possible explanations for this: (i) this additional variability in the D_e distributions are caused by extrinsic factors, e.g. microdosimetry (see review by Duller, 2008), partial bleaching and/or post-depositional sediment mixing (e.g. Rodnight et al., 2006; Bateman et al., 2007); (ii) we have underestimated the instrinsic variability in our dose estimates, i.e. the variability in dose estimation using SAR is not adequately described by counting statistics, fitting errors and gamma-dose recovery over-dispersion. At this stage we cannot choose between these two possibilities.

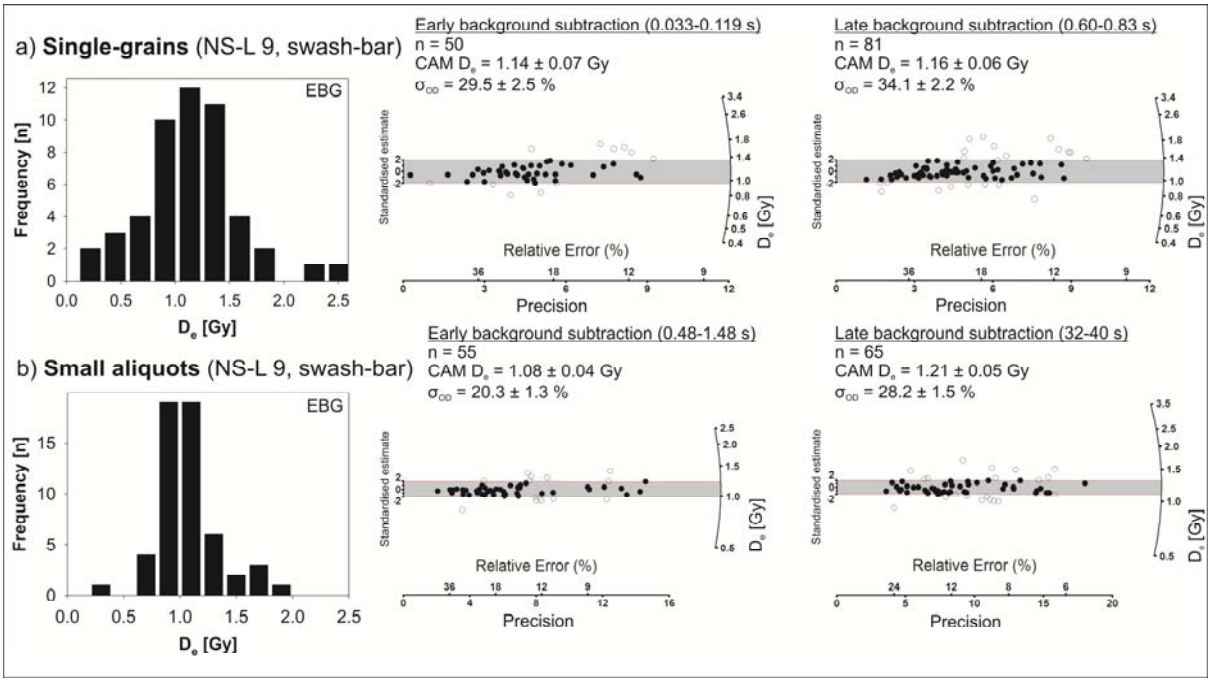

Figure 5.6: D_e distributions from the uncontaminated swash-bar sample NS-L 9. Histograms (left) and radial plots (centre, right) of D_e distributions derived from single-grain **(a)** and small aliquot measurement **(b)** of the swash-bar sample NS-L 9 are shown. The data shown in the central radial plot was analysed using the early background subtraction; the data of the right radial plot was analysed using the late background subtraction.

For the swash-bar sample (NS-L 9) we also obtain close to symmetric D_e distributions for both single-grain and small aliquot measurements (Fig. 5.7) and the CAM D_e of these distributions are consistent with each other (Fig. 5.7 a, b). As for the aeolian sample above, the distributions obtained by using the LBG are more dispersed (see radial plots in Fig. 5.7 a, b) and as a result the σ_{OD} for the EBG subtraction is smaller than that for the LBG subtraction, especially for the small aliquot data. The LBG σ_{OD} is 34.1 ± 2.2 % (single-grains) and 28.2 ± 1.4 % (small aliquots) whereas the EBG σ_{OD} is 29.5 ± 2.5 % (single-grains) and 20.3 ± 1.3 % (small aliquots). This reduction in σ_{OD} is presumably for two reasons. Firstly, when using the EBG, 31 low sensitivity grains (i.e. those with a low test dose (T_N) response) were removed from the distribution (Fig. 5.8 a, b) because the uncertainty on the test dose exceeded the 20 % threshold (see section 5.3.3). Removing these grains appears to reduce the σ_{OD} in the D_e distributions: the σ_{OD} of the D_e distribution of the 31 grains (Fig. 5.8 b) accepted using LBG, but not accepted if EBG is used, is 39.5 ± 5.0 %; if only those 50 grains are considered which are accepted using EBG (and also LBG) this decreases to 30.7 ± 2.3 % (Fig. 5.8 a), although one cannot be confident that these two over-dispersions are distinguishable because of the relatively large uncertainty on the σ_{OD} of the first value. Secondly, we deduce that the apparently acceptable signal strength using LBG in some of these grains was derived from the slow/medium components, and that when this contribution is removed the fast component is found to be unacceptably weak and the T_N error threshold is exceeded. In order to evaluate this we calculated the fast ratio (Madsen et al., 2009; Durcan and Duller, 2011) for the single-grains of sample NS-L 9 to estimate the contribution of the fast component to the OSL signals. In this approach, the OSL intensity of the fast component (*F*) is divided by the OSL intensity of the medium component (*M*). Here, *F* is derived from the summation of the first 0.016 s and *M* from the summation between 0.048-0.112 s of the OSL decay curve. A background summed over the last 0.21 s is subtracted from both *F* and *M*. Fig. 5.9 a and 5.9 b shows the intrinsic luminescence brightness as a function of the fast ratio. The average fast ratio for the grains rejected in EBG (4.2 ± 0.8, n = 31) is significantly lower than that for the accepted

grains (6.7 ± 0.6, n = 50) confirming that using the EBG biases is preferentially rejecting grains with a relatively weak fast component. By applying the EBG we remove ~30-40 % of the single-grain dose estimates (Fig. 5.6 a and 5.7 a) and 5-15 % of the small aliquots (Fig. 5.6 b and 5.7 b) because the test dose uncertainty of these aliquots exceeds the threshold for single-grains and small aliquots of 20 % and 15 %, respectively.

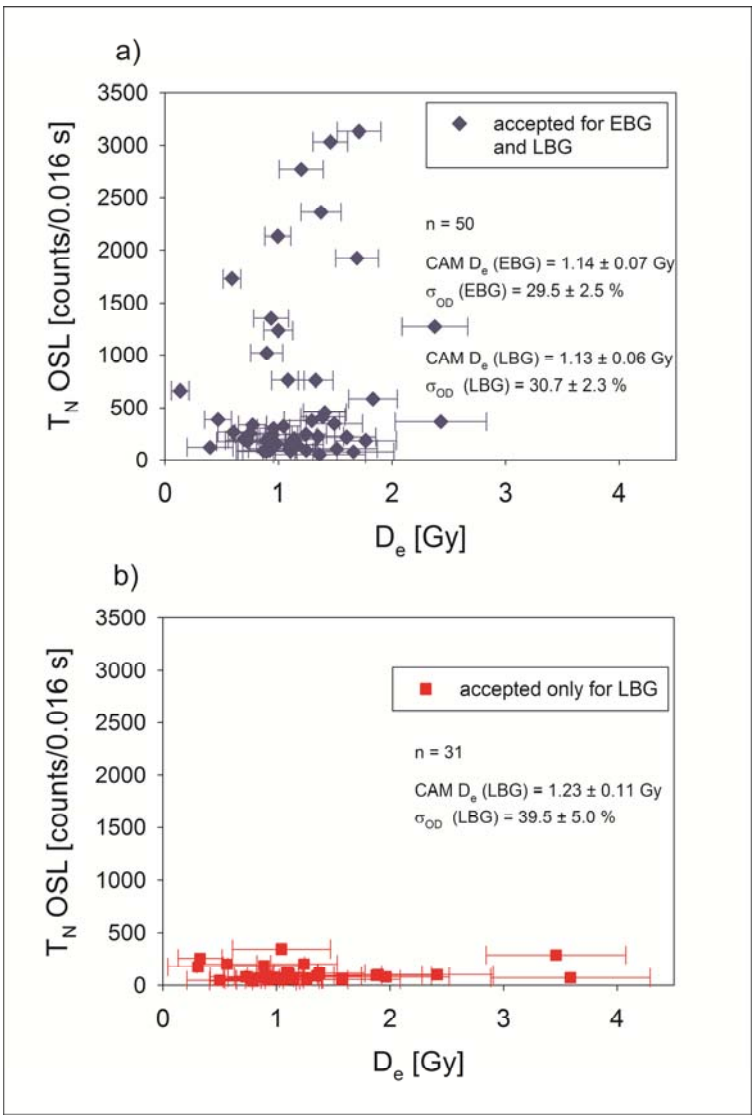

Figure 5.8: Intrinsic OSL brightness (T_N response) versus D_e. The over-dispersions were calculated using the CAM (Galbraith et al., 1999).

We now examine the effects of EBG analysis of the accepted aliquots on the D_e values. In Figure 5.10, the D_e estimates calculated using EBG subtraction are shown against the corresponding estimates calculated using LBG subtraction for both single-grain and small aliquots for sample NS-L 10 (Fig. 5.10 a) and NS-L 9 (Fig. 5.10 b). Figure 5.10 shows that the background subtraction has no significant effect on the D_e values. Only two small aliquots (one in each sample) have significantly larger doses using the LBG approach compared to the EBG approach. The decay curves for these aliquots are shown in Fig. 5.10 a and 5.10 b, respectively. Both aliquots appear to have a weak fast component compared to the more typical behaviour (a typical small aliquot decay curve is shown in Fig. 5.3 b), and will thus have a larger contribution from the slower components using LBG. Summarising these observations, it appears that the estimated doses are not significantly affected by the choice of background summation interval, but the EBG subtraction does reduce the σ_{OD} values. We find this

surprising, because we had expected that at least some of the over-dispersion arose because of such factors as poor bleaching, instability, and poor sensitivity correction of the medium and/or slow components. Had this been the case the average dose would have been expected to change as the σ_{OD} decreased. Nevertheless, the reduction in σ_{OD} means that there are clear advantages in using the EBG dose distribution.

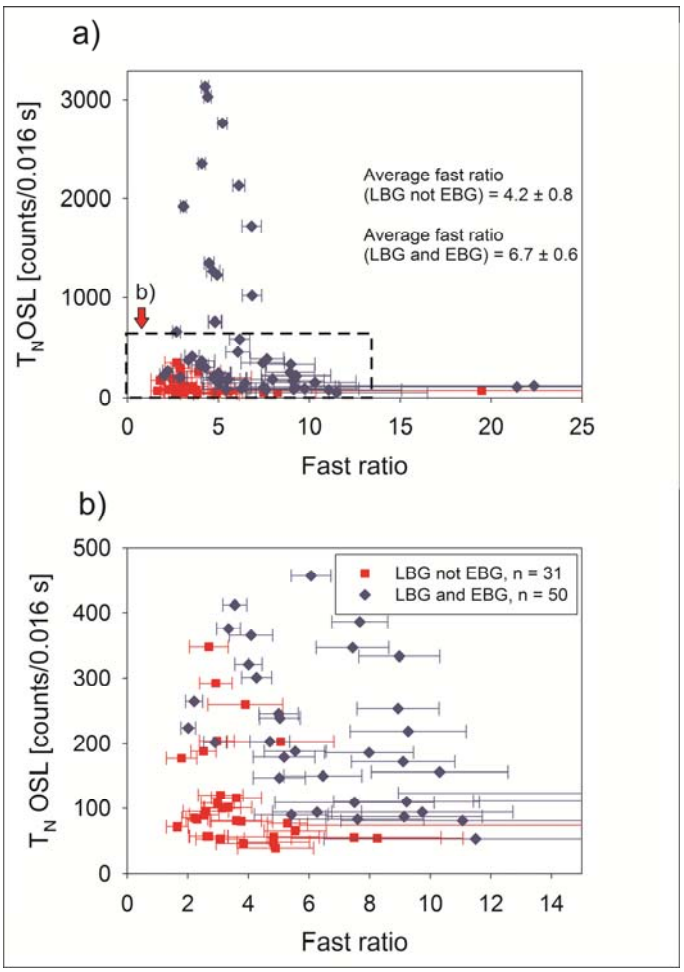

Figure 5.9: T_N response versus fast ratio. The fast ratio (F-LBG/M-LBG) was calculated according to Madsen et al. (2009) and Durcan and Duller (2011). The integral of the first channel (first 0.016s) was used for F, channel 3-7 (0.048-0.112s, M) of the OSL signal were used for M. The background (LBG) was calculated from channel 40-50 (0.64-83s).

Using the EBG for analyses of the swash-bar sample NS-L 9 we obtained over-dispersions of 29.5 ± 2.5 % (single-grain) and 20.3 ± 1.3 % (small aliquots). The CAM D_es of these D_e distributions agree within uncertainties. For sample NS-L 10 the CAM D_e values and σ_{OD} values derived from the single-grain (Fig. 5.6 a) and small aliquot D_e distributions (Fig. 5.6 b) are also consistent with each other when the EBG is applied. Thus, for the uncontaminated samples examined here the use of small aliquots gives a result similar to that obtained using single-grain analysis.

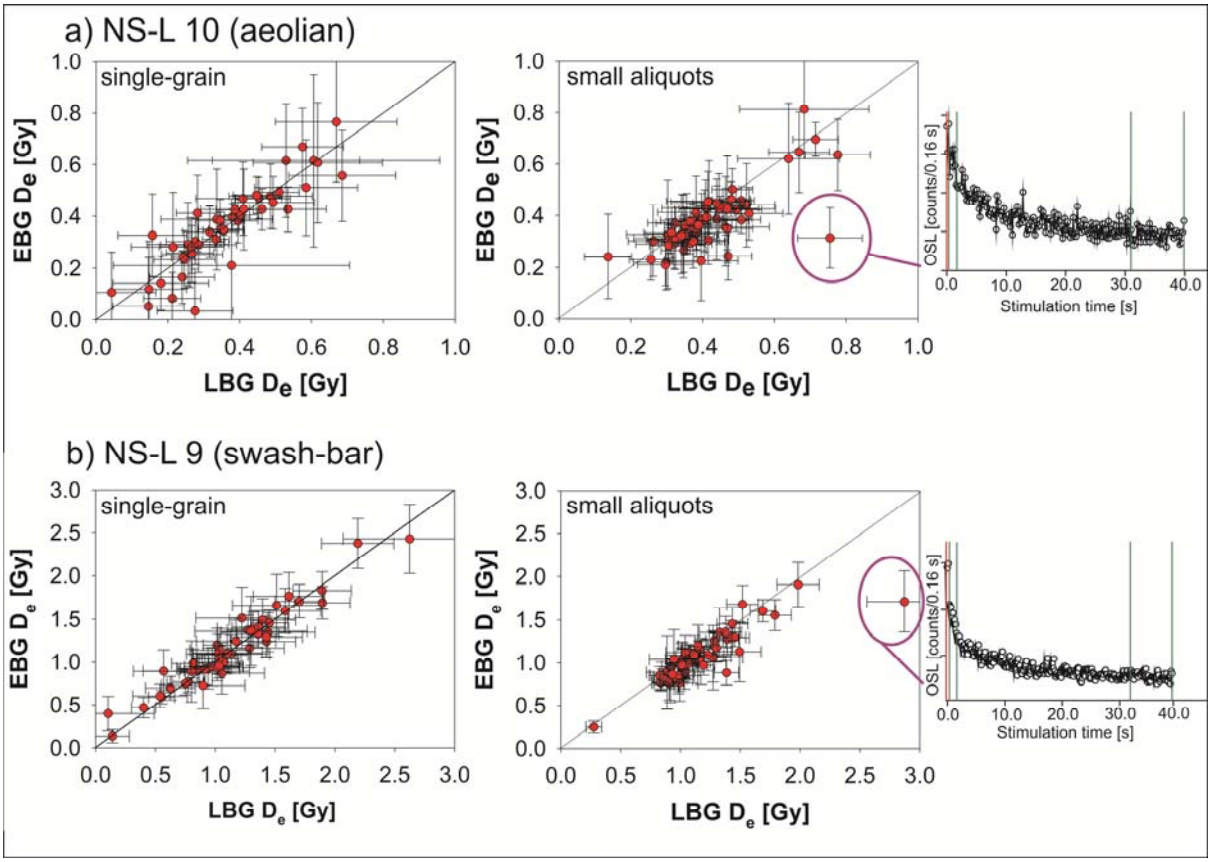

Figure 5.10: Comparison of D_e using LBG and EBG. For single-grains the time interval from 0.033 s to 0.119 s and from 0.63 s to 0.83 s was subtracted from the initial 0.033 s of the OSL signal to obtain EBG D_e and LBG D_e, respectively. For small aliquot measurements the time interval from 0.48 s to 1.48 s and from 32 s to 40 s was subtracted from the initial 0.48 s of the OSL signal to obtain the EBG D_e and LBG D_e, respectively.

In summary, we regard both NS-L 10 and NS-L 9 as being well-bleached despite the single-grain over-dispersion values of 15.9 ± 2.3 % and 29.5 ± 2.5 %. Note that these σ_{OD} values are in addition to those found for 'ideal' gamma dosed distributions. Our σ_{OD} values found in the aeolian and swash-bar D_e distributions are comparable to other values reported for well-bleached sediments (e.g. Olley et al., 2004; Pietsch, 2009; Lüthgens et al., 2011). Olley et al. (2004) observed overestimation in the weighted mean ages of Holocene sediments of various settings, which show over-dispersion values of more than 20 % in the respective D_e distributions, whereas they found agreement of the weighted mean age with the independent age control for σ_{OD} values of 21 % or lower. However, we suggest that any over-dispersion threshold for well-bleached samples is generally not very useful. Obviously, incomplete bleaching should give a decreasing relative over-dispersion as the mean dose increases. However, the σ_{OD} is essentially the unexplained dispersion after all known sources are taken into account; this over-dispersion is less likely to decrease with increasing dose, and if some laboratory contributions are not recognised it will be overestimated. In the remaining part of this paper, we take the σ_{OD} parameter for single-grain and small aliquot analyses of NS-L 10 and NS-L 9 (see Fig. 5.6 and 5.7) as representative of well bleached and uncontaminated aeolian and swash-bar sediment sample, respectively.

Table 5.2: Analyses of the uncontaminated samples and the laboratory mixture.

Sample	Single-grains						Small aliquots (20 grains)				
	measured/accepted	L_f [%][a]	σ_{OD} [%][b]	CAM D_e [Gy][c]	FMM Db_1 [Gy][d]	FMM Db_2 [Gy][d]	measured/accepted	σ_{OD} [%][b]	CAM D_e	FMM Db_1 [Gy][d]	FMM Db_2 [Gy][d]
NS-L 10	1800/52	4	15.9 ± 2.3	0.40 ± 0.03	-	-	96/63	16.0 ± 1.5	0.38 ± 0.04	-	-
NS-L 9	1900/50	3	29.5 ± 2.5	1.14 ± 0.07	-	-	96/55	20.3 ± 1.3	1.08 ± 0.04	-	-
NS-L 9+10 mix	2100/53	3	49.1 ± 5.0	0.83 ± 0.07	0.42 ± 0.08	1.14 ± 0.10	144/52	43.5 ± 4.4	0.77 ± 0.06	0.49 ± 0.06	1.14 ± 0.07

Foot notes:
[a] Percentage of grains giving a detectable test dose response.
[b] σ_{OD} is the over-dispersion parameter (Galbraith et al., 1999).
[c] Central Age Model (CAM) dose estimate (Galbraith et al., 1999).
[d] Finite Mixture Model (FMM) dose estimate (Roberts et al., 2000).

5.4.3.2 Applying the Finite Mixture Model (FMM) to a laboratory sediment mixture

The main objective of this work is to determine best estimates of the burial doses of the contaminated swash-bar samples. To derive these estimates, we apply the Finite Mixture Model (FMM, Roberts et al, 2000). Before doing so we test the ability of the model to identify discrete dose populations using a 50:50 (by mass) laboratory mixture of the uncontaminated aeolian sample NS-L 10 and the uncontaminated swash-bar sample NS-L 9. This laboratory mixture was measured using both single-grains and small aliquots (Fig. 5.11 a, 5.11 b, respectively). The results are summarised in Table 5.2. The FMM requires estimates of the σ_{OD} values for the individual dose populations as an input parameter. We used the σ_{OD} values determined for the uncontaminated swash-bar sample (20.0 % and 29.5 % for small aliquots and single-grains, respectively; see previous section).

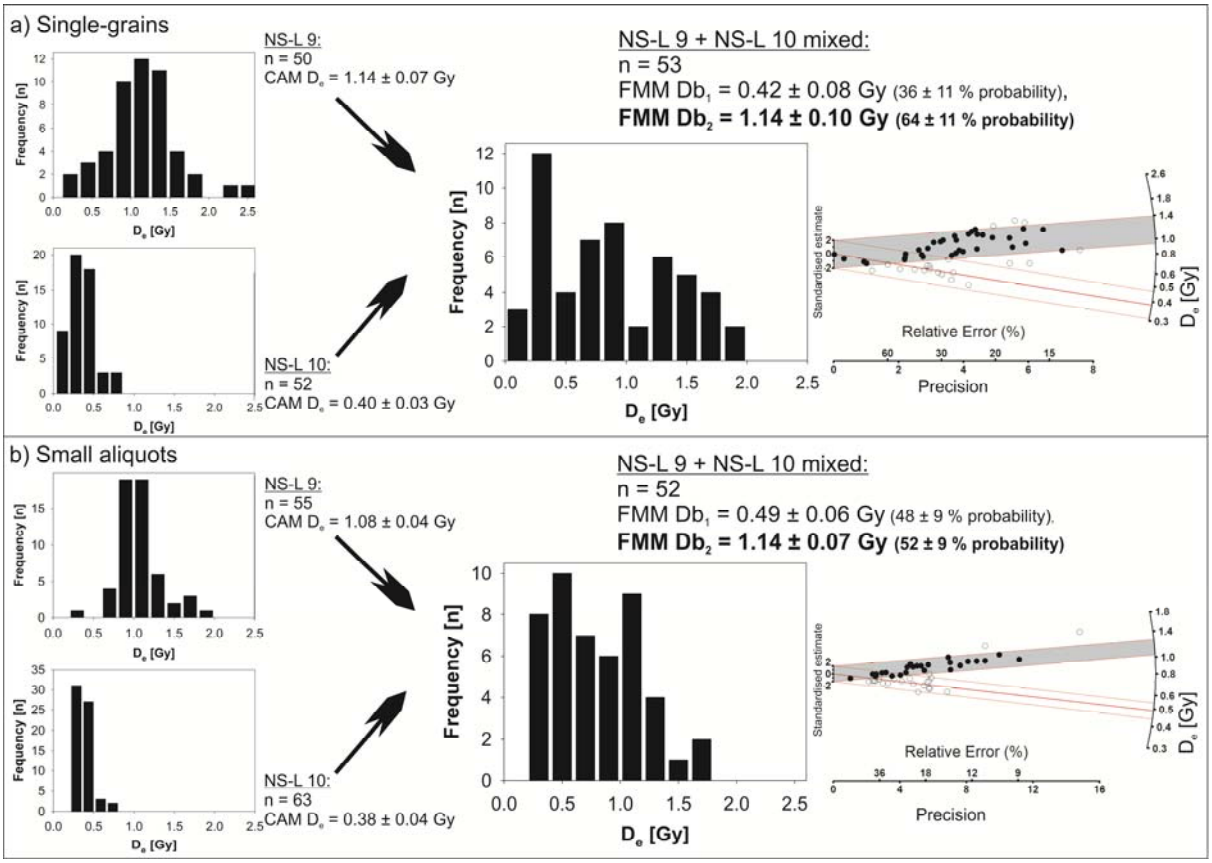

Figure 5.11: Analysis of a laboratory sediment mixture. D_e distributions derived from single-grain **(a)** and small aliquot **(b)** measurements are show. On the left the histograms of the original aeolian (NS-L 10) and swash-bar (NS-L 9) D_e distributions, on the right histograms and radial plots of the resulting 50:50 laboratory mixture are shown. The CAM D_e was calculated according to Galbraith et al. (1999). The burial doses (Db) and the probabilities of the dose components were calculated using the Finite Mixture Model of Galbraith and Green (1990). In both radial plots at the right (a,b), the burial doses of the older dose components (Db_2) are grey shaded; the lower dose components (Db_1) are light shaded.

To assess the most suitable FMM fitting with increasing values of k (number of discrete dose components) the BIC (Bayesian Information Criterion) score was used as suggested by Galbraith (2005) and then applied by Jacobs et al. (2008a) and Arnold and Roberts (2009) and others. For both data sets (Fig. 5.11 a and b) the most suitable fit for the 50:50 laboratory mixture was obtained for k = 2 (Fig. 5.11). Figure 5.11 a shows that the two dose populations Db_2 (1.14 ± 0.10 Gy) and Db_1 (0.42 ± 0.08 Gy) derived from the laboratory mixture are consistent with the CAM D_e of the swash-bar sample NS-L 9 (1.14 ± 0.07 Gy) and the CAM D_e of aeolian sample NS-L 10 (0.40 ± 0.03 Gy). The FMM also suggests that the two components are present in approximately equal portions (Fig. 5.11 a). It appears that the FMM applied to single-grain data is able to successfully identify the weighted mean dose and relative contribution of the original D_e components as previously demonstrated by others for artificial and natural sediment mixtures (e.g. Bateman et al., 2007; David et al., 2007). The FMM was also applied to the small aliquot D_e distribution measured from the laboratory mixture (Fig. 5.11 b). The FMM correctly identifies two dose populations in equal proportions with doses consistent with the expected doses. This agreement between FMM results and expected results shows that the FMM is able to identify the dose populations successfully.

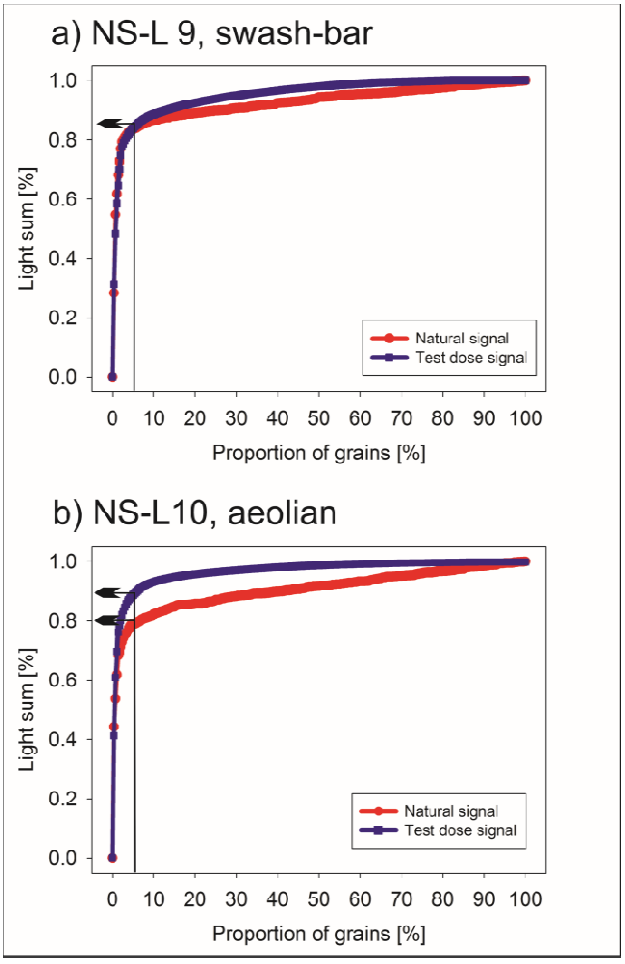

Figure 5.12: Light sum curves of sample NS-L 9 and NS-L 10. The light sum curves of the swash-bar sample NS-L 9 **(a)** and the aeolian sample NS-L 10 **(b)** are shown. The black lines indicate the theoretical contribution to the light sum of the brightest grain on a 20 grain aliquot.

The FMM burial dose components in the artificially-mixed sample based on single-grain or small aliquot analyses appear to be in good agreement with each other and the derived relative contribution of the two components in the known 50:50 laboratory mixture has been estimated accurately. Importantly, by applying the FMM to small aliquot data, we were able to correctly identify the dose population originating from the older swash-bar sample; this suggests that for

these samples small aliquot analyses are adequate. Indeed, Figure 5.12 shows that 80 % to 90 % of the signal arises from only 5 % of the grains. Thus, in an aliquot containing 20 grains, 80-90 % of the signal is likely to come from a single grain. Thus, for our samples it would appear that using small aliquots each of 20 grains is effectively the same as undertaking single-grain measurements of these samples and that D_e averaging effects are negligibly small. However, within the single-grain analyses we rejected 30-40 % low sensitivity grains from the distribution by applying the EBG. In contrast, only 5-15 % of the small aliquots were rejected by applying the EBG. Thus, it is likely that a few dim grains contribute to the signal in the small aliquots. Nevertheless, it is clear that these grains have no significant systematic effect upon the D_e (Fig. 5.10). Furthermore it is well know that the detection efficiency of a standard reader (i.e. without single-grain attachment) used for the measurements of small aliquots is ~40 % higher than that of a single-grain machine because the photomultiplier tube of a single-grain system is further away from the sample. Thus, more single-grains should be rejected compared to small aliquots.

5.4.3.3 Investigating the sensitivity of the FFM outcome to the over-dispersion parameter

Roberts et al. (2000) and Galbraith (2005) stressed that it is important to assess the over-dispersion parameter for the expected (unaffected by mixing or partial bleaching) dose component as accurately as possible. Various approaches (e.g. aeolian samples, sun-bleached portions, dose recovery experiments) are suggested in order to define the expected σ_{OD} (e.g. Roberts et al., 2000; Rodnight et al., 2006; David et al., 2007; Lüthgens et al., 2011). In the previous section we showed that our choice of the σ_{OD} parameter enabled the FMM to accurately extract the correct dose components from a laboratory mixture. In the following, we test how sensitive the FMM results are to σ_{OD} ranging between 1 and 50% with respect to (i) the apparent burial doses corresponding to the oldest dose component (Db_{old}), (ii) the number of dose components (k) and (iii) the probable contribution of each of these components to the mixture. Again, we use the BIC score to determine the most appropriate outcome of the FMM.

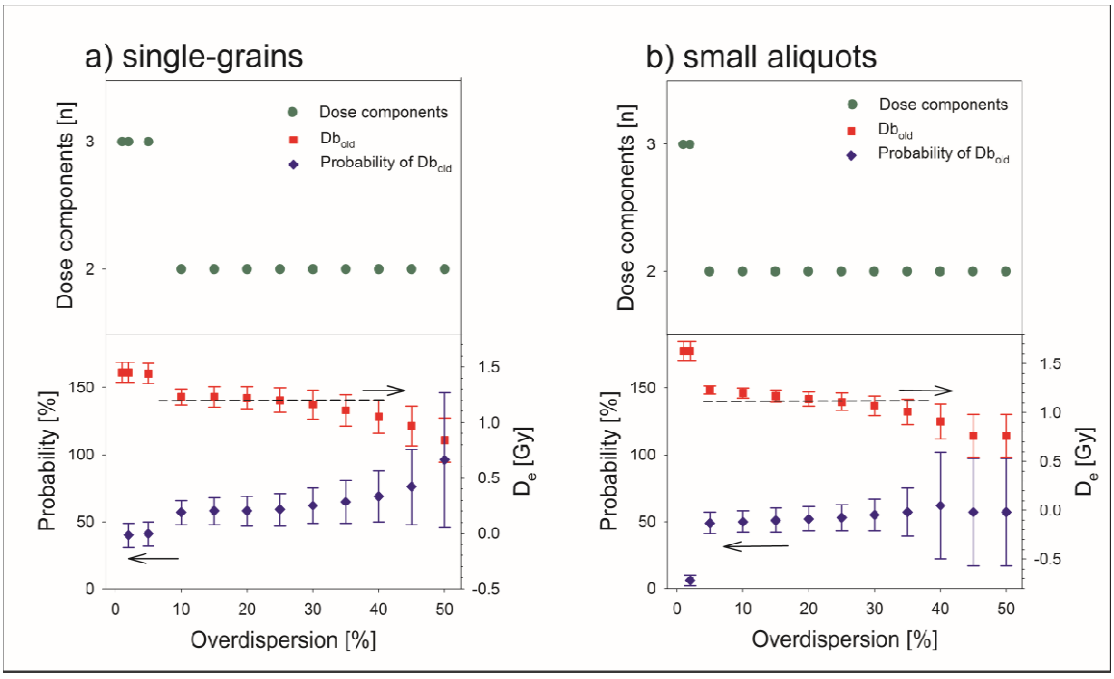

Figure 5.13: The importance of the σ_{OD} parameter to the FMM.

Figure 5.13 shows that the FMM results are largely insensitive to the choice of σ_{OD} parameter for this laboratory mixture; the Db_{old} values are all consistent with the expected value, although both for single-grains and small aliquots Db_{old} tends to decrease with increasing σ_{OD} (Fig. 5.13 a,b). The probabilities of about 50 % are also consistent with expectation. For small aliquots, the apparently correct number of dose components and expected probability was found for a σ_{OD} of only 5 %. These observations indicate that the results of the FMM when applied to our samples should be very insensitive to the exact overdispersion values selected, and that the selected over-dispersion values based on uncontaminated swash-bar and aeolian samples (section 5.4.3.1) are entirely appropriate.

In the previous sections we have demonstrated that no advantage is gained by using the more challenging single-grain measurements compared to small aliquot measurements for these samples. Thus, we are justified in using small aliquot measurements for the remaining samples. In Figure 5.14, we present the dose distributions obtained from the five swash-bar sediment samples (NS-L 5, 6, NS-L 13, 14 and NS-L 20) suspected of suffering from contamination of overlying sediment units due to the sampling method employed. Over-dispersions, CAM ages and the FMM ages derived from the oldest dose components (Db_{old}) are given in Table 5.3. The σ_{OD} estimates from the potentially contaminated swash-bar samples are, as expected, significantly higher than the σ_{OD} for the uncontaminated swash-bar sample NS-L 9 (20.3 ± 1.3 %) with the possible exception of the potentially contaminated NS-L 20 which has an over-dispersion of 24.8 ± 1.8 %.

5.4.3.4 Dating the contaminated samples

For sample NS-L 5 two discrete dose components at 1.02 ± 0.11 Gy and at 0.66 ± 0.09 Gy were obtained (Fig. 5.14 a). The proportion of accepted D_e values contributing to the older component is 59 ± 26% and this component gives an age of 1.6 ± 0.2 ka (Table 5.3). Three dose components were found for sample NS-L 6. The oldest component has a dose (Db_{old}) of 1.12 ± 0.14 Gy, the proportion of accepted D_e values contributing to Db_{old} amounts to of 25 ± 14 % and an age of 1.9 ± 0.2 ka (Fig. 5.14 b, Table 5.3). For sample NS-L 13 three dose components were found. The oldest (Db_{old}) has a D_e of 0.93 ± 0.18 Gy but a probability of only 10 ± 4 % (Fig. 5.14 c). A similar problem was found for sample NS-L 14. The older of two dose populations has a D_e of 0.79 ± 0.08 Gy and a probability of 15 ± 5 % (Fig. 5.14 d). The ages derived from Db_{old} are 0.87 ± 0.17 ka and 0.75 ± 0.05 ka for sample NS-L 13 and NS-L 14, respectively (Table 5.3). Sample NS-L 20 appears to contain two dose components with doses of 0.68 ± 0.04 Gy and 1.08 ± 0.11 Gy (Fig. 5.14 e). The proportion of accepted D_e values contributing to Db_{old} is 20 ± 10 %, and the resulting age is 1.7 ± 0.2 ka (Table 5.3).

In summary it would appear that the D_e distributions of the potentially contaminated samples do contain an older dose population, but that this component represents an unexpectedly small fraction of the accepted grains – it is hard to accept that only 10 to 20 % of the target layer was present in the sampling tube after recovery. To test whether this analysis is could be the result of a statistical artefact, we attempted to apply the FMM model to the D_e distributions of the two samples (NS-L 10 and NS-L 9) in which we were confident that no contamination had occurred. The best FMM fit is obtained for k=2; Db_{old} is 0.37 ± 0.03 Gy and 1.09 ± 0.04 Gy for sample NS-L 10 and NS-L 9, respectively. The contribution of accepted D_e values to Db_{old} was 96 ± 4 % for NS-L 10 and 98 ± 2 % for NS-L 9. Thus, both Db_{old} values agree with the results from the CAM (Fig. 5.6 and 5.7) and the FMM calculated a probability consistent with 100 % for these D_e components.

Table 5.3: Dating results.

Sample			Total dose rate	Measured/given ratio[a]	Overdispersion [%][b]		n	Central age model[c]		Finite Mixture Model[e]			
core	sample	depth [m]	[Gy/ka]		medium aliquots	small aliquots		D_b [Gy] (small)	Age [ka]	Db_{old} [Gy][f]	k	Proportion [%]	Age [ka]
ME-02	NS-L 10	0.55-0.65	0.91 ± 0.06	1.00 ± 0.02	-	16.0 ± 1.5	63	0.38 ± 0.04	0.42 ± 0.03	-	-	-	-
ME-02	NS-L12	2.40-2.50	0.73 ± 0.06	1.02 ± 0.04	9.1 ± 0.5	-	17	0.36 ± 0.01	0.49 ± 0.04	-	-	-	-
ME-02	NS-L13	3.40-3.55	1.07 ± 0.06	1.06 ± 0.03	-	42.8 ± 5.0	87	0.40 ± 0.06	0.37 ± 0.03	0.93 ± 0.18	3	10 ± 5	0.87 ± 0.17
ME-02	NS-L14	3.60-3.80	1.06 ± 0.06	1.00 ± 0.02	-	34.7 ± 1.9	81	0.44 ± 0.04	0.42 ± 0.03	0.79 ± 0.08	2	15 ± 5	0.75 ± 0.05
WSS-04	NS-L5	3.60-3.75	0.63 ± 0.06	0.97 ± 0.02	-	32.0 ± 2.0	48	0.86 ± 0.04	1.4 ± 0.1	1.02 ± 0.11	2	59 ± 26	1.6 ± 0.2
WSS-04	NS-L6	2.60-2.70	0.58 ± 0.06	0.99 ± 0.01	-	36.2 ± 2.2	57	0.77 ± 0.05	1.3 ± 0.1	1.12 ± 0.14	3	25 ± 14	1.9 ± 0.2
WSS-05	NS-L9	2.40-2.50	0.68 ± 0.06	1.03 ± 0.03	-	20.3 ± 1.3	55	1.14 ± 0.07	1.7 ± 0.2	-	-	-	-
WSS-06	NS-L20	4.55-4.65	0.64 ± 0.06	0.97 ± 0.02	-	24.8 ± 1.8	52	0.74 ± 0.04	1.2 ± 0.1	1.08 ± 0.14	2	20 ± 10	1.7 ± 0.2
SWS-02	NS-L16	0.10-0.20	1.03 ± 0.06	1.07 ± 0.02	-	-	38	0.02 ± 0.01[d]	0.02 ± 0.01	-	-	-	-

Foot notes:
[a] Measured to given ratio was measured at 180 °C preheat and cutheat and is indicated as the mean of four aliquots and the standard error.
[b] Overdispersion parameter was calculated using the Central Age Model of Galbraith et al. (1999).
[c] Burial doses and burial ages were calculated using the Central Age Model (CAM) according to Galbraith et al. (1999).
[d] Burial dose was calculated using an unlog version of CAM (Arnold et al., 2009).
[e] Burial doses (Db), dose components (k), probability and burial ages were calculated using the Finite Mixture Model (FMM) of Galbraith and Green (1990) and Roberts et al. (2000).
[f] Db_{oe} is the burial dose of the oldest dose component.

It has been widely demonstrated that aeolian, beach and shallow marine sediments along the continental North Sea and Baltic Sea coast are in general well suited for OSL dating. OSL analyses of quartz provide reliable age estimates, in agreement with independent age control, if a secure (uncontaminated) sample is dated (e.g. Ballarini et al., 2003; Madsen et al., 2005, 2007, 2010; Reimann et al. 2011a, b). Here, in the detailed analysis of the uncontaminated samples (NS-L 9, 10 and NS-L 12) in section 5.4.2 we also feel confident to regard these CAM ages as reliable estimates and take these numbers as the anchor points to discuss the calculated ages (CAM and FMM) of the contaminated samples (NS-L 5, 6, NS-L 13, 14 and NS-L 20) in relation to the stratigraphy of the sediment succession.

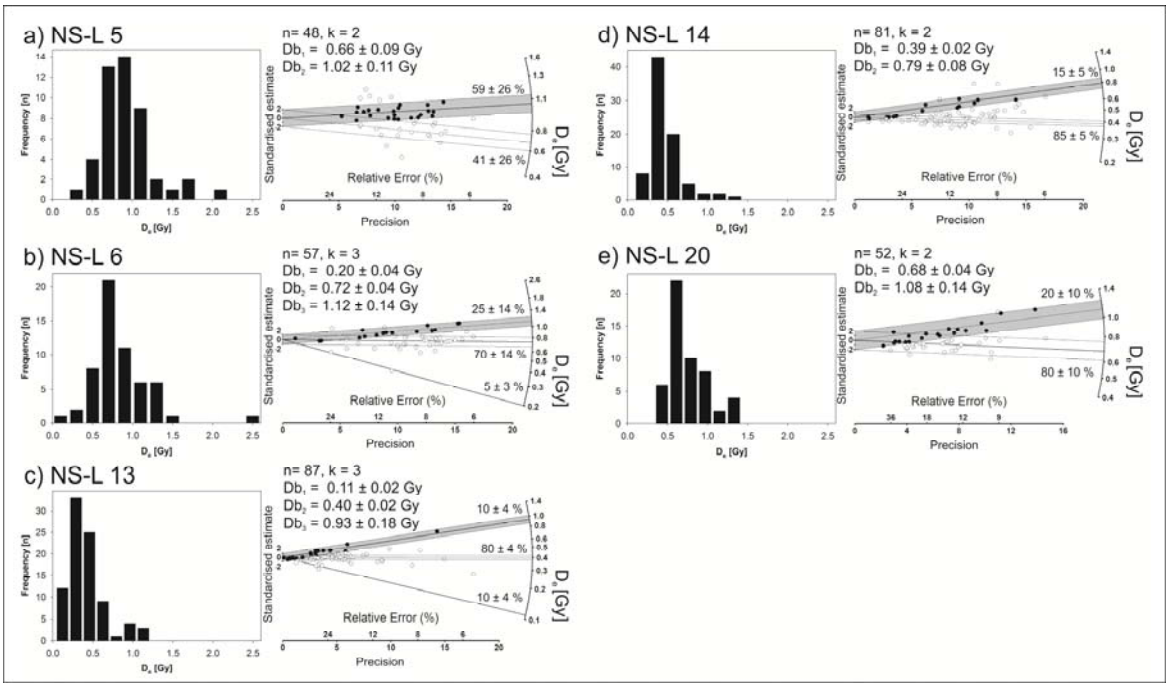

Figure 5.14: Dating results of the contaminated coastal samples. Histograms and radial plots of the contaminated swash-bar samples NS-L 5 **(a)**, NS-L 6 **(b)**, NS-L 13 **(c)**, NS-L 14 **(d)**, and NS-L 20 **(e)**. The burial dose components (Db) and the probabilities were calculated using the Finite Mixture Model of Galbraith and Green (1990). The best fit of the model (including the number of dose components) was selected using the BIC score.

Sample NS-L 5, 6 and NS-L 20 are stratigraphically older than the uncontaminated swash-bar sample NS-L 9 (1.7 ± 0.2 ka), but despite this the ages of samples NS-L 5, 6 and NS-L 20 are systematically younger (1.2-1.4 ka) than the overlying material (1.7 ka) when the CAM is applied for age calculation, presumably as a result of contamination by younger aeolian and wash-over sediments. If taken at face value, the CAM ages would suggest a simultaneous swash-bar deposition at ~1.4 ka. However, the four burial ages based on the oldest dose component identified using the FMM (FMM age in Fig. 5.2) from the three contaminated samples are all indistinguishable (i.e. consistent within 1σ-uncertainties) from the uncontaminated NS-L 9; these ages all indicate a simultaneous deposition of the swash-bar succession at ~1.7 ka. We conclude that the CAM ages of samples NS-L 5, 6 and NS-L 20 are too young due to contamination during sampling by younger sediments with smaller burial doses. This contamination was also observed in the D_e distributions of these samples (Fig. 5.14). The FMM age of a contaminated sample appear to be more reliable because it presumably represents the burial ages of the oldest D_e components which in turn we take to represent the genuine burial age of uncontaminated swash-bar sediments. Nevertheless we are surprised at the level of contamination; in one of these samples this appears to amount to about 90% of the accepted grains (and therefore presumably of the mass in the sampling tube).

A similar picture emerges for the northernmost drilling ME-02 (Fig. 5.2). The upper two aeolian samples (NS-L 10 and 12) are uncontaminated because both samples were taken in a closed liner (excluding sediment mixing) and so the CAM ages of 0.42 ± 0.03 and 0.49 ± 0.04 ka, respectively, are considered reliable. The CAM ages of both the contaminated lower samples (NS-L 13: 0.37 ± 0.03 ka and NS-L 14: 0.42 ± 0.03 ka) were taken from an older beach sediment facies. According to the geological model of Fig. 5.2, this facies should be older than the overlying aeolian facies, and yet the CAM ages are younger compared to the overlying uncontaminated aeolian sample NS-L 12 (0.49 ± 0.04 ka). However, the CAM ages agree within 2-σ uncertainties. On the other hand, the burial ages using the oldest dose components from the FMM are 0.87 ± 0.17 ka and 0.75 ± 0.05 ka for sample NS-L 13 and NS-L 14, respectively; these ages are significant older than the overlying aeolian sediments and thus in stratigraphic order. However, it should be pointed out that these ages (Db_{old}) are only based upon a few aliquots (about 10-20 % of the aliquots) and thus sediment contamination is severe in these two samples (NS-L 13, 14).

In summary, we obtain burial ages in good agreement with the stratigraphy using dose components made up of the largest D_e values and these ages are (unlike the ages calculated from the younger D_e population) in good stratigraphic agreement with the less contestable ages calculated for the uncontaminated samples (NS-L 9, 10, 12). This is consistent with the expectation from sampling and from the geological model of the sediment succession (Fig. 5.2). From this model we expected a contamination of the older swash-bar sediments by sediments from two different overlying (i.e. younger) units (i) aeolian for all the drillings (ME-02, WSS-04-06) and (ii) an additional wash-over unit for drilling WSS-04 (Fig. 5.2). Thus, we feel confident to regard these ages made up of the largest D_e population as reliable estimates for our stratigraphically oldest sediments. The geological model also explains the presence of 2 or 3 age populations (derived from swash-bar, aeolian, and wash-over sediments). We interpret the probabilities of the oldest dose populations to represent the fraction of the target facies present in the sample tube after recovery; these seem to us to be remarkably low. For three out of five samples (NS-L 13, 14, 20) Db_{old} includes <20 % of the grains (Fig. 5.14). Nevertheless, using the FMM under controlled conditions, we derived probabilities consistent with

the known values for a 50:50 laboratory mixture (Fig. 5.11) indicating that the selection of different D_e components using the FMM and small aliquots can be accurate under laboratory controlled conditions. We are forced to conclude that the sampling technique (open core probe) used for these sediments gave rise to an unexpectedly high level of contamination from overlying material. We expected a contamination of ~10 %, certainly no more than 50 %. We assume that the unexpectedly high contamination resulted from wash-out effects during drilling (in particular during lifting the probe) because we took the samples below the present water table. We have to conclude that this open-core sampling technique was inappropriate to these water-logged deposits.

Finally it is interesting to note that our small aliquots perform very well in comparison to single-grains. The two data sets were analysed using the same statistical tools to give largely indistinguishable results, indicating that our 20 grain aliquots are behaving essentially as single-grains. This is not surprising given the low fraction of sensitive grains in this material, and can be contrasted with the opposite conclusions reached by Arnold and Roberts (2009) and Olley et al. (2004); their analysis, however, was based on a much larger proportion of sensitive grains. In our view the decision as to whether to work with single-grains or small aliquots must be taken on a case by case basis, taking into account both the fraction of grains giving light and practical issues.

5.5 Conclusions

This study demonstrates that the Finite Mixture Model (FMM) is able to reliably identify the maximum dose population from small aliquot (~20 grains) D_e distributions. These doses are then used to derive burial ages for beach samples contaminated during sampling. We conclude that:

- For quartz from the central part of the continental North Sea coast, small aliquots of about 20 grains are adequate proxies for single-grains. In general, it is concluded that small aliquots can be used instead of true single-grains if, on average, more than 80 % of the luminescence sum from the aliquot in response to a known dose is emitted by only one grain. From our data, it appears that under these conditions signal averaging in the multi-grain aliquot is reduced to a negligible level. Information from some single-grain analyses is required to define the appropriate size (number of grains) of such a small aliquot, but this information can be obtained from very limited single-grain sensitivity study.
- For our samples a part of the observed over-dispersion in the D_e distributions arises from low senstivity quartz grains dominated by medium and slow components; these were successfully rejected when the background interval was moved close to the initial signal. Nevertheless, no significant systematic effect on the average D_e was observed.
- The FMM can reliably identify maximum dose populations derived from suitable small aliquot D_e distributions. The burial ages are consistent with the stratigraphy and with the uncontaminated samples. For the two component laboratory mixture it is shown that the FMM results (burial doses, number of components, probability of components) are relatively insensitive to changes of the over-dispersion parameter between 10 and 40 %.

Acknowledgement

We thank the Amt für ländliche Räume in Husum (ALR) for providing the working permits in the nature protection area of northern Sylt, and for providing the data for the terrain model presented in Fig. 5.1. Many thanks also to the Diedrichsen family for allowing our work on northern Sylt. For field assistance special thanks to Juliane Ludwig, Ilona Schutter and Hauke Petersen.

References

- Adamiec, G., Aitken, M., 1998. Dose-rate conversion factors: update. Ancient TL 16, 37-50.
- Aitken, M.J., 1985. Thermoluminescence Dating. Academic Press, London.
- Alappat, L., Frechen, M., Ramesch, R., Tsukamoto, S., Srinivasalu S., 2011. Evolution and chronology of late Holocene coastal dunes in the Cauvery delta region of Tamil Nadu, India. Journal of Asian Earth Science, doi.org/10.1016/j.jseaes.2011.05.019)
- Arnold, L.J., Roberts, R.G., 2009. Stochastic modelling of multi-grain equivalent dose (D_e) distributions: Implications for OSL dating of sediment mixtures. Quaternary Geochronology 4, 204-230.
- Arnold, L.J., Roberts, R.G., Galbraith, R.F., DeLong, S.B., 2009. A revised burial dose estimation procedure for optical dating of young and modern-age sediments. Quaternary Geochronology 4, 306-325.
- Ballarini, M., Wallinga, J., Murray, A.S., van Heteren, S., Oost, A.P., Bos, A.J.J., van Eijk, C.W.E., 2003. Optical dating of young coastal dunes on a decadal time scale. Quaternary Science Reviews 22, 1011-1117.
- Ballarini, M., Wallinga, J., Wintle, A.G., Bos, A.J.J., 2007. A modified SAR protocol for optical dating of individual grains from young quartz samples. Radiation Measurements 42, 360-369.
- Bateman, M.D., Boulter, C.H., Carr, A.S., Frederick, C.D., Peter, D., Wilder, M., 2007. Detecting post-depositional sediment disturbance in sandy deposits using optical luminescence. Quaternary Geochronology 2, 57–64.
- Bøtter-Jensen, L., Bulur, E., Duller, G.A.T., Murray A.S., 2000. Advances in luminescence instrument systems. Radiation Measurements 32, 523-528.
- Buynevich, I. V., FitzGerald, D. M., Goble, R. J., 2007. A 1500 yr record of North Atlantic storm activity based on optically dated relict beach scarps. Geology 35, 543-546.
- Cunningham, A.C., Wallinga, J., 2010. Selection of integration time intervals for quartz OSL decay curves. Quaternary Geochronology, doi:10.1016/j.quageo.2010.08.004.
- David, B., Roberts, R.G., Magee, J., Mialanes, J., Turney, C., Bird, M., White, C., Fifield, L.K., Tibby, J., 2007. Sediment mixing at Nonda Rock: investigations of stratigraphic integrity at an early archaeological site in northern Australia and implications for the human colonisation of the continent. Journal of Quaternary Science 22, 449-479.
- Duller, G.A.T., 2003. Distinguishing quartz and feldspar in single grain luminescence measurements. Radiation Measurements 37, 161-165.
- Duller, G.A.T., 2007. Assessing the error on equivalent dose estimates derived from single aliquot regenerative dose measurements. Ancient TL 25, 15-24.

- Duller, G.A.T., 2008. Single-grain optical dating of Quaternary sediments: why aliquot size matters in luminescence dating. Boreas 37, 589-612.
- Duller, G.A.T., Bøtter-Jensen, L., Murray, A.S., Truscott, A.J., 1999. Single grain laser luminescence (SGLL) measurements using a novel automated reader. Nuclear Instruments and Methods: B 155, 506–514.
- Duller, G.A.T., Bøtter-Jensen, L., Murray, A. S., 2000. Optical dating of single sand sized grains of quartz: Sources of variability. Radiation Measurements 32, 453–457.
- Durcan, J., Duller, G.A.T., 2011. The fast ratio: a rapid measure for testing the dominance of the fast component in the initial OSL signal from quartz. Radiation Measurements, doi: 10.1016/j.radmeas.2011.07.016
- Galbraith, R.F., 2005. Statistics for Fission Track Analysis. Chapman and Hall/CRC Press, Boca Raton, Florida.
- Galbraith, R.F., Green, P.F., 1990. Estimating the component ages in a finite mixture. Nuclear Tracks and Radiation Measurements 17, 197-206.
- Galbraith, R.F., Roberts, R.G., Laslett, G.M., Yoshida, H., Olley, J.M., 1999. Optical dating of single and multiple grains of quartz from Jinmium rock shelter, Northern Australia: part 1, experimental details and statistical models. Archaeometry 41, 339-364.
- Gibbard, P.L., Boreham, S., Cohen, K.M., Moscariello, A., 2005. Global chronostratigraphical correlation table for the last 2.7 million years. Boreas 34, unpaginated.
- Gripp, K., Simon, G., 1940. Untersuchungen über den Aufbau und die Entstehung der Insel Sylt: I. Nord-Sylt. Westküste 2, 1-70.
- Gripp, K., Becker, W., 1940. Untersuchungen über den Aufbau und die Entstehung der Insel Sylt: II. Mittel-Sylt. Westküste 2, 71–84.
- Hoffmann, D., 1974. Zum geologischen Aufbau der Hörnumer Halbinsel auf Sylt. Meyniana 23, 63-68.
- Jacobs, Z., Duller, G.A.T., Wintle, A.G., 2006. Interpretation of single grain D_e distributions and calculation of D_e. Radiation Measurements 41, 264–277.
- Jacobs, Z., Wintle, A.G., Duller, G.A.T., Roberts, R.G., Wadley, L., 2008a. New ages for the post-Howiesons Poort, late and final Middle Stone Age at Sibudu, South Africa. Journal of Archaeological Science 35, 1790–1807.
- Jacobs, Z., Wintle, A.G., Roberts, R.G., Duller, G.A.T., 2008b. Equivalent dose distributions from single grains of quartz at Sibudu, South Africa: context, causes and consequences for optical dating of archaeological deposits. Journal of Archaeological Science 35, 1808–1820.
- Jain, M., Murray, A.S., Bøtter-Jensen, L., 2003. Characterisation of blue-light stimulated luminescence components in different quartz samples: implications for dose measurement. Radiation Measurements 37, 441-449.
- Jain, M., Thomsen, K.J., Bøtter-Jensen, L., Murray, A.S., 2004. Thermal transfer and apparent-dose distributions in poorly bleached mortar samples: results from single grains and small aliquots of quartz. Radiation Measurements 38, 101-109.
- Lindhorst, S., Betzler, C., Hass, H.C., 2008. The sedimentary architecture of a Holocene barrier spit (Sylt, German Bight): Swash-bar accretion and storm erosion. Sedimentary Geology 206, 1-16.
- Lindhorst, S., Fürstenau, J., Hass, H.C., Betzler, C., 2010. Anatomy and sedimentary model of a hooked spit (Sylt, southern North Sea). Sedimentology 57, 935-955.

- Lopez, G. I., Rink, W. J., 2007. Characteristics of the burial environment related to quartz SAR-OSL dating at St. Vincent Island, NW Florida, USA. Quaternary Geochronology 2, 65-70.
- Lüthgens, C. Böse, M., Preusser, F., 2011. Age of the Pomeranian ice-marginal position in northeastern Germany determined by Optically Stimulated Luminescence (OSL) dating of glaciofluvial sediments. Boreas, doi: 10.1111/j.1502-3885.2011.00211.
- Madsen, A.T., Murray, A.S., Andersen, T.J., Pejrup, M., Breuning-Madsen, H., 2005. Optically stimulated luminescence dating of young estuarine sediments: a comparison with ^{210}Pb and ^{137}Cs dating. Marine Geology 214, 251-268.
- Madsen, A.T., Murray, A.S., Andersen, T.J., 2007. Optical dating of dune ridges on Rømø, a barrier island in the Wadden Sea, Denmark. Journal of Coastal Research 23, 1259–1269.
- Madsen, A.T., Duller, G.A.T., Donnelly, J.P., Roberts, H.M., Wintle, A.G., 2009. A chronology of hurricane landfalls at Little Sippewisset Marsh, Massachusetts, USA, using optical dating. Geomorphology 109, 36-45.
- Madsen, A.T., Murray, A.S., Andersen, T.J., Pejrup, M., 2010. Luminescence dating of Holocene sedimentary deposits on Rømø, a barrier island in the Wadden Sea, Denmark. The Holocene, doi:10.1177/0959683610374883.
- Mejdahl, V., 1979. Thermoluminescence dating: beta attenuation in quartz grains. Achaeometry 21, 61-73.
- Murray, A.S., Wintle, A.G., 2000. Luminescence dating of quartz using an improved single-aliquot regenerative-dose protocol. Radiation Measurements 32, 57-73.
- Murray-Wallace, C.V., Banerjee, D., Rourman, R.P., Olley, J.M., Brooke, B.P., 2002. Optically stimulated luminescence dating of Holocene relict foredunes, Guichen Bay, South Australia. Quaternary Science Reviews 21, 1077-1086.
- Nielsen, A., Murray, A.S., Pejrup, M., Elberling, B., 2006. Optically stimulated luminescence dating of al Holocene beach ridge plain in Northern Jutland, Denmark. Quaternary Geochronology 1, 305-312.
- Olley, J.M., Caitcheon, G.G., Roberts, R.G., 1999. The origin of dose distributions in fluvial sediments, and the prospect of dating single grains from fluvial deposits using optically stimulated luminescence. Radiation Measurements 30, 207–217.
- Olley, J.M., Pietsch, T., Roberts, R.G., 2004. Optical dating of Holocene sediments from a variety of geomorphic settings using single grains of quartz. Geomorphology 60, 337-358.
- Pietsch, T.J., 2009. Optically stimulated luminescence dating of young (<500 years old) sediments: Testing estimates of burial dose. Quaternary Geochronology 4, 406-422.
- Prescott, J.R., Stephan, L.G., 1982. The contribution of cosmic radiation to the environmental dose for thermoluminescent dating - Latitude, altitude and depth dependences. PACT 6, 17-25.
- Prescott, J.R., Hutton, J.T., 1994. Cosmic ray distributions to dose rates for luminescence and ESR dating: large depths and long-term variations. Radiation Measurements 23, 497–500.
- Reimann, T., Tsukamoto, S., Naumann, M., Frechen, M., 2010. The potential of using K-rich feldspars for optical dating of young coastal sediments – a test case from Darss-Zingst peninsula (southern Baltic Sea coast). Quaternary Geochronology, doi: 10.1016/j.quageo.2010.10.001.

- Reimann, T., Tsukamoto, S., Harff, J., Osadczuk, K., Frechen, M. Reconstruction of Holocene coastal foredune progradation using luminescence dating – an example from the Świna barrier (southern Baltic Sea, NW Poland). Accepted for publication in Geomorphology.
- Roberts, H.M., Plater, A.J., 2007. Reconstruction of Holocene foreland progradation using optically stimulated luminescence (OSL) dating: an example from Dungeness. The Holocene 17, 495-505.
- Roberts, R., Yoshida, H., Galbraith, R., Laslett, G., Jones, R., Smith, M., 1998. Single aliquot and single-grain optical dating confirm thermoluminescence age estimates at Malakunanja II rock shelter in northern Australia. Ancient TL 16, 19–25.
- Roberts, R.G., Galbraith, R.F., Yoshida, H., Laslett, G.M., Olley, J.M., 2000. Distinguishing dose populations in sediment mixtures: a test of single-grain optical dating procedures using mixtures of laboratory-dosed quartz. Radiation Measurements 32, 459–465.
- Roberts, R.G., Flannery, T.F., Ayliffe, L.K., Yoshida, H., Olley, J.M., Prideaux, G.J., Laslett, G.M., Baynes, A., Smith, M.A., Jones, R., Smith, B.L., 2001. New ages for the last Australian megafauna: continent-wide extinction about 46,000 years ago. Science 292, 1888–1892.
- Rodnight, H., Duller, G.A.T., Wintle, A.G., Tooth, S., 2006. Assessing the reproducibility and accuracy of optical dating of fluvial deposits. Quaternary Geochronology 1, 109-120.
- Singarayer, J.S., Bailey, R.M., 2003. Further investigations of the quartz optically stimulated luminescence components using linear modulation. Radiation Measurements 37, 451-458.
- Singarayer, J.S., Bailey, R.M., 2004. Component-resolved bleaching spectra of quartz optically stimulated luminescence: preliminary results and implications for dating. Radiation Measurements 38, 111-118.
- Thomas, P.J., Jain, M., Juyal, N., Singhvi, A.K., 2005. Comparison of single-grain and small-aliquot OSL dose estimates in <3000 years old river sediments from South India. Radiation Measurements 39, 457-469.
- Thomsen, K.J., Bøtter-Jensen, L., Murray, A.S., Solongo, S., 2002. Retrospective dosimetry using unheated quartz: a feasibility study. Radiation Protection Dosimetry 101, 345-348.
- Thomsen, K.J., Jain, M., Bøtter-Jensen, L., Murray, A.S., Jungner, H., 2003. Variation with depth of dose distributions in single grains of quartz extracted from an irradiated concrete block. Radiation Measurements 37, 315–321.
- Thomsen, K.J., Murray, A.S., Bøtter-Jensen, L., 2005. Sources of variability in OSL dose measurements using single grains of quartz. Radiation Measurement 39. 47-61.
- Thomsen, K.J., Murray, A.S., Bøtter-Jensen, L., Kinahan, J., 2007. Determination of burial dose in incompletely bleached fluvial samples using single grains of quartz. Radiation Measurements 42, 370-379.
- Wintle, A.G., Murray, A.S., 2006. A review of quartz optically stimulated luminescence characteristics and their relevance in single-aliquot regeneration dating protocols. Radiation Measurements 41, 369–391.

Chapter 6, Paper IV:

Tony Reimann[a], Sumiko Tsukamoto[a], Michael Naumann[b,c], Manfred Frechen[a]
2011.

[a] Leibniz Institute for Applied Geophysics (LIAG): Geochronology and Isotope Hydrology, Stilleweg 2, 30655 Hannover, Germany
[b] Leibniz Institute for Baltic Sea Research, Department for Marine Geology, Warnemünde, Germany
[c] Institute of Geography and Geology, Greifswald University, Greifswald, Germany

The potential of using K-rich feldspars for optical dating of young coastal sediments – a test case from Darss-Zingst peninsula (southern Baltic Sea coast).

Quaternary Geochronology 6, 207-222.

(www.sciencedirect.com/science/article/pii/S1871101410000634)

Abstract

The potential use of a modified elevated temperature post-IR IRSL (pIRIR) SAR protocol for K-rich feldspar was tested for seven late Pleistocene and Holocene samples from a coastal sediment succession from the southern Baltic Sea (Darss-Zingst peninsula). This modified pIRIR protocol observes a pIRIR signal at 180 °C after the IRSL measurement at 50 °C. After thorough performance testing, equivalent doses (D_e) were measured and corrected for the residual doses and fading. The results showed that thermal transfer and residual doses are more significant for pIRIR signal than for quartz OSL and IRSL signal. The calculated K-feldspar ages (IRSL and pIRIR) were then compared with quartz-SAR and two independent radiocarbon ages.

The ages of the investigated sediments range from the late Pleistocene (~13.5 ka) to a few hundred years. The laboratory fading rate of the pIRIR signal was significantly lower (g-value of 0-2 %/decade) than that of the IRSL (g-values of 3-10 %/decade). We observed a systematic overestimation of fading-corrected IRSL ages based on high g-values (>5 %), whereas the pIRIR ages showed a good agreement with the quartz ages and with the radiocarbon ages for the well-bleached mid-Holocene and the late Pleistocene samples, suggesting that our modified pIRIR protocol is suitable for well bleached young sediments. For the incompletely bleached uppermost samples the minimum age model (MAM) was applied. For these samples it is concluded that both IRSL and pIRIR ages derived from K-feldspar overestimated the true burial age.

6.1 Introduction

Sediment dating is an important tool in coastal research because it contributes to the unravelling and understanding of the dynamics and processes along our coasts. Successions of beach ridges, foredune ridges and/or coastal dunes provide high-resolution chronologies for the Holocene coastal evolution and hence the development of coastal landforms e.g. spits, barrier-spits and barrier islands. Until recently, most chronologies of coastal sediment successions, for example along the southern Baltic Sea coast, were mainly based on radiocarbon data derived mostly from the coastal hinterland and a limited number of archaeological findings (e.g. Lampe, 2005; Hoffmann et al., 2005). But radiocarbon based chronologies are often incomplete and complicated due to the absence of suitable non-reworked organic material (e.g. peat, wood or shells) and calibration problems within the last 350 years (Hua, 2009).

Luminescence dating methods provide an excellent chronological tool in coastal environments (e.g. Jacobs, 2008) because they can provide burial ages for sand- or silt-sized sediments for the Holocene period. In recent years, optical dating of quartz applying the single-aliquot regenerative-dose (SAR) protocol (Murray and Wintle, 2000) is commonly used for geochronological studies in a sand dominated coastal environment (e.g. Ballarini et al., 2003; Madsen et al., 2005, 2007, 2009; Nielsen et al., 2006; Lopez and Rink, 2007; Roberts and Plater, 2007). Quartz optical dating has also been applied frequently and successfully to sediments younger than 1000 years (see recent review by Madsen and Murray, 2009). However, in some regions of the world the use of quartz as a dosimeter is not possible due to a poor OSL sensitivity of the quartz minerals (e.g. Preusser et al. 2006; Hülle et al., 2010; Steffen et al., 2009; Kunz et al., 2010). Furthermore, Davids et al. (2010) pointed out that the quartz OSL signal of very young samples is dim and produces a broad distribution of equivalent doses (D_e) due to a poor signal to noise ratio. The dim OSL signal of very young quartz samples also limits the use of small-aliquot techniques for samples from the recent past, necessary to detect incomplete bleaching (Madsen and Murray, 2009). In addition, Davids et al. (2010) as well as Madsen et al. (2009) identified problems of broad D_e distributions, if the dosimetry is complex due to inhomogeneously-deposited sediments and/or large variations in the water content.

Wallinga et al. (2000) and Blair et al. (2005) developed the single-aliquot regenerative-dose protocol for infrared-stimulated luminescence (SAR-IRSL) of coarse grain feldspar. Li et al. (2007a) and Davids et al. (2010) demonstrated that SAR-IRSL of K-feldspars gives more reproducible and precise D_e values than quartz for their Holocene dune sand and coastal overwash sediment. Both authors interpreted this to be caused by the higher OSL sensitivity of feldspar grains and because the internal potassium content of K-feldspars reduce the impact of variations in the external dose. Nevertheless, ages derived from SAR-IRSL dating of K-feldspars need to be corrected for anomalous fading. Wallinga et al. (2007) showed the limitations of the assumptions made by the common fading correction procedures (e.g. Huntley and Lamothe, 2001; Lamothe et al., 2003). Wallinga et al. (2007) also reported a decreasing fading rate (g-value according to Aitken, 1985) as a function of dose rate. In contrary, Li et al. (2008b) found a negative correlation between dose rate and the amount of underestimation of feldspar ages, suggesting a higher fading rate might be related to a higher environmental dose rate.

In this paper we test the potential of an elevated temperature post-IR IRSL (pIRIR) SAR protocol which was originally proposed by Thomsen et al. (2008) and recently applied by Buylaert et al., (2009). This protocol measures a standard IRSL signal at 50°C as well as a pIRIR signal at an elevated temperature for dating of young coastal sediments. The pIRIR signal is supposed to be much less affected by anomalous fading (Thomsen et al., 2008; Buylaert et al., 2009). However, signal resetting might be a problem for the pIRIR protocol. Buylaert et al. (2009) reported residual doses of less than 2 Gy which do not affect for their old samples but be important for young samples. In order to apply the pIRIR protocol to young sediments it should make use of a lower preheat temperature than that originally suggested to minimize thermal transfer. Furthermore, the subtraction dating technique (e.g. Aitken, 1985; Davids et al., 2010) is applied to test the reliability of this method. The subtraction method uses the difference between the quartz and the feldspar D_e (Aitken, 1985) and was recently applied by Davids et al. (2010) for SAR-IRSL and SAR-OSL dating of feldspar and quartz from hurricane overwashed sediments. In this study, we measured seven samples from a sediment core from the Darss-Zingst peninsula (southern Baltic Sea coast, Germany) having an age range from about 13.5 ka to a few hundred years. We compare IRSL and pIRIR ages with ages obtained from SAR measurements of quartz and the subtraction method. Radiocarbon dating of three organic layers within the sediment core is used as an independent age control. Only two of the radiocarbon dates are used because the third one is regarded as unreliable. The aim of this study is to test and modify the pIRIR protocol to make it suitable for dating of young coastal sand-sized samples.

6.2 Geological setting and samples

6.2.1 Geological setting

The drilling site of Zi-43 is located at the Darss-Zingst Peninsula (NE Germany) which belongs to the southern Baltic Sea coast (Fig. 6.1). The Darss-Zingst peninsula is a part of the Fischland-Darss-Zingst island chain. The drilling was done in the east of the artificially closed coastal inlet “Prerowstrom” which subdivides the Darss from the Zingst, and in the west of the sampling sites Zingst-Osterwald and Windwatt of Reimann et al. (2010) where they obtained OSL ages of ~1500-1900 years and ~40-900 years from the beach ridge successions, respectively (Fig. 6.1). The development of the southern Baltic Sea coastline started with the Littorina transgression at ~8 ka (Janke and Lampe, 1998; Lampe, 2005; Hoffmann et al., 2005). The pre-Littorina relief was mainly shaped by the Weichselian glaciation during the late Pleistocene. Morainic and glaciofluvial/glacilacustrine depositions were modified by glacial tectonic and fluvial processes and formed the basement and sediment supply for the coastal evolution (Naumann et al., 2009). Between 8 and 6 ka the sea level rose rapidly with rates of up to 2.5 cm/a (Kliewe and Janke, 1991) resulting in a level of around 2 m below the present sea level at about 6 ka. The cliffs from the Pleistocene headlands were eroded and the morphological depressions were subsequently filled with sediment. The shallowing of the depressions and the decrease of the sea level rise since 6.5 ka (Schumacher and Bayerl, 1999; Hoffmann et al., 2005; Lemke, 2005; Lampe, 2005) led to the development of spits and barrier-spits between the islands isolating bays and lagoons from the open sea. These processes formed the typical southern Baltic coast with a system of beach ridges and dunes at the front and peatlands in the coastal hinterland.

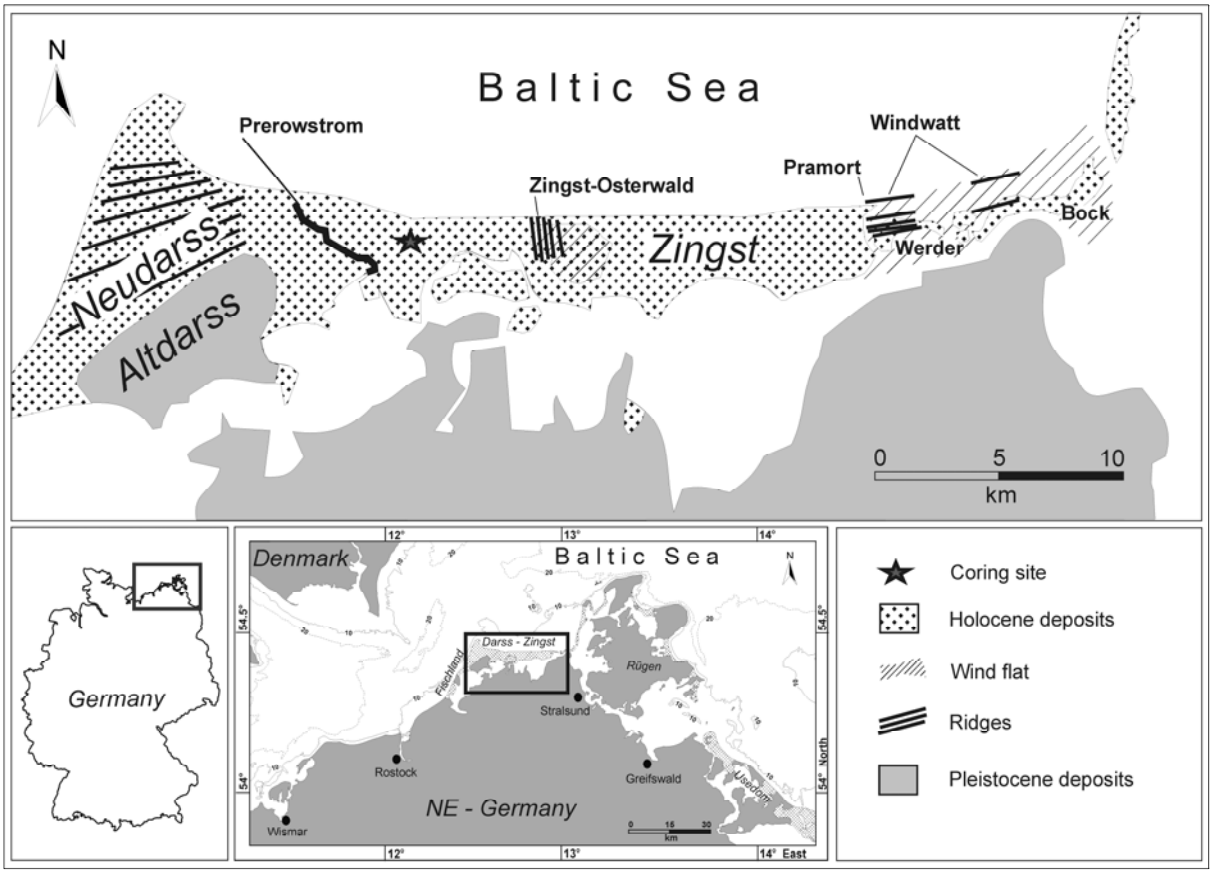

Figure 6.1: Map of Darss-Zingst peninsula. Map showing the sampling location and regional context.

6.2.2 Samples and preparation

The core was taken with a hydraulic powered extracting tool. Black PVC liners with a diameter of 80 mm were used for coring to avoid light exposure of the luminescence samples. The core (Zi-43, Fig. 6.2) contains a sediment succession of ~5.3 m. The succession starts at the bottom with late Pleistocene glaciofluvial and/or galciolacustrine fine sand. Between 4.9 m and 4.5 m a peat was developed with an obvious and undisturbed soil development underneath (Fig. 6.2). It is therefore very likely that this peat is “in situ”. Above this first peat layer, the Holocene succession started with shallow water or coastal fine sand between 4.5 to 2.5 m. This sand is very quartz-rich and has only low shell content. Interstratified organic and peat layers were also found and the most pronounced one (at about 4 m) was sampled for radiocarbon dating (Fig. 6.2). As this peat horizon has a very sharp border to the Holocene sand beneath, we assume it is not “in situ”. The succession continues with an organic-silicate gyttja representing slack water conditions, which is related to the closing or shallowing process of the “Prerowstrom”, and the isolation from the open sea. On the top of the succession a quartz-rich fine sand layer follows, which is structured by interstratified thin organic or peat layers. Altogether, seven luminescence samples (W-Zi 1-7) were taken from the glaciofluvial/glaciolacustrine, the shallow marine, and the cover sand units (Fig. 6.2). Samples for dose rate determination were taken from each sediment surrounding the luminescence sample. In addition, we took three samples from the two peat layers and the gyttja for radiocarbon dating.

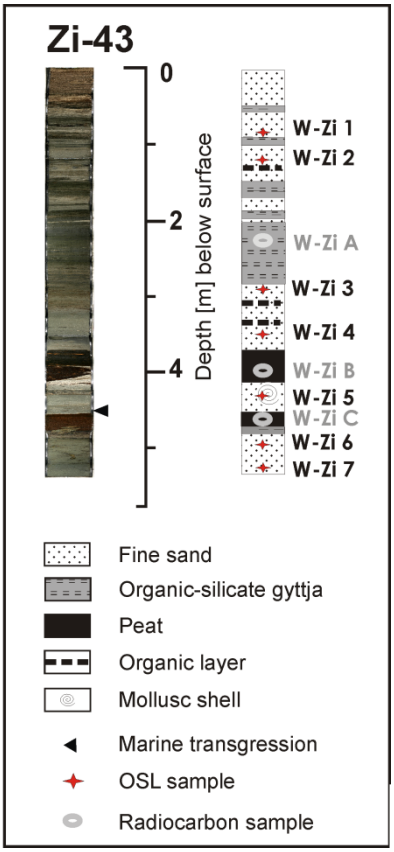

Figure 6.2: Lithology and position of radiocarbon and luminescence samples of the core Zi-43 (Westzingst).

The Zi-43 core (Fig. 6.2) was opened, sub-sampled, and the samples were prepared in the luminescence laboratory under subdued red light conditions. The seven samples were dry-sieved to recover grains either 100-150 µm (Zi-W 1, 3-7) or 150-200 µm (Zi-W 2) in diameter. The sand was treated with HCl to dissolve carbonate, with $Na_2C_2O_4$ to dissolve aggregates, and with H_2O_2 to remove organic matter. The quartz minerals were then density separated by a heavy liquid (sodium polytungstate) from the feldspars (<2.62 g/cm^3) and the heavy minerals (>2.70 g/cm^3). Using the same method, the K-rich feldspars (<2.58 g/cm^3) were separated from the Na-rich feldspars (>2.58 g/cm^3). The quartz grains were then treated with 40% HF for about 60 minutes to etch the outer surface of the grains, to avoid a contribution of the α-irradiated outer part of the quartz mineral, and to remove remaining feldspar minerals. After HF-etching, the quartz grains were sieved again with a 100 µm (Zi-W 1, 3-7) and 150 µm (Zi-W 2) mesh to reject small particels. The K-rich feldspar separates were not treated with HF. The samples for dose rate determination were dried and homogenised.

6.3 Methods

6.3.1 Luminescence measurement

The measurements were made on an automated luminescence reader (Risø TL/OSL DA-15) equipped with a $^{90}Sr/^{90}Y$ beta source (Bøtter-Jensen et al., 2000). The quartz and K-feldspar extracts were mounted on stainless steel discs with the grains covering the area with a diameter of 6 mm (medium aliquots) or 2 mm (small aliquots) using silicon oil. For the quartz OSL blue LEDs (470 nm) were used

for stimulating the aliquots and a 7.5 mm Hoya U-340 filter was used as the signal detection filter in front of the photomultiplier tube. For the IR stimulation of K-feldspar infrared LEDs (870 nm) were used and the IRSL signal was detected through a combination of Schott BG-39 and Corning 7-59 filters in the blue light spectrum between 320 and 450 nm. Quartz and feldspar decay curves for sample W-Zi 3 are shown in Figure 6.3. The luminescence intensities were integrated over the first 0.8 s for quartz and the first 2.4 s for feldspar. The last 4.8 s and 24 s of the signal were subtracted as background for quartz and feldspar, respectively.

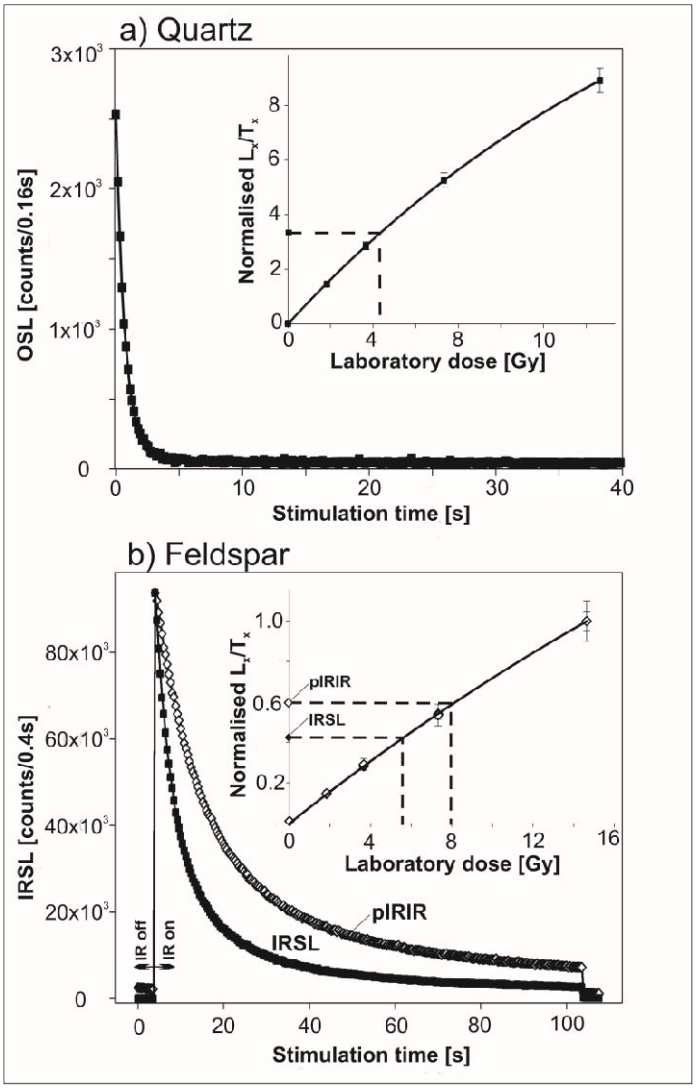

Figure 6.3: Quartz and feldspar decay curves and dose response curves of sample W-Zi 3. (a) A typical quartz decay curve. The inset shows a SAR dose response curve of W-Zi 3 from the same aliquot. **(b)** Typical IRSL and pIRIR decay curves. The inset shows the dose response curves of the pIRIR from the same aliquot.

6.3.2 Dose rate and subtraction dating

For determination of the external dose rate, the radionuclide concentrations (U, Th and K content) of the surrounding sediment were measured in 50 g boxes using high-resolution gamma spectrometry. The activities of ^{234}Th, ^{214}Bi, ^{214}Pb and ^{210}Pb for U, and ^{228}Ac, ^{212}Pb, and ^{208}Tl, for Th were measured for the seven samples, respectively. In addition, the activity of the ^{40}K nuclide was measured to obtain the K content. A potential problem for water-lain sediments is the disequilibrium of the U decay chain resulting in time-dependent changes in dose rate (Olley et al., 1996, 1997; Li et al., 2008a). To check if there is disequilibrium, the activities of ^{234}Th, ^{214}Pb, ^{214}Bi and ^{210}Pb were compared. No significant discrepancy of the activities was observed indicating

equilibrium for the U decay chain. The conversion factors of Adamiec and Aitken (1998) and the β-attenuation factors after Mejdahl (1979) were used to obtain the external β- and γ-dose rates. The "in situ" water content of the samples was measured to correct the α-, β- and γ-dose rates for the water attenuation (Aitken, 1985). At present the "in situ" water content of 20 ± 4 % is equivalent to 100 % water saturation because the present water table is only a few decimetres below the surface. For samples W-Zi 6 and W-Zi 7 this saturation water content does not represent the water content over the burial time because both samples were deposited considerably prior to the littorina transgression and hence the onset of the coastal evolution. In contrast to the samples above, we assumed a lower water content for W-Zi 6 and W-Zi 7 for the time before the sea level reached this area (at about 6 ka following Lampe, 2005) thus causing the water table to rise to the present level. A value of 8 ± 4 % (according to Reimann et al., 2010) was selected as water content for the pre-Littorina time from ~14 to 6 ka. An averaged water content of 13 ± 4 % was calculated for the whole burial time for W-Zi 6 and W-Zi 7. The cosmic dose rate was calculated according to Prescott and Stephan (1982) and Prescott and Hutton (1994) from the altitude and latitude of the sampling sites, the burial depth, and the density of the overburden.

Table 6.1: Results of dose rate determination.

Sample ID	Method	Depth [m]	Grain size [µm]	Water content[a] [%]	Cosmic dose rate [Gy/ka]	U content [ppm]	Th content [ppm]	K content [%]	External dose rate [Gy/ka]	Internal dose rate [Gy/ka]	Total dose rate [Gy/ka]
W-Zi 1	Quartz	0.95	100-150	20 ± 4	0.18 ± 0.02	0.37 ± 0.02	0.97 ± 0.04	0.88 ± 0.01	0.81 ± 0.05	-	0.99 ± 0.05
	K-feldspar (IRSL)				0.18 ± 0.02	0.37 ± 0.02	0.97 ± 0.04	0.88 ± 0.01	0.84 ± 0.06	0.51 ± 0.08	1.53 ± 0.10
	K-feldspar (pIRIR)				0.18 ± 0.02	0.37 ± 0.02	0.97 ± 0.04	0.88 ± 0.01	0.84 ± 0.06	0.51 ± 0.08	1.53 ± 0.10
	Subtraction				-	-	-	-	0.03 ± 0.04	0.51 ± 0.08	0.54 ± 0.09
W-Zi 2	Quartz	1.25	150-200	20 ± 4	0.17 ± 0.02	0.57 ± 0.02	2.03 ± 0.04	1.05 ± 0.01	1.02 ± 0.05	-	1.19 ± 0.05
	K-feldspar (IRSL)				0.17 ± 0.02	0.57 ± 0.02	2.03 ± 0.04	1.05 ± 0.01	1.06 ± 0.06	0.68 ± 0.09	1.74 ± 0.11
	K-feldspar (pIRIR)				0.17 ± 0.02	0.57 ± 0.02	2.03 ± 0.04	1.05 ± 0.01	1.06 ± 0.06	0.68 ± 0.09	1.74 ± 0.11
	Subtraction				-	-	-	-	0.04 ± 0.04	0.68 ± 0.09	0.72 ± 0.10
W-Zi 3	Quartz	2.70	100-150	20 ± 4	0.13 ± 0.01	1.07 ± 0.02	3.19 ± 0.05	1.38 ± 0.02	1.44 ± 0.05	-	1.57 ± 0.05
	K-feldspar (IRSL)				0.13 ± 0.01	1.07 ± 0.02	3.19 ± 0.05	1.38 ± 0.02	1.53 ± 0.06	0.51 ± 0.08	2.17 ± 0.10
	K-feldspar (pIRIR)				0.13 ± 0.01	1.07 ± 0.02	3.19 ± 0.05	1.38 ± 0.02	1.53 ± 0.06	0.51 ± 0.08	2.17 ± 0.10
	Subtraction				-	-	-	-	0.09 ± 0.04	0.51 ± 0.08	0.60 ± 0.09
W-Zi 4	Quartz	3.45	100-150	20 ± 4	0.12 ± 0.01	0.81 ± 0.02	2.10 ± 0.05	1.04 ± 0.02	1.07 ± 0.05	-	1.19 ± 0.05
	K-feldspar (IRSL)				0.12 ± 0.01	0.81 ± 0.02	2.10 ± 0.05	1.04 ± 0.02	1.13 ± 0.06	0.51 ± 0.08	1.76 ± 0.10
	K-feldspar (pIRIR)				0.12 ± 0.01	0.81 ± 0.02	2.10 ± 0.05	1.04 ± 0.02	1.13 ± 0.06	0.51 ± 0.08	1.76 ± 0.10
	Subtraction				-	-	-	-	0.06 ± 0.04	0.51 ± 0.08	0.57 ± 0.09
W-Zi 5	Quartz	4.30	100-150	20 ± 4	0.10 ± 0.01	0.64 ± 0.02	1.74 ± 0.04	1.17 ± 0.01	1.13 ± 0.06	-	1.23 ± 0.06
	K-feldspar (IRSL)				0.10 ± 0.01	0.64 ± 0.02	1.74 ± 0.04	1.17 ± 0.01	1.18 ± 0.07	0.51 ± 0.08	1.79 ± 0.11
	K-feldspar (pIRIR)				0.10 ± 0.01	0.64 ± 0.02	1.74 ± 0.04	1.17 ± 0.01	1.18 ± 0.07	0.51 ± 0.08	1.79 ± 0.11
	Subtraction				-	-	-	-	0.05 ± 0.04	0.51 ± 0.08	0.56 ± 0.09
W-Zi 6	Quartz	4.95	100-150	13 ± 4	0.09 ± 0.01	0.73 ± 0.02	2.03 ± 0.04	1.16 ± 0.02	1.23 ± 0.06	-	1.32 ± 0.06
	K-feldspar (IRSL)				0.09 ± 0.01	0.73 ± 0.02	2.03 ± 0.04	1.16 ± 0.02	1.30 ± 0.08	0.51 ± 0.08	1.90 ± 0.11
	K-feldspar (pIRIR)				0.09 ± 0.01	0.73 ± 0.02	2.03 ± 0.04	1.16 ± 0.02	1.30 ± 0.08	0.51 ± 0.08	1.90 ± 0.11
	Subtraction				-	-	-	-	0.07 ± 0.05	0.51 ± 0.08	0.58 ± 0.09
W-Zi 7	Quartz	5.05	100-150	13 ± 4	0.09 ± 0.01	1.02 ± 0.02	2.87 ± 0.04	1.02 ± 0.01	1.30 ± 0.06	-	1.39 ± 0.06
	K-feldspar (IRSL)				0.09 ± 0.01	1.02 ± 0.02	2.87 ± 0.04	1.02 ± 0.01	1.39 ± 0.08	0.51 ± 0.08	1.99 ± 0.11
	K-feldspar (pIRIR)				0.09 ± 0.01	1.02 ± 0.02	2.87 ± 0.04	1.02 ± 0.01	1.39 ± 0.08	0.51 ± 0.08	1.99 ± 0.11
	Subtraction				-	-	-	-	0.09 ± 0.05	0.51 ± 0.08	0.60 ± 0.09

Foot note:
[a] Water content is expressed as mass of dry sediment

Additionally, the external α-dose rate for α-irradiated outer rim of the K-feldspar grains and the internal dose rate have to be considered for K-feldspar age calculation. An a-value of 0.15 ± 0.05 was used according to Balescu and Lamothe (1994) for external α-dose rate calculation of the outer 0.25 µm (following Aitken, 1998) of the feldspar grains. For the internal β-dose rate a K concentration of 12.5 ± 0.5 % (Huntley and Baril, 1997) and an Rb content of 400 µg/g (following Huntley and Hancock, 2001) was assumed. Both values were comparable to those reported by Zhao and Li (2005) obtained from EMPA and ICP-MS measurement of individual K-feldspar grains taken from granite

and sediment samples. They also measured the concentration of U and Th in K-feldspar grains, but Li et al. (2007b) concluded that the contribution of U and Th to the internal β-dose rate (of ~1 %) is negligible compared to K and Rb. However, U and Th within the K-rich feldspar fraction could possibly contribute to an internal α-dose rate which would have a significant effect upon the luminescence signal (Zhao and Li, 2005; Li et al., 2007b). Nevertheless, Duller (1992) pointed out that it is not clear whether U and Th are located within the feldspar grains and it is likely that the distribution of internal U and Th is inhomogeneous (Mejdahl, 1987). Thus, an internal α-dose rate contribution from U and Th was not taken into consideration following Duller (1992) who concluded that the effect of a localised internal α-dose upon the luminescence signal is small. A significant effect would only occur if U and Th are evenly distributed within the feldspar grains (Duller, 1992). The conversion factors according to Adamiec and Aitken (1998) were used for calculation of the internal dose rate. Since only a part of the β-energy is deposited within the feldspar grain, the absorbed beta dose fraction for K was calculated according to Mejdahl (1979) and for Rb according to Readhead (2002). The results of dose rate calculation are listed in Table 6.1. If the equivalent dose of feldspar is independent of fading (e.g. after fading correction) subtraction ages can be calculated (e.g. Aitken, 1985; Davids et al, 2010). The differences between the corrected feldspar and quartz D_es were calculated to obtain subtraction D_es. To obtain subtraction ages, these subtraction D_es were divided by the sum of the internal dose rates and the external α-dose rate of K-feldspar for each sample, respectively.

6.3.3 Radiocarbon dating

Conventional radiocarbon dating was applied to two peat samples and one gyttja bulk sample. Additionally, the organic acid of the peat bulk samples (Zi-W C and W-Zi A) was dated to ensure that no modern humic acid contaminated the peat. The specific ^{14}C activity was measured radiometrically by means of proportional counters and $\delta^{13}C$ corrected according to Geyh (2005). The programme CALIB 5.0 according to Stuiver and Reimer (1993) and Reimer et al. (2004) was used for calibration of radiocarbon ages. All uncertainties of the technical and chemical treatment of the samples were included in the expressed age error (2-sigma standard deviation). The calibrated radiocarbon ages, which are given in ages BC, were recalculated to ka before the sampling date 2008 (Table 6.2). Only two of the three radiocarbon dates are regarded as reliable (Zi-W A and Zi-W C). The peat sample Zi-W B has an age of ~6.8 ka (Tab. 6.2). Thus, it is considered to have formed before or during the Littorina transgression reached the study area (see section 6.2.1). The peat horizon (Zi-W B) has a very sharp border to the shallow marine Holocene sand beneath (Fig. 6.2, layer with mollusc shell), which was clearly deposited after the Littorina transgression. Because of the stratigraphic position and the sharp horizon to the underlying shallow marine sand, we assume that the peat (Zi-W B) was re-deposited and thus it is not “in situ”.

Table 6.2: Results of radiocarbon dating.

Sample ID	Material	Depth [m]	$\delta^{13}C$ (‰)	^{14}C age [ka BP]	calibrated age range[a] [ka cal. BC]	calibrated age range[b] [ka ago]
W-Zi A	gyttja	2.08-2.18	22.6	2.40 ± 0.05	0.40-0.71	2.41-2.72
W-Zi B	peat	3.95-4.05	27.2	5.97 ± 0.09	4.73-4.96	6.74-6.95
	organic acid	3.95-4.05	27.2	5.95 ± 0.08	4.73-4.93	6.74-6.94
W-Zi C	peat	4.70-4.80	30.8	11.3 ± 0.1	11.2-11.3	13.2-13.3
	organic acid	4.70-4.80	31.1	11.1 ± 0.2	10.9-11.2	12.9-13.2

Foot notes:
[a]The ^{14}C ages were calibrated using CALIB 5.0 according to Stuiver and Reimer (1993) and Reimer et al. (2004).
[b]To obtain the age range in ka ago, 2.01 ka was added on the calibrated ^{14}C age BC.

6.4 Results

6.4.1 Performance of quartz-SAR

For the quartz-OSL the single-aliquot regenerative-dose (SAR) protocol after Murray and Wintle (2000) was applied for pre-tests (dose recovery, thermal transfer, and preheat plateau test) and D_e measurements. The quartz-SAR protocol was applied without preheat. Three quality criteria were included in each measurement sequence. The second regenerative dose was recycled at the end of the measurement sequence to obtain the recycling ratio (Wintle and Murray, 2006) to check if the sensitivity change was corrected for successfully. Furthermore, the IR/blue OSL depletion ratio (Duller, 2003) was measured for quartz aliquots to identify the presence of any feldspar contamination for each disc. Aliquots with a recycling ratio and/or IR/blue OSL depletion ratio >10% from unity were rejected, as suggested by Murray and Wintle (2000). Additionally, the measurement of a zero-dose point (recuperation) was conducted to check if there is any thermally-transferred charge from light-insensitive traps to the OSL traps (Wintle and Murray, 2006). A dose response curve of the applied quartz SAR for sample W-Zi 3 is shown in the inset of Figure 6.3a.

Figure 6.4 shows the pre-test results for the quartz-SAR measurement using sample W-Zi 3. Each data point is the mean of four medium aliquots (6 mm) and the given uncertainty is the standard deviation. A preheat plateau was obtained for the preheat temperatures between 160 to 260 °C (Fig. 6.4a). For the thermal transfer test, the D_e values from bleached aliquots (using blue LEDs for two times 40s) were measured applying the quartz-SAR protocol for preheats between 160 to 260 °C (Fig. 6.4b). Thermal transfer is detectable for preheat temperatures above 220 °C, but is small (e.g. < 0.25 Gy). The dose recovery ratios (Fig. 6.4c) were also independent of preheat temperature, and distribute within the range of acceptability (after Wintle and Murray, 2006). We therefore chose a preheat of 180 °C for the D_e measurement. The observed recycling ratios were close to unity and the very low recuperation level (1-2 % of the natural signal) supports the appropriateness of the applied quartz-SAR protocol.

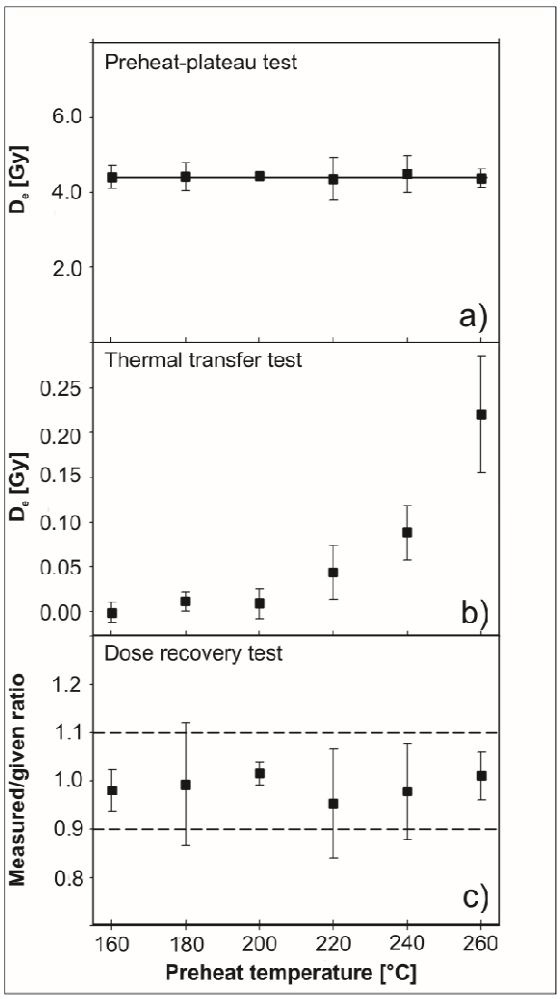

Figure 6.4: Performance tests of quartz-SAR. (a) Preheat plateau test, **(b)** thermal transfer test and **(c)** dose-recovery test results of Sample W-Zi 3. Black squares show the mean value of four medium aliquots. The uncertainties are indicated as the 1-σ standard deviation.

6.4.2 Performance of the pIRIR on K-feldspar

Preheat plateau and dose recovery tests were also applied for K-feldspar using the pIRIR protocol shown in Table 6.3. The individual results shown in Figure 6.5 are based on the average of four aliquots. The pIRIR stimulation temperature was fixed to 180 °C, and the D_e values were obtained using various preheat temperatures between 180 and 280 °C for 60 s. The pIRIR protocol was applied without a cleanout at high temperature at the end of each cycle because a test measurement using a cleanout temperature of 290 °C (according to Buylaert et al., 2009) showed no significant reduction of recuperation by this step. Moreover, we obtained better dose recovery ratios (within 10 % of unity) when the pIRIR protocol was applied without the cleanout.

Table 6.3: Modified pIRIR protocol used for equivalent dose determination of IRSL and post-IR IRSL.

Step	Treatment	Observe
1	Dose	
2	Preheat (200 °C for 60 s)	
3	IRSL, 100 s @ 50 °C	Lx_1
4	IRSL, 100 s @ 180 °C	Lx_2
5	Test dose	
6	Preheat (200 °C for 60 s)	
7	IRSL, 100 s @ 50 °C	Tx_1
8	IRSL, 100 s @ 180 °C	Tx_2
9	Return to step 1	

A preheat-plateau between 180 °C and 280 °C was obtained for the IRSL signal (Fig. 6.5a). The measured D_e values appear to decrease with increasing preheat temperature for the pIRIR signal. To estimate the thermal transfer as a function of preheat temperatures a part of sample Zi-W 3 was bleached for 4 h in a solar simulator and stimulated with IR at 50 for 200 s at room temperature. The aliquots were then measured using the pIRIR protocol and the results are presented in Figure 6.5b. Additionally, the measurement conditions proposed by Thomsen et al. (2008) (250 °C preheat and 225 °C pIRIR stimulation) and by Murray et al. (2009) and Thiel et al. (2010) (320 °C preheat and 290 °C pIRIR stimulation) were also tested. The doses measured in this experiment originate from any unbleacheable residual signal as well as any thermally transferred. Figure 6.5b shows the increase of measured dose with increasing preheats (180-320 °C) and pIRIR stimulation temperature (180 °C, 225 °C and 290 °C) for both IRSL and pIRIR signals. For the preheat temperature at 200 °C and a pIRIR stimulation at 180 °C, the thermal transfer or residual dose were small (~1 Gy) for both signals, whereas much larger doses were observed for the 320 °C preheat and 290 °C pIRIR stimulation (2.3 ± 0.5 Gy for the IRSL at 50 °C and 6.4 ± 1.2 Gy for the pIRIR stimulation at 290 °C). A similar trend was detected for the recuperation level (see Fig. 6.6a). The recuperation increases with preheat temperature.

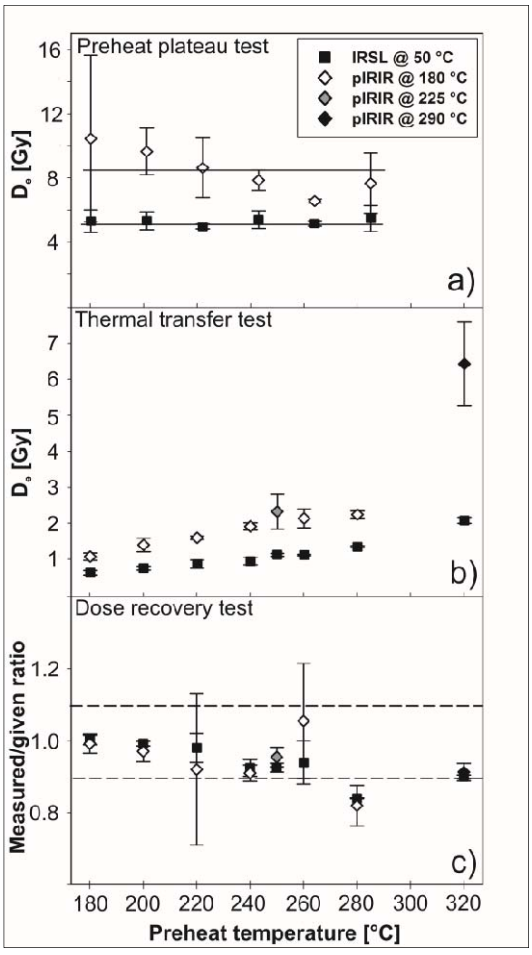

Figure 6.5: Performance tests of K-feldspar pIRIR 1. (a) Preheat plateau test, **(b)** thermal transfer test and **(c)** dose recovery-test results of Sample W-Zi 3. Black squares show the mean value of four aliquots for the IRSL signal at 50 °C. The open diamonds represent the mean value (four aliquots) of the post-IR IR signal at 180 °C. The filled diamonds represent the pIRIR signal at 225 °C for 250 °C preheat (following Thomsen et al., 2008) and 290 °C for 320 °C preheat (following Thiel et al., 2010). The values of the dose recovery experiment shown in c) represent the mean of six aliquots for preheats at 220 °C and 260 °C, respectively. The given dose for the dose recovery experiment was 12.1 Gy. The dose recovery ratios were not corrected for thermal transfer. All uncertainties are indicated as the 1-σ standard deviation.

A dose recovery experiment was conducted employing the same sets of preheat and the pIRIR stimulation temperatures as stated above using β-irradiated bleached (for 4h in the solar simulator

and IR stimulation for 200 s at room temperature) aliquots. We obtained good dose recovery ratios (close to unity) for both IRSL at 50 °C as well as the pIRIR signal for preheat temperatures of 180 °C and 200 °C (Fig. 6.5c). For preheat temperatures above 200 °C the ratios decreased. For 250 °C preheat and 225 °C pIRIR stimulation, the dose recovery ratios were within the acceptable range (0.93 ± 0.01 for the IRSL and 0.95 ± 0.03 for the pIRIR) but less promising than the lower preheat and pIRIR temperatures (at 200 °C preheat and 180 °C pIRIR stimulation; 0.99 ± 0.01 for the IRSL and 0.97 ± 0.03 for the pIRIR, respectively). Using 320 °C preheat and 290 °C pIRIR stimulation gave dose recovery ratios of 0.90 ± 0.01 for the IRSL and 0.91 ± 0.02 for the pIRIR.

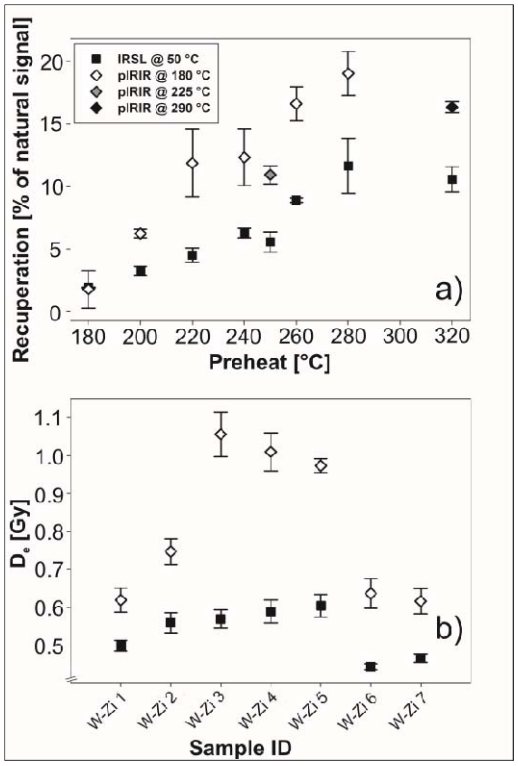

Figure 6.6: Performance of the K-feldspar pIRIR 2. (a) Recuperation obtained from the dose-recovery test of W-Zi 3 and **(b)** result of residual-dose test for W-Zi samples. Black squares show the mean value of four aliquots for the IRSL signal at 50 °C. The open diamonds represent the mean value (four aliquots) of the pIRIR signal at 180 °C. The filled diamonds represent the pIRIR signal at 225 °C for 250 °C preheat (following Buylaert et al., 2009) and 290 °C for 320 °C preheat (following Thiel et al., 2010).

We chose a preheat at 200 °C and a pIRIR stimulation at 180 °C for the D_e measurements. Since the residual dose (including the thermal transfer) is not negligible compared to the D_e value (Fig. 6b, Table 6.4), the residual dose, which were obtained after bleaching four aliquots of each sample for 4h in the solar simulator, was subtracted from the D_e values (Table 6.4). Note that the performance test data (Fig. 6.5) was not corrected for fading and residual doses. Dose response curves of the IRSL and pIRIR signals are shown in the inset of Figure 6.3b.

6.4.3 Fading rates

It is well-known that most feldspar samples suffer from anomalous fading. Huntley and Lamothe (2001) showed that the luminescence signal decays logarithmically with time (t) and attributed this loss to anomalous fading; the dependence was predicted by a quantum-mechanical tunnelling based model. A substantive review of anomalous fading and the theoretical background (e.g. the underlying model) is given by Aitken (1985, Appendix F and 1998, Appendix D). If fading is present, it induces a systematic underestimation of the feldspar ages. Anomalous fading is usually quantified by the g-value which represents the signal loss per decade of normalised storage time. A dose similar to the natural dose of each sample was given by the beta source and the normalised luminescence was

measured following various time delays (Fig. 6.7a). The pIRIR protocol described above (Table 6.3) was used to calculate g-values for the IRSL at 50 °C and the pIRIR at 180 °C using six aliquots for each sample (Fig. 6.7b). The preheat was conducted immediately following the irradiation, and thus prior to the delays (Auclair et al., 2003). The g-value of each aliquot was obtained by fitting a linear regression line to the sensitivity corrected IRSL and pIRIR signals as a function of logarithmic normalised storage time (Fig. 6.7a).

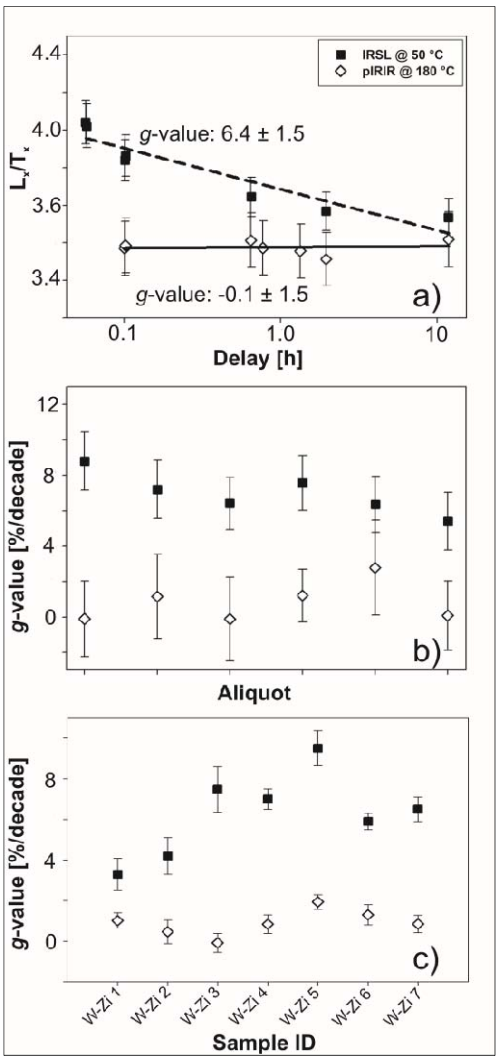

Figure 6.7: Fading correction for K-feldspar pIRIR. Fading rate (g-value) determination for W-Zi 4 **(a)** for a representative aliquot, **(b)** for six aliquots. The g-value as mean of six aliquots and the standard error of each sample (W-Zi 1-7) is shown in (c). Black squares show the mean value for the IRSL signal at 50 °C. The open diamonds represent the mean value of the pIRIR signal at 180 °C.

We obtained laboratory-fading rates (average of six aliquot and the standard error) between 3.3 ± 0.8 and 9.5 ± 0.9 %/decade for the IRSL at 50 °C and between 0.1 ± 0.5 to 1.9 ± 0.4 %/decade for the pIRIR signal at 180 °C. The g-values for the pIRIR signal are therefore significantly lower compared to the g-values of the IRSL (Fig. 6.7a, b, c; Table 6.4). Figure 6.7a shows a typical g-value determination for one aliquot of sample W-Zi 4 for both feldspar signals. It shows a pronounced difference in the slopes of the fitted linear function between the two feldspar signals, which is equivalent to the g-value. Figure 6.7b shows the individual g-values measured for sample W-Zi 4. The errors of the individual g-values are comparable for the IRSL and the pIRIR (Fig. 6.7b). Furthermore, the g-values of the IRSL signals from our seven samples revealed a wider range (between 3.29 and 9.50 %/decade) compared to those of the post-IR IRSL (between 0.08 and 1.93 %/decade) (Fig. 6.7c).

6.4.4 D_e distributions

The natural D_e distributions for both quartz and feldspar were measured for all seven samples using 6 mm aliquots each containing about 500 to 1000 individual grains. The resulting D_e distributions for sample W-Zi 6 are shown in Fig. 6.8.

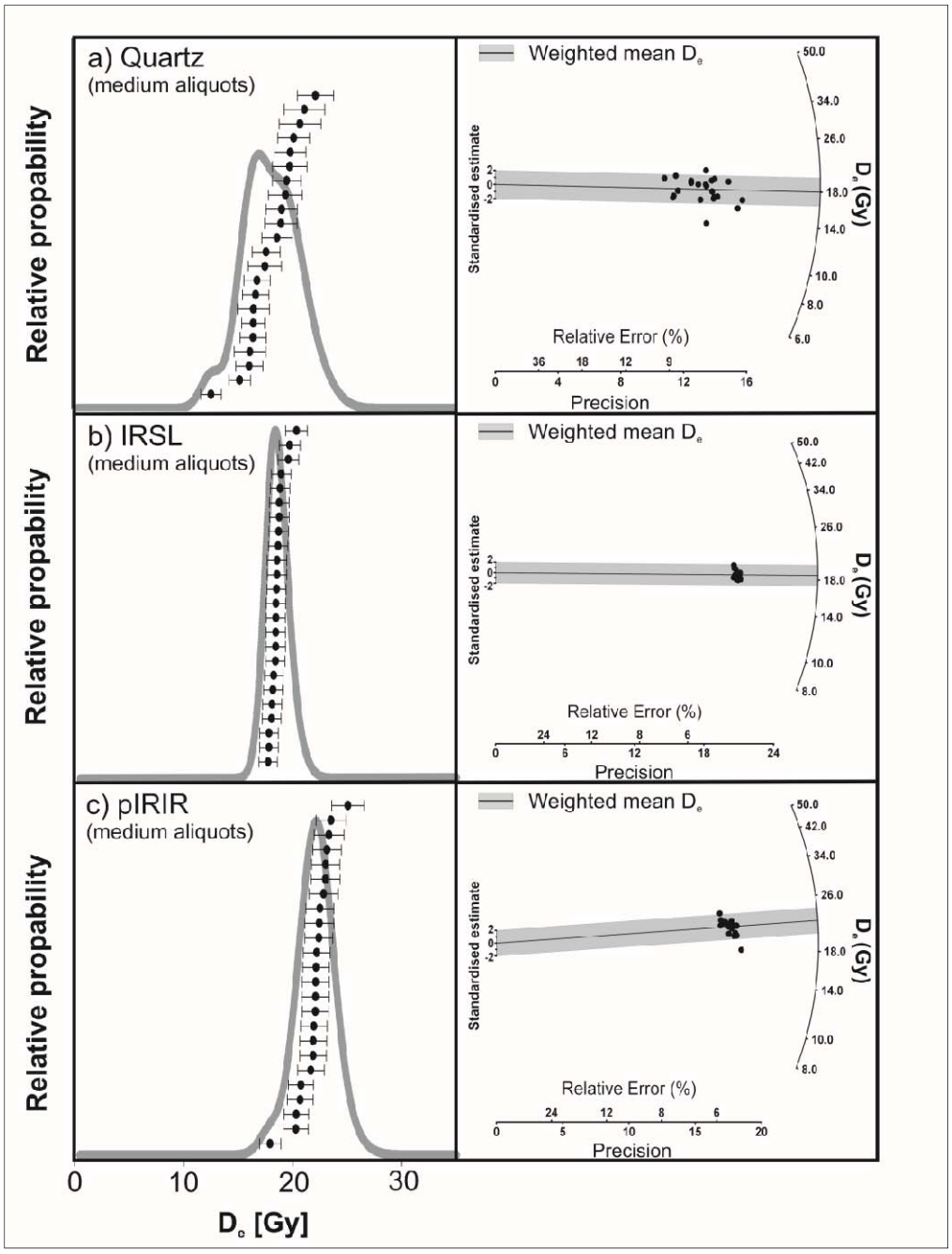

Figure 6.8: D_e distributions of W-Zi 6: probability density and radial plots of quartz (a), IRSL (b) and pIRIR (c) D_e distributions. The probability-density curves were calculated according to Singhvi et al. (2001, Appendix A) and the radial plots arccording to Galbraith et al. (1999). Des of W-Zi 2 were estimated as the weighted mean. The lines of the radial plots (a, b, c) were positioned at the weighted mean D_e.

Similar D_e distributions were obtained for samples W-Zi 3, 4, 5 and 7. All distributions appear normal with small (<20%) overdispersion values (see Table 6.4). The overdispersion values were calculated using the Central Age Model (Galbraith et al., 1999). For these five samples the weighted means are used as estimates of the uncorrected equivalent dose.

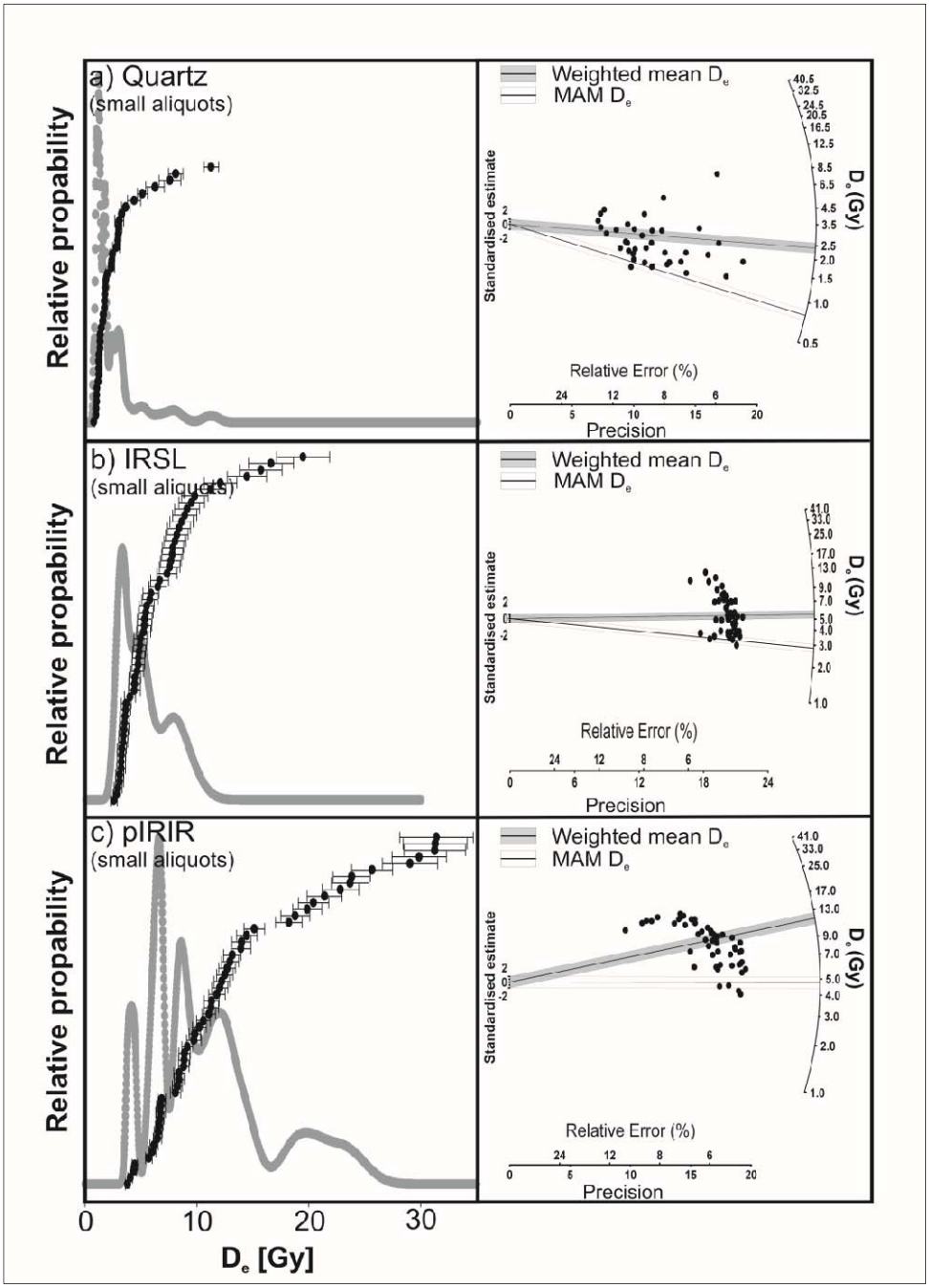

Figure 6.9: D_e distributions of W-Zi 2: probability density and radial plots of quartz (a), IRSL (b) and pIRIR (c) D_e distributions. The probability-density curves were calculated according to Singhvi et al. (2001, Appendix A) and the radial plots arccording to Galbraith et al. (1999). D_es of W-Zi 2 were estimated as the weighted mean and using the minimum age model (Galbraith et al., 1999). The lines of the radial plots (a, b, c) were positioned at the weighted mean D_e (grey shaded) and the MAM D_e (light shaded).

However, for one of the two youngest samples (W-Zi 2) the overdispersion values were generally higher; possibly indicating the presence of incomplete bleaching. For this sample we therefore

undertook additional small aliquots (2 mm) dose measurements in which each aliquot contain about 50-100 individual grains. The resulting dose distributions are shown in Fig. 6.9 and 6.10. For sample W-Zi 2 (Fig. 6.9) all signals result in positively skewed D_e distributions with overdispersion values of about 50%. Thus, for this sample we suspect that none of the signals investigated were well-bleached at the time of deposition. All though the overdispersion values are similar for the three signals it appears that by simply comparing the weighted means that quartz was better bleached than feldspar at the time of deposition. For feldspar the D_e distributions may indicate that the IRSL signal was better bleached than the pIRIR signal.

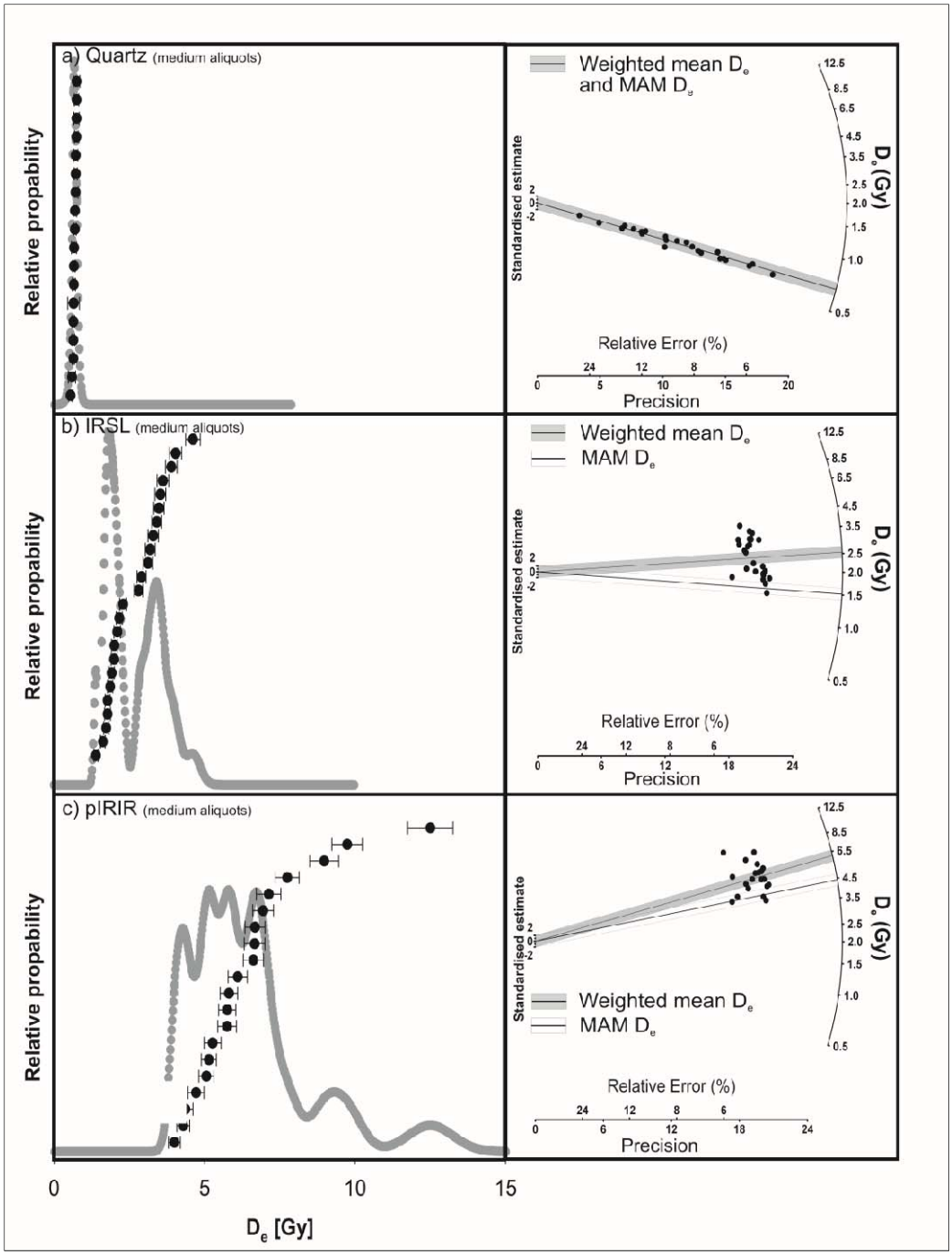

Figure 6.10: Radial plots of quartz (a), IRSL (b) and pIRIR (c) for sample W-Zi 1 D_e distributions. The radial plots are according to Galbraith et al. (1999). D_es of W-Zi 1 were estimated as the weighted mean and using the minimum age model (Galbraith et al., 1999). The lines of the radial plots (a, b, c) were positioned at the weighted mean D_e (grey shaded) and the MAM D_e (light shaded).

Sample W-Zi 1 (Fig. 10) showed, based on measurement of medium aliquots, normally distributed D_es for quartz whereas the feldspar distributions all appear to be positively skewed. The overdispersion value for quartz is 4.6% whereas it is ~50% for both feldspar signals. This presumably indicates that the quartz was well-bleached whereas the feldspar was not. Thus, in both these samples suspected of incomplete bleaching (W-Zi 1 and 2) there is some indication that quartz bleaches faster than feldspar in agreement with previously published results (e.g. Godfrey-Smith et al., 1988 and Thomsen et al., 2008).

6.4.5 Equivalent dose and age determination

For the five older samples (W-Zi 3-7) the uncorrected D_e was simply estimates as the weighted mean. The uncertainty given is the standard error (see Table 6.4). For the two younger samples (W-Zi 1 and 2) suspected of varying degrees of incomplete bleaching the Minimum Age Model (MAM, Galbraith et al., 1999) was employed for D_e estimation. For W-Zi 1 we believe that the quartz was well-bleached and consequently it makes no difference to the estimated D_e whether a weighted mean or the MAM is used for dose calculation. For the signals suspected of suffering from incomplete bleaching the MAM produces significantly lower estimates of the uncorrected D_e. For all quartz samples the luminescence age was simply calculated by dividing the uncorrected D_e by the dose rate. For all feldspar samples the uncorrected D_e was corrected for thermal transfer/residual dose and for anomalous fading. The uncertainty on the feldspar age is strongly affected by the uncertainty of the g-value; particular for samples with high g-values. The higher the g-value, the larger the relative uncertainty on the age. For our well-bleached samples the relative uncertainties on the age varied between 8 and 16% for the IRSL signals and between 6 and 8% for the pIRIR signals; i.e. the relative uncertainty on the age is always smaller for the pIRIR signal than for the IRSL signal. Thus, in order to minimize the uncertainty on the subtraction ages we decided to use the corrected pIRIR equivalent doses. All age estimates of W-Zi 6 and 7 (except for the subtraction age of W-Zi 7) indicate a late Pleistocene age of these sediments (~14 ka). For samples W-Zi 3-5 we obtained mid Holocene ages ranging from ~2 to 5.5 ka. The two uppermost samples (W-Zi 1 and 2) gave quartz ages of ~0.7 ka.

Table 6.4: Results of luminescence dating.

Sample ID	Method	Depth [m]	Total dose rate [Gy/ka]	No. of aliquotes	σ_{OD}-value [%][b]	uncorr. D_e [Gy][c]	Relative errors [%][d]	uncorr. MAM D_e [Gy][e]	g-value [%/decade]	Residual dose [Gy][f]	corr. D_e [Gy][g]	Fading uncorr. Age [ka][i]	Age [ka][j]
W-Zi 1	Quartz	0.95	0.99 ± 0.05	24	4.6	0.68 ± 0.01	1.5	0.68 ± 0.01	-	-	0.68 ± 0.01	0.69 ± 0.05	0.69 ± 0.05
	K-feldspar (IRSL)		1.53 ± 0.10	24	50.1	2.55 ± 0.14	5.5	1.52 ± 0.12	3.29 ± 0.79	0.50 ± 0.01	1.30 ± 0.18[h]	0.67 ± 0.07	0.85 ± 0.13
	K-feldspar (pIRIR)		1.53 ± 0.10	24	49.8	6.14 ± 0.20	3.3	4.42 ± 0.36	1.02 ± 0.58	0.62 ± 0.03	3.92 ± 0.44[h]	2.48 ± 0.26	2.56 ± 0.33
	Subtraction		0.54 ± 0.09	-	-	-	-	-	-	-	3.24 ± 0.44	-	2.12 ± 0.32
W-Zi 2	Quartz	1.25	1.19 ± 0.05	39[a]	53.0	2.78 ± 0.15	5.4	0.81 ± 0.07	-	-	0.81 ± 0.07[h]	0.68 ± 0.07	0.68 ± 0.07
	K-feldspar (IRSL)		1.74 ± 0.11	54[a]	41.8	5.40 ± 0.32	5.9	2.85 ± 0.18	4.20 ± 0.90	0.56 ± 0.03	3.18 ± 0.28[h]	1.31 ± 0.14	1.84 ± 0.20
	K-feldspar (pIRIR)		1.74 ± 0.11	54[a]	52.7	11.1 ± 0.8	7.2	4.78 ± 0.38	0.47 ± 0.58	0.75 ± 0.03	4.15 ± 0.45[h]	2.32 ± 0.26	2.40 ± 0.30
	Subtraction		0.72 ± 0.10	-	-	-	-	-	-	-	3.34 ± 0.46	-	4.64 ± 0.91
W-Zi 3	Quartz	2.70	1.57 ± 0.05	20	4.7	4.22 ± 0.07	1.7	-	-	-	4.22 ± 0.07	2.69 ± 0.10	2.69 ± 0.10
	K-feldspar (IRSL)		2.17 ± 0.10	16	10.4	5.41 ± 0.11	2.0	-	7.47 ± 1.12	0.57 ± 0.02	8.88 ± 1.40	2.23 ± 0.11	4.09 ± 0.67
	K-feldspar (pIRIR)		2.17 ± 0.10	16	19.1	8.05 ± 0.20	2.5	-	0.08 ± 0.46	1.06 ± 0.06	7.03 ± 0.32	3.22 ± 0.18	3.24 ± 0.21
	Subtraction		0.60 ± 0.09	-	-	-	-	-	-	-	2.81 ± 0.33	-	6.85 ± 0.89
W-Zi 4	Quartz	3.45	1.19 ± 0.05	18	1.0	3.79 ± 0.05	1.3	-	-	-	3.79 ± 0.05	3.18 ± 0.14	3.18 ± 0.14
	K-feldspar (IRSL)		1.76 ± 0.10	16	0.0	4.79 ± 0.05	1.0	-	7.00 ± 0.50	0.59 ± 0.03	7.94 ± 0.49	2.39 ± 0.14	4.51 ± 0.38
	K-feldspar (pIRIR)		1.76 ± 0.10	16	7.3	5.99 ± 0.14	2.3	-	0.84 ± 0.46	1.01 ± 0.05	5.32 ± 0.25	2.83 ± 0.18	3.02 ± 0.22
	Subtraction		0.57 ± 0.09	-	-	-	-	-	-	-	1.53 ± 0.25	-	2.68 ± 0.61
W-Zi 5	Quartz	4.30	1.23 ± 0.06	15	6.1	4.02 ± 0.22	5.5	-	-	-	4.02 ± 0.22	3.27 ± 0.24	3.27 ± 0.24
	K-feldspar (IRSL)		1.79 ± 0.11	24	0.0	4.99 ± 0.05	1.0	-	9.50 ± 0.87	0.60 ± 0.03	11.6 ± 1.6	2.45 ± 0.15	6.47 ± 0.99
	K-feldspar (pIRIR)		1.79 ± 0.11	24	6.8	6.21 ± 0.12	2.0	-	1.93 ± 0.36	0.97 ± 0.03	5.62 ± 0.29	2.93 ± 0.20	3.27 ± 0.25
	Subtraction		0.56 ± 0.09	-	-	-	-	-	-	-	1.60 ± 0.36	-	2.86 ± 0.79
W-Zi 6	Quartz	4.95	1.32 ± 0.06	22	12.6	18.1 ± 0.6	3.3	-	-	-	18.1 ± 0.6	13.7 ± 0.8	13.7 ± 0.8
	K-feldspar (IRSL)		1.90 ± 0.11	24	0.0	18.6 ± 0.1	0.6	-	5.90 ± 0.40	0.44 ± 0.01	32.2 ± 1.7	9.56 ± 0.56	16.6 ± 1.3
	K-feldspar (pIRIR)		1.90 ± 0.11	24	3.1	22.0 ± 0.1	0.5	-	1.30 ± 0.50	0.64 ± 0.03	23.9 ± 1.0	11.2 ± 0.7	12.6 ± 0.9
	Subtraction		0.58 ± 0.09	-	-	-	-	-	-	-	5.81 ± 1.10	-	10.0 ± 2.5
W-Zi 7	Quartz	5.05	1.39 ± 0.06	22	6.1	19.0 ± 0.8	4.2	-	-	-	19.0 ± 0.8	13.7 ± 0.8	13.7 ± 0.8
	K-feldspar (IRSL)		1.99 ± 0.11	20	0.0	19.2 ± 0.2	1.0	-	6.50 ± 0.60	0.47 ± 0.01	35.6 ± 2.9	9.41 ± 0.53	17.9 ± 1.8
	K-feldspar (pIRIR)		1.99 ± 0.11	20	3.2	22.7 ± 0.3	1.3	-	0.85 ± 0.43	0.62 ± 0.03	23.7 ± 1.4	11.1 ± 0.6	11.9 ± 1.0
	Subtraction		0.60 ± 0.09	-	-	-	-	-	-	-	4.73 ± 1.58	-	7.88 ± 2.50

Foot notes:
[a] Small aliquots were used for D_e estimation.
[b] Overdispersion (σ_{OD}-value) was calculated according to the Central Age Model of Galbraith et al. (1999).
[c] Uncorrected D_e is indicated as weighted mean of measured aliquots and the one sigma standard error.
[d] Relative errors are derived from the one sigma standard error and the weighted mean.
[e] D_e value determined using the minimum age model (MAM) of Galbraith et al. (1999).
[f] Residual doses are indicated as mean and the standard error.
[g] Value after correcting the uncorrected D_e for fading and residual dose.
[h] The value of [e] was taken for correction.
[i] The fading uncorrected age is corrected for residual doses.
[j] Fading corrected age.

6.5 Discussion

6.5.1 Luminescence dating

Figure 6.11 compares the four sets of luminescence dating (quartz-SAR, IRSL, pIRIR, subtraction dating) with radiocarbon ages. The seven quartz ages are in stratigraphic order and in perfect agreement with the two radiocarbon ages from the in situ peat (W-Zi A) and the organic-silicate gyttja (W-Zi C), which are regarded as reliable. The reliability of the quartz ages is supported by the pre-test results (Fig. 6.4). In particular, the absence of thermal transfer, residual doses, and very low recuperations (1-2 % of the natural signal) enforces the confidence of the the appropriateness. The uncertainties of the quartz ages are lower than those of the K-feldspars. The pIRIR ages are in stratigraphic order and W-Zi 7, 6, 5, and 4 are in agreement with the quartz-SAR within the 1-σ uncertainties. The age of sample W-Zi 3 is in agreement with the quartz age within the 2-σ uncertainty (Fig. 6.11, Table 6.4). However, the pIRIR ages of the two incompletely bleached upper samples, W-Zi 1 and 2, considerably overestimated the quartz age presumably because we employed multi-grain analyses. In quartz the number of light emitting grains is often small (<10%) which implies that small aliquots containing less than 50 grains per aliquot can be regarded as a sufficient proxy for single grain measurements (e.g. Duller, 2008). However, in feldspar the number of light emitting grains are generally found to be much higher (e.g. >40%) implying that several grains contribute significantly to the natural signal in a multi-grain approach. Thus, in samples suffering from incomplete bleaching it is to be expected that no multi-grain feldspar aliquot will

record the true burial dose. Thus, for feldspar one would presumably need to undertake true single grain measurements in the hope of identifying well-bleached grains.

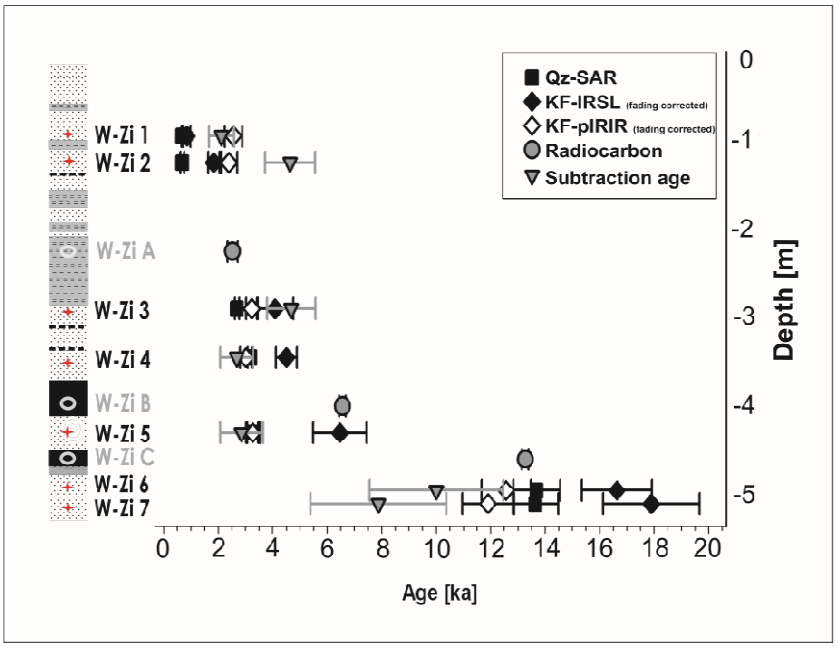

Figure 6.11: Comparision of radiocarbon and luminescence ages. The plotted feldspar ages (IRSL and pIRIR) are corrected for residual doses plus thermal transfer and furthermore for anomalous fading (corrected ages, see also Table 6.4). The set of subtraction ages is derived from the corrected pIRIR age and the quartz age (see Table 6.4).

The fading rates obtained for the pIRIR are significantly lower than those from IRSL (Table 6.4 and Fig. 6.7) suggesting the potential of the pIRIR protocol developed by Thomsen et al. (2008) for dating our young coastal coarse-grain feldspar samples. The seven IRSL ages are in stratigraphic order but overestimated the quartz-SAR ages in six out of seven samples. Only the uppermost sample, for which the minimum age model was used to calculate the IRSL age, is in good agreement with the quartz age. This sample (W-Zi 1) also has the lowest g-value (Table 6.4).

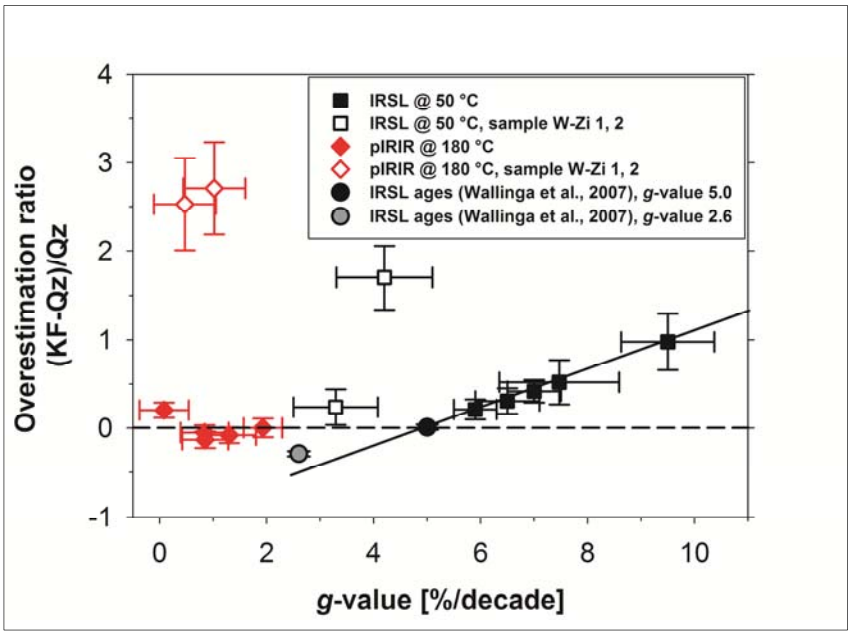

Figure 6.12: False estimation of feldspar ages compare to quartz ages as a function of g-value. The open symbols represent the upper samples (W-Zi 1 and W-Zi 2), which are affected by incomplete bleaching. The squares indicate IRSL (50 °C) ages and the diamonds indicate pIRIR (180 °C) ages. The cycles represent average ratios (from sample 1-1 to 14-1) for g-values of 2.6 %/decade (filled grey) and 5.0 %/decade (filled black) reported by Wallinga et al. (2007). The linear relationship between the false estimation ratio and the g-value is indicated as a straight line.

One reason should be considered in order to explain the tendency of overestimation of the IRSL at 50 °C; the overestimation of feldspar ages is strongly dependent on the applied fading correction (based on the papers of Huntley and Lamothe, 2001; Auclair et al., 2003) and hence the g-value. Wallinga et al. (2007) also found a systematic false estimation of feldspar ages after the fading correction using the method of Lamothe et al. (2003) and attributed this to the questionable assumptions made by the common fading correction methods regarding natural situations. In contrast to Wallinga et al. (2007), our IRSL feldspar ages overestimated or rather overcorrected when compared to the quartz OSL ages. The correlation between the feldspar age overestimation and the g-value is shown in Figure 6.12. This graph shows a linear relationship between the overestimation ratio (KF-Qz)/Qz and the g-value for the IRSL except for the two upper samples which are very likely affected by incomplete bleaching. It appears that the overestimation of the IRSL ages increases systematically with the fading rate for g-values above 5 %/decade (Fig. 6.12). According to the agreement of pIRIR ages (g-values <2 %/decade) with the quartz ages for well bleached mid-Holocene and late Pleistocene samples, we consider the overestimation of the IRSL ages is related to a systematic overcorrection of young samples having high g-values (>5 %/decade). The IRSL fading rates reported by Wallinga et al. (2007) are significant lower (~2.6 %/decade). They found an agreement for their IRSL ages with the quartz-OSL ages if a g-value of 5 %/decade was used instead. The average overestimation ratio of Wallinga et al. (2007) for the two different g-values 2.6 and 5 %, are also shown in Fig. 6.12. Their underestimated IRSL ages are almost in agreement with the linear relationship between (KF-Qz)/Qz and the IRSL g-values determined for these samples (Fig. 6.12). Correction for anomalous fading also increased the uncertainty of the derived feldspar ages significantly for our samples. Nevertheless, a fading correction is needed for those feldspar ages. A comparison of the uncorrected feldspar ages (IRSL and pIRIR) and the reliable quartz-SAR ages is shown in Fig. 6.13.

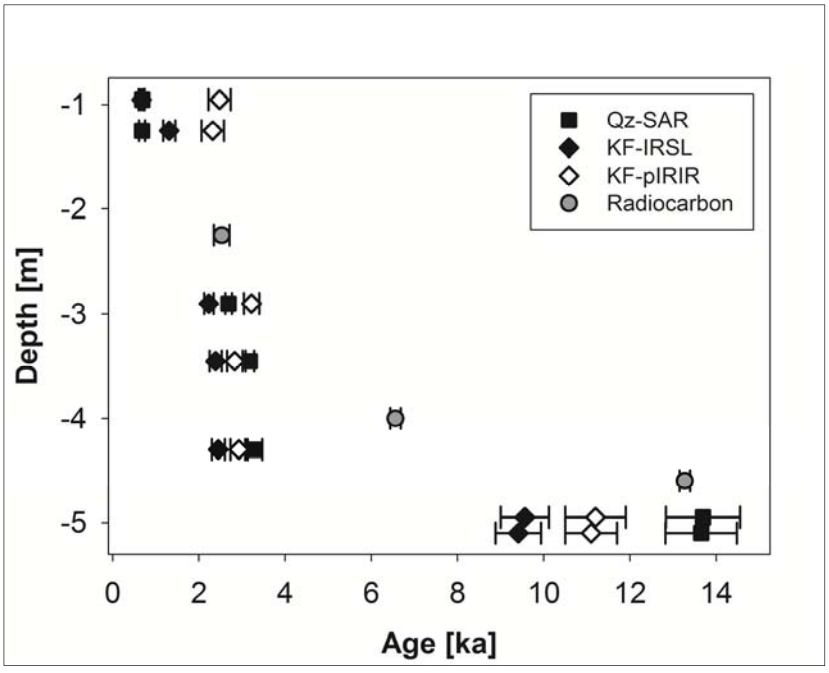

Figure 6.13: Comparison of fading uncorrected feldspar ages with quartz and radiocarbon ages. The plotted feldspar ages (IRSL and pIRIR) are corrected for residual doses plus thermal transfer but not for anomalous fading. The feldspar ages show a tendency to underestimate the reliable quartz-SAR and radiocarbon ages (the uppermost and lowermost) for the well bleached mid-Holocene and Late Pleistocene samples (W-Zi 3-7) due to anomalous fading.

Figure 6.8a, b, c shows the uncorrected D_e distributions for sample W-Zi 6. The distribution obtained from feldspar measurements of this sample indicated a very high precision with a relative standard

error of 0.6 % and 0.5 % for the IRSL and pIRIR, respectively, whereas the quartz has a standard error of 3.0 %. The same pattern was found for sample W-Zi 5 and W-Zi 7 (Table 6.4). These results support the studies of Li et al. (2007a), Li et al. (2007b) and Davids et al. (2010), who obtained higher precisions for K-feldspar than for quartz. Huntley and Lamothe (2001) already described the advantages of K-feldspar dating of young sediments due to the greater luminescence intensity. In contrast to those papers, the relative errors of both corrected feldspar ages for these samples (W-Zi 5-7) are larger mainly owing to the large uncertainties of the fading corrections for each of our seven samples.

The overestimation and the relatively large feldspar errors of W-Zi 1 and W-Zi 2 are additionally related to the different rates of zeroing of the quartz-OSL, the IRSL, and the post-IR IRSL signals. Godfrey-Smith et al. (1988) demonstrated that the bleaching of the optical signal from quartz is more rapid compared to that from IRSL. The relative probability and radial plots of the incompletely bleached sample W-Zi 2 (Fig. 6.9a, b, and c) support and extend this classic investigation. The comparison of these plots indicates that the quartz bleached most rapidly. Furthermore, the pIRIR D_e-distributions of sample W-Zi 2 appears to be wider than this of the IRSL (Fig. 6.9b, c). This possibly suggests that the IRSL signal was better bleached than the pIRIR prior to the burial. The different quantity of bleaching contributes significantly to the overestimation of the corrected IRSL and post-IR IR ages for samples W-Zi 2 (Fig. 6.11 and Fig. 6.12). This observation is also supported by the D_e results of sample W-Zi 1. The quartz of W-Zi 1 was sufficiently bleached prior to deposition and hence the weighted mean and the MAM give exactly the same D_e value (Table 6.4, Fig. 6.10). Whereas the K-feldspar D_e distributions indicate incomplete bleaching (see σ_{OD}-values, Table 6.4 and also radial plots Fig. 6.10) and therefore the D_e values of IRSL and post-IR IR calculated from minimum age model are smaller than the weighted mean. The MAM age (W-Zi 1) of the IRSL is consistent with the quartz age, whereas the weighted mean age is not. Finally, we conclude that the application of the statistical methods (e.g. MAM) using multi-grain analyses of small aliquots in order to obtain more reliable equivalent doses for incompletely-bleached samples is more promising for quartz than for feldspar. One reason is that the quartz bleached more rapidly than feldspar. The other reason is that small aliquot measurement of quartz in many samples appears to be a good proxy for single grain measurement whereas the small aliquot measurement of feldspar is not. For feldspar one would presumably need to undertake true single grain measurements to have any chance of obtaining the true burial dose.

The set of subtraction ages is not consistent with the stratigraphic order and not in agreement with the quartz ages for five of the seven samples. This method only shows agreement with the quartz ages when the quartz and pIRIR ages agree within the 1-σ uncertainties (W-Zi 4 and W-Zi 5, Table 6.4). The underestimation of the subtraction ages for the late Pleistocene samples (W-Zi 6, 7) might be related to an overestimated internal dose rate, which would affect the subtraction age more severely than the post-IR IR age. Huntley and Baril (1997) reported internal K contents in a range from 6.5 ± 0.9 to 16.9 ± 1.5 % from their 21 different K-feldspar extracts from sediments. If for example a lower potassium content of 11.0 ± 1.0 % (according to Mejdahl, 1987) is applied instead of 12.5 ± 0.5 % (mean value of Huntley and Baril, 1997) the subtraction ages would increase to 11.0 ± 2.7 and 8.6 ± 3.1 ka for W-Zi 6 and W-Zi 7, respectively. Thus, the subtraction age of W-Zi 6 would agree in this case (internal K content according to Mejdahl, 1987) with the quartz and radiocarbon ages within the 1-σ uncertainties. The pIRIR ages would change to 12.9 ± 0.9 ka and 12.2 ± 1.0 ka for

samples W-Zi 6 and W-Zi 7, respectively. These ages would be still consistent with the ages from quartz and radiocarbon. Thus, we assume that a systematic application of subtraction dating requires a sample or rather aliquot dependent determination of internal K and Rb content. The subtraction dating approach therefore merits further investigation, because it has great potential for dating studies with very complex external dosimetry (e.g. large fluctuations of the water content).

6.5.2 Stratigraphic context

The ages of glaciolacustrine fine sand W-Zi 6 and W-Zi 7 (between about 13 and 14.5 ka, Fig. 6.14) revealed an pre-Allerød age (Older Dryas, Bølling, or Oldest Dryas), which is in agreement with previous investigations of the late Pleistocene regional landscape history of the Altdarss area based on radiocarbon chronology (Kaiser, 2001; Görsdorf and Kaiser, 2001 and Kaiser et al., 2006). Hilgers (2007) also dated a similar glaciolacustrine fine sand unit and obtained Younger Dryas to Allerød ages, but expected pre-Allerød ages (>13.5 ka) as well and hence concluded that these samples were underestimated. Our luminescence ages however, in particular the quartz ages, have a pre-Allerød age within the errors. The peat sample of W-Zi C was dated by radiocarbon to 13.2 ± 0.1 ka and hence has an Early Allerød age (Fig. 6.14). It is also in agreement with the luminescence ages below.

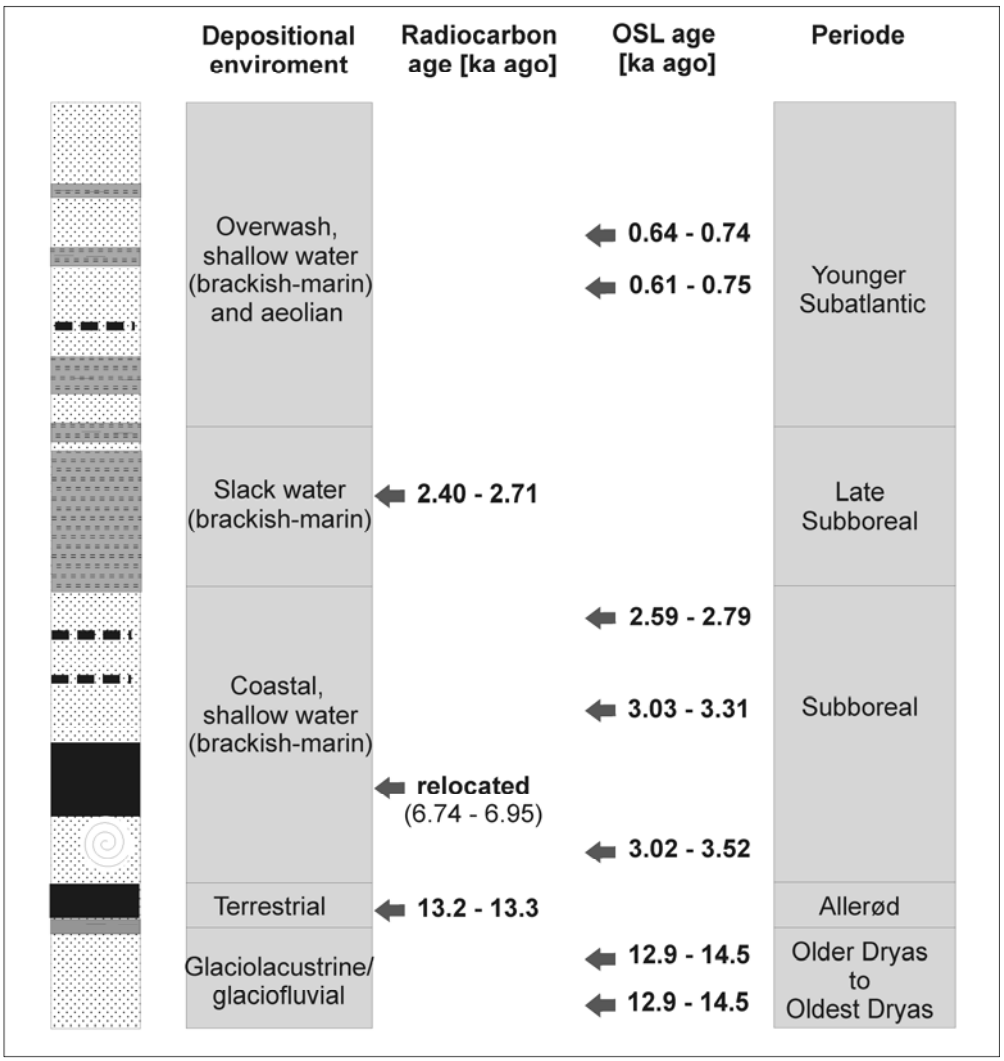

Figure 6.14: Chronostratigraphy of the investigated sediment succession. The radiocarbon and OSL ages are indicated in ka before 2008. The OSL estimates were taken from the most reliable quartz-SAR chronology. See Figure 6.2 for the lithological description.

The aeolian sand unit of Hilgers (2007), which was dated to Younger Dryas to Early Preboreal ages, is not exposed in our sediment succession. For the time between ~12.5 and 3.5 ka (Younger Dryas to Early Sub-Boreal) a large hiatus is assumed (Fig. 6.14). The succession of Zi-43 continues with shallow water or coastal sand, which is related to the development of beach ridges or a coastal-sand flat. This coastal sand has to be younger than ~6.5 ka cal. BP (according to Hoffmann et al., 2005, Lampe, 2005) because the fast-rising sea level (~15 mm/yr) reached this area between 8 and 6 ka (Early to Middle Atlantic period) and slowed down to a rate of ~1.5 mm per year at about 6.5 ka cal. BP (Hoffmann and Lampe, 2007). At the time of rapid sea level rise, the accommodation space grew faster than the sediment supply, which resulted in erosive conditions (Hoffmann et al., 2005). The development of a large sand flat behind beach ridges is therefore related to the subsequent Late Atlantic and Sub-Boreal period (<6.5 ka). Another beach ridge succession of the barrier-spit (Darss-Zingst) at Zingst-Osterwald (~5 km eastward, Fig. 6.1) was dated by quartz OSL to between about 2.0 and 1.5 ka (Reimann et al., 2010). Our quartz and post-IR IR ages of the mid-Holocene coastal sand unit between 2.6 and 3.5 ka (Sample W-Zi 3, 4 and 5) support the model of spit and coastal-barrier evolution proposed by Hoffmann et al. (2005), and are in agreement with the previous OSL investigations at Zingst-Osterwald. The radiocarbon age of sample W-Zi B, on the other hand, does not support the model, but we think this is because the organic matter was taken from relocated peat and hence this radiocarbon age is not reliable.

The organic silicate gyttja (Fig. 6.2) of the sediment succession was dated by radiocarbon to 2.5 ± 0.2 ka ago and hence developed in the Late Sub-Boreal period (Fig. 6.14). This phase of coastal development was characterized according to Hoffmann et al. (2005) by ongoing beach-ridge and dune development, which continuously narrowed and truncated the coastal inlets (e.g. the Prerowstrom as in our case, Fig. 6.1) and resulted in slack-water conditions with the development of gyttja and/or peat.

The reliable luminescence ages (in this case only the quartz ages) of the uppermost sand unit reveal a Younger Subatlantic or medieval age (~0.7 ka or ~1300 AD, Fig. 6.14). This cover sand could be related to a temporary reactivation (e.g. after a storm surge) of the coastal inlet Prerowstrom (Fig. 6.1) and thus overwash sedimentation under coastal conditions. This relatively fast sediment rearrangement is a good explanation for the insufficiently bleached sample W-Zi 2. An additional scenario could be the sand reactivation related to a period of aeolian activity between 1100 and 1350 AD, which was also found by Hilgers (2007) in NE Germany in four of the five sections investigated. The medieval dune reactivation period was related to a period of deforestation owing to a rapidly increased population, and an expansion of settlements within the German colonisation of today's NE Germany (Hilgers, 2007).

6.6 Conclusion

This case study has demonstrated that our modified pIRIR protocol with the measurement of the pIRIR signal at 180 °C was successfully applied for dating young coastal sediment samples. Nevertheless, the ages obtained for the quartz-SAR OSL are the more reliable than those of feldspar, because they are in excellent agreement with the stratigraphy and independent radiocarbon ages

and are not affected by residual doses, thermal transfer, and fading. The fading corrected IRSL ages systematically overestimate the reliable quartz ages for g-values higher than 5 %/decade. We conclude that the common fading correction approach, which was applied in this study, generated a systematic overcorrection and is thus not suitable for our samples. The only agreement with quartz-SAR was obtained for sample W-Zi 1 with the lowest g-value. Reliable pIRIR ages were obtained for the mid-Holocene and the late Pleistocene part of our succession, as these sediments were well bleached. In contrast, pIRIR dating was problematic for very young samples (<1 ka) because of higher residuals and thermal transfer, when compared to the IRSL and quartz-SAR. The pIRIR signal may bleach more slowly than IRSL and quartz OSL thus resulting in a higher probability of partially-bleached grains within the samples. The big advantages of the pIRIR signal are the very low g-values, which lead to a more reliable fading correction and fading corrected ages for the lower and the middle part of the sediment succession. Subtraction dating has great potential, if reliable quartz and feldspar De values are obtained. However, the internal dose determination has to be further investigated because it has a large importance on the precision and reliability of the subtraction dating method. The established luminescence chronology is in very good agreement with the regional stratigraphy and supports the geomorphologic models (e.g. Hoffmann et al., 2005) of spit and barrier-island evolution at the southern Baltic Sea coast.

Acknowledgements

This study was financially supported by the “Leibniz-Pakt für Innovation und Forschung”. The authors thank Gudrun Drewes, Petra Posimowski and Astrid Techmer for technical help and radiocarbon data interpretation. Helena Rodnight is thanked for improving the English and providing very helpful comments on an earlier draft of the manuscript. Kristina Thomsen and Bo Li are appreciated for their constructive comments, recommendations and criticism which helped to improve the manuscript significantly. Furthermore we thank Bert Roberts for the editorial handling.

References

- Adamiec, G., Aitken, M.J., 1998. Dose-rate conversion factors: update. Ancient TL 16, 37-50.
- Aitken, M.J., 1985. Thermoluminescence Dating. Academic Press, London.
- Aitken, M.J., 1998. An Introduction to Optical Dating. Oxford University Press, Oxford.
- Auclair, M., Lamothe, M., Huot, S., 2003. Measurements of anomalous fading for feldspar IRSL using SAR. Radiation Measurements 37, 487-492.
- Balescu, S., Lamothe, M. 1994. Comparison of TL and IRSL age estimates of feldspar coarse grains from waterlain sediments. Quartnerary Geochronology (Quaternary Science Reviews) 13, 437-444.
- Ballarini, M., Wallinga, J., Murray, A.S., van Heteren, S., Oost, A.P., Bos, A.J.J., van Eijk, C.W.E., 2003. Optical dating of young coastal dunes on a decadal time scale. Quaternary Science Reviews 22, 1011-1117.
- Blair, M.W., Yukihara, E.G., Mckeever, S.W.S., 2005. Experiences with single-aliquot OSL procedures using coarse-grain feldspars. Radiation Measurements 39, 361-374.

- Bøtter-Jensen, L., Bulur, E., Duller, G.A.T., Murray A.S., 2000. Advances in luminescence instrument systems. Radiation Measurements 32, 523-528.
- Buylaert, J.P., Murray, A.S., Thomsen, K.J., Jain, M., 2009. Testing the potential of an elevated temperature IRSL signal from K-feldspar. Radiation Measurements 44, 560-565.
- Davids, F., Duller, G.A.T., Roberts, H.M., 2010. Testing the use of feldspars for optical dating of hurricane overwash deposits. Quaternary Geochronology 5, 125-130.
- Duller, G.A.T., 1992. Luminescence Chronology of Raised Marine Terraces, South-West North Island, New Zealand. PhD thesis, University of Wales, Aberystwyth.
- Duller, G.A.T., 2003. Distinguishing quartz and feldspar in single grain luminescence measurements. Radiation Measurements 37, 161-165.
- Duller, G.A.T., 2004. Luminescence dating of Quaternary sediments recent advances. Journal of Quaternary Science 19, 183-192.
- Duller, G.A.T., 2008. Single-grain optical dating of Quaternary sediments: why aliquot size matters in luminescence dating. Boreas 37, 589-612.
- Duller, G.A.T, Bøtter-Jensen, L., Murray, A.S., 2003. Combining infrared- and green-laser stimulation sources in single-grain luminescence measurements of feldspar and quartz. Radiation Measurements 37, 543-550.
- Galbraith, R.F., Roberts, R.G., Laslett, G.M., Yoshida, H., Olley, J.M., 1999. Optical dating of single and multiple grains of quartz from Jinmium rock shelter, Northern Australia: part 1, experimental details and statistical models. Archaeometry 41, 339-364.
- Geyh, M.A., 2005. Handbuch der Physikalischen und Chemischen Altersbestimmung. Wissenschaftliche Buchgesellschaft, Darmstadt.
- Godfrey-Smith, D., Huntley, D., Chen, W.-H., 1988. Optical dating studies of quartz and feldspar sediments extracts. Quaternary Science Reviews 7, 373-380.
- Görsdorf, J., Kaiser, K., 2001. Radiokohlenstoffdaten aus dem Spätpleistozän und Frühholozän von Mecklenburg-Vorpommern. Meyniana 53, 91-118.
- Hilgers, A., 2007. The chronology of Late Glacial and Holocene dune development in the northern Central European lowland reconstructed by optically stimulated luminescence (OSL) dating. PhD thesis, University of Cologne, Cologne.
- Hoffmann, G., Lampe, R., 2007. Sediment budget calculation to estimate Holocene coastal changes on the southwest Baltic Sea (Germany). Marine Geology 243, 143-156.
- Hoffmann, G., Lampe, R., Barnasch, J., 2005. Postglacial evolution of coastal barriers along the West Pomeranian coast, NE Germany. Quaternary International 133-134, 47-59.
- Hülle, D., Hilgers, A., Radtke, U., Stolz, C., Hempelmann, N., Grunert, J., Felauer, T., Lehmkuhl, F, 2010. OSL dating of sediments from the Gobi Desert, Southern Mongolia. Quaternary Geochronology 5, 107-113.
- Huntley, D.J., Baril, M.R., 1997. The K content of the K-feldspars being measured in optical dating or in thermoluminescence dating. Ancient TL 15, 11-13.
- Huntley, D.J., Hancock, R.G.V., 2001. The Rb contents of the K-feldspars being measured in optical dating. Ancient TL 19, 43-46.
- Huntley, D.J., Lamothe, M., 2001. Ubiquity of anomalous fading in K-feldspars and the measurement and correction for it in optical dating. Canadian Journal of Earth Science 38, 1093-1106.

- Jacobs, Z., 2008. Luminescence chronologies for coastal and marine sediments. Boreas 37, 508-535.
- Janke, W., Lampe, R., 1998. Die Entwicklung der Nehrung Fischland-Darß-Zingst und ihres Umlandes seit der Litorina-Transgression und die Rekonstruktion ihrer subrezenten Dynamik mittels historischer Karten. Zeitschrift für Geomorphologie N.F., Suppl. Bd. 112, 177-194.
- Kaiser, K., 2001. Die spätpleistozäne bis frühholozäne Beckenentwicklung in Mecklenburg-Vorpommern – Untersuchungen zur Startigraphie, Geomorphologie und Geoarchäologie. Greifswalder Geographische Arbeiten 24, 1-208.
- Kaiser, K., Barthelmes, A., Czako Pap, S., Hilgers, A., Janke, W., Kühn, P., Theuerkauf, M., 2006. A Lateglacial palaeosol cover in the Altdarss area, southern Baltic Seacoast (Northeast Germany): investigations on pedology, geochronology and botany. Netherlands Journal of Geosciences 85, 199-222.
- Kliewe, H., Janke, W., 1991. Holozäner Küstenausgleich im südlichen Ostseegebiet bei besonderer Berücksichtigung der Boddenausgleichsküste Vorpommerns. Petermanns Geographische Mitteilungen 135, 1-15.
- Kunz, A., Frechen, M., Ramesh, R., Urban, B., 2010. Revealing the coastal event-history of the Andaman Islands (Bay of Bengal) during the Holocene using radiocarbon and OSL dating. International Journal of Earth Sciences, in press, doi: 10.1007/s00531-009-0507-4.
- Lamothe, M., Auclair, M., Hamzaoui, C., Huot, S., 2003. Towards a prediction of long-term anomalous fading of feldspar IRSL. Radiation Measurements 37, 493-503.
- Lampe, R., 2005. Lateglacial and Holocene water-level variations along the NE German Baltic Sea coast: review and new results. Quarternary International 133-134, 121-136.
- Lemke, W., 2005. Die kurze und wechselvolle Entwicklungsgeschichte der Ostsee – Aktuelle meeresgeologische Forschungen zum Verlauf der Litorina-Transgression. Jahrbuch der Bodendenkmalpflege in Mecklenburg-Vorpommern 52, 43-54.
- Li, S.H., Chen, Y.Y., Li, B. Sun, J., Yang, L.R., 2007a. OSL dating of sediments from deserts in northern China. Quaternary Geochronology 2, 23-28.
- Li, B. Li, S.H., Wintle, A.G., Zhao, H., 2007b. Isochron measurement of naturally irradiated K-feldspar grains. Radiation Measurements 42, 1315-1327.
- Li, B., Li, S.H., Wintle, A.G., 2008a. Overcoming environmental dose rate changes in luminescence dating of waterlain deposits. Geochronometria 30, 33-40.
- Li, B., Li, S.H., Wintle, A.G., Zhao, H., 2008b. Isochron dating of sediments using luminescence of K-feldspar grains. Journal of Geophysical Research-Earth Surface 113, F02026. 02010.01029/02007JF000900.
- Madsen, A.T., Murray A.S., 2009. Optically stimulated luminescence dating of young sediments: a review. Geomorphology 109. 3-16.
- Madsen, A.T., Murray, A.S., Andersen, T.J., Pejrup, M., Breuning-Madsen, H., 2005. Optically stimulated luminescence dating of young estuarine sediments: a comparison with ^{210}Pb and ^{137}Cs dating. Marine Geology 214, 251-268.
- Madsen, A.T., Murray, A.S., Andersen, T.J., 2007. Optical dating of dune ridges on Rømø, a barrier island in the Wadden Sea, Denmark. Journal of Coastal Research 23, 1259–1269.
- Madsen, A.T., Duller, G.A.T., Donnelly, J.P., Roberts, H.M., Wintle, A.G., 2009. A chronology of hurricane landfalls at Little Sippewisset Marsh, Massachusetts, USA, using optical dating. Geomorphology 109, 36-45.

- Mejdahl, V., 1979. Thermoluminescence dating: beta attenuation in quartz grains. Achaeometry 21, 61-73.
- Mejdahl, V., 1987. Internal radioactivity in quartz and feldspar grains. Ancient TL 5, 10-17.
- Murray, A.S., Wintle, A.G., 2000. Luminescence dating of quartz using an improved single-aliquot regenerative-dose protocol. Radiation Measurements 32, 57-73.
- Murray, A.S., Buylaert, J.P., Thomsen, K.J., Jain, M, 2009. The effect of preheating on the IRSL signal from feldspar. Radiation Measurements 44, 554-559.
- Naumann, M., Lampe, R., Hoffmann, G, 2009. Geological structure and palaeogeographic reconstruction of the Bug peninsula /NW-Rügen island. E&G (Eiszeitalter und Gegenwart) Quaternary Science Journal 58, 164-173.
- Nielsen, A., Murray, A.S., Pejrup, M., Elberling, B., 2006. Optically stimulated luminescence dating of al Holocene beach ridge plain in Northern Jutland, Denmark. Quaternary Geochronology 1, 305-312.
- Olley, J.M., Murray, A.S., Roberts, R.G., 1996. The effect of disequilibria in the uranium and thorium decay chains on burial dose rates in fluvial sediments. Quaternary Science Reviews 15, 751-760.
- Olley, J.M., Roberts, R.G., Murray, A.S., 1997. Disequilibria in the uranium decay series in sedimentary deposits at Allen´s Cave, Nullarbor Plain, Australia: implications for dose rate determinations. Radiation Measurements 27, 433-443.
- Olley, J.M., Caitcheon, G.G., Roberts, R.G., 1999. The origin of dose distributions in fluvial sediments, and the prospect of dating single grains from fluvial deposits using optically stimulated luminescence. Radiation Measurements 30, 207-217.
- Prescott, J.R., Stephan, L.G., 1982. The contribution of cosmic radiation to the environmental dose for thermoluminescent dating - Latitude, altitude and depth dependences. PACT 6, 17-25.
- Prescott, J.R., Hutton, J.T., 1994. Cosmic ray distributions to dose rates for luminescence and ESR dating: large depths and long-term variations. Radiation Measurements 23, 497–500.
- Preusser, F., Ramsmeyer, K., Schlüchter, Ch., 2006. Characterisation of low OSL intensity quartz from New Zealand Alps. Radiation Measurements 41, 871-877.
- Readhead, M.L., 2002. Absorbed dose fraction for ^{87}Rb β particels. Ancient TL 20, 25-27.
- Reimann, T., Naumann, M., Tsukamoto, S., Frechen, M., 2010. Luminescence dating of coastal sediments from the Baltic Sea coastal barrier-spit Darss-Zingst, NE Germany. Geomorphology 122, 264-273.
- Reimer, P.J., Baillie, M.G.L., Bard, E., Bayliss, A., Beck, J.W., Bertrand, C.J.H., Blackwell, P.G., Buck, C.E., Burr, G.S., Cutler, K.B., Damon, P.E., Edwards, R.L., Fairbanks, R.G., Friedrich, M., Guilderson, T.P., Hogg, A.G., Hughen, K.A., Kromer, B., McCormac, F.G., Manning, S., Bronk Ramsey, C., Reimer, R.W., Remmele, S., Southon, J.R., Stuiver, M., Talamo, S., Taylor, F.W., van der Plicht, J., Weyhenmeyer, C.E., 2004. IntCal04 terrestrial radiocarbon age calibration, 0‑26 cal kyr BP. Radiocarbon 46, 1029‑1058.
- Roberts, H.M., Plater, A.J., 2007. Reconstruction of Holocene foreland progradation using optically stimulated luminescence (OSL) dating: an example from Dungeness. The Holocene 17, 495–505.
- Schumacher, W., Bayerl, K.-A., 1999. The shoreline displacement curve of Rügen Island (Southern Baltic Sea). Quaternary International 56, 107-113.

- Singhvi, A.K., Bluszcz, A., Bateman, M.D., Someshwar Rao, M., 2001. Luminescence dating of loess-palaeosol sequences and coversands: methodological aspects and paleoclimatic implications. Earth-Science Reviews 54, 193-211.
- Steffen, D., Preusser, F., Schlunegger, F., 2009. OSL quartz age underestimation due to unstable signal components. Quaternary Geochronology 4, 353-362.
- Stuiver, M., Reimer, P.J., 1993. Extended 14C database and revised CALIB radiocarbon calibration program. Radiocarbon 35, 215–230.
- Thiel, C., Buylaert, J.P., Terhorst, B., Murray, A.S., Hofer, I., Tsukamoto, S., Frechen, M., 2010. Luminescence dating of Stratzing loess profile (Austria) – Testing the potential of an elevated temperature post-IR IRSL protocol. Quaternary International, in press, doi:10.1016/j.quaint.2010.05.018
- Thomsen, K.J., Murray, A.S., Bøtter-Jensen, L., 2005. Sources of variability in OSL dose measurements using single grains of quartz. Radiation Measurements 39, 47-61.
- Thomsen, K.J., Murray, A.S., Jain, M., Bøtter-Jensen, L., 2008. Laboratory fading rates of various luminescence signals from feldspar-rich sediment extracts. Radiation Measurements 43, 1474-1486.
- Wallinga, J., Murray, A.S., Wintle, A.G., 2000. The single-aliquote regenrative-dose (SAR) protocol applied to coarse-grain feldspar. Radiation Measurements 32, 529-533.
- Wallinga, J., Bos A.J.J., Dorenbos, P., Murray, A.S., Schokker, J., 2007. A test case for anomalous fading correction in IRSL dating. Quaternary Geochronology 2, 216-221.
- Wintle, A.G., Murray, A.S., 2006. A review of quartz optically stimulated luminescence characteristics and their relevance in single-aliquot regeneration dating protocols. Radiation Measurements 41, 369–391.
- Zhao, H., Li, S.H., 2005. Internal dose rate to K-feldspar grains from radioactive elements other than potassium. Radiation Measurements 40, 84-93.

Chapter 7, Paper V:

Tony Reimann[a], Kristina J. Thomsen[b], Mayank Jain[b], Andrew S. Murray[c], Manfred Frechen[a].

[a] Leibniz Institute for Applied Geophysics (LIAG), Section S3: Geochronology and Isotope Hydrology, Hannover, Germany
[b] Radiation Research Division, Risø DTU, Roskilde, Denmark
[c] Nordic Laboratory for Luminescence Dating, Department of Earth Sciences, Aarhus University, Risø DTU, Roskilde, Denmark

Single-grain dating of young sediments using the pIRIR signal from feldspar

Submitted in revised form to Quaternary Geochronology.

(www.sciencedirect.com/science/journal/18711014)

Abstract

In this article we test for the first time the potential of single-grains of K-rich feldspar to date well-bleached and poorly-bleached sediments using a post-IR IRSL (pIRIR) protocol. We measure natural dose distributions using K-rich feldspars from four coastal samples applying the pIRIR protocol with a preheat of 200 °C and a pIRIR stimulation temperature of 180 °C; each sample had an independent age control obtained from quartz OSL and radiocarbon dating. We also analyse single-grain dose distributions of "zero-dose" and γ-irradiated samples to determine thermal transfer/residual doses and the intrinsic sources of variability of pIRIR single-grain measurements, respectively. Based on these experiments, we conclude that thermal transfer/residual dose give rise to an off-set of ~0.6 Gy in these samples and that the uncertainty assigned to individual pIRIR single grain dose estimates cannot be smaller than 16.5%.

The analysis of the well-bleached samples shows that only the brightest 30% of the grains give pIRIR single-grain ages in agreement with the age control; this effect may arise from the suggested correlation between blue emission and potassium content of individual grains. Comparison of single-grain quartz and feldspar dose distributions from the poorly bleached samples shows that quartz is relatively better bleached; nevertheless, selection of a reliable 'minimum' feldspar dose was achieved using two different statistical models.

7.1 Introduction

Over the past two decades optically stimulated luminescence (OSL) has been applied widely in Quaternary research to establish chronologies for a variety of sedimentary settings (e.g. see reviews by Wallinga, 2002; Jain et al., 2004a; Bateman, 2008; Fuchs and Owen, 2008; Madsen and Murray, 2009). The vast majority of studies have used quartz as a natural dosimeter and quartz has generally been found to yield precise and accurate ages (e.g. Murray and Olley, 2002). Incomplete bleaching of the OSL signal prior to burial has in some samples been shown to result in an age overestimation, this is especially significant for young samples (<1ka; Jain et al. 2004a). To overcome the problem of incomplete bleaching, the OSL technique has been applied to single-grains of quartz in an attempt to identify the grain population most likely to have been well-bleached at burial. This approach has been successful in several studies (e.g. Murray and Roberts, 1997; Roberts et al., 1999, 2000; Olley et al., 1999, 2004; Bateman et al., 2007, Buylaert et al., 2009a). The methological development of single-grain techniques and the various dating applications employing single-grain analyses have been reviewed by Duller (2008). However, a drawback of using quartz as a dosimeter is its highly variable OSL sensitivity. There are some regional and sedimentary settings where the use of quartz as a natural dosimeter is limited or even impossible due to very low luminescence sensitivity (e.g. Duller, 2006; Preusser et al., 2006; Lukas et al., 2007; Steffen et al., 2009; Kunz et al., 2010). Such low sensitivities are usually encountered in samples in which the mineral grains have only recently been released from the source rock, e.g. samples from the European Alps, the New Zealand Alps or the Andes (Preusser et al., 2009). In general, low quartz OSL sensitivity makes it difficult to obtain precise OSL age estimates. Single-grain studies on such quartz samples have shown that only very few grains emit a detectable OSL signal in response to a laboratory dose (e.g. Thomsen et al., 2002, 2003; Jain et al., 2004b) and the majority of these are poorly known. In contrast, feldspar seems to have inherently strong IRSL signals regardless of the regional and sedimentary setting, and it may prove beneficial to use K-rich feldspar as the natural dosimeter instead of quartz in some settings.

Only a few single-grain feldspar studies have been published so far. Duller et al. (2003) showed that for two samples at least 40% of the individual feldspar grains emit a significant IRSL signal and stated that the large proportion of feldspar grains giving a significant signal is of great benefit when measuring single-grains of feldspar. Recently, Li et al. (2011) came to the same conclusion. In the past the widespread use of feldspar as a natural dosimeter has been held back for two main reasons: (1) the presence of anomalous fading in the feldspar thermoluminescence (TL) signal (e.g. Wintle, 1973) or IRSL signal (Spooner, 1994; Lamothe and Auclair, 1997, 1999; Huntley and Lamothe, 2001; Wallinga et al., 2007) (2) a slower resetting of the luminescence signal by exposure to sunlight (e.g. Godfrey-Smith et al., 1988; Thomsen et al., 2008), which makes the potential problem of incomplete bleaching more severe in feldspar than in quartz. Recently, significant progress has been made in finding luminescence signals from feldspar which are less prone to the effects of anomalous fading. Thomsen et al. (2008) proposed the use of a post-IR IRSL (pIRIR) signal measured at elevated temperature; this signal appears to be less affected by anomalous fading than the conventional IRSL signal. Jain and Ankjærgaard (2011) proposed a comprehensive model for feldspar luminescence based on time-resolved OSL measurements, which suggests this signal arises from distant pair recombination routed through the band tail states. This pIRIR measurement protocol has been successfully applied to older sediments by Buylaert et al. (2009b) Stevens et al. (2011), and Thiel et al. (2011). Reimann et al. (2011) applied the pIRIR protocol to Holocene coastal samples and

obtained pIRIR feldspar ages that agreed with associated quartz and radiocarbon ages. However, this study also showed that feldspar multi-grain pIRIR measurements of incompletely bleached coastal overwash sediments (W-Zi1 and W-Zi2) overestimated the true burial dose significantly even if the Minimum Age Model (MAM) of Galbraith et al. (1999) was applied to small aliquot (~100 grains) dose distributions. This overestimation is not surprising given the fact that a significantly larger proportion of feldspar grains emit a detectable signal compared to quartz grains, and so it is unlikely that one will measure a multi-grain aliquot containing only well-bleached feldspar grains. In this study we examine the potential of using single-grains of K-rich feldspar to date both well-bleached and incompletely bleached sediments using the pIRIR protocol suggested by Reimann et al. (2011) for young feldspar samples. We have measured the natural single-grain dose distributions of four of the samples (W-Zi2, W-Zi3, W-Zi6 and W-Zi7) presented in Reimann et al. (2011) using the same pIRIR measurement protocol. The multi-grain feldspar ages of samples W-Zi6 and W-Zi7 agreed well with independent age control (quartz OSL and radiocarbon dating) and these samples are thus considered to be well-bleached. In contrast, the feldspar ages of W-Zi2 and W-Zi3 both overestimated the ages given by quartz OSL age. These samples are thus suspected of being affected by the presence of incompletely bleached feldspar grains (particularly sample W-Zi2 where even the quartz multi-grain dose distribution also showed indications of poor bleaching). As well as examining the natural dose distributions of these samples we estimate the contribution of thermal transfer/residual dose likely to be present in these samples using both a modern analogue and a laboratory bleached sample (W-Zi7). To assess the over-dispersion expected from intrinsic sources of variability we also examine the results obtained from two gamma irradiated samples. Finally, we estimate the burial dose in the two samples which are possibly affected by incomplete bleaching (W-Zi2 and W-Zi3).

7.2 Experimental details

7.2.1 Samples

The four samples measured in this study were taken from the Westzingst core (Zi-43). The sampling site is located on the southern Baltic Sea coast (NE Germany) and shown in Fig. 7.1A. More information about the sampling location and the geological context are given in Reimann et al. (2011). From quartz OSL and radiocarbon dating it is known that the sediment record spans ~13.5 ka. The sampling position, the radiocarbon ages and the multi-grain quartz ages are shown in Figure 7.1B. Furthermore, a modern sample (Zi-modern) with a quartz OSL age of ~35-40 years was taken from the recent beach of Zingst peninsula. The lowermost samples have multi-grain fading corrected pIRIR feldspar ages of 12.6 ± 0.9 ka and 11.9 ± 1.0 ka for samples W-Zi6 and W-Zi7, respectively, both showing good agreement with quartz OSL ages and the radiocarbon age of an overlying peat horizon; thus, both samples are regarded as well bleached. Based on multi-grain measurements, the fading corrected pIRIR age of the mid-Holocene sample W-Zi3 was, estimated to be 3.24 ± 0.21 ka. The fading corrected pIRIR age of sample W-Zi3 slightly exceeds the quartz OSL age (2.69 ± 0.10 ka) and the radiocarbon age of an overlying gyttja (2.57 ± 0.16 ka) within the 1-σ uncertainty suggesting that the apparent feldspar age of this sample may be affected by incomplete bleaching. The upper sample W-Zi2 showed incomplete bleaching in small aliquot dose distributions for both pIRIR feldspar and quartz OSL (Reimann et al., 2011).

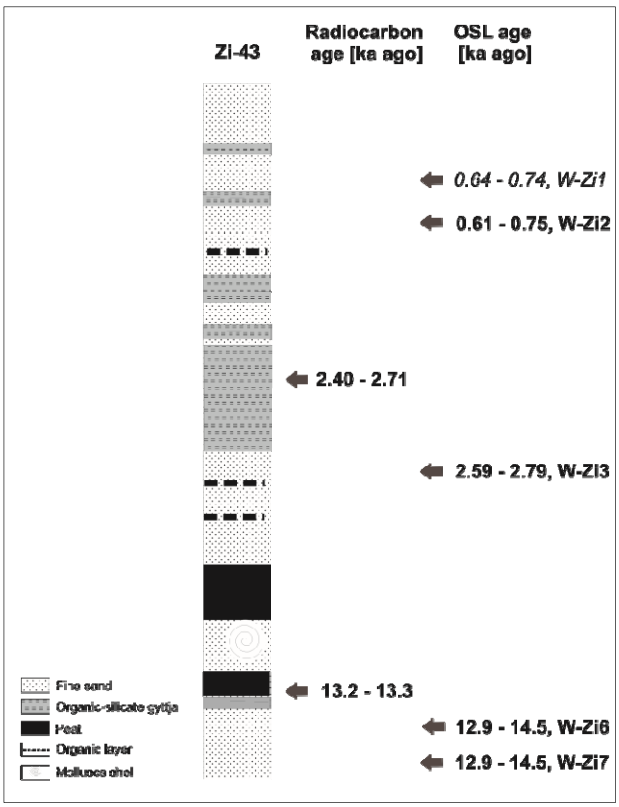

Figure 7.1: Sample position, radiocarbon ages and multi-grain quartz ages of the samples under study, modified after Reimann et al. (2011). Sample WZi-1, displayed in italic font, is not analysed in this study.

7.2.2 Sample preparation

The samples from Westzingst core were sieved and subsequently treated with HCl and H_2O_2 to take away carbonates and organics. To obtain K-rich feldspar extracts ($\rho < 2.58$ g/cm^3) the 100-150 µm fraction of samples W-Zi6, 7, 3 and the 150-200 µm fraction of sample W-Zi2 were density separated using a heavy liquid. Furthermore, the quartz fraction (2.62 g/cm^3 < ρ < 2.70 g/cm^3) was treated with concentrated HF to remove the outer rim of the quartz grains. The K-rich feldspar extracts were not HF treated. The dose rates were determined using high-resolution gamma spectrometry and the total dose rates are shown in Table 7.1. Details of dose rate determination are reported by Reimann et al. (2011).

7.2.3 Luminescence equipment and measurement procedures

An automated Risø TL/OSL reader (DA 15) fitted with a dual (red and green) laser single-grain attachment (Bøtter-Jensen et al., 2003; Duller et al., 2003) was used for luminescence measurements. The grains were loaded into aluminium single-grain discs with a 10 x 10 grid of 200 µm grain holes. To confirm that only one grain was loaded into each hole the discs were visual inspected using a microscope. The feldspar grains were optically stimulated for 1.68 s with a 150 mW 830 nm IR laser. The IRSL at 50 °C was released prior to the pIRIR single-grain measurement using an array of infrared LEDs (870±40 nm, ~140 mW/cm^2) for 200 s stimulation. All feldspar signals were detected through a combination of Schott BG-39 and Corning 7-59 filters transmitting between 320 and 450 nm. The quartz grains were stimulated for 0.83 s with a 10 mW Nd : YVO_4 solid-state diode-pumped laser emitting at 532 nm. The signal was detected trough a 7.5 mm Hoya U-340 detection filter. For details of the dual laser system and the adjustment of the lasers see Bøtter-Jensen et al. (2003) and Duller et al. (2003). In situ irradiations were made using a $^{90}Sr/^{90}Y$ beta

source (produced before 2000). The source uniformity was mapped with radiosensitive film and a dose rate map was consequently derived (see Lapp et al.; submitted for details). The dose uniformity across the sample area was found to be ~4% and is thus not expected to contribute significantly to the observed variability in the measured single-grain dose distributions. Correcting the measured single dose distributions for source non-uniformity did not change the obtained over-dispersion values significantly.

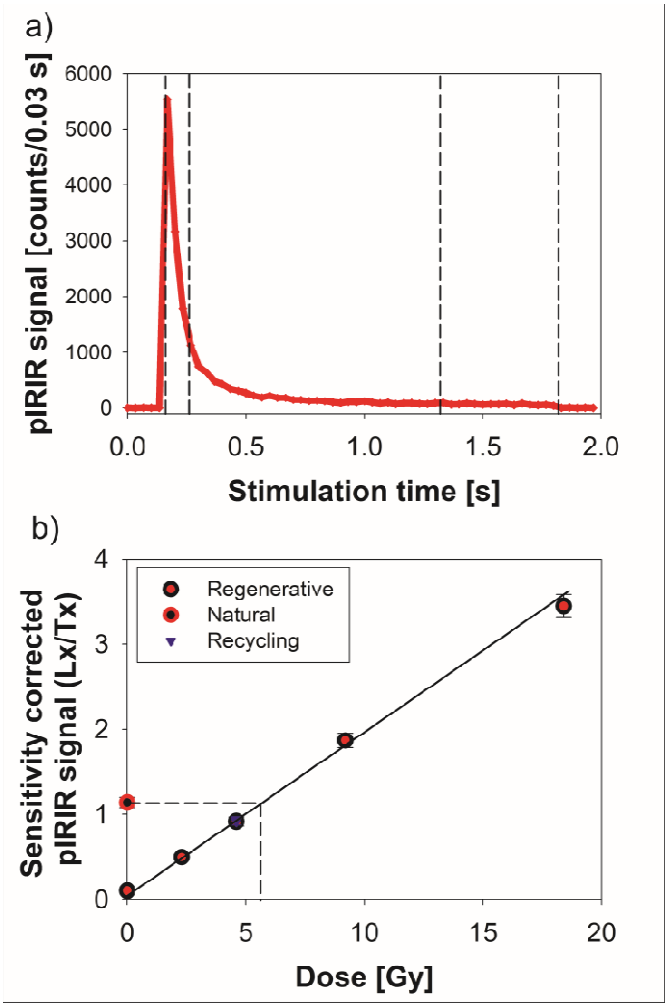

Figure 7.2: Typical pIRIR single-grain feldspar decay curve (a) and dose response curve (b) of sample W-Zi2. The applied pIRIR protocol is described in Reimann et al. (2011).

A pIRIR protocol (Thomsen et al., 2008) was employed using a preheat of 200 °C for 60 s and a pIRIR stimulation temperature of 180 °C (Reimann et al., 2011). The pIRIR measurement time was 1.68 s. A typical single-grain pIRIR decay curve is shown in Fig. 7.2A. The signal of the first 0.07 s after the IR laser was switched on was used as the initial signal and the signal observed in the last 0.48 s was subtracted as background (Fig. 7.2). Furthermore, Reimann et al. (2011) also calculated (using multi-grain measurements) fading rates (g-values) of the pIRIR signal of between 0 and 1.8 %/decade suggesting that fading is low for the samples under study (W-Zi2, 3, 6, and 7). The multiple-grain pIRIR g-values are listed in Table 7.1.

Quartz was measured using a single-aliquot regenerative-dose (SAR) protocol (Murray and Wintle, 2000) employing a preheat of 180 °C for 10s. For single-grain quartz the time interval of the last 0.23 s was subtracted as background from the initial 0.033 s. All dose estimates were derived by fitting

the regenerated dose points by a linear function (for pIRIR see Fig. 7.2B). For dose estimation each dose response curve was forced through the origin and the fitting was carefully checked. For all experiments only single-grains with a test dose error of less than 20% and a recycling consistent with unity within 2σ were accepted. Furthermore, all grains displaying non-monotonically growing dose response curves or other "abnormal" luminescence behaviour were rejected from further analysis. Recuperation is an important effect for dating of young samples. However, since the natural signals are small, the recuperation values (R_0/N) are by definition rather high, of the order of 15-30 % for the young incompletely bleached samples. Thus it is difficult to use recuperation as a measure of satisfactory applicability of the SAR procedure or otherwise. For such young samples the use of recuperation as a rejection parameter, as suggested by Li et al. (2011), could result in biased distributions, where the lower dose values are automatically rejected because of their correspondingly smaller natural signals. To avoid this problem the recuperation was calculated relative to the sensitivity corrected response to the first regenerative dose (R_0/R_1) which is independent of D_e. However, no systematic relationship between the dose recovery ratio, the grain brightness and the R_0/R_1 recuperation was found.

Gamma irradiation was performed using a calibrated ^{137}Cs point source at a distance of 2 m to deliver a dose of 4.81 Gy. The samples were loaded into glass tubes with an internal diameter of 5 mm and a wall thickness of 2 mm. The ^{137}Cs source is calibrated using a standardised ionisation chamber measuring air kerma by Statens Institut for Strålehygiejne (Danish State Institute for Radiation Hygiene).

Table 7.1: Results.

Sample	Total dose rate [Gy/ka][a]	n measured/accepted /brightest 30%[b]	CAM D_e [Gy][c]	σ_{OD} [%][c]	MAM-4 D_e [Gy][d]	IEU [Gy][e]	g-value [%/decade][f]	Corrected CAM age [ka][g]	Corrected MAM age [ka][g]	corrected IEU age [ka][g]	Expected age [ka]
W-Zi 2 (KF)	1.74 ± 0.10	1000/330/99	5.44 ± 0.78	135 ± 12	1.69 ± 0.09	1.69 ± 0.09	0.47 ± 0.58	2.88 ± 0.46	0.57 ± 0.06	0.63 ± 0.06	0.84
W-Zi 2 (Qz)	1.19 ± 0.05	2400/131/-	1.75 ± 0.17	92.3 ± 7.6	1.12 ± 0.06	0.98 ± 0.06	-	1.47 ± 0.16	0.94 ± 0.06	0.82 ± 0.05	0.84
W-Zi 3	2.17 ± 0.09	500/154/46	7.15 ± 0.50	44.9 ± 3.7	5.58 ± 0.62	5.80 ± 0.20	0.08 ± 0.46	2.86 ± 0.29	2.30 ± 0.37	2.53 ± 0.14	2.69
W-Zi 6	1.90 ± 0.10	500/250/75	22.3 ± 0.5	10.4 ± 1.1	-	-	1.30 ± 0.50	12.8 ± 0.9	-	-	13.7
W-Zi 7	1.99 ± 0.10	700/330/99	23.6 ± 0.7	17.0 ± 1.2	-	-	0.85 ± 0.43	12.5 ± 0.9	-	-	13.7

Foot notes:

[a] For details of dose rate determination see Reimann et al. (2011).

[b] See section 3.4.

[c] Calculated using the Central Age Model (CAM) of Galbraith (1999). The uncertainties on the individual dose points include an additional uncertainty of 16.5% derived from the gamma dose recovery experiment (section 3.3).

[d] Minimum Age Model (MAM) according to Galbraith et al. (1999). Overdispersion of a well-bleached dose component was defined to be 15%.

[e] IEU according to Thomsen et al. (2007).

[f] For details of fading correction see Reimann et al. (2011).

[g] Feldspar ages are corrected for thermal transfer (see section 3.2) and fading.

7.3 Results and discussion

7.3.1 Sensitivity of individual feldspar grains

Reimann et al. (2011) made use of small aliquots (each containing ~100 grains) for their measurements of sample W-Zi2. They obtained dose distributions for both quartz and feldspar indicating the presence of incomplete bleaching. Using the Minimum Age Model (MAM, Galbraith et al., 1999) they were able to extract a quartz dose consistent with the dose expected from radiocarbon dating, indicating that the small aliquot measurements were a sufficiently good proxy for single-grain measurements. However, applying the MAM to the feldspar distribution resulted in

a considerable overestimation (~250%). In the literature it has been shown that the proportion of grains contributing significantly to the measured signal in multi-grain measurements is higher for feldspar than for quartz (e.g. Duller et al., 2003; Li et al., 2011), which may mean that the small aliquot measurements of the feldspar fraction are not a good proxy for single-grain measurements.

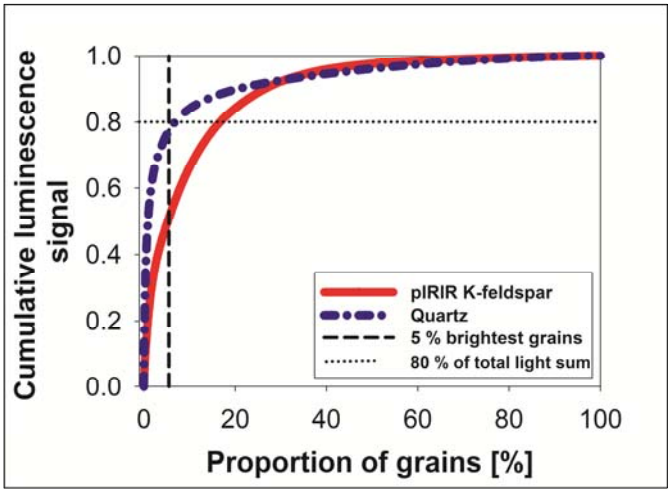

Figure 7.3: Total light sum curves of sample W-Zi2.

In this study we have undertaken true single-grain measurements of sample W-Zi2 to verify the conclusion of Reimann et al. (2011). Figure 7.3 shows the normalised cumulative light sum for the natural test dose signal as a function of the proportion of grains (Duller and Murray, 2000). For quartz (n = 2400) about 80% of the light comes from about 5% of the grains, and only these grains gave a statistical uncertainty on the natural test dose of less than 20%. Thus, in the small aliquot measurements (~100 grains), on average only ~5 grains gave a detectable OSL signal, and the total light emitted from these small aliquots must be dominated by the brightest 1-2 grains. Thus, it seems reasonable to conclude that it was indeed possible to measure individual aliquots containing only well-bleached grains.

In Fig. 7.3 we show the normalised cumulative light sum for single-grains of feldspar extracted from W-Zi2 (n=1000). For feldspar 80% of the light comes from about 20% of the grains and 33% of the grains had a test dose response known to better than 20%; on average each 100 grain aliquot would have included 33 grains giving a detectable signal and 6-7 grains giving 80% of the cumulative light sum. Thus, in multi-grain measurements one would expect a significantly larger averaging effect for feldspar than for quartz.

7.3.2 Dose distributions from the modern and laboratory bleached samples

One of the potential problems of using feldspar as a natural dosimeter is that the feldspar IRSL signal bleaches significantly more slowly than the quartz OSL signal and thus is more prone to incomplete signal resetting at burial. A second, problem particularly associated with young samples, is the amount of thermal transfer (see review by Madsen and Murray, 2009). This term describes a transfer of charge from thermally shallow, light-insensitive traps to deeper, light-sensitive traps. If the thermal transfer is a significant fraction of the luminescence signal it can cause an offset in dose estimates. Lowering the preheat temperature should reduce the importance of thermal transfer (e.g. Bailey et al. 2001). Thermal transfer in quartz at a single-grain scale was investigated by Jain et

al. (2004b); they showed that thermal transfer was strongly variable from grain to grain, and that dose distributions systematically moved to higher doses with preheat. The feldspar multi-grain study of Reimann et al. (2011) showed that their pIRIR protocol (applying a preheat of 200 °C) resulted in a significant thermal transfer. They examined feldspar multi-grain dose distributions of laboratory bleached samples to correct for this effect.

In this study we examine zero age (modern) samples to determine possible residual doses/thermal transfer in sediments. In Fig. 7.4A we show the resulting K-rich feldspar single-grain pIRIR dose distribution from a modern beach sample (sample Zi-modern; dated to be ~35 years using quartz OSL, and so a predicted feldspar dose of ~0.06 Gy) from the study area. A total of 400 grains was measured and 129 of these grains passed the rejection criteria (see section 7.2.3). The distribution is clearly symmetric and centred around 0.6 Gy. To estimate the weighted mean we used a modified version of the Central Age Model (CAM_{unlog}), which makes use of non-logarithmic D_e values. The CAM_{unlog} D_e was calculated to be 0.63 ± 0.03 Gy with an over-dispersion (σ_{OD}) of 0.29 ± 0.04 Gy (45.5 ± 5.9%). The underlying assumptions regarding the calculation of the over-dispersion are specified in the next section.

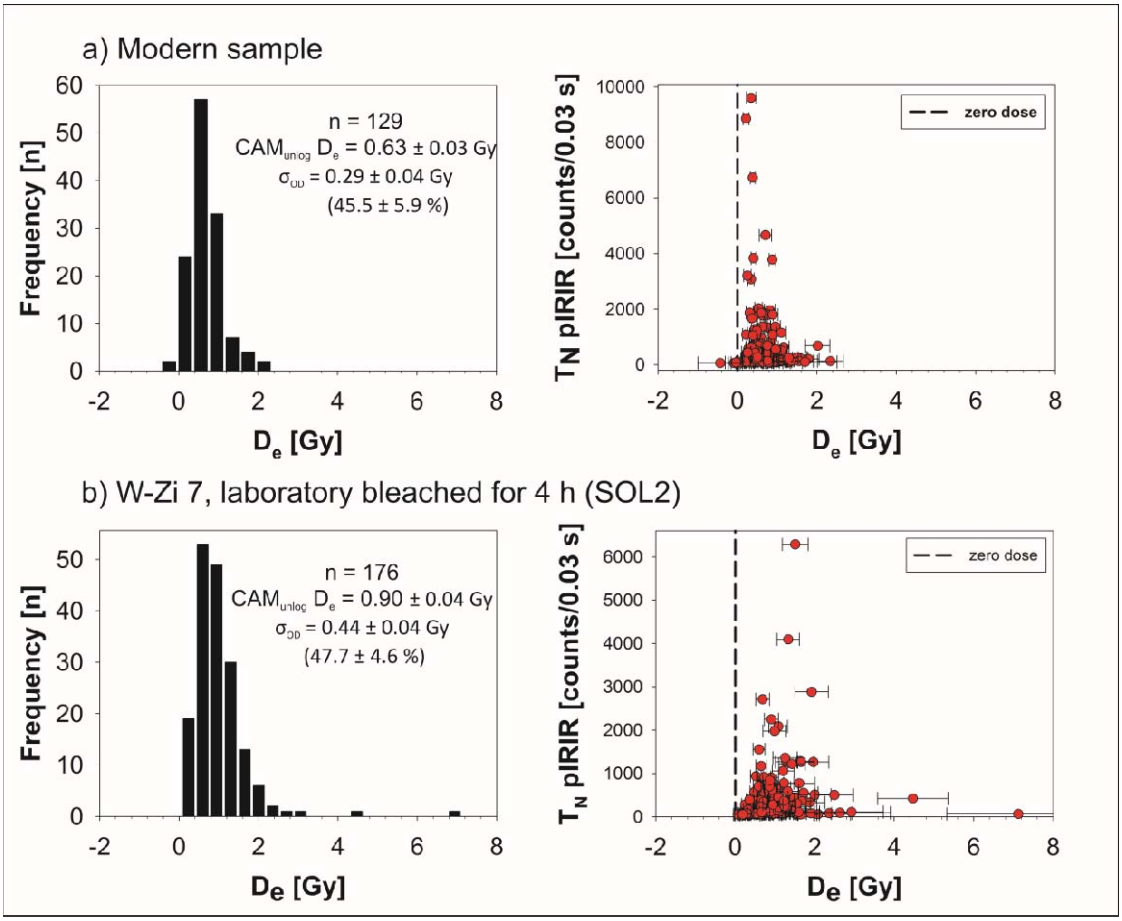

Figure 7.4: pIRIR single-grain dose distributions of a modern sample Zi-modern (a), and the laboratory bleached W-Zi7 (b). On the left a histogram on the right a T_N vs. D_e plot is shown for (a) and (b), respectively.

We also bleached a portion of sample W-Zi7 (D_e = ~23 Gy, Reimann et al., 2011) for four hours using a daylight simulator (SOL2). The resulting D_e distribution is shown in Fig. 7.4B. A total of 600 grains were measured and 176 grains passed the rejection criteria. The distribution is approximately symmetric and centred on 0.8 Gy. However, the distribution appears slightly wider than the distribution of the modern sample suggesting that bleaching in nature was more effective than four

hours bleaching using the SOL2 in the laboratory. The CAM_{unlog} D_e of the laboratory bleached sample is 0.90 ± 0.04 Gy and the over-dispersion (σ_{OD}) is 0.44 ± 0.04 Gy (47.7 ± 4.6%). The CAM estimates of both experiments were used to correct for thermal transfer and residual doses in the dose recovery experiments.

7.3.3 Quantification of the intrinsic over-dispersion

In general, the observed dispersion in a natural single-grain dose distribution is attributed to intrinsic factors (e.g. counting statistics, instrument reproducibility, thermal transfer and other OSL characteristics) and extrinsic factors (e.g. small scale variations of the radiation field, partial bleaching, post-depositional mixing). Thus, in order to be able to evaluate the contribution of external sources of variability to the observed over-dispersion in natural dose distributions, it is important to assign appropriate intrinsic uncertainties to the individual dose estimates. In order to assess the appropriateness of the assigned intrinsic uncertainties a gamma dose recovery experiment was performed. In a dose recovery experiment the extrinsic factors are eliminated and thus only intrinsic factors contribute to the observed over-dispersion. Similar experiments were performed by Thomsen et al. (2005) on heated quartz samples and by Thomsen et al. (2007) on both heated and unheated quartz. They suggested that the minimum over-dispersion resulting from intrinsic factors alone in quartz is of the order of 9-12%.

Portions of the modern (Zi-modern) and the laboratory bleached (W-Zi7) samples were placed in separate glass tubes and irradiated simultaneously using a 662 keV ^{137}Cs point source providing a dose rate in feldspar of 0.10 Gy/h in a scatter-free geometry. Both samples were given a γ-dose of 4.81 Gy and were measured ~10 days after irradiation. To check for fading, the measurement of the γ-irradiated sample was repeated after 137 days (equivalent to a delay of more than 2 decades relative to the irradiation time). The resulting dose distributions are shown in Fig. 7.5A, B, C. The expected dose is the sum of the given γ-dose (4.81 Gy) and the estimate of the residual dose of ~0.63 Gy and ~0.90 Gy for the modern sample and the laboratory bleached sample, respectively. The D_e estimates in Fig. 7.5A and B (prompt and delay measurement, respectively) agree within uncertainties suggesting that fading is not detectable at this level. The calculated measured–to-given dose ratio is 1.08 ± 0.02 for the modern sample (Fig. 7.5A, B) and 1.05 ± 0.02 for laboratory bleached sample (Fig. 7.5C) suggesting that the applied pIRIR protocol is working satisfactorily.

The uncertainty on individual D_e values is made up of contributions from counting statistics and curve fitting errors calculated using “Analyst 3.24” (Duller, 2007). However, over-dispersions of 16.5 ± 0.6%, 19.3 ± 0.6% and 22.9 ± 0.8% (Fig. 7.5A, B, C, respectively) were measured using the γ-dose distributions suggesting that the associated uncertainties based on counting statistics and fitting errors alone are too small to account for the observed variability and furthermore, that no single-grain D_e can be known to better than ~16.5% in these samples. Thus, from now on, we add in quadrature 16.5% to the uncertainties on the individual D_es to account for other intrinsic sources of uncertainty (e.g. instrumental reproducibility, luminescence characteristics of the grains).

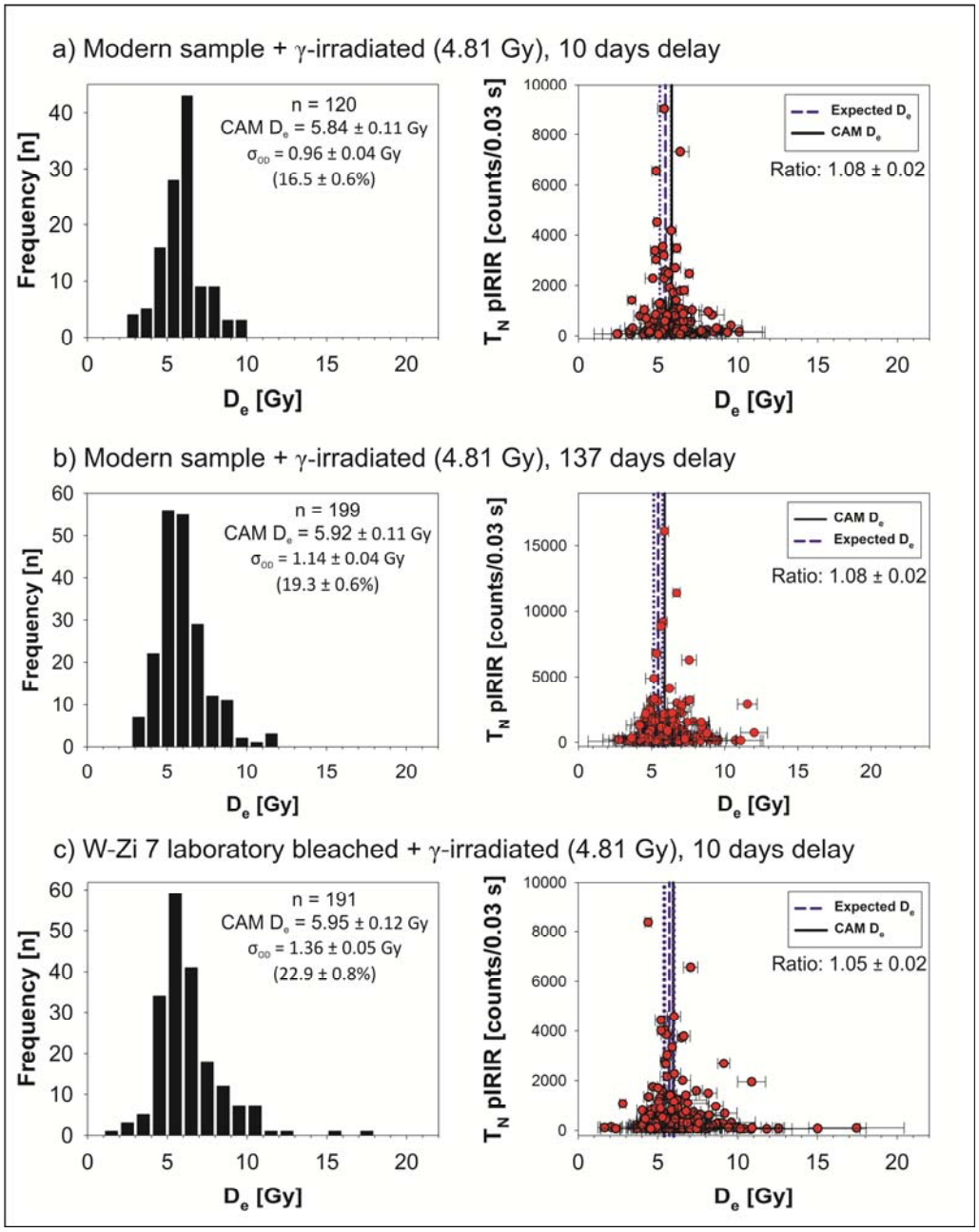

Figure 7.5: pIRIR single-grain dose distributions of the γ-irradiated (4.81 Gy) samples. (a) Shows the distributions of modern γ-irradiated sample measured after 10 days and **(b)** after 137 days; **(c)** shows the distribution of γ-irradiated laboratory bleached sample. On the right a histogram on the left a T_N vs. D_e plot is shown for (a), (b) and (c), respectively. The expected dose is indicated as medium-dashed line, the weighted mean (CAM, Galbraith et al., 1999) is indicated as solid line.

The same experiment was conducted using γ-dosed (4.81 Gy) quartz extracts from the modern sample (Zi-modern) and the laboratory bleached sample W-Zi7. The over-dispersions in the resulting quartz single-grain dose distributions are 11.0 ± 1.2% (n = 41) and 8.5 ± 1.1% (n = 67) for the modern sample and the laboratory bleached sample, respectively. Thus, the over-dispersions in the quartz single-grain dose distributions are significantly lower than those observed in the pIRIR feldspar single-grain distribution.

7.3.4 Dose distribution analysis for the well bleached coastal samples

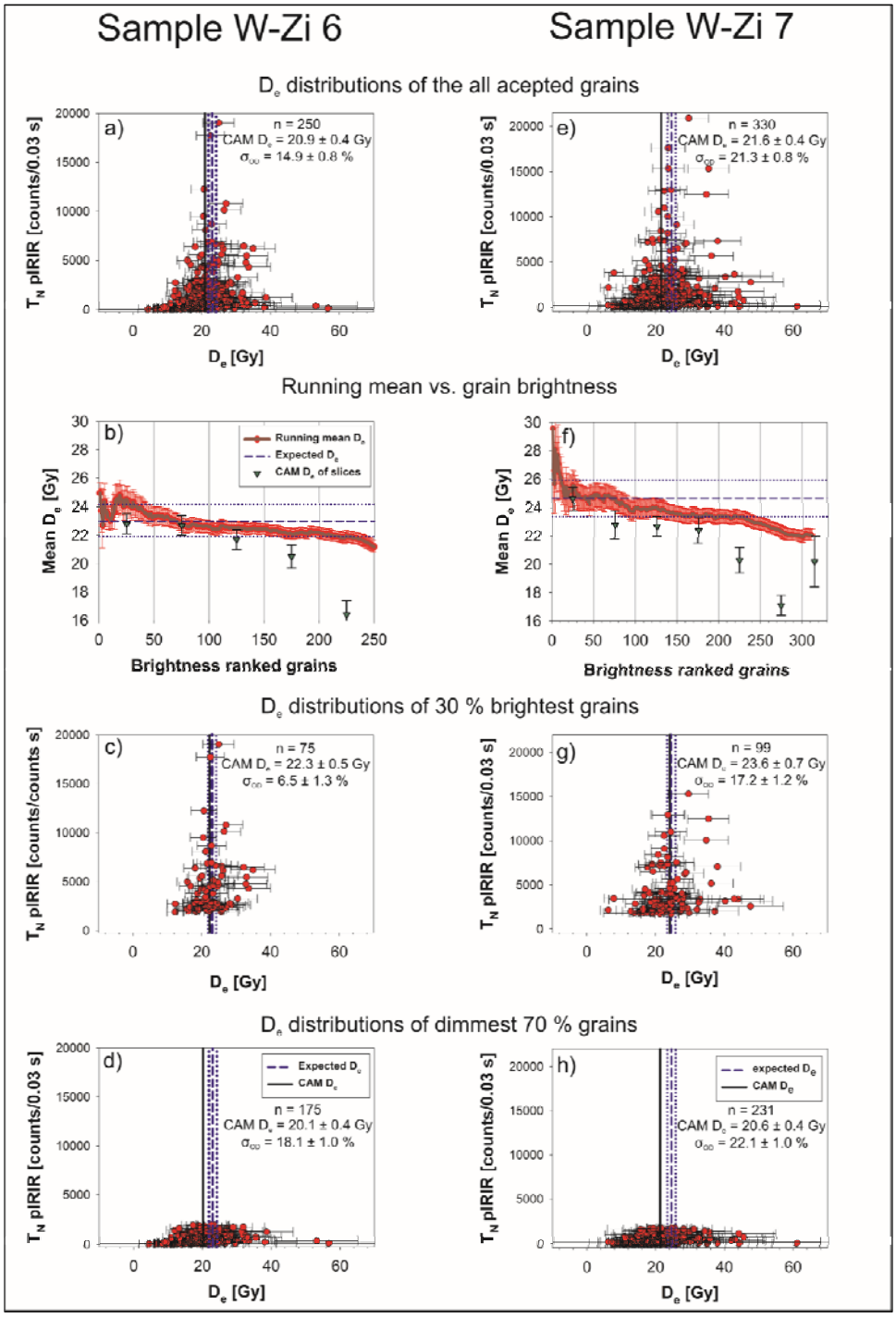

Figure 7.6: Single-grain pIRIR distributions of well bleached coastal samples (W-Zi6 and W-Zi7). In the left column **(a), (b), (c), (d)** dose distributions of W-Zi6 are shown. In the right column **(e), (f), (g), and (h)** dose distributions of sample W-Zi7 are shown. In the first row (a) and (b) D_e distributions of all accepted grains are shown for W-Zi6 and W-Zi7, respectively. In the second row (b) and (f) the running mean and the weighted mean (CAM, shown as diamonds) of bins of 50 grains (slices) in function of the intrinsic grain brightness are shown for W-Zi6 and W-Zi7, respectively. In the third row (c) and (g) D_e distributions of the 30% brightest grains (according to intrinsic grain brightness) are shown for W-Zi6 and W-Zi7, respectively. In the fourth row (d) and (h) D_e distributions of the dimmest 70 % (according to intrinsic grain brightness) are shown for W-Zi6 and W-Zi7, respectively. The expected dose is indicated as medium-dashed line, the weighted mean (CAM, Galbraith et al., 1999) is indicated as solid line.

Two well bleached samples (W-Zi6 and W-Zi7) were analysed to investigate the behaviour of natural pIRIR feldspar single-grain D_e distributions and to assess the contribution of other extrinsic sources

of D_e scatter apart from incomplete bleaching. Multi-grain quartz OSL dating provided ages of both samples of 13.7 ± 0.8 ka; these are supported by a radiocarbon age of ~13.2 ka cal. BP from an overlying peat layer. The ages of W-Zi6 and W-Zi7 are 12.6 ± 0.9 ka and 11.9 ± 1.0 ka using K-rich feldspar multi-grain aliquots (Reimann et al., 2011). The good agreement between the feldspar ages and the independent age control suggests that these samples are not significantly affected by incomplete bleaching.

Single-grain pIRIR dose distributions including all accepted feldspar grains of W-Zi6 and W-Zi7 are shown in Fig. 7.6A and 7.6E, respectively. The expected D_e for these two samples is 23.7 ± 1.1 Gy and 24.6 ± 1.2 Gy for W-Zi6 and W-Zi7, respectively. The calculation of the expected D_e is based on the multi-grain quartz OSL age (~13.7 ka), the observed residual doses (see section 7.3.2) and the total dose rate reported by Reimann et al. (2011). However, the CAM D_e is 20.9 ± 0.4 Gy and 21.3 ± 0.4 Gy for W-Zi6 and W-Zi7, respectively; these slightly underestimate the expected D_e (Fig. 7.6A, E).

To examine the cause of this apparent underestimation we ranked the accepted grains according to their pIRIR natural test dose response (starting with the brightest grain) and calculated a running mean of the D_e as a function of the number of grains included in the running mean. As can be seen from Figure 7.6B, F, we observe that the mean dose decreases as the dimmer grains are included. Consequently, we binned the dose estimates in bins each containing 50 grains (e.g. the first bin contains the dose estimates arising from the 50 brightest grains, and so on) and calculated the weighted mean using CAM. The CAM D_e decreases systematically for the dimmer grain fractions; the CAM D_e of the dimmest grain populations is about 30% lower than the CAM D_e of the brightest grain populations.

To examine whether this observation of D_e dependence on intrinsic grain brightness can be attributed to experimental factors we analysed the gamma-irradiated samples (see section 7.3.3) in the same manner. For these γ-dosed distributions there is no significant systematic variation in the average dose as a function of intrinsic brightness (Fig. 7.7), which indicates that the observation of the apparent dose dependence on grain brightness only applies to natural samples. To explain this observation we examine two different hypotheses: (1) differential fading and (2) internal dosimetry.

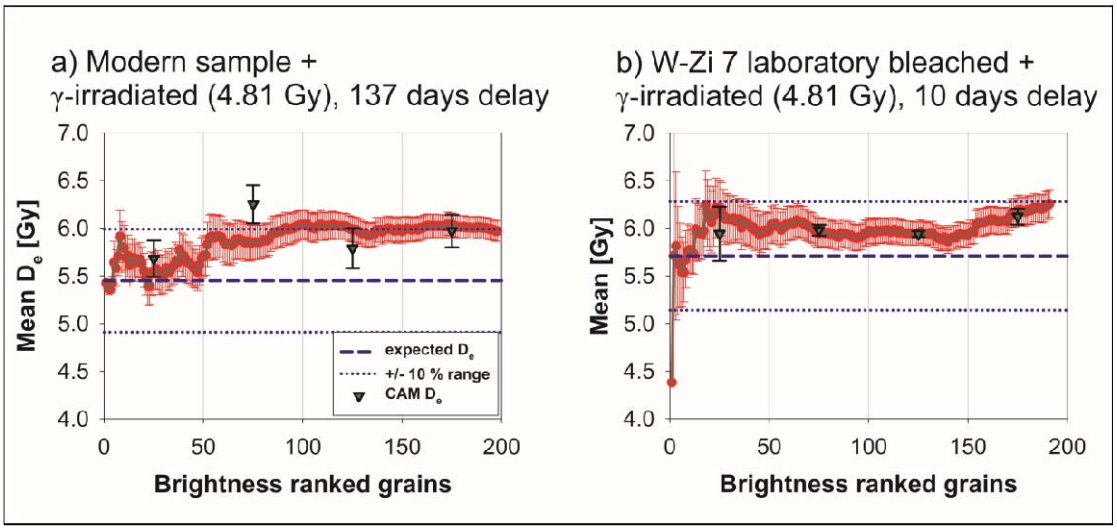

Figure 7.7: Dose recovery ratio in function of the intrinsic grain brightness. The γ-irradiated modern sample is shown in **(a)**, the γ-irradiated laboratory bleached sample is shown in **(b).** The expected dose is indicated as medium-dashed line.

7.3.4.1 Differential fading

The observed D_e dependence on intrinsic brightness could be caused by differential fading, i.e. bright grains fade more slowly than dim grains. To examine this suggestion the fading rate for individual grains was determined. A portion of the modern sample was given a beta dose of 20 Gy (~7 min of irradiation) in the reader prior to a prompt D_e measurement (D_{prompt}). Subsequent to D_e measurement the grains were re-dosed (20 Gy) and stored for seven days (equivalent to ~10000 min of storage time and more than three decades of the half irradiation time) prior to D_e measurement (D_{delay}). In Fig. 7.8 the ratio of D_{delay} and D_{prompt} is shown for the individual grains as a function of the brightness ranked grains. The average ratio is 0.95 ± 0.02, and the individual ratios do not appear to depend on intrinsic brightness; this indicates that differential fading of dim and bright grains is not likely to be the cause of the D_e dependence on grain brightness.

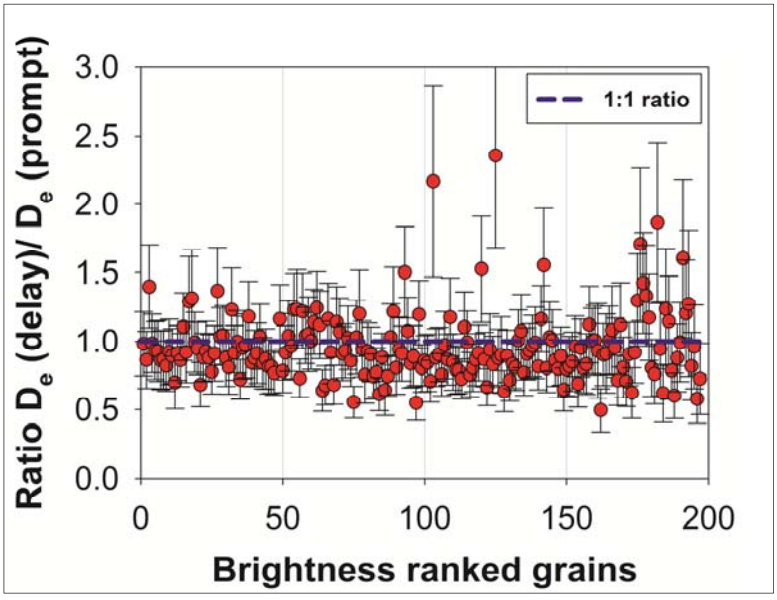

Figure 7.8: Fading in function of intrinsic grain brightness. The modern sample (Zi-modern) was given a β-dose of 20 Gy (equivalent to ~7 min) prior to prompt D_e measurement (D_{prompt}). After prompt measurement the same grains were re-dosed (20 Gy) and stored for seven days prior to the delay D_e measurement (D_{delay}). The average ratio of D_{prompt}/D_{delay} is 0.95 ± 0.02.

7.3.4.2 Internal dosimetry

A major reason why single-grain studies on feldspar have not been more widely undertaken relates to internal dosimetry. According to Huntley and Baril (1997) the average internal potassium content for orthoclase feldspar is 12.5 ± 0.5% based on multi-grain measurements (blue detection). For our study, the K-rich feldspar fractions were extracted from the sediment using density separation (see section 7.2.1) and it is well-known that this technique does not provide a pure K-feldspar extract, e.g. it is very likely that the samples contain a broad distribution of feldspar with varying contents of potassium, including some end members with no potassium, e.g. albite, anorthite. Nevertheless, there is an indication that the blue emission (centred around 400 nm) tends to be stronger in K-rich feldspars (Prescott and Fox, 1993; Huntley and Baril, 1997), and that feldspars with K content over 11% tends to be the brightest. Thus, an average internal potassium content of 12.5% is presumably an acceptable estimate in multi-grain measurements. But for single-grain measurements this assumption is unlikely to apply to all light emitting grains. If we postulate that dim grains have a lower potassium content than bright grains, then the actual dose rate to dim grains will be lower than that to bright grains.

This hypothesis correlates very well with our observation that there is a decrease in the D_e with decreasing intrinsic grain brightness for two well-bleached K-rich feldspar samples (Fig. 7.6B, F). The D_e calculated using the brightest grains (30%) agrees with the dose expected from the independent age control whereas the dim grains underestimate the expected dose. Assuming a maximum internal K content of ~14% for orthoclase feldspars (applicable to the brightest grains in the distribution) and an internal K content of 0% for the dimmest grains, the expected internal β-doses would vary between ~0.6 Gy and zero for pure orthoclase and pure non-potassium phases, respectively. In Fig. 7.9 we have calculated the ratio of measured to expected age for seven bins of 50 grains each, which were ranked according to their intrinsic grain brightness (T_N response), assuming a constant internal K content of 12.5 ± 0.5% (Huntley and Baril, 1997). We obtain a decreasing trend of the ratios, with an underestimation up to 30% (green diamonds in Fig. 7.9). Note that the ages of the dimmest 100-150 grains are 20-30% younger than the expected age. In Fig. 7.9 we also show the ratio of measured to expected age for the same seven bins assuming a smoothly decreasing internal K content starting with 14.0 ± 0.5% for the brightest 50 grains and decreasing to 0% for the dimmest 50 grains, in steps of 2%. If a decreasing internal K content with decreasing intrinsic grain brightness is assumed the apparent age dependence of grain brightness vanishes (red squares in Fig. 7.9). If our assumption is valid the relation of intrinsic grain brightness and the K content can also be used to calculate the effective K content of the multi-grain single aliquot feldspar ages. If we assumed that the K content systematically increases with grain brightness (i.e. the dimmest yield 0 % and the brightest 14 %) and weighted the K content according to the signal intensity (i.e. the contribution to the total light sum) to calculated the effective K content, we obtained an effective internal K content of 11.2 % and 11.6 % for W-Zi 6 and W-Zi 7, respectively. This changes the fading corrected multi-grain pIRIR ages of Reimann et al. (2011) to 12.8 ± 0.9 ka (W-Zi 6) and 12.1 ± 1.0 ka (W-Zi 7). Both multi-grain pIRIR ages are consistent with the corresponding quartz OSL ages (both 13.7 ± 0.8 ka) within 1-σ uncertainties.

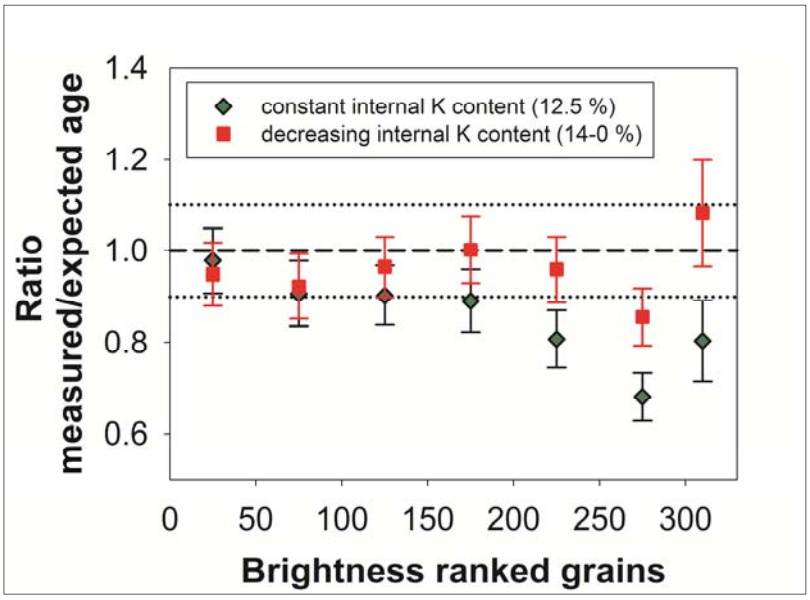

Figure 7.9: Ratio of measured/expected age in function of intrinsic grain brightness of well-bleached sample W-Zi7. The ratios are calculated for bins of 50 grains each, which were ranked according to their intrinsic grain brightness. Ratios assuming a constant internal K content of 12.5 ± 0.5% according to Huntely and Baril (1997) are shown as diamonds; ratios assuming a smoothly decreasing internal K content are shown as squares. Unity is indicated as medium-dashed line.

The mean values of the brightest 30% of the grains are in a good agreement with the expected dose (Fig. 7.6B, F) based on the radiocarbon and quartz OSL technique, suggesting that this fraction of grains provides reliable D_e estimates. Thus, we calculated the feldspar D_e for our samples based on

the single-grain distributions of the brightest 30% (Fig. 7.6C, G) and excluded the dim grains from dose estimation. For comparison, the dose distribution of the 70% dimmest grains is shown for sample W-Zi6 and W-Zi7 in Fig. 7.6D and Fig. 7.6H, respectively. The ratios of the CAM D_es of the distributions of the brightest 30% to the expected doses are 0.94 ± 0.05 and 0.96 ± 0.05 for W-Zi6 and W-Zi7, respectively. Thus, in the following we used the fraction of the brightest 30% of the grains for further analyses.

The distributions of the two well-bleached samples are approximately symmetric and the over-dispersions are 10.4 ± 1.1% (W-Zi6, Fig. 7.6C) and 17.0 ± 1.2% (W-Zi7, Fig. 7.6G), implying that the assigned intrinsic uncertainties of 16.5% (see section 7.3.1.2) are not accounting for the observed variability in D_e in our well-bleached dose distributions. Thus, we have to consider extrinsic sources of D_e scatter as well. Incomplete bleaching is considered to be an unlikely cause of the observed over-dispersion because of the good agreement between quartz and feldspar small aliquot measurements. Other possible sources of extrinsic variability are microdosimetry (small scale variation of the radiation field) and grain migration (e.g. Duller, 2008). Although, it is difficult to compare relative over-dispersions between different studies because of the variations in how intrinsic uncertainties are assigned, the observed values for well-bleached single-grain distributions are in general similar to these reported by Li et al. (2011) for IRSL feldspar or OSL quartz studies (e.g. Olley et al., 2004).

7.3.5 Dose evaluation from incompletely bleached coastal samples

In this section we present the single-grain dose distributions of two samples (W-Zi3 and W-Zi2). Reimann et al. (2011) showed that the fading corrected multi-grain pIRIR age of W-Zi3 (3.24 ± 0.21 ka) exceeds the weighted mean quartz OSL age (2.69 ± 0.10 ka). The accuracy of the quartz OSL age was confirmed by a radiocarbon age of 2.57 ± 0.16 ka cal. BP from an overlying gyttja layer. However, both quartz and feldspar ages agree within 2σ with the radiocarbon age. Although the fading corrected multi-grain pIRIR age tends to be older than the quartz OSL age no internal indication of incomplete bleaching was observed in the pIRIR feldspar multi-grain dose distribution (e.g. a positive skewed distribution).

In contrast, skewed quartz OSL and feldspar pIRIR multi-grain dose distributions were observed in sample W-Zi2 suggesting that this sample suffers from poor bleaching. Reimann et al. (2011) used the Minimum Age Model (MAM; Galbraith et al., 1999) to estimate the burial dose from the multi-grain dose distributions, and found that that the fading corrected multi-grain pIRIR age (2.40 ± 0.30 ka) for feldspar severely overestimated that of quartz (0.68 ± 0.07 ka). The radiocarbon age of 2.57 ± 0.16 ka cal. BP from the underlying Gyttja layer gives a maximum burial age for sample W-Zi2. Thus, both quartz and feldspar ages are consistent with this independent age control. However, bearing in mind that quartz bleaches faster than feldspar (e.g. Godfrey-Smith et al., 1988, Thomsen et al., 2008) it is assumed that the quartz MAM age is more reliable. In section 7.3.5.2 and 7.3.5.3 we use the measured natural dose distributions for sample W-Zi2 obtained from quartz and feldspar, respectively, to test this assumption.

In order to derive minimum D_e estimates we use both the MAM and the so-called IEU approach (Thomsen et al., 2003, 2007) to estimate the burial dose from both quartz and feldspar single-grain dose distributions. Both methods attempt to identify the minimum dose population that is most likely to contain grains that were well-bleached at burial.

We used the logged version of the 4-parameter MAM model (Galbraith et al., 1999). Using the results of the well-bleached samples (see section 7.3.4) we defined the over-dispersion of a well-bleached dose component to be 15%.

The IEU approach requires knowledge of the variation in absolute over-dispersion as a function of the burial dose. We used the over-dispersions obtained from the "zero-dose" samples (modern sample, laboratory bleached, section 7.3.2) and the corresponding γ-irradiated samples (see section 7.3.3) and fitted a straight line to the data. A slope *a* of 0.15 ± 0.03 and an intercept *b* of -0.26 ± 0.04 Gy was determined and these values were subsequently used as input parameters in the equation given below

$$\sqrt{\sigma_c^{\,2} + \left(a \cdot D_{burial} + b\right)^2} \qquad \text{(Eq. 1)}$$

In this equation σ_c is the uncertainty derived from counting statistics and fitting errors (i.e. the errors derived from Analyst). To solve this equation we need to know the mean dose (D_{burial}) that we are trying to determine; here we used the iterative approach described in Thomsen et al. (2007).

7.3.5.1 Sample W-Zi3

Based on the overlying radiocarbon age, the observed residual doses in the modern sample (0.63 ± 0.03 Gy, section 7.3.2) and the multi-grain g-value (0.08 ± 0.46 %/decade, Reimann et al., 2011) the expected dose in this sample is estimated to be 6.40 ± 0.40 Gy.

Figure 7.10A shows the measured single-grain K-feldspar D_e distribution. The distribution appears positively skewed. Figure 7.10B shows the "synthetic aliquot" distribution derived from the single-grain data by summing of the light emitted from individual grains to produce a "synthetic aliquot" comprising of 100 grains. Figure 7.10C show the "true" multi-grain distribution obtained using aliquots approximately containing 1000 grains. The single-grain dose distribution (Fig. 7.10A) is positively skewed and the apparent leading edge dose population is at ~4 Gy. Both multi-grain distributions appear more symmetric and the leading edge dose population is at ~7 Gy. The CAM D_e of the single-grain distribution is 7.15 ± 0.50 Gy and thus agrees within 1-σ uncertainty with the expected dose. The CAM D_e of the synthetic aliquots (9.17 ± 0.92 Gy) and medium aliquots (8.05 ± 0.20 Gy) overestimate the expected dose.

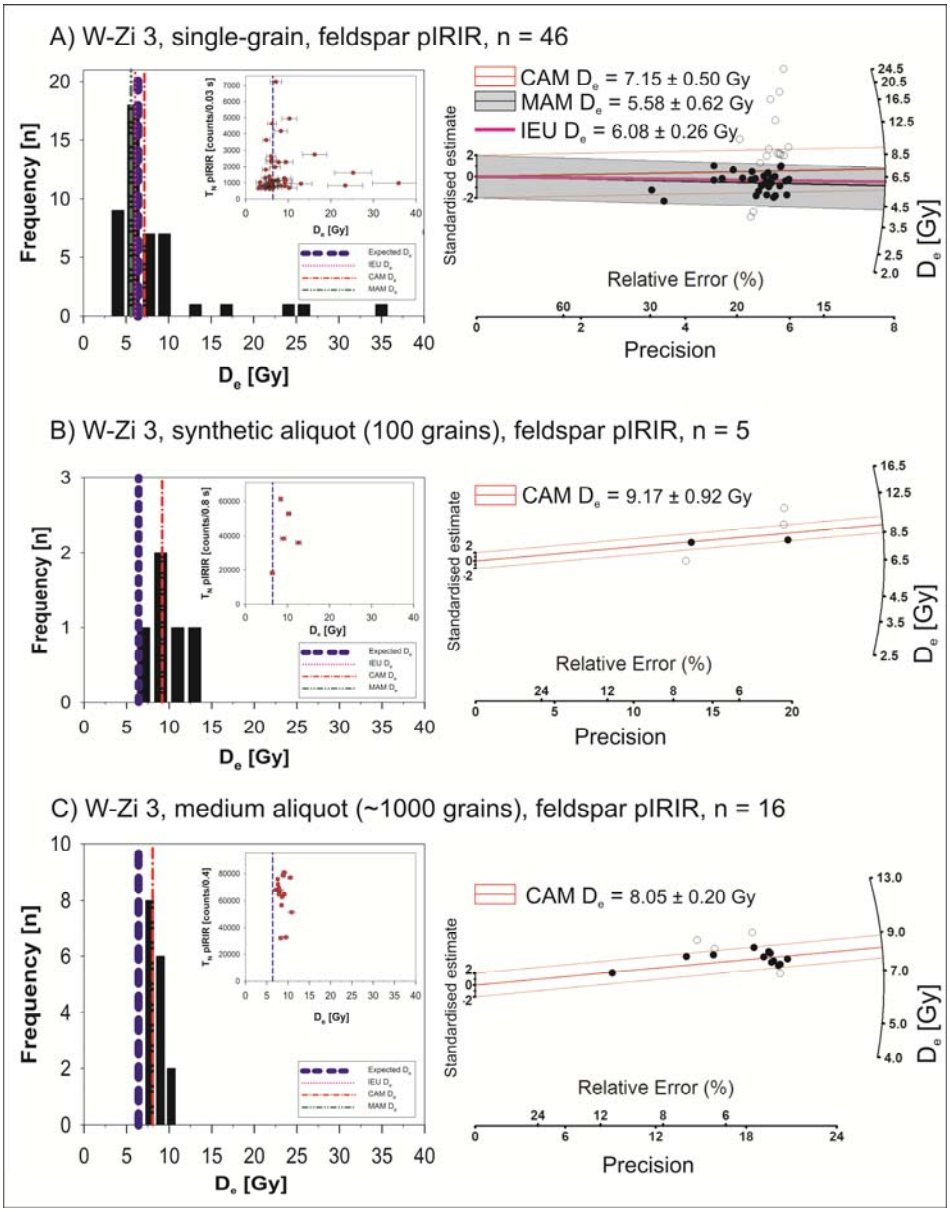

Figure 7.10: D_e distributions of sample W-Zi 3. Distribution of pIRIR feldspar single-grain is shown in **(a),** synthetic 100 grain aliquots are shown in **(b)** and the distribution of 1000 grain medium aliquots is shown in **(c).** On the left histograms and T_N vs. D_e plots are shown for (a), (b), and (c), respectively. On the right radial plots are shown for (a), (b), and (c), respectively. Central Age Model (CAM) D_e and Minimum Age Model (MAM) D_e was calculated according to Galbraith et al. (1999). The IEU D_e was calculated according to Thomsen et al. (2003, 2007).

To estimate the grain population containing the lowest D_e values, we used both the 4-parameter minimum age model (MAM) of Galbraith et al. (1999) and the IEU approach as described in the previous section. The MAM D_e is 5.58 ± 0.62 Gy and is consistent with the expected dose within 1-σ uncertainty. The IEU dose estimate is 5.80 ± 0.27 Gy and thus agrees with both the expected dose and the MAM D_e. The IEU dose estimate contains 76% of the grains whereas the MAM D_e contains only ~52% of the grains (p0—parameter of the 4-parameter MAM). The multi-grain CAM D_es slightly overestimate the expected dose (Fig. 7.10B, C).

7.3.5.2 Sample W-Zi2

The small aliquot distributions of W-Zi2 indicate incomplete bleaching for both quartz and feldspar. Thus, the expected dose is not so well-known for this sample. However, the sample W-Zi1 above

(0.68 ± 0.07 ka; Reimann et al., 2011) appeared to be well bleached and we expect W-Zi2 to be equivalent to, or older than, W-Zi1. In the following sections we present the observed single-grain dose distributions for both quartz and feldspar.

7.3.5.3 SG quartz dose distributions of W-Zi 2

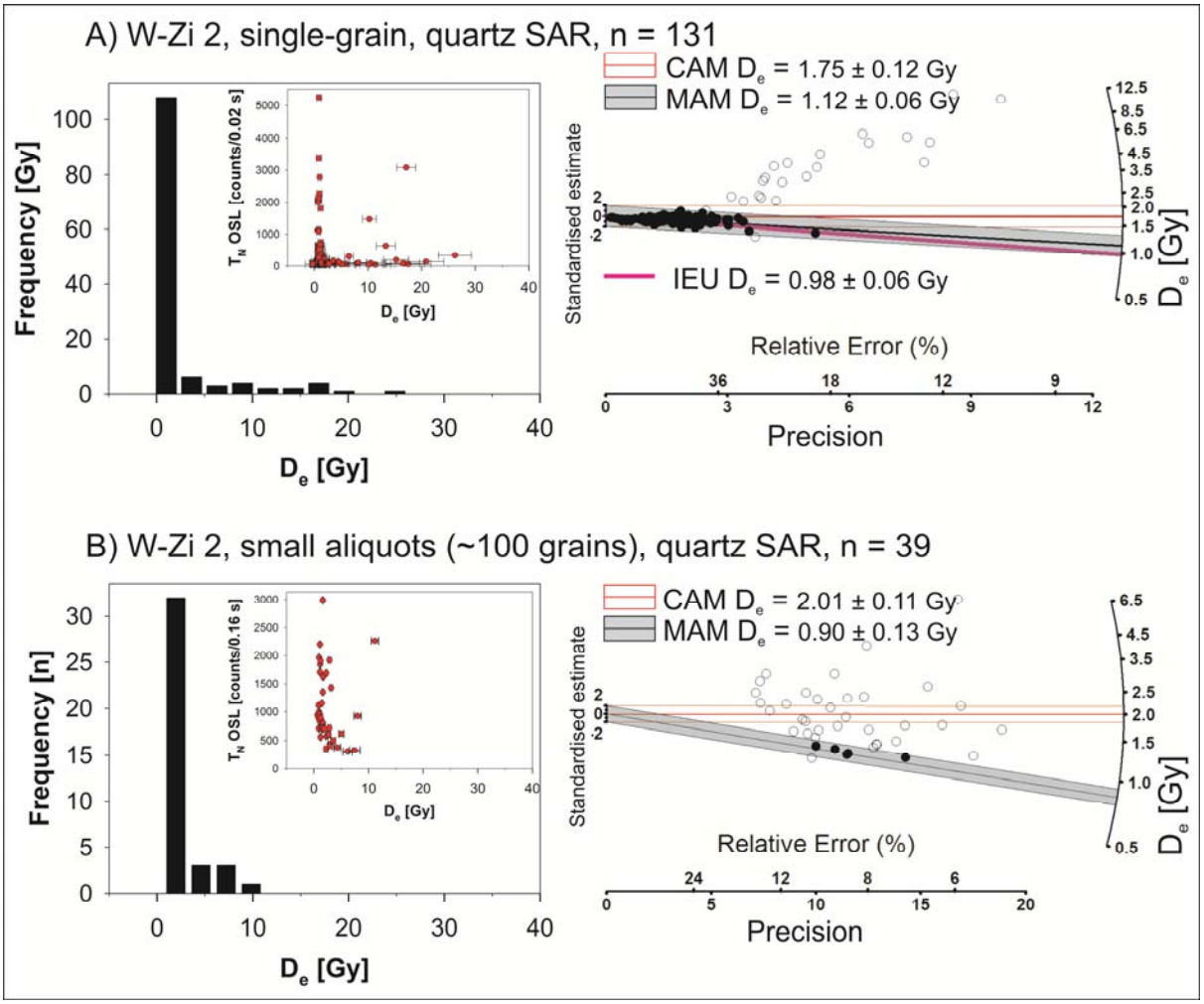

Figure 7.11: Quartz D_e distributions of sample W-Zi2. Histograms (left) and a radial plot (right) of quartz single-grain dose distribution are shown in **(a);** histograms and radial plots of the small aliquot (~100 grains) distribution are shown in **(b)**. Central Age Model (CAM) D_e and Minimum Age Model (MAM) De was calculated according to Galbraith et al. (1999). The IEU D_e was calculated according to Thomsen et al. (2003, 2007).

The quartz single-grain distribution of sample W-Zi2 is shown in Figure 7.11A. These single-grain measurements show that the majority of the quartz grains belong to a well-defined dose population centred at about 1 Gy with a few high dose points. Using the MAM we obtained a D_e of 1.12 ± 0.06 Gy (83% included grains) corresponding to an age of 0.94 ± 0.06 ka. Using the IEU we obtained 0.98 ± 0.06 Gy (89% included grains) corresponding to an age of 0.82 ± 0.05 ka. For comparison, we show the quartz small aliquot dose distribution of Reimann et al. (2011) in Fig. 7.11B and recalculate the MAM and CAM dose estimates using the small aliquots. Using the 4-parameter MAM on the quartz small aliquot distribution of Reimann et al. (2011) gave a D_e of 0.90 ± 0.13 Gy (10% included aliquots) and an age of 0.76 ± 0.11 ka. Thus, we obtained consistent ages of 0.94 ± 0.06 ka, 0.82 ± 0.05 ka, and 0.76 ± 0.11 ka for the MAM (single-grains), the IEU (single-grains) and the MAM (small aliquots),

respectively. We take the average of these ages (0.84 ± 0.05 ka) as the most reliable estimate for the expected age of sample W-Zi2.

7.3.5.4 SG feldspar dose distributions of W-Zi2

Figure 7.12 shows pIRIR dose distributions of single-grains (Fig. 7.12A) and small aliquots (Fig. 7.12B) of sample W-Zi2. Both dose distributions appear skewed towards high D_e values as is expected for an incompletely bleached sample. The single-grain feldspar distribution clearly contains a leading edge dose population centred at ~1.5 Gy (Fig. 7.12A), and a significant number of bright grains containing doses up to 80 Gy. Thus, it would appear that the feldspar fraction is affected by incomplete bleaching to a greater degree than quartz; this is to be expected from their different bleaching rates. The MAM D_e derived from the single-grain distribution is 1.59 ± 0.08 Gy (p0 = 43%), and the IEU estimate is 1.69 ± 0.10 Gy (based on 49% of the grains). The MAM D_e derived from the small aliquot distribution is 4.78 ± 0.38 Gy, and thus significantly overestimates the minimum dose derived from the single-grain dose distribution, presumably because a significant averaging of light signals occur in these multi-grain dose measurements. From the cumulative light sum data (Figure 7.3) we estimate the multi-grain feldspar aliquot would need to consist of <5 grains in order to be confident of measuring some aliquots which contain only well-bleached grains. However, we observed a significantly higher spread in the single-grain feldspar distribution of the incomplete bleached sample W-Zi2 than in corresponding single-grain quartz distribution. This suggests that also the differences in the natural signals of the well bleached feldspar grains (i.e. low dose grains) and the incomplete bleached feldspar grains (i.e. high dose grains) within the single-grain pIRIR D_e distributions are larger. Even if the test dose signal (a measure of sensitivity) of a small aliquot is dominated by a very bright well-bleached grain, the natural signal may nevertheless be dominated by the signal from a low sensitivity grain, if this grain was poorly bleached and so retained a large natural signal. As a result, it appears unlikely that measurement of small aliquots of feldspar is useful; it is probably necessary to use single-grain measurements in studies of incomplete bleaching in feldspar.

The MAM and IEU pIRIR single-grain ages (after correction for residual doses and anomalous fading) are 0.57 ± 0.06 ka and 0.63 ± 0.06 ka, respectively (Table 7.1). The IEU age is consistent (within 2σ) with the expected age based on the quartz measurements of W-Zi2 (see previous section). The MAM age slightly underestimates the quartz age.

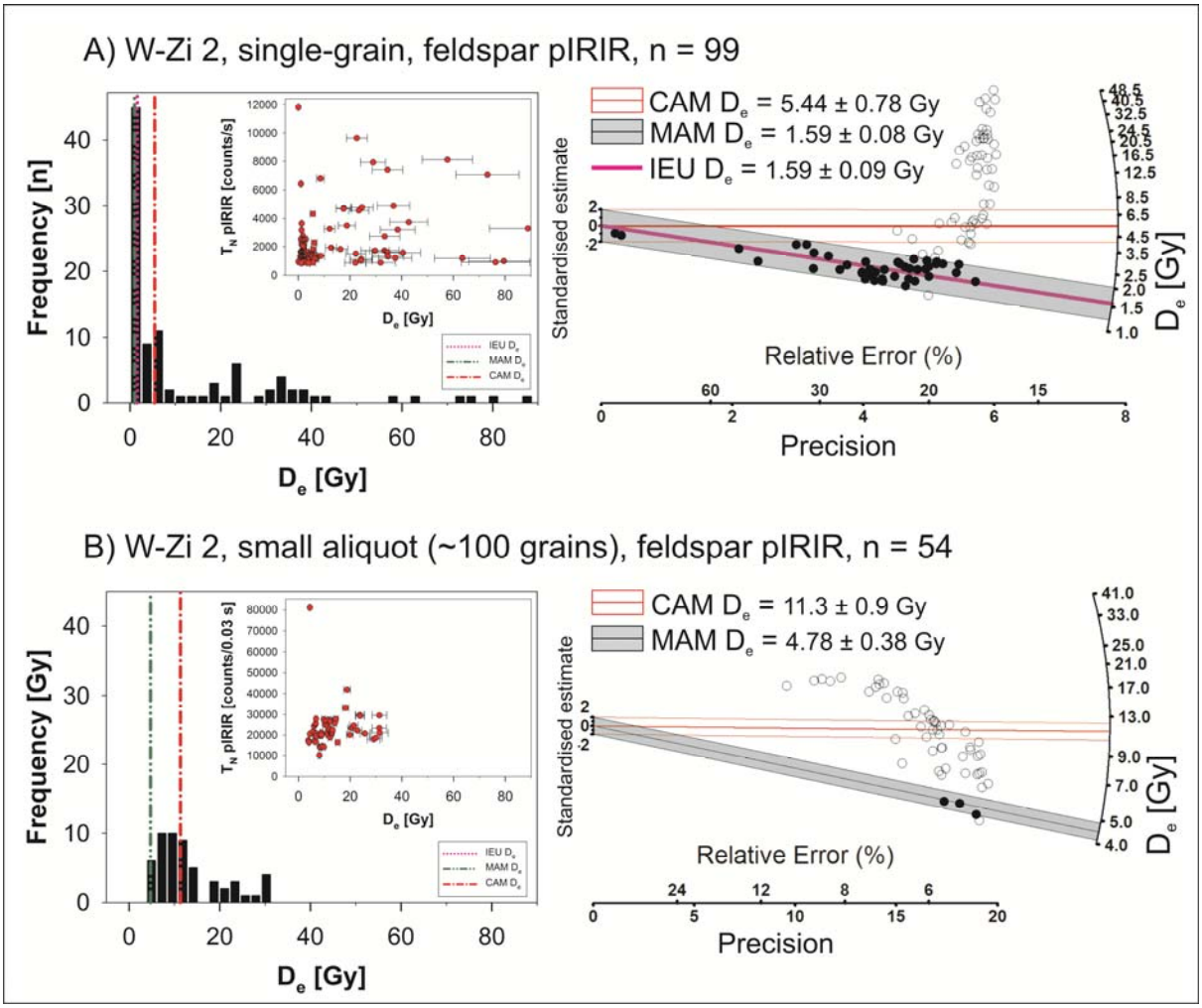

Figure 7.12: Feldspar pIRIR D_e distributions of sample W-Zi2. Histograms (left) and radial plots (right) of pIRIR feldspar single-grain dose distribution are shown in **(a)**; histograms and radial plots of the small aliquot (~100 grains) distribution are shown in **(b)**. Central Age Model (CAM) D_e and Minimum Age Model (MAM) D_e was calculated according to Galbraith et al. (1999). The IEU D_e was calculated according to Thomsen et al. (2003, 2007).

7.4 Conclusion

This is the first study to demonstrate the potential of single-grains of feldspars in the dating of young well-bleached and poorly-bleached sediments. This has become possible because the use of a pIRIR protocol reduces the problem of anomalous fading significantly, thus allowing examination of the extrinsic controls on over-dispersion such as dose-rate heterogeneity and partial bleaching. Nevertheless, the analysis of two γ-irradiated samples suggests that the dose of an individual feldspar grain cannot be known to better than ~16.5% in our samples.

In this study we have measured the feldspar single-grain dose distributions from two samples (W-Zi6 and W-Zi7) believed to be well-bleached because of the good agreement between quartz and feldspar multi-grain measurements (Reimann et al., 2011). We find that the average single-grain doses only agree with the multi-grain doses if the brightest 30% of the grains are included in the dose estimation. Based on this observation we suggest that only the brightest grains have an average K-content of 12.5%. The dimmer grains may contain less K. This observation highlights the

importance of measuring internal K content in single-grains of feldspar, and, perhaps, indicates that luminescence intensity may be used as a proxy for K-content. However, the measurement of internal K content is not a straightforward task because it is likely that potassium is not evenly distributed within the feldspar grains. Furthermore, it seems advisable for future single-grain feldspar studies to improve the separation process in order to purify the K-rich feldspar fraction.

We have also measured K-feldspar single-grain distributions for two samples (W-Zi2 and W-Zi3) that appear to suffer from incomplete bleaching. For both samples minimum age models were used to estimate the burial dose, again using the brightest 30% grains. For W-Zi3 the quartz appear to be well-bleached (Reimann et al., 2011), and we obtain a good agreement between the single-grain feldspar age and the multi-grain quartz age (consistent within 1σ). For sample W-Zi2 both quartz and feldspar appear to suffer from incomplete bleaching. Quartz single-grain measurements give minimum ages of 0.94 ± 0.06 ka and 0.82 ± 0.05 ka for the MAM and the IEU, respectively. However, applying minimum age models to the K-feldspar single-grain distribution gives fading corrected pIRIR ages of 0.57 ± 0.06 ka and 0.63 ± 0.06 ka for the MAM and IEU, respectively,which slightly underestimate the expected age. At such low doses (~1.5 Gy) the contribution from thermal transfer/residual dose is significant (~45%) for pIRIR feldspar measurements and the underestimation is perhaps a consequence of inappropriate correction.

For these samples, quartz multi-grain (~100 grains) analysis can successfully be applied because of relatively few light emitting grains; however, the same is not applicable to feldspar. In feldspar multi-grain aliquots (~100 grains) a greater proportion of the grains contribute to the measured signal (see Figure 7.3), and thus it is very unlikely that aliquots containing only well-bleached grains will be measured from a sample suffering from incomplete bleaching. We conclude that multi-grain analysis is unlikely to be useful when measuring incompletely bleached feldspars.

The study demonstrates the reliability of an alternative method to the more commonly used MAM approach for identifying the well-bleached component in a single-grain D_e distribution; the IEU age is completely consistent with the MAM age.

References

- Aitken, M.J., 1985. Thermoluminescence dating. Academic Press, London.
- Aitken, M.J., 1998. An Introduction to optical dating. Oxford University Press, Oxford.
- Bailey, S.D., Wintle, A.G., Duller, G.A.T., Bristow, C.S., 2001. Sand deposition during the last millennium at Aberffraw, Anglesey, North Wales as determined by OSL dating of quartz. Quaternary Science Reviews 20, 710-704.
- Bateman, M. D., Boulter, C. H., Carr, A. S., Frederick, C. D., Peter, D., Wilder, M. 2007. Detecting post-depositional sediment disturbance in sandy deposits using optical luminescence. Quaternary Geochronology 2, 57–64.
- Bateman, M.D., 2008. Luminescence dating of periglacial sediments and structures. Boreas 37, 574-588.
- Bøtter-Jensen, L., Andersen, C. E., Duller, G. A. T., Murray, A. S., 2003. Developments in radiation, stimulation and observation facilities in luminescence measurements. Radiation Measurements 37, 535–541.

- Buylaert, J.P., Ghysels, G., Murray, A.S., Thomsen, K.J., Vandenberghe, D., DeCorte, F., Heyse, Van den haute, P., 2009a. Optical dating of relict sand wedges and composite-wedge pseudomorphs in Flanders, Belgium. Boreas 38, 160-175.
- Buylaert, J.P., Murray, A.S., Thomsen, K.J., Jain, M., 2009b. Testing the potential of an elevated temperature IRSL signal from K-feldspar. Radiation Measurements 44, 560-565.
- Davids, F., Duller, G.A.T., Roberts, H.M., 2010. Testing the use of feldspars for optical dating of hurricane overwash deposits. Quaternary Geochronology 5, 125-130.
- Duller, G. A. T. 2006. Single grain optical dating of glacigenic sediments. Quaternary Geochronology 1, 296–304.
- Duller, G.A.T., 2007. Assessing the error on equivalent dose estimates derived from single aliquot regenerative dose measurements. Ancient TL 25, 15-24.
- Duller, G.A.T., 2008. Single-grain optical dating of Quaternary sediments: why aliquot size matters in luminescence dating. Boreas 37. 589-612.
- Duller, G. A. T., Murray, A.S., 2000. Luminescence dating of sediments using individual mineral grains. Geologos 5, 87-106.
- Duller, G. A. T., Bøtter-Jensen, L., Murray, A. S. 2003. Combining infrared- and green-laser stimulation sources in single-grain luminescence measurements of feldspar and quartz. Radiation Measurements 37, 543–550.
- Fuchs, M., Owen, L. A., 2008. Luminescence dating of glacial and associated sediments: review, recommendations and future directions. Boreas 37, 636-659.
- Galbraith, R.F., Roberts, R.G., Laslett, G.M., Yoshida, H., Olley, J.M., 1999. Optical dating of single and multiple grains of quartz from Jinmium rock shelter, Northern Australia: part 1, experimental details and statistical models. Archaeometry 41, 339-364.
- Godfrey-Smith, D., Huntley, D., Chen, W.-H., 1988. Optical dating studies of quartz and feldspar sediments extracts. Quaternary Science Reviews 7, 373-380.
- Huntley, D.J., Baril, M.R., 1997. The K content of the K-feldspars being measured in optical dating or in thermoluminescence dating. Ancient TL 15, 11-13.
- Huntley, D.J., Lamothe, M., 2001. Ubiquity of anomalous fading in K-feldspars and the measurement and correction for it in optical dating. Canadian Journal of Earth Science 38, 1093-1106.
- Jain, M., Ankjærgaard, C., 2011. Towards a non-fading signal in feldspar: Insight into charge transport and tunnelling from time-resolved optically stimulated luminescence. Radiation Measurements, doi:10.1016/j.radmeas.2010.12.004.
- Jain, M., Murray, A.S., Bøtter-Jensen, L., 2004a. Optically stimulated luminescence dating - how significant is incomplete light exposure in fluvial environments ? Quaternaire 15, 143-157.
- Jain, M., Thomsen, K.J., Bøtter-Jensen, L., Murray, A.S., 2004b. Thermal transfer and apparent-dose distributions in poorly bleached mortar samples: results from single grains and small aliquots of quartz. Radiation Measurements 38, 101-109.
- Kunz, A., Frechen, M., Ramesh, R., Urban, B., 2010. Revealing the coastal event-history of the Andaman Islands (Bay of Bengal) during the Holocene using radiocarbon and OSL dating. International Journal of Earth Sciences, doi: 10.1007/s00531-009-0507-4.

- Lamothe, M., Balescu, S., Auclair, M. 1994. Natural IRSL intensities and apparent luminescence ages of single feldspar grains extracted from partially bleached sediments. Radiation Measurements 23, 555–561.
- Lamothe, M., and Auclair, M., 1997. Assessing the datability of young sediments by IRSL using an intrinsic laboratory protocol. Radiation Measurements 27, 107–117.
- Lamothe, M., and Auclair, M. 1999. A solution to anomalous fading and age shortfalls in optical dating of feldspar minerals. Earth and Planetary Science Letters 171, 319–323.
- Lapp, T., Jain, M., Thomsen, K.J., Murray, A.S., Buylaert, J.P. New Luminescence Measurement Facilities in Retrospective Dosimetry. Submitted to Radiation Measurements.
- Li, B., Li, S.H., Duller, G.A.T., Wintle, A.G., 2010. Infrared stimulated luminescence measurements of single grains of K-rich feldspar for isochron dating. Quaternary Geochronology, doi:10.1016/j.quageo.2010.02.003.
- Li, S.H., Chen, Y.Y., Li, B. Sun, J., Yang, L.R., 2007a. OSL dating of sediments from deserts in northern China. Quaternary Geochronology 2, 23-28.
- Lukas, S., Spencer, J.Q.G., Robinson, R.A.J., Benn, D.I., 2007. Problems associated with luminescence dating of Late Quaternary glacial sediments in the NW Scottish Highlands. Quaternary Geochronology 2, 243-248.
- Madsen, A.T., Murray A.S., 2009. Optically stimulated luminescence dating of young sediments: a review. Geomorphology 109, 3-16.
- Murray, A. S., Roberts, R. G. 1997. Determining the burial time of single grains of quartz using optically stimulated luminescence. Earth and Planetary Science Letters 152, 163–180.
- Murray, A.S., Wintle, A.G., 2000. Luminescence dating of quartz using an improved single-aliquot regenerative-dose protocol. Radiation Measurements 32, 57-73.
- Murray, A.S., Olley, J.M., 2002. Precision and accuracy in the optically stimulated luminescence dating of sedimentary quartz: a status review. Geochronometria 21, 1-16.
- Olley, J.M., Caitcheon, G.G., Roberts, R.G., 1999. The origin of dose distributions in fluvial sediments, and the prospect of dating single grains from fluvial deposits using optically stimulated luminescence. Radiation Measurements 30, 207-217.
- Olley, J.M., Pietsch, T., Roberts, R.G., 2004. Optical dating of Holocene sediments from a variety of geomorphic settings using single grains of quartz. Geomorphology 60, 337-358.
- Prescott, J.R., Fox, P.J., 1993. Three-dimensional thermoluminescence spectra of feldspars. Journal of Physics D. 26, 2245-2254.
- Preusser, F., Ramsmeyer, K., Schlüchter, Ch., 2006. Characterisation of low OSL intensity quartz from New Zealand Alps. Radiation Measurements 41, 871-877.
- Preusser, F., Chithambo, M.L., Götte, T., Martini, M., Ramseyer, K., Sendezera, E.J., Susino, G.J., Wintle, A.G., 2009. Quartz as a natural luminescence dosimeter. Earth-Science Reviews 97, 184-214.
- Reimann, T., Tsukamoto, S., Naumann, M., Frechen, M., 2011. The potential of using K-rich feldspars for optical dating of young coastal sediments – a test case from Darss-Zingst peninsula (southern Baltic Sea coast). Quaternary Geochronology 6, 207-222.
- Roberts, R.G., Galbraith, R.F., Olley, J.M., Yoshida, H., Laslett, G.M. 1999. Optical dating of single and multiple grains of quartz from Jinmium rock shelter, northern Australia: Part II. Results and implications. Archaeometry 41, 365–395.

- Roberts, R.G., Galbraith, R.F., Yoshida, H., Laslett, G.M., Olley, J.M., 2000. Distinguishing dose populations in sediment mixtures: a test of single-grain optical dating procedures using mixtures of laboratory-dosed quartz. Radiation Measurements 32, 459–465.
- Rodnight, H., Duller, G.A.T., Wintle, A.G., Tooth, S., 2006. Assessing the reproducibility and accuracy of optical dating of fluvial deposits. Quaternary Geochronology 1, 109-120.
- Spooner, N.A., 1994. The anomalous fading of infrared-stimulated luminescence from feldspars. Radiation Measurements 23, 625–632.
- Southgate, G.A. 1985. Thermoluminescence dating of beach and dune sands: Potential of single-grain measurements. Nuclear Tracks and Radiation Measurements 10, 743–747.
- Steffen, D., Preusser, F., Schlunegger, F., 2009. OSL quartz age underestimation due to unstable signal components. Quaternary Geochronology 4, 353-362.
- Stevens, T., Marković, S.B., Zech, M., Hambach, U., Sümegi, P. 2011. Dust deposition and climate in the Carpathian Basin over an independently dated last glacial – interglacial cycle. Quaternary Science Reviews 30, 662-681.
- Thiel, C., Buylaert, J.P., Terhorst, B., Murray, A.S., Hofer, I., Tsukamoto, S., Frechen, M, 2010. Luminescence dating of Stratzing loess profile (Austria) – Testing the potential of an elevated temperature post-IR IRSL protocol. Quaternary International, in press, doi:10.1016/j.quaint.2010.05.018
- Thomsen, K.J., Bøtter-Jensen, L., Murray, A.S., Solongo, S., 2002. Retrospective dosimetry using unheated quartz: a feasibility study. Radiation Protection Dosimetry 101, 345-348.
- Thomsen, K. J., Jain, M., Bøtter-Jensen, L., Murray, A. S., Jungner, H. 2003. Variation with depth of dose distributions in single grains of quartz extracted from an irradiated concrete block. Radiation Measurements 37, 315–321.
- Thomsen, K.J., Murray, A.S., Bøtter-Jensen, L., 2005. Sources of variability in OSL dose measurements using single grains of quartz. Radiation Measurements 39. 47-61.
- Thomsen, K. J., Murray, A. S., Bøtter-Jensen, L., Kinahan, J. 2007. Determination of burial dose in incompletely bleached fluvial samples using single grains of quartz. Radiation Measurements 42, 370–379.
- Thomsen, K.J., Murray, A.S., Jain, M., Bøtter-Jensen, L., 2008. Laboratory fading rates of various luminescence signals from feldspar-rich sediment extracts. Radiation Measurements 43, 1474-1486.
- Wallinga, J., 2002. Optically stimulated luminescence dating of fluvial deposits: a review. Boreas 31, 303-322.
- Wallinga, J., Bos A.J.J., Dorenbos, P., Murray, A.S., Schokker, J., 2007. A test case for anomalous fading correction in IRSL dating. Quaternary Geochronology 2, 216-221.
- Wintle, A.G., 1973. Anomalous fading of thermoluminescence in mineral samples. Nature 245, 143-144.
- Wintle, A.G., Murray, A.S., 2006. A review of quartz optically stimulated luminescence characteristics and their relevance in single-aliquot regeneration dating protocols. Radiation Measurements 41, 369–391.

8 Conclusions and outlook

8.1 Overall conclusions

Luminescence dating method was applied to investigate coastal sedimentary archives along the southern Baltic Sea and southern North Sea coast, to establish numerical chronologies for important coastal sediment successions and to set up an improved chronostratigraphy for the Holocene barrier-spit evolution in particular for the southern Baltic Sea. In combination with geomorphological and sedimentological studies the cause-effect relationship of environmental parameters (e.g. sea-level, climate) and Holocene barrier-spit evolution was systematically examined. Furthermore, different analytical set-ups were tested in order to obtain reliable burial ages of contaminated and incompletely bleached coastal sediment samples. Finally, the potential of feldspar minerals as alternative luminescence dosimeter in Holocene coastal settings was thoroughly investigated. The outcome of the five presented research papers enables to make five sets of conclusions.

8.1.1 Chronostratigraphy of foredunes at the southern Baltic Sea

The classic relative foredune stratigraphy of Keilhack (1912, 1914) was quantified by a numerical chronology (see chapter 3). The brown foredunes formed from about 5000 BC until about 500 AD. The brown foredunes at Zingst-Osterwald (Darss-Zingst, see chapter 4) aggregated from 100 AD to 400 AD and thus the ages agree with the findings from the Świna barrier. The formation of foredunes started subsequently after the main phase of the Littorina transgression, when the former fast sea-level rise decelerated. The yellow dunes formed after ~1000 AD, i.e. shortly after the late Subatlantic transgression. Thus, it appears that the formation of the brown dune generation and the yellow dune generation were separated by the late Subatlantic transgression, which caused an alteration of the sediment dynamics (chapter 3 and 4). White dunes formed after ~1500 AD. However, Keilhack´s relative stratigraphy was confirmed.

8.1.2 Holocene barrier-spit evolution and Holocene sea-level fluctuation

The chronologies of the investigated sedimentary archives (Świna-barrier, Darss-Zingst, Sylt) indicated that under conditions of a fast sea-level rise (i.e. during the Littorina or Flandrian transgression) no established foredunes or swash-bars were formed. The accretion of the oldest foredune ridges at the Świna-barrier (4000-5000 BC, chapter 3) started subsequently after the main phase of the Littorina transgression, when the average sea-level rise decelerated from ~15 mm/yr during the main phase to ~1.5 mm/yr after the main phase (i.e. after 5000-5500 BC, see e.g. Hoffmann and Lampe, 2007; Lampe et al., 2007). However, the ages of the oldest foredune ridges at the Świna-barrier revealed that foredune plains can grow even under conditions of a moderate sea-level rise. The minor sea-level fluctuations after 5000 BC were not recorded in the chronologies of the sedimentary archives, e.g. as phases of intensified or reduced foredune plain or beach plain progradation. Only the late Subatlantic transgression (~800 AD, see Lampe et al., 2007) caused a significant decrease of the progradation dynamics and alteration of the sediment dynamics, which is recorded in the sediment archives of the Świna-barrier (chapter 3) and Darss-Zingst (chapter 4), respectively. However, it is concluded that under conditions of an overall moderate sea-level rise (1.0-1.5 mm/yr) the condition of a beach plain or foredune plain (progradative, or erosive) is highly

depending on other controlling parameters. In particular it depends on the relation of sediment supply and accumulation space, i.e. the local geology and morphology.

8.1.3 Holocene barrier-spit evolution and climate change

Based on chapter 3, 4, and 5 it is concluded that under conditions of moderate sea-level fluctuations the vegetation cover and thus the climate is an important control on the evolution of beach plains and foredune plains. The formation of foredunes and swash-bars was likely correlated to warmer, milder and calmer phases within the mid- to late-Holocene. At the Świna barrier a phase of intensive foredune plain progradation took place in early Subboreal before ~2100 BC during the time of the Holocene climate optimum. Furthermore, a phase of beach plain and foredune plain progradation occurred during the Roman Warm Period (0-400 AD) in the sedimentary archives of the Świna barrier, Darss-Zingst, and Sylt in chapter 3, 4, and 5, respectively. However, time gaps within the chronology of Świna barrier foredune progradation (chapter 3) were detected probably indicating a stagnant or erosive foredune plain at ~2100 BC, ~900 BC, 600 AD, and during the time of the Little Ice Age (LIA) at ~1550 AD. These time gaps correlate with well known phases of enhanced aeolian activity along the coasts of West and Northwest Europe (e.g. Wilson et al., 2004; Clemmensen et al., 2009) in coherency with abrupt climatic shifts (known as LIA-type events) to cooler and stormier conditions (e.g. Bond et al., 1997). These climatic shifts (i.e. higher frequency and magnitude of storm events, shorter vegetation period) likely caused a regressive vegetation cover and accordingly induced a sediment transport from the beach/foredune plain to the coastal hinterland providing the sediment for transgressive dunes or aeolian sand-sheets. Indeed, the formation of a transgressive dune at the Świna barrier and the deposition of aeolian cover sands in Sylt were dated to ~1500-1600 AD indicating enhanced aeolian activity during the main phase of the LIA.

8.1.4 Are small aliquots a reliable proxy for single-grains?

In chapter 5, 6 and 7 it is shown that analyses of Holocene sediment mixtures or incomplete bleached sediments require luminescence measurements on a single-grain scale. However, for sedimentary quartz from the North Sea (chapter 5) and Baltic Sea (chapter 6, 7) small aliquots are a reliable proxy for single-grain measurements if the averaging effect in multi-grain aliquots is limited to a negligible level. For sedimentary quartz from the North Sea (chapter 5) this is the case if on average 80 % of the luminescence signal is emitted by the brightest grain in the multi-grain aliquot. Thus, information from single-grain measurement is recommended in order to define the right number of grains on a small aliquot. Chapter 5 revealed that the Finite Mixture Model applied to D_e distributions of approved small aliquots can reliably identify discrete D_e population within sedimentary mixture. These findings contradict the results of Arnold and Roberts (2009) that used a stochastic model to simulate sediment mixtures.

In contrast to quartz single-grains from the Baltic Sea or North Sea, a large portion of feldspar grains (~40 %) emitted a detectable luminescence signal (chapter 7). Furthermore, the contribution to the total light sum in a multi-grain aliquot is more evenly (i.e. unlike quartz the average luminescence signal in a multi-grain aliquot is dominated by only a few bright grains) suggesting that the averaging effect in feldspar multi-grain aliquots is more severe than in quartz. Moreover, in contrast to quartz, a significant higher spread (~3-4 times higher) in the feldspar single-grain D_e distribution of incompletely bleached samples was observed, an effect that could probably cause an additional averaging effect (chapter 7). Thus, it is concluded that small aliquot feldspar is unlikely to be useful

in studies of incomplete bleaching or sediment mixing. However, the first feldspar single-grain results of well-bleached and incompletely bleached samples (presented in chapter 7) are encouraging.

8.1.5 Feldspar as alternative luminescence dosimeter in Holocene coastal settings

In regions and settings where quartz is not suitable as luminescence dosimeter (e.g. Scandinavia, West Coast Canada, New Zealand) feldspar can be taken as an alternative. Chapter 6 showed that pIRIR ages of mid-Holocene and late Pleistocene samples were in good agreement with reliable quartz and with independent radiocarbon ages. In contrast, the conventional IRSL ages systematically overestimated the more reliable quartz (see chapter 6) and radiocarbon ages mainly due to the applied fading correction procedure (following Huntely and Lamothe, 2001), which generated a systematic overcorrection for fading rates above 5 %/decade. The fading rates of the pIRIR signal were significantly lower (0-2 %/decade) and the fading corrected pIRIR ages are, in contrast to the fading corrected IRSL ages, considered as reliable. However, pIRIR dating of very young samples (<1.0 ka) was problematic because of a higher significance of residuals and thermal transfer. Furthermore, the pIRIR signal bleaches more slowly than the quartz signal and thus residual doses generated by incompletely bleached feldspar grains have a higher importance as well (chapter 7). Nevertheless, the feldspar pIRIR protocol of Thomsen et al. (2008), which was originally developed to date older sediments (>100 ka), was successfully modified in order to reliably date late Pleistocene and Holocene samples (chapter 6). The first single-grain pIRIR results (chapter 7) revealed that it is possible to identify well-bleached feldspar grains within incomplete bleached sediments.

8.2 Suggestions for future research

Although the results presented in this thesis enable an improved view on coastal evolution of barrier-spits along the southern Baltic Sea and North Sea (Świna-barrier, Darss-Zingst, northern Sylt) and furthermore the thesis established new methodological procedures to date Holocene coastal sediments using feldspars as luminescence dosimeter, there are still open questions leaving space for future research. In the following, the most important of these open research questions are addressed.

The Świna-barrier turned out to be a very detailed, rich and thus a very important sedimentary archive, which merits further investigations. Future studies should systematically combine methods of Applied Geophysics (e.g. GPR measurments), Sedimentology, and OSL dating in order to estimate the sediment volume of the barrier-spit systems (to quantify sediment transport over the time) and furthermore to unravel the sedimentary processes of foredune plain evolution in a higher resolution and in more detail. Although, the presented chronology of the Świna-barrier (based on 28 OSL ages) is significantly improved compared to the radiocarbon based chronology, future studies should take minimum one sample per foredune ridge (~150-200 OSL samples) in order to examine the cause-effect relationship of foredune plain evolution and Holocene sea-level and climate fluctuations in the highest possible resolution.

Future studies should investigate the regional and local significance of fluctuations of supraregional environmental parameters (e.g. sea-level, climate). Therefore, similar studies should investigate other important barrier-spits at the southern Baltic Sea (e.g. in NE Poland) and at the southern North Sea (e.g. East Frisian Islands).

Feldspar is a reliable alternative luminescence dosimeter, which can be used to date Holocene coastal sediments if the quartz is not a sufficient luminescence dosimeter; however, feldspar pIRIR dating of sediments younger than ~1.0 ka is still problematic due to an increasing significance of thermal transfer, residual doses and due to a higher probability of incomplete bleached grains. In order to use the pIRIR protocol to date feldspars of the recent past a study is required that systematically investigates thermal transfer and residuals in pIRIR feldspar in order to minimize both to a negligible level or to establish a reliable correction procedure. Furthermore, incomplete bleaching of the different feldspar signals should be studied in more detail.

The measurement of feldspar single-grains can be used to identify well bleached feldspar grains within an incompletely bleached sediment sample. However, this technique is in a very early experimental stage. Thus, future studies should still concentrate on the methodology of feldspar single-grain dating, e.g. the mineral separation needs to be improved and the bleaching behaviour of feldspar single-grains should be tested for different sedimentary settings. However, above all, it is prudent to develop techniques that reliably enable potassium content measurements on a single-grain scale in order to determine dose and internal dose rate on the same grain.

List of references

Aagaard, T., Orford, J., Murray, A.S., 2007. Environmental controls on the coastal dune formation; Skallingen Spit, Denmark. Geomorphology 83, 29-47.

Adamiec, G., Aitken, M., 1998. Dose-rate conversion factors: update. Ancient TL 16, 37-50.

Aitken, M.J., 1985. Thermoluminescence Dating, Academic Press, London.

Aitken, M.J., 1998. An Introduction to optical dating. Oxford University Press, Oxford.

Alappat, L., Frechen, M., Ramesch, R., Tsukamoto, S., Srinivasalu S., 2011. Evolution and chronology of late Holocene coastal dunes in the Cauvery delta region of Tamil Nadu, India. Journal of Asian Earth Science, doi.org/10.1016/j.jseaes.2011.05.019)

Alappat, L., Vink, A., Tsukamoto, S., Frechen, M., 2010. Establishing the Late Pleistocene-Holocene sedimentation boundary in the southern North Sea using OSL dating of shallow continental shelf sediments. Proceedings of the Geologists´ Association 121, 43-54.

Arnold, L.J., Roberts, R.G., 2009. Stochastic modelling of multi-grain equivalent dose (D_e) distributions: Implications for OSL dating of sediment mixtures. Quaternary Geochronology 4, 204-230.

Arnold, L.J., Bailey, R.M., Tucker, G.E., 2007. Statistical treatment of fluvial dose distributions from southern Colorado arroyo deposits. Quaternary Geochronology 2, 162-167.

Arnold, L.J., Roberts, R.G., Galbraith, R.F., DeLong, S.B., 2009. A revised burial dose estimation procedure for optical dating of young and modern-age sediments. Quaternary Geochronology 4, 306-325.

Auclair, M., Lamothe, M., Huot, S., 2003. Measurement of anomalous fading for feldspar IRSL using SAR. Radiation Measurements 37, 487-492.

Bailey, R.M., Arnold, L.J., 2006. Statistical modelling of single grain quartz De distributions and the assessement of procedures for estimating burial dose. Quaternary Science Reviews 25, 2475-2502.

Bailey, S.D., Wintle, A.S., Duller, G.A.T., Bristow, C.S., 2001. Sand deposition during the last millennium at Aberffraw, Anglesey, North Wales as determined by OSL dating of quartz. Quaternary Science Reviews 20, 701-704.

Balescu, S., Lamothe, M., 1994. Comparison of TL and IRSL age estimates of feldspar coarse grains from waterlain sediments. Quartnerary Geochronology (Quaternary Science Reviews) 13, 437-444.

Ballarini, M., Wallinga, J., Murray, A.S., van Heteren, S., Oost, A.P., Bos, A.J.J., van Eijk, C.W.E., 2003. Optical dating of young coastal dunes on a decadal time scale. Quaternary Science Reviews 22, 1011-1017.

Ballarini, M., Wallinga, J., Wintle, A.G., Bos, A.J.J., 2007. A modified SAR protocol for optical dating of individual grains from young quartz samples. Radiation Measurements 42, 360–369.

Bateman, M.D., 2008. Luminescence dating of periglacial sediments and structures. Boreas 37, 574-588.

Bateman, M.D., Frederick, C.D., Jaiswal, M.K., Shingvi, A.S., 2003. Investigations into the effect of pedoturbation on luminescence dating. Quaternary Science Reviews 22, 1169-1176.

Bateman, M.D., Boulter, C.H., Carr, A.S., Frederick, C.D., Peter, D., Wilder, M., 2007. Detecting post-depositional sediment disturbance in sandy deposits using optical luminescence. Quaternary Geochronology 2, 57–64.

Berger, G.W., Murray, A.S., Havholm, K.G., 2003. Photonic dating of Holocene back-barrier coastal dunes, northern North Carolina, USA. Quaternary Science Reviews 22, 1043-1050.

Bird, E.C.F., 1990. Classification of European dune coast. Catena Supplement 18, 15-24.

Björck, S., 1995. A review of the history of the Baltic Sea 13.0-8.0 ka BP. Quaternary International 27, 19-40.

Blair, M.W., Yukihara, E.G., Mckeever, S.W.S., 2005. Experiences with single-aliquot OSL procedures using coarse-grain feldspars. Radiation Measurements 39, 361-374.

Bond, G., Showers, W., Cheseby, M., Lotti, R., Almasi, P., deMenocal, P., Priore, P., Cullen, H., Hajdas, I., Bonani, M., 1997. A pervasive millennial-scale cycle in North Atlantic Holocene and Glacial climates. Science 278, 1257-1266.

Borówka, R.K., 1990. Coastal dunes in Poland. Catena Supplement 18, 25-30.

Borówka, R.K., Gonera, P., Kostrzewski, A., Nowaczyk, B., Zwoliński, Z., 1986. Stratigraphy of eolian deposits in Wolin Island and the surrounding area, North-West Poland. Boreas 15, 301–309.

Borówka, R.K., Osadczuk, A., Witkowski, A., Wawrzyniak-Wydrowska, B., Duda, T., 2005. Late Glacial and Holocene depositional history in the eastern part of the Szczecin Lagoon (Great Lagoon) basin-NW Poland. Quaternary International 130, 87–96.

Bøtter-Jensen, L., Bulur, E., Duller, G.A.T., Murray A.S., 2000. Advances in luminescence instrument systems. Radiation Measurements 32, 523-528.

Bøtter-Jensen, L., Andersen, C.E., Duller, G.A.T., Murray A.S., 2003. Developments in radiation, stimulation and observation facilities in luminescence measurement. Radiation Measurements 37, 535-541.

Bristow, C.S., Chroston, P.N., Bailey, S.D., 2000. The structure and development of foredunes on a locally prograding coast: insights from ground-penetrating radar surveys, Norfolk, UK. Sedimentology 47, 923–944.

Buylaert, J.P., Ghysels, G., Murray, A.S., Thomsen, K.J., Vandenberghe, D., DeCorte, F., Heyse, Van den haute, P., 2009a. Optical dating of relict sand wedges and composite-wedge pseudomorphs in Flanders, Belgium. Boreas 38, 160-175.

Buylaert, J.P., Murray, A.S., Thomsen, K.J., Jain, M., 2009b. Testing the potential of an elevated temperature IRSL signal from K-feldspar. Radiation Measurements 44, 560-565.

Buynevich, I. V., FitzGerald, D. M., Goble, R. J., 2007. A 1500 yr record of North Atlantic storm activity based on optically dated relict beach scarps. Geology 35, 543-546.

Clarke, M., Rendell, H., 2009. The impact of North Atlantic storminess on western European coasts: A review. Quaternary International 195, 31-41.

Clarke, M., Rendell, H., Tastet, J.-P., Clave, B., Masse, L., 2002. Late-Holocene sand invasion and North Atlantic storminess along the Aquitaine Coast, southwest France. The Holocene 12, 231-238.

Clemmensen, L.B., Murray, A., 2006. The termination of the last major phase of aeolian sand movement, coastal dunefields, Denmark. Earth Surface Processes and Landforms 31, 795–808.

Clemmensen, L.B., Pye, K., Murray, A., Heinemeier, J., 2001a. Sedimentology, stratigraphy, and landscape evolution of a Holocene coastal dune system, Lodbjerg, NW Jutland, Denmark. Sedimentology 48, 3-27.

Clemmensen, L.B., Murray, A., Beck, J.H., Clausen, A., 2001b. Large-scale aeolian sand movement on the west coast of Jutland, Denmark in late Subboreal to early Subatlantic time - a record of climate change or cultural impact? GFF (Geologiska Föreningens i Stockholm Förhandlingar) 123, 193-203.

Clemmensen, L.B., Murray, A., Heinemeier, J., de Jong, R., 2009. The evolution of Holocene coastal dunefields, Jutland, Denmark: A record of climate change over the past 5000 years. Geomorphology 105, 303-313.

Cooper, W.S., 1958. Coastal sand dunes of Oregon and Washington. Memoirs of Geological Society of America 72. Boulder, Co.

Cunningham, A.C., Wallinga, J., 2010. Selection of integration time intervals for quartz OSL decay curves. Quaternary Geochronology, doi:10.1016/j.quageo.2010.08.004.

David, B., Roberts, R.G., Magee, J., Mialanes, J., Turney, C., Bird, M., White, C., Fifield, L.K., Tibby, J., 2007. Sediment mixing at Nonda Rock: investigations of stratigraphic integrity at an early archaeological site in northern Australia and implications for the human colonisation of the continent. Journal of Quaternary Science 22, 449-479.

Davids, F., Duller, G.A.T., Roberts, H.M., 2010. Testing the use of feldspars for optical dating of hurricane overwash deposits. Quaternary Geochronology 5, 125-130.

Dawson, A.G., Hickey, K., Holt, T., Elliott, L., Dawson, S., Foster, I.D.L., Wadhams, P. Jonsdottir, I., Wilkinson, J., McKenna, J., Davis, N.R., Smith, D.E., 2002. Complex North Atlantic Oscillation (NAO) index signal of historic North Atlantic storm-track changes. The Holocene 12, 363–369.

Duller, G.A.T., 1991. Equivalent dose determination using single aliquots. Nuclear Tracks and Radiation Measurements 18, 371-378.

Duller, G.A.T., 1992. Luminescence Chronology of Raised Marine Terraces, South-West North Island, New Zealand. PhD thesis, University of Wales, Aberystwyth.

Duller, G.A.T, 1994. Luminescence dating of sediments using single aliquots: new procedures. Quaternary Science Reviews 13, 149-156.

Duller, G.A.T., 2003. Distinguishing quartz and feldspar in single grain luminescence measurements. Radiation Measurements 37, 161-165.

Duller, G.A.T., 2004. Luminescence dating of Quaternary sediments recent advances. Journal of Quaternary Science 19, 183-192.

Duller, G.A.T. 2006. Single grain optical dating of glacigenic sediments. Quaternary Geochronology 1, 296–304.

Duller, G.A.T., 2007. Assessing the error on equivalent dose estimates derived from single aliquot regenerative dose measurements. Ancient TL 25, 15-24.

Duller, G.A.T., 2008. Single-grain optical dating of Quaternary sediments: why aliquot size matters in luminescence dating. Boreas 37. 589-612.

Duller, G.A.T., Murray, A.S., 2000. Luminescence dating of sediments using individual mineral grains. Geologos 5, 87-106.

Duller, G.A.T., Bøtter-Jensen, L., Murray, A.S., Truscott, A.J., 1999. Single grain laser luminescence (SGLL) measurements using a novel automated reader. Nuclear Instruments and Methods: B 155, 506–514.

Duller, G.A.T., Bøtter-Jensen, L., Murray, A.S., 2000. Optical dating of single sand sized grains of quartz: Sources of variability. Radiation Measurements 32, 453–457.

Duller, G.A.T., Bøtter-Jensen, L., Murray, A.S. 2003. Combining infrared- and green-laser stimulation sources in single-grain luminescence measurements of feldspar and quartz. Radiation Measurements 37, 543–550.

Durcan, J., Duller, G.A.T., 2011. The fast ratio: a rapid measure for testing the dominance of the fast component in the initial OSL signal from quartz. Radiation Measurements, doi: 10.1016/j.radmeas.2011.07.016

Erfurt, G., Krbetschek, M.R., 2003. Studies on the physics of the infrared radioluminescence of potassium feldspar and on the methodology of its application to sediment dating. Radiation Measurements 37, 505-510.

Forbes, D.L., Orford, J.D., Carter, R.W.G., Shaw, J., Jennings, S.C., 1995. Morphodynamic evolution, self-organisation, and instability of coarse-clastic barriers on paraglacial coasts. Marine Geology 126, 63-85.

Fuchs, M., Lang, A., 2001. OSL dating of coarse-grain fluvial quartz using single-aliquot protocols on sediments from NE Peloponnese, Greece. Quaternary Science Reviews 20, 783-787.

Fuchs, M., Owen, L. A., 2008. Luminescence dating of glacial and associated sediments: review, recommendations and future directions. Boreas 37, 636-659.

Galbraith, R.F., 2005. Statistics for Fission Track Analysis. Chapman and Hall/CRC Press, Boca Raton, Florida.

Galbraith, R.F., Green, P.F., 1990. Estimating the component ages in a finite mixture. Nuclear Tracks and Radiation Measurements 17, 197-206.

Galbraith, R.F., Roberts, R.G., Laslett, G.M., Yoshida, H., Olley, J.M., 1999. Optical dating of single and multiple grains of quartz from Jinmium rock shelter, Northern Australia: part 1, experimental details and statistical models. Archaeometry 41, 339-364.

Geyh, M.A., 2005. Handbuch der Physikalischen und Chemischen Altersbestimmung. Wissenschaftliche Buchgesellschaft, Darmstadt.

Gibbard, P.L., Boreham, S., Cohen, K.M., Moscariello, A., 2005. Global chronostratigraphical correlation table for the last 2.7 million years. Boreas 34, unpaginated.

Godfrey-Smith, D., Huntley, D., Chen, W.-H., 1988. Optical dating studies of quartz and feldspar sediments extracts. Quaternary Science Reviews 7, 373-380.

Görsdorf, J., Kaiser, K., 2001. Radiokohlenstoffdaten aus dem Spätpleistozän und Frühholozän von Mecklenburg-Vorpommern. Meyniana 53, 91-118.

Gripp, K., Simon, G., 1940. Untersuchungen über den Aufbau und die Entstehung der Insel Sylt: I. Nord-Sylt. Westküste 2, 1-70.

Gripp, K., Becker, W., 1940. Untersuchungen über den Aufbau und die Entstehung der Insel Sylt: II. Mittel-Sylt. Westküste 2, 71–84.

Grunewald, R., 2006. Assement of damages from recreational activities on coastal dunes of the southern Baltic Sea. Journal of Coastal Research 22, 1145-1157.

Harff, J., Lüth, F., (eds.) 2007. Sincos – Sinking Coast. Geosphere. Ecosphere and Anthroposphere of the Holocene Southern Baltic Sea. Bericht der Römisch-Germanischen Kommission 88, 7-266.

Harff, J., Meyer, M., 2007. Changing Holocene coastal zones of the Baltic Sea. Bericht der Römisch-Germanischen Kommission 88, 241-266.

Harff, J., Lampe, R., Lemke, W., Lübke, H., Lüth, F., Meyer, M., Tauber, F., 2005. The Baltic Sea — a model ocean to study interrelations of geosphere, ecosphere, and anthroposphere in the coastal zone. Journal of Coastal Research 21, 441–446.

Hass, H.C., 1996. Northern Europe climate variations during late Holocene: evidence from marine Skagerrak. Palaeogeography, Palaeoclimatology, Palaeoecology 123, 121–145.

Hesp, P.A., 1988. Morphology, dynamics and internal stratification of some established foredunes in southeast Australia. Journal of Sedimentary Geology 55, 17– 41.

Hesp, P., 2002. Foredunes and blowouts: initiation, geomorphology and dynamics. Geomorphology 48, 245-268.

Hilgers, A., 2007. The chronology of Late Glacial and Holocene dune development in the northern Central European lowland reconstructed by optically stimulated luminescence (OSL) dating. PhD thesis, University of Cologne.

Hilgers, A., Murray, A.S., Schlaak, N., Radtke, U., 2001. Comparison of quartz OSL protocols using Lateglacial and Holocene dune sands from Brandenburg, Germany. Quaternary Science Reviews 20, 731-726.

Hoffmann, D., 1974. Zum geologischen Aufbau der Hörnumer Halbinsel auf Sylt. Meyniana 23, 63-68.

Hoffmann, G., Lampe, R., 2007. Sediment budget calculation to estimate Holocene coastal changes on the southwest Baltic Sea (Germany). Marine Geology 243, 143-156.

Hoffmann, G., Lampe, R., Barnasch, J., 2005. Postglacial evolution of coastal barriers along the West Pomeranian coast, NE Germany. Quaternary International 133-134, 47-59.

Hoffmann, G., Schmedeman, N., Schafmeister, M.Th., 2009. Relative sea-level curve for SE Rügen and Usedom Island (SW Baltic Sea Coast, Germany) – using decompacted profiles. Zeitschrift der Deutschen Gesellschaft für Geowissenschaften (ZDGG) 160, 69-78.

Hua, Q., 2009. Radiocarbon: A chronological tool fort the recent past. Quaternary Geochronology 4, 378-390.

Hülle, D., Hilgers, A., Radtke, U., Stolz, C., Hempelmann, N., Grunert, J., Felauer, T., Lehmkuhl, F., 2010. OSL dating of sediments from the Gobi Desert, Southern Mongolia. Quaternary Geochronology 5, 107-113.

Huntley, D.J., Baril, M.R., 1997. The K content of the K-feldspars being measured in optical dating or in thermoluminescence dating. Ancient TL 15, 11-13.

Huntley, D.J., Hancock, R.G.V., 2001. The Rb contents of the K-feldspars being measured in optical dating. Ancient TL 19, 43-46.

Huntley, D.J., Godfrey-Smith, D.I., Thewalt, M.L.W., 1985. Optical dating of sediments. Nature 313, 105-107.

Hütt, G., Jaek, I., Tchonka, J., 1988. Optical dating – K-feldspars optical-response stimulation spectra. Quaternary Science Reviews 7, 381-385.

IPCC, 2007. Summary of Policymakers. In: Climate Change 2007: The Physical Science Basis. Contribution of Working Group I to the Fourth Assessement Report of the Intergovernmental Panel on Climate Change. Cambridge University Press, Cambridge (UK), and New York (USA).

ISSS-ISRIC-FAO, 1998. World reference base for soil resources. FAO, World Soil Resources Report 84, Rome.

Jacobs, Z., 2008. Luminescence chronologies for coastal and marine sediments. Boreas 37, 508-535.

Jacobs, Z., Duller, G.A.T., Wintle, A.G., 2006. Interpretation of single grain D_e distributions and calculation of D_e. Radiation Measurements 41, 264–277.

Jacobs, Z., Wintle, A.G., Duller, G.A.T., Roberts, R.G., Wadley, L., 2008a. New ages for the post-Howiesons Poort, late and final Middle Stone Age at Sibudu, South Africa. Journal of Archaeological Science 35, 1790–1807.

Jacobs, Z., Wintle, A.G., Roberts, R.G., Duller, G.A.T., 2008b. Equivalent dose distributions from single grains of quartz at Sibudu, South Africa: context, causes and consequences for optical dating of archaeological deposits. Journal of Archaeological Science 35, 1808–1820.

Jain, M., Ankjærgaard, C., 2011. Towards a non-fading signal in feldspar: Insight into charge transport and tunnelling from time-resolved optically stimulated luminescence. Radiation Measurements, doi:10.1016/j.radmeas.2010.12.004.

Jain, M., Murray, A.S., Bøtter-Jensen, L., 2003. Characterisation of blue-light stimulated luminescence components in different quartz samples: implications for dose measurements. Radiation Measurements 37, 441-449.

Jain, M., Murray, A.S., Bøtter-Jensen, L., 2004a. Optically stimulated luminescence dating - how significant is incomplete light exposure in fluvial environments? Quaternaire 15, 143-157.

Jain, M., Thomsen, K.J., Bøtter-Jensen, L., Murray, A.S., 2004b. Thermal transfer and apparent-dose distributions in poorly bleached mortar samples: results from single grains and small aliquots of quartz. Radiation Measurements 38, 101-109.

Janke, W., Lampe, R. 1998. Die Entwicklung der Nehrung Fischland-Darß-Zingst und ihres Umlandes seit der Litorina-Transgression und die Rekonstruktion ihrer subrezenten Dynamik mittels historischer Karten. Zeitschrift für Geomorphology N.F., Suppl. Bd. 112, 177-194.

Kaiser, K., 2001. Die spätpleistozäne bis frühholozäne Beckenentwicklung in Mecklenburg-Vorpommern – Untersuchungen zur Startigraphie, Geomorphologie und Geoarchäologie. Greifswalder Geographische Arbeiten 24, 1-208.

Kaiser, K., Barthelmes, A., Czako Pap, S., Hilgers, A., Janke, W., Kühn, P., Theuerkauf, M., 2006. A Lateglacial palaeosol cover in the Altdarss area, southern Baltic Seacoast (Northeast Germany): investigations on pedology, geochronology and botany. Netherlands Journal of Geosciences 85, 199-222.

Keilhack, K., 1912. Die Verlandung der Swinepforte. Jahrbuch der Königliche-Preussischen Geologischen Landesanstalt XXXII, 209-244.

Keilhack, K., 1914. Erläuterungen zu Geologischen Karten von Preussen und benachtbarten Bundesstaaten. Blatt Swinemünde. Berlin.

Kiyak, K.G., Canel, T., 2006. Equivalent dose in quartz from young samples using the SAR protocol and the effect of preheat temperature. Radiation Measurements 41, 917-922.

Kliewe, H., Janke, W., 1991. Holozäner Küstenausgleich im südlichen Ostseegebiet bei besonderer Berücksichtigung der Boddenausgleichsküste Vorpommerns. Petermanns Geographische Mitteilungen 135, 1-15.

Klijn, J.A., 1990. The younger dunes in the Netherlands; chronology and causation. Catena, Supplement 18, 89-100.

Krbetschek, M.R., Götze, J., Dietrich, A., Trautmann, T., 1997. Spectral information from minerals relevant for luminescence dating. Radiation Measurements 27, 695-748.

Kunz, A., Frechen, M., Ramesh, R., Urban, B., 2010a. Luminescence dating of late holocene dunes showing remnants of early settlement in Cuddalore and evidence of monsoon activity in south east India. Quaternary International 222, 194-208.

Kunz, A., Frechen, M., Ramesh, R., Urban, B., 2010b. Revealing the coastal event-history of the Andaman Islands (Bay of Bengal) during the Holocene using radiocarbon and OSL dating. International Journal of Earth Sciences, doi: 10.1007/s00531-009-0507-4.

Labuz, T., 2009. The west Pomerania coastal dunes – alert state of their development. Zeitschrift der Deutschen Gesellschaft für Geowissenschaften (ZDGG) 160, 113-122.

Lamothe, M., Balescu, S., Auclair, M., 1994. Natural IRSL intensities and apparent luminescence ages of single feldspar grains extracted from partially bleached sediments. Radiation Measurements 23, 555–561.

Lamothe, M., and Auclair, M., 1997. Assessing the datability of young sediments by IRSL using an intrinsic laboratory protocol. Radiation Measurements 27, 107–117.

Lamothe, M., and Auclair, M. 1999. A solution to anomalous fading and age shortfalls in optical dating of feldspar minerals. Earth and Planetary Science Letters 171, 319–323.

Lamothe, M., Auclair, M., Hamzaoui, C., Huot, S., 2003. Towards a prediction of long-term anomalous fading of feldspar IRSL. Radiation Measurements 37, 493-503.

Lampe, R., 2002. Holocene evolution and coastal dynamics of the Fischland-Darss-Zingst peninsula. Greifswalder Geographische Arbeiten 27, 155-163.

Lampe, R., 2005. Lateglacial and Holocene water-level variations along the NE German Baltic Sea coast: review and new results. Quarternary International 133-134, 121-136.

Lampe, R., Meyer, H., Ziekur, R., Janke, W., Endtmann, E. 2007. Holocene evolution of the irregularly sinking southern Baltic Sea coast and the interactions of sea-level rise, accommodation space and sediment supply. Bericht der Römisch-Germanischen Kommission 88, 14-46.

Lemke, W., 2005. Die kurze und wechselvolle Entwicklungsgeschichte der Ostsee – Aktuelle meeresgeologische Forschungen zum Verlauf der Litorina-Transgression. Jahrbuch der Bodendenkmalpflege in Mecklenburg-Vorpommern 52, 43-54.

Li, S.H., Chen, Y.Y., Li, B. Sun, J., Yang, L.R., 2007a. OSL dating of sediments from deserts in northern China. Quaternary Geochronology 2, 23-28.

Li, B., Li, S.H., Wintle, A.G., Zhao, H., 2007b. Isochron measurement of naturally irradiated K-feldspar grains. Radiation Measurements 42, 1315-1327.

Li, B., Li, S.H., Wintle, A.G., 2008a. Overcoming environmental dose rate changes in luminescence dating of waterlain deposits. Geochronometria 30, 33-40.

Li, B., Li, S.H., Wintle, A.G., Zhao, H., 2008b. Isochron dating of sediments using luminescence of K-feldspar grains. Journal of Geophysical Research-Earth Surface 113, F02026. 02010.01029/02007JF000900.

Li, B., Li, S.H., Duller, G.A.T., Wintle, A.G., 2010. Infrared stimulated luminescence measurements of single grains of K-rich feldspar for isochron dating. Quaternary Geochronology, doi:10.1016/j.quageo.2010.02.003.

Lindhorst, S., 2007. Stratigraphy and development of a Holocene barrier-spit (Sylt, southern North Sea). PhD thesis, University of Hamburg.

Lindhorst, S., Betzler, C., Hass, H.C., 2008. The sedimentary architecture of a Holocene barrier spit (Sylt, German Bight): Swash-bar accretion and storm erosion. Sedimentary Geology 206, 1-16.

Lindhorst, S., Fürstenau, J., Hass, H.C., Betzler, C., 2010. Anatomy and sedimentary model of a hooked spit (Sylt, southern North Sea). Sedimentology 57, 935-955.

Lopez, G.I., Rink, W.J., 2007. Characteristics of the burial environment related to quartz SAR-OSL dating at St. Vincent Island, NW Florida, USA. Quaternary Geochronology 2, 65-70.

Lukas, S., Spencer, J.Q.G., Robinson, R.A.J., Benn, D.I., 2007. Problems associated with luminescence dating of Late Quaternary glacial sediments in the NW Scottish Highlands. Quaternary Geochronology 2, 243-248.

Lüthgens, C. Böse, M., Preusser, F., 2011. Age of the Pomeranian ice-marginal position in northeastern Germany determined by Optically Stimulated Luminescence (OSL) dating of glaciofluvial sediments. Boreas, doi: 10.1111/j.1502-3885.2011.00211.

Madsen, A.T., Murray A.S., 2009. Optically stimulated luminescence dating of young sediments: a review. Geomorphology 109, 3-16.

Madsen, A.T., Murray, A.S., Andersen, T.J., Pejrup, M., Breuning-Madsen, H., 2005. Optically stimulated luminescence dating of young estuarine sediments: a comparison with ^{210}Pb and ^{137}Cs dating. Marine Geology 214, 251-268.

Madsen, A.T., Murray, A.S., Andersen, T.J., 2007. Optical dating of dune ridges on Rømø, a barrier island in the Wadden Sea, Denmark. Journal of Coastal Research 23, 1259–1269.

Madsen, A.T., Duller, G.A.T., Donnelly, J.P., Roberts, H.M., Wintle, A.G., 2009. A chronology of hurricane landfalls at Little Sippewisset Marsh, Massachusetts, USA, using optical dating. Geomorphology 109, 36-45.

Madsen, A.T., Murray, A.S., Andersen, T.J., Pejrup, M., 2010. Luminescence dating of Holocene sedimentary deposits on Rømø, a barrier island in the Wadden Sea, Denmark. The Holocene, doi:10.1177/0959683610374883.

Mauz, B., Bungenstock, F., 2007. How to reconstruct trends of late Holocene relative sea level: A new approach using tidal flat clastic sediments and optical dating. Marine Geology 237, 225-237.

McDermott, F., Mattey, D.P., Hawkesworth, C., 2001. Centennial-scale Holocene climate variability revealed by a high-resolution speleothem ^{18}O record from SW Ireland. Science 294, 1328–1331.

Mejdahl, V., 1979. Thermoluminescence dating: Beta-dose attenuation in quartz grains. Archaeometry 21, 61-72.

Mejdahl, V., 1987. Internal radioactivity in quartz and feldspar grains. Ancient TL 5, 10-17.

Mejdahl, V., Bøtter-Jensen, L., 1994. Luminescence dating of archaeological materials using a new technique based on single aliquot measurements. Quaternary Science Reviews 13, 551-554.

Müller, A., 1996. Zu Sedimentationsgeschichte und Paläomilieu der Darß-Zingster Boddenkette (Barther Bodden und Grabow). Zeitschrift für geologische Wissenschaften 25, 1996, 465-480.

Murray, A.S., Roberts, R.G. 1997. Determining the burial time of single grains of quartz using optically stimulated luminescence. Earth and Planetary Science Letters 152, 163–180.

Murray A.S., Roberts R.G., 1998. Measurements of the equivalent dose in quartz using a regenerative-dose single aliquot protocol. Radiation Measurements 29, 503-515.

Murray, A.S., Wintle, A.G., 2000. Luminescence dating of quartz using an improved single-aliquot regenerative-dose protocol. Radiation Measurements 32, 57-73.

Murray, A.S., Clemmensen, L.B., 2001. Luminescence dating of Holocene aeolian sand movement, Thy, Denmark. Quaternary Science Reviews 20, 751-754.

Murray, A.S., Olley, J.M., 2002. Precision and accuracy in the optically stimulated luminescence dating of sedimentary quartz: a status review. Geochronometria 21, 1-16.

Murray, A.S., Wintle, A.G., 2003. The single aliquot regenerative dose protocol: potential for improvements in reliability. Radiation Measurements 37, 377-381.

Murray, A.S., Mohanti, 2006. Luminescence dating of the barrier spit at Chilika Lake, Orissa, India. Radiation Protection Dosimetry 119, 442–445.

Murray, A.S., Marten, R., Johnston, A., Martin, P., 1987. Analysis for naturally occuring radionuclides at environmental concentrations by gammaspectrometry. Journal of Radioanalytical and Nuclear Chemistry 115/2, 263-288.

Murray, A.S., Buylaert, J.P., Thomsen, K.J., Jain, M, 2009. The effect of preheating on the IRSL signal from feldspar. Radiation Measurements 44, 554-559.

Murray-Wallace, C.V., Banerjee, D., Rourman, R.P., Olley, J.M., Brooke, B.P., 2002. Optically stimulated luminescence dating of Holocene relict foredunes, Guichen Bay, South Australia. Quaternary Science Reviews 21, 1077-1086.

Naumann, M., Lampe, M. The evolution of a southern Baltic coastal barrier system, deduced from geostatistical based volume calculations and relative sea level rise (Darss-Zingst Hiddensee area / NE Germany). Submitted to Bericht der Römisch-Germanischen Kommission.

Naumann, M., Lampe, R., Hoffmann, G, 2009. Geological structure and palaeogeographic reconstruction of the Bug peninsula /NW-Rügen island. E&G (Eiszeitalter und Gegenwart) Quaternary Science Journal 58, 164-173.

Nielsen, A., Murray, A.S., Pejrup, M., Elberling, B., 2006. Optically stimulated luminescence dating of al Holocene beach ridge plain in Northern Jutland, Denmark. Quaternary Geochronology 1, 305-312.

Olley, J.M., Murray, A.S., Roberts, R.G., 1996. The effect of disequilibria in the uranium and thorium decay chains on burial dose rates in fluvial sediments. Quaternary Science Reviews 15, 751-760.

Olley, J.M., Roberts, R.G., Murray, A.S., 1997. Disequilibria in the uranium decay series in sedimentary deposits at Allen´s Cave, Nullarbor Plain, Australia: implications for dose rate determinations. Radiation Measurements 27, 433-443.

Olley, J.M., Caitcheon, G.G., Roberts, R.G., 1999. The origin of dose distributions in fluvial sediments, and the prospect of dating single grains from fluvial deposits using optically stimulated luminescence. Radiation Measurement 30, 207-217.

Olley, J.M., Pietsch, T., Roberts, R.G., 2004. Optical dating of Holocene sediments from a variety of geomorphic settings using single grains of quartz. Geomorphology 60, 337-358.

Oszadczuk, K., 2002. Evolution of the Świna barrier spit. Greifswalder Geographische Arbeiten 27, 119-125.

Otvos, E.G., 2000. Beach ridges—definitions and significance. Geomorphology 32, 83–108.

Pedersen, K., Clemmensen, L.B., 2005. Unveiling past aeolian landscapes: a groundpenetrating radar survey of a Holocene coastal dunefield system, Thy, Denmark. Sedimentary Geology 177, 57–86.

Pietsch, T.J., 2009. Optically stimulated luminescence dating of young (<500 years old) sediments: Testing estimates of burial dose. Quaternary Geochronology 4, 406-422.

Prescott, J.R., Stephan, L.G., 1982. The contribution of cosmic radiation to the environmental dose for thermoluminescent dating - Latitude, altitude and depth dependences. PACT 6, 17-25.

Prescott, J.R., Fox, P.J., 1993. Three-dimensional thermoluminescence spectra of feldspars. Journal of Physics D. 26, 2245-2254.

Prescott, J.R., Hutton, J.T., 1994. Cosmic ray distributions to dose rates for luminescence and ESR dating: large depths and long-term variations. Radiation Measurements 23, 497–500.

Preusser, F., Andersen, B.G., Denton, G.H., Schlüchter, C., 2005. Luminescence chronology of Late Pleistocene glacial deposits in North Westland, New Zealand. Quaternary Science Reviews 24, 2207–2227.

Preusser, F., Ramsmeyer, K., Schlüchter, Ch., 2006. Characterisation of low OSL intensity quartz from New Zealand Alps. Radiation Measurements 41, 871-877.

Preusser, F., Degering, D., Fuchs, M., Hilgers, A., Kadereit, A., Klasen, N., Krbetschek, M., Richter, D., Spencer, J.Q.G., 2008. Luminescence dating: basics, methods and applications. Eiszeitalter und Gegenwart 57, 95–149.

Preusser, F., Chithambo, M.L., Götte, T., Martini, M., Ramseyer, K., Sendezera, E.J., Susino, G.J., Wintle, A.G., 2009. Quartz as a natural luminescence dosimeter. Earth-Science Reviews 97, 184-214.

Prusinkiewicz, K., Noryśkiewicz, B., 1966. Zagadnienie wieku bielic na wydmach brunatnych Mierzei Świny w świetle analizy palynologicznej i datowania radioweglem C14. Zeszyty Naukowe Uniwersytetu Mikołaja Kopernika w Toruniu. Geografia 5, 75-88.

Readhead, M.L., 2002. Absorbed dose fraction for 87Rb β particels. Ancient TL 20, 25-27.

Reimann, T., Naumann, M., Tsukamoto, S., Frechen, M., 2010. Luminescence dating of coastal sediments from the Baltic Sea coastal barrier-spit Darss-Zingst, NE Germany. Geomorphology 122, 264-273.

Reimann, T., Tsukamoto, S., Naumann, M., Frechen, M., 2011a. The potential of using K-rich feldspars for optical dating of young coastal sediments – a test case from Darss-Zingst peninsula (southern Baltic Sea coast). Quaternary Geochronology 6, 207-222.

Reimann, T., Harff, J., Tsukamoto, S., Osadczuk, K., Frechen, M, 2011b. Reconstruction of Holocene coastal foredune progradation using luminescence dating – an example from the Świna barrier (southern Baltic Sea, NW Poland). Geomorphology 132, 1-16.

Reimann, T., Lindhorst, S., Thomsen, K.J., Murray, A.S., Frechen, M. OSL dating of mixed coastal sediments (Sylt, German Bight, North Sea). Submitted to Quarternary Geochronology

Reimer, P.J., Baillie, M.G.L., Bard, E., Bayliss, A., Beck, J.W., Bertrand, C.J.H., Blackwell, P.G., Buck, C.E., Burr, G.S., Cutler, K.B., Damon, P.E., Edwards, R.L., Fairbanks, R.G., Friedrich, M., Guilderson, T.P., Hogg, A.G., Hughen, K.A., Kromer, B., McCormac, F.G., Manning, S., Bronk Ramsey, C., Reimer, R.W., Remmele, S., Southon, J.R., Stuiver, M., Talamo, S., Taylor, F.W., van der Plicht, J., Weyhenmeyer, C.E., 2004. IntCal04 terrestrial radiocarbon age calibration, 0‐26 cal kyr BP. Radiocarbon 46, 1029‐1058.

Roberts, H.M., 2008. The development and application of luminescence dating to loess deposits: a perspective on the past, present and future. Boreas 37, 483-507.

Roberts, H.M., Plater, A.J., 2007. Reconstruction of Holocene foreland progradation using optically stimulated luminescence (OSL) dating: an example from Dungeness. The Holocene 17, 495-505.

Roberts, R., Yoshida, H., Galbraith, R., Laslett, G., Jones, R., Smith, M., 1998. Single aliquot and single-grain optical dating confirm thermoluminescence age estimates at Malakunanja II rock shelter in northern Australia. Ancient TL 16, 19–25.

Roberts, R.G., Galbraith, R.F., Olley, J.M., Yoshida, H., Laslett, G.M., 1999. Optical dating of single and multiple grains of quartz from Jinmium rock shelter, northern Australia: Part II. Results and implications. Archaeometry 41, 365–395.

Roberts, R.G., Galbraith, R.F., Yoshida, H., Laslett, G.M., Olley, J.M., 2000. Distinguishing dose populations in sediment mixtures: a test of single-grain optical dating procedures using mixtures of laboratory-dosed quartz. Radiation Measurements 32, 459–465.

Roberts, R.G., Flannery, T.F., Ayliffe, L.K., Yoshida, H., Olley, J.M., Prideaux, G.J., Laslett, G.M., Baynes, A., Smith, M.A., Jones, R., Smith, B.L., 2001. New ages for the last Australian megafauna: continent-wide extinction about 46,000 years ago. Science 292, 1888–1892.

Rodnight, H., 2008. How many equivalent dose values are needed to obtain a reproducible distribution? Ancient Tl 26, 1-9.

Rodnight, H., Duller, G.A.T., Wintle, A.G., Tooth, S., 2006. Assessing the reproducibility and accuracy of optical dating of fluvial deposits. Quaternary Geochronology 1, 109-120.

Schumacher, W., 2000. Zur geomorphologischen Entwicklung des Darsses - ein Beitrag zur Küstendynamik und zum Küstenschutz an der südlichen Ostseeküste. Zeitschrift für geologische Wissenschaften 28, 601-613.

Schumacher, W., 2002. Coastal evolution of the Darss Peninsula. Greifswalder Geographische Arbeiten 27, 165-168.

Schumacher, W., Bayerl, K.-A., 1999. The shoreline displacement curve of Rügen Island (Southern Baltic Sea). Quaternary International 56, 107-113.

Schütze, H., 1939. Morphologischer Beitrag zur Entstehung des Darß und Zingst. Geologie der Meere und Binnengewässer 3, 173-200.

Shofield, J.C., 1975. Sea-level fluctuations cause periodic postglacial progradation, South Kaipara Barrier, North Island, New Zealand. Journal of Geology and Geophysics 28, 295-316.

Singarayer, J.S., Bailey, R.M., 2003. Further investigations of the quartz optically stimulated luminescence components using linear modulation. Radiation Measurements 37, 451-458.

Singarayer, J.S., Bailey, R.M., 2004. Component-resolved bleaching spectra of quartz optically stimulated luminescence: preliminary results and implications for dating. Radiation Measurements 38, 111-118.

Singhvi, A.K., Bluszcz, A., Bateman, M.D., Someshwar Rao, M., 2001. Luminescence dating of loess-palaeosol sequences and coversands: methodological aspects and paleoclimatic implications. Earth-Science Reviews 54, 193-211.

Sommerville, A.A., Hansom, J.D., Housley, R.A., Sanderson, D.C.W., 2007. Optically stimulated luminescence (OSL) dating of coastal aeolian sand, Orkney Islands, Scotland. The Holocene 17, 627–637.

Spooner, N.A., 1994. The anomalous fading of infrared-stimulated luminescence from feldspars. Radiation Measurements 23, 625–632.

Steffen, D., Preusser, F., Schlunegger, F., 2009. OSL quartz age underestimation due to unstable signal components. Quaternary Geochronology 4, 353-362.

Stevens, T., Marković, S.B., Zech, M., Hambach, U., Sümegi, P. 2011. Dust deposition and climate in the Carpathian Basin over an independently dated last glacial – interglacial cycle. Quaternary Science Reviews 30, 662-681.

Stone, A.E.C., Thomas, D.S.G., 2008. Linear dune accumulation chronologies from the southwest Kalahari, Namibia: challanges of reconstructing late Quaternary palaeoenvironments from aeolian landforms. Quaternary Science Reviews 27, 1667-1681.

Streif, H., 2004. Sedimentary record of Pleistocene and Holocene marine inundations along the North Sea coast of Lower Saxony, Germany. Quaternary International 112, 3‑28.

Stuiver, M., 1978. Radiocarbon timescale tested against magnetic and other dating methods. Nature 273, 271-274.

Stuiver, M., Reimer, P.J., 1993. Extended 14C database and revised CALIB radiocarbon calibration program. Radiocarbon 35, 215–230.

Szkornik, K., Gehrels, W.R., Murray, A.S., 2008. Aeolian sand movement and relative sea-level rise in Ho Bugt, western Denmark, during the “Little Ice Age”. Holocene 18, 951-965.

Telfer, M.W., Bailey, R.M., Burrough, S.L., Stone, A.E.S., Thomas, D.S.G., Wiggs, G.S.F., 2010. Understanding linear dune chronologies: Insights from a simple accumulation model. Geomorphology 122, 195-208.

Thiel, C., Buylaert, J.P., Terhorst, B., Murray, A.S., Hofer, I., Tsukamoto, S., Frechen, M, 2010. Luminescence dating of Stratzing loess profile (Austria) – Testing the potential of an elevated temperature post-IR IRSL protocol. Quaternary International, in press, doi:10.1016/j.quaint.2010.05.018.

Thomas, P.J., Jain, M., Juyal, N., Singhvi, A.K., 2005 Comparison of single-grain and small-aliquot OSL dose estimates in <3000 years old river sediments from South India. Radiation Measurements 39, 457–469.

Thomsen, K.J., Bøtter-Jensen, L., Murray, A.S., Solongo, S., 2002. Retrospective dosimetry using unheated quartz: a feasibility study. Radiation Protection Dosimetry 101, 345-348.

Thomsen, K.J., Jain, M., Bøtter-Jensen, L., Murray, A.S., Jungner, H., 2003. Variation with depth of dose distributions in single grains of quartz extracted from an irradiated concrete block. Radiation Measurements 37, 315–321.

Thomsen, K.J., Murray, A.S., Bøtter-Jensen, L., 2005. Sources of variability in OSL dose measurements using single grains of quartz. Radiation Measurements 39. 47-61.

Thomsen, K.J., Murray, A.S., Bøtter-Jensen, L., Kinahan, J., 2007. Determination of burial dose in incompletely bleached fluvial samples using single grains of quartz. Radiation Measurements 42, 370-379.

Thomsen, K.J., Murray, A.S., Jain, M., Bøtter-Jensen, L., 2008. Laboratory fading rates of various luminescence signals from feldspar-rich sediment extracts. Radiation Measurements 43, 1474-1486.

Trautmann, T., Krbetschek, M.R., Dietrich, A., Stolz, W., 1999. Feldspar radioluminescence: a new dating method and its physical background. Journal of Luminescence 85, 45-58.

Tsukamoto, S., Denby, P.M., Murray, A.S., Bøtter-Jensen, L., 2006. Time-resolved luminescence from feldspars: New insight into fading. Radiation Measurements 41, 790-795.

Uścinowicz, S., 2006. A relative sea-level curve for the Polish Southern Baltic Sea. Quaternary International 145-146, 86-105.

Vandenberghe, D., 2004. Investigations of the Optically Stimulated Luminescence dating method for application to young geological sediments. PhD thesis, Ghent University.

Wallinga, J., 2002. Optically stimulated luminescence dating of fluvial deposits: a review. Boreas 31, 303-322.

Wallinga, J., Murray, A.S., Wintle, A.G., 2000. The single-aliquote regenrative-dose (SAR) protocol applied to coarse-grain feldspar. Radiation Measurements 32, 529-533.

Wallinga, J., Bos A.J.J., Dorenbos, P., Murray, A.S., Schokker, J., 2007. A test case for anomalous fading correction in IRSL dating. Quaternary Geochronology 2, 216-221.

Wilson, P., Orford, J.D., Knight, J., Braley, S.M., Wintle, A.G., 2001. Late-Holocene (post-4000 yr BP) coastal due development in Northumberland, northeast England, The Holocene 11, 215-229.

Wilson, P., McGourty, J., Bateman, M.D., 2004. Mid- to late-Holocene coastal dune event stratigraphy for the north coast of Northern Ireland. The Holocene 14, 406-416.

Wintle, A.G., 1973. Anomalous fading of thermoluminescence in mineral samples. Nature 245, 143-144.

Wintle, A.G., Murray, A.S., 2006. A review of quartz optically stimulated luminescence characteristics and their relevance in single-aliquot regeneration dating protocols. Radiation Measurements 41, 369–391.

Zeeberg, J.J., 1998. The European sand belt in Eastern Europe and comparison of Late Glacial dune orientation with GCM simulation results. Boreas 27, 127-139.

Zhao, H., Li, S.H., 2005. Internal dose rate to K-feldspar grains from radioactive elements other than potassium. Radiation Measurements 40, 84-93.

Appendix I: Curriculum Vitae

For reasons of data protection, the curriculum vitae is not included in the online version.

Contact: Tony.Reimann@liag-hannover.de

Appendix II: Publications

Publication (peer reviewed)

(1) **Reimann, T.**, Naumann, M., Tsukamoto, S., Frechen, M., 2010. Luminescence dating of coastal sediments from the Baltic Sea coastal barrier-spit Darss-Zingst, NE Germany. Geomorphology 122, 264-273.

(2) **Reimann, T.**, Tsukamoto, S., Harff, J., Osadczuk, K., Frechen, M., 2011a. Reconstruction of Holocene coastal foredune progradation using luminescence dating – an example from the Świna barrier (southern Baltic Sea, NW Poland). Geomorphology 132, 1-16.

(3) **Reimann, T.**, Tsukamoto, S., Naumann, M., Frechen, M., 2011b. The potential of using feldspars for optical dating of young coastal sediments – a test case from Darss-Zingst peninsula (southern Baltic Sea coast). Quaternary Geochronology 6, 207-222.

(4) **Reimann, T.**, Lindhorst, S., Thomsen, K.J., Murray, A.S., Frechen, M. OSL dating of mixed coastal sediments (Sylt, North-Sea, German Bight). Submitted to Quaternary Geochronology.

(5) **Reimann, T.**, Thomsen, K.J., Jain, M., Murray, A.S., Frechen, M. Single-grain dating of young feldspars using the pIRIR procedure. Submitted to Quaternary Geochronology.

(6) **Reimann, T.**, Tsukamoto, S. Dating the recent past (<500 years) by post-IR IRSL feldspar – examples from the North Sea and Baltic Sea coast. Submitted to Quaternary Geochronology.

(7) Dörschner, N., **Reimann, T.**, Wenske, D., Lüthgens, Ch., Tsukamoto, S., Böse, M., Frechen, M. Reconstruction of Holocene coastal development at Fulong beach in north-east Taiwan using optically stimulated luminescence (OSL) dating. Accepted in Quaternary International.

(8) Wenske, D., Frechen, M., Böse, M., **Reimann, T.**, Tseng, C-H., Hoelzmann, P. Late Quaternary Terraces in the Central Mountain Range of Taiwan. Accepted in Quaternary International.

(9) Costas, I., **Reimann, T.,** Ludwig, J., Lindhorst, S., Tsukamoto, S., Hass, C.H., Betzler, C. Comparison of OSL ages from young dune sediments with a high-resolution age model. Submitted to Quaternary Geochronology.

(10) Lindhorst, S., **Reimann, T.**, Hass, C.H., Betzler, C. Sea level and climate – a mixed signal reflected in Holocene barrier spit architecture (Southern North Sea). In preparation.

Publication (not peer reviewed)

(10) Bölscher, J., **Reimann, T.,** Böse, M., 2008. Geomorphologische Untersuchungen zum Verhältnis von Trockentälern zu den Flussterrassen der Niederlausitzer Neiße zwischen Bad Muskau und Zelz. Tagungsband zum 7. Geopark-Treffen in Bad Muskau, Förderverein Geopark Muskauer Faltenbogen e. V., Jerischke (Ed). Tagungsband zum 7. Geopark-Treffen in Forst (Lausitz) 2008, 2009.

(11) **Reimann, T.,** Lindhorst, S., 2011. Interrelation of Holocene beach progradation and aeolian sand movement at Baltic Sea and North Sea coast – insights from OSL dating. In: van Heteren, S. (Ed). Coastal Development. NCL Symposium Series 8, 3-4.

Appendix III: Conference and workshop contributions (only lead author)

(1) **Reimann, T.,** Lindhorst, S., 2011. Interrelation of Holocene beach progradation and aeolian sand movement at Baltic Sea and North Sea coast – insights from OSL dating. 8th NCL Symposium TUDelft (The Netherlands), 30 August. Oral presentation.

(2) **Reimann, T.**, Tsukamoto, S., Frechen, M., 2011. Dating the recent past (<500 years) by post-IR IRSL feldspar – examples from the North Sea and Baltic Sea coast. 13th International LED conference, Toruń (Poland), 10-14 July. Poster.

(3) **Reimann, T.**, Lindhorst, S., Thomsen, K.J., Murray, A.S., Frechen, M., 2010. OSL dating of contaminated coastal sediments from Sylt (North Sea) – single-grain vs. small aliquots. German-LED meeting, Innsbruck (Austria), 05-07. November. Oral presentation.

(4) **Reimann, T.**, Thomsen, K.J., Murray, A.S., Tsukamoto, S., Lindhorst, S., Frechen, M., 2010. Dating young quartz and feldspar – Insights from multi-grain and single grain analyses. Leibniz-pact workshop, Hannover (Germany), 24-26. October, Oral presentation.

(5) **Reimann, T.**, Harff, J., Tsukamoto, S., Osadczuk, K., Frechen, M., 2010. Reconstruction of Holocene coastal foredune progradation using luminescence dating – an example from the Świna barrier (southern Baltic Sea, NW Poland). 35. Hauptversammlung der Deutschen Quartärvereinigung (DEUQUA), 12th Annual meeting of the INQUA PeriBaltic Working Group, Greifswald (Germany), 13-17. September. Oral presentation.

(6) **Reimann, T.**, Thomsen, K.J., Murray, A.S., Tsukamoto, S., Frechen, M, 2010. The potential of K-feldspar for the optical dating of young coastal sediments - multi-grain and single-grain analyses. UK TL/OSL/ESR Meeting, Oxford (UK), 08-10. September. Oral presentation.

(7) **Reimann, T.**, Lindhorst, S., Thomsen, K.J., Murray, A.S., Hass, C., Frechen, M., 2010. OSL dating of mixed coastal sediments from Sylt (German Bight, North Sea). UK TL/OSL/ESR Meeting, Oxford (UK), 08-10. September. Poster.

(8) **Reimann, T.**, Lindhorst, S., Frechen, M., Hass, C.H., 2010. Unravelling Holocene coastal dynamics of Sylt (German Bight) using optically stimulated luminescence dating method. The Wadden Sea: Changes and Challenges in a World Heritage Site, Workshop Alfred-Wegner-Institut, List (Sylt, Germany), 03-07. May. Oral presentation.

(9) **Reimann, T.**, Lindhorst, S., Frechen, M., Hass, C.H., 2010. Applied Geophysics and Geochronology - tools to unravel Holocene coastal dynamics of Sylt (German Bight). 70. Jahrestagung der Deutschen Geophysikalischen Gesellschaft, Bochum (Germany), 15–18. March. Oral presentation.

(10) **Reimann, T.**, Tsukamoto, S., Naumann, M., Frechen, M., 2009. The potential of feldspars for optical dating of late Pleistocene and Holocene coastal deposits – a test case from Darss-Zingst peninsula (Baltic Sea coast). German Conference on Luminescence and Electron Spin Resonance Dating (German-LED), Hannover (Germany), 9-10. October. Oral presentation.

(11) **Reimann, T**., Harff, J., Tsukamoto, S., Osadczuk, K., Frechen, M., 2009. Luminescence dating of coastal sand deposits from the Baltic Sea – examples from Darss-Zingst and the Swina Gate. International Conference on Climate Change: The environmental and socio-economic response in the southern Baltic region. University of Szczecin (Poland), 25-28. May. Poster.

(12) **Reimann, T.**, Tsukamoto, S., Frechen, M., 2009. Luminescence dating of coastal sand deposits from the Baltic Sea and North Sea. 10th International Coastal Symposium (ICS), Lisbon (Portugal), 13-18. April. Oral presentation.

(13) **Reimann, T.**, Naumann, M., Tsukamoto, S., Frechen, M., 2008. OSL dating of coastal sand deposits from the Baltic Sea coastal barrier Zingst-Werder-Bock, NE Germany. 12th International Conference on Luminescence and Electron Spin Resonance Dating (LED 2008), Beijing (China), 19-25. September. Poster.

(14) **Reimann, T.**, Naumann, M., Tsukamoto, S., Frechen, M., 2008. OSL-Datierungen von Küstensanden des Nehrungssystems Zingst-Werder-Bock (Deutsche Ostseeküste). DEUQUA-Tagung, Wien (Österreich), 31. Mai-5. September. Poster.

Appendix IV: Eidesstattliche Erklärung

Hiermit erkläre ich, dass ich die vorgelegte Arbeit selbständig und ohne fremde Hilfe verfasst habe. Alle verwendeten Quellen und Hilfsmittel wurden ordnungsgemäß angeben. Ich erkläre, dass die Arbeit erstmalig am Fachbereich Geowissenschaften der Freien Universität Berlin eingereicht wurde und somit noch keiner anderen Fakultät oder Universität zur Prüfung vorgelegt wurde. Die Bestimmungen der Promotionsordnung sind mir bekannt. Die Doktorarbeit wurde von Prof. Dr. Manfred Frechen betreut.

Tony Reimann

Berlin, 21.März.2011